Regulation of SIRT1 protein in cancer metabolism and ribosome biogenesis

John R. P. Knight

A thesis submitted for the degree of Ph.D

University of York

Department of Biology

December 2011

Abstract

The deacetylase signalling enzyme SIRT1 has been subject of much research interest, in part due to its ability to promote the survival of cancer cells, and redundancy in non-cancer cell viability. The deacetylation and downregulation of p53 and the FOXO family of tumour suppressors has been identified among the downstream effects of SIRT1 in cancer. Importantly, the regulation of cancer cell survival upstream of SIRT1 has not been well characterised, creating the possibility of targeting SIRT1 via its endogenous regulatory mechanisms for anti-cancer therapeutic gain. This *Thesis* validates two putative anti-cancer targets that promote SIRT1 activity and have also been implicated in essential processes that are commonly aberrant in cancer: cellular metabolism and translational control.

SIRT1 is a sirtuin, which are unique deacetylases due to their requirement for the redox metabolite NAD^+ as a co-enzyme. The potential to promote SIRT1 activity via provision of NAD^+ is analysed here by targeting the metabolic enzyme lactate dehydrogenase A (LDH-A). LDH-A catalyses NAD^+ production and promotes aberrant cancer metabolism by perpetuating the Anaerobic Glycolysis cycle. A link is found between cancer metabolism and SIRT1 activity, with LDH-A observed to suppress cancer cell apoptosis via a mechanism consistent with SIRT1 activation.

SIRT1 is also subject to regulation by direct interaction with the protein AROS (Active Regulator Of SIRT1). AROS associates with and promotes SIRT1 pro-survival function in cancer cells. Here, AROS is found to specifically promote cancer cell survival, via a mechanism appearing to involve SIRT1 and downstream substrates. However, AROS regulation of SIRT1 is not as simple as originally thought, varying by cell context and substrate. Further to its role in directing SIRT1 activity, AROS also forms a binding interaction with the ribosomal protein RPS19. The effect of AROS upon RPS19 protein and function is analysed for the first time, revealing a role for AROS in 40S ribosomal subunit biogenesis. Beyond this, AROS is discussed as a regulator of translation, and the functional interplay between RPS19, AROS and SIRT1 is described. This provides a link between cancer associated anti-apoptotic signalling and ribosome biogenesis centred on regulation of SIRT1 activity, which could be exploited by anti-cancer therapeutics.

List of Contents

List of Figures

Chapter 1

Chapter 2

Chapter 3

Chapter 4

Chapter 5

Chapter 6

Chapter 7

Chapter 8

Chapter 9

Appendices

List of Tables

Chapter 2

Chapter 4

Chapter 6

Appendices

Acknowledgements

The completion of this Thesis would not have been possible without the support and help of the many people around me over the past 3 and half years. My gratitude goes out to everyone who has helped in any way over this time to make this possible. However, special thanks are needed for certain people.

First to both of my supervisors Prof. Jo Milner and Dr Simon Allison, who have helped with discussion, direction and instilled the drive in me to carry out work of the highest quality. From the early days, through each set back and into the final reckoning assistance was at hand. Also to Yorkshire Cancer Research, a great thank you for awarding funding to this project.

Of course, thanks are due to the other members of the YCR p53 Cancer Research Unit. Their day-to-day assistance and distractions helped keep the project moving, despite many difficulties for themselves during the course of my studies. Special thanks go to the 11am coffee brigade (Julie Mercer, Julie Wainwright, Lorna Warnock, Euan Baxter and Jack Ford) for assistance and topical discussion and to Zahid Shah, Shafiq Ahmed and Cian Lynch for discussions, both scientific and sport-related!

Thank you to my potentially long-suffering housemates, Ben Thompson, Nick Bradley and Paul McKeegan for the help along the way. Without you, and a supporting cast of other friends, it would have been a lonely journey.

I am hugely indebted to my family, who have shown me that hard work will bear the fruit it deserves, something this process has proven to me! To my Mum and Dad, Brother Dave and grandparents, thank you for your support whenever required and the ability to put things into perspective.

Finally, a huge thank you to Fiona Warrander for her patience, often pre-emptive advice and unending inspiration. This *Thesis* is dedicated to you and everyone else who has believed in and invested their time in me.

Declaration

I declare that this *Thesis* represents my own unaided work, except where acknowledge otherwise in the text. This work has not been submitted previously, in whole or in part, at the University of York or any other institution.

John Knight

December 2011

1 Introduction

1.1 *The functions of SIRT1*

SIRT1 is a member of the sirtuin family of histone deacetylase enzymes. The founding member of the family was the *Saccharomyces cerevisiae* Sir2 protein, named Silent Information Regulator 2 for its ability to silence repetitive DNA sequences (Rine and Herskowitz 1987). The discovery that Sir2 could silence telomeres and rDNA (Gottschling et al. 1990; Bryk et al. 1997; Smith and Boeke 1997) coincided with the emergence of histone post-translational modification as a means to regulate chromatin, in particular by acetylation (Braunstein et al. 1993; Thompson et al. 1994; Braunstein et al. 1996). This lead to the discovery that Sir2 acts as a histone deacetylase (Imai et al. 2000), correlating the regulation of chromatin by Sir2 with the role of reversible acetylation in chromatin biology.

1.1.1 NAD^+-dependent enzymatic activity

Sir2 has homologues in bacteria, archaea and eukaryotes, which collectively are referred to as the sirtuins (Frye 2000). After the identification of Sir2 as a deacetylase enzyme, Sir2 homologues were analysed and found to be conserved deacetylases acting via a novel mechanism (Landry et al. 2000; Smith et al. 2000). Unexpectedly, the analyses of sirtuin enzymatic activity uncovered a strict requirement for the redox metabolite NAD^+ (Imai et al. 2000; Landry et al. 2000; Smith et al. 2000). NAD^+ is required for catalytic removal of acetyl groups from substrate lysine residues, creating nicotinamide and a novel metabolite O-acetyl-ADP-ribose (Tanner et al. 2000). The majority of sirtuins are deacetylases, although some do not appear to have enzymatic activity or catalyse alternative reactions, such as removal of larger post-translational modifications (Du et al. 2011) or ribosyl-transferase activity (Bell et al. 2002).

The closest mammalian homologue to Sir2 is the SIRT1 protein (Frye 2000), which has NAD^+-dependent deacetylase activity. As well as regulating chromatin via deacetylation of histones, SIRT1 was the first sirtuin found to deacetylate a non-histone protein – namely the p53 tumour suppressor (Luo et al. 2001; Vaziri et al.

2001). This expanded the repertoire of the sirtuins, which have since been identified as wide ranging protein deacetylases.

The sirtuins act as sensors of cellular metabolism via their NAD^+-dependence, and can modulate substrate function via reversible deacetylation. For example, SIRT1 modulates ribosomal RNA transcription via epigenetic silencing of rDNA loci (Murayama et al. 2008). This enables SIRT1 to react to low nutrient availability, which manifests as an increase in NAD^+ abundance (Canto et al. 2009), and promote lysine methylation of chromatin by catalysing the initial deacetylation reaction. Through this mechanism SIRT1 is hypothesised to be integral to a metabolism responsive 'throttle' for cell growth (Grummt and Ladurner 2008). This serves to demonstrate the strict dependence SIRT1 has upon NAD^+, and the precise modulation of SIRT1 possible via NAD^+ abundance.

1.1.2 Longevity

The first ascribed physiological function of the sirtuins was in the determination of organismal lifespan. Deletion of the Sir2 gene in *Saccharomyces cerevisiae* reduced life span, whereas insertion of an extra copy of Sir2 increased lifespan by up to 30% (Kaeberlein et al. 1999). Interestingly, overexpression of the closest homologues of Sir2 in both the nematode worm (*Caenorhabditis elegans*) and fruit fly (*Drosophila melanogaster*) also resulted in an increase in lifespan (Tissenbaum and Guarente 2001; Rogina and Helfand 2004).

SIRT1 was therefore believed to hold the same capacity in mammals, potentially allowing lifespan extension by activation. However, recent analysis of mice overexpressing SIRT1 revealed no lifespan extension compared to mice expressing SIRT1 at normal levels (Herranz et al. 2011). Despite this, intense study has revealed crucial roles for SIRT1 in the aetiology in a number of human diseases, as follows.

1.1.3 Type-2 diabetes

SIRT1 has been implicated in type-2 diabetes via two potential mechanisms; firstly, the regulation of the insulin signalling pathway; and secondly, regulation of

the metabolic pathways involved in management of carbon bound energy. SIRT1 protects against insulin resistance associated with type-2 diabetes in mice by ensuring correct function of the insulin signalling cascade in the liver (Wang et al. 2011b). In type-2 diabetes insulin production is normal but the effect insulin has upon the liver, and other organs, is lost. Thus, by ensuring the insulin signal is correctly received in the liver SIRT1 may suppress the onset of type-2 diabetes.

SIRT1 also directly deacetylates the metabolic regulator PGC-1α, modulating glycolysis, anaerobic respiration and gluconeogenesis in metabolic tissue (Nemoto et al. 2005; Rodgers et al. 2005). Through PGC-1α, SIRT1 appears to integrate nutrient availability (via NAD^+, see above) with the transcriptional control of enzymes involved in carbon uptake, usage and storage. Thus, SIRT1 may also ensure the correct processing of carbon, which may be aberrant in type-2 diabetes. The most compelling evidence that SIRT1 protects against type-2 diabetes comes with the observation that upregulation of SIRT1 reduces the incidence of type-2 diabetes in mice (Banks et al. 2008; Yoshino et al. 2011). Thus, SIRT1 contributes to resistance to pathology in type-2 diabetes, likely via modulating the response to insulin and subsequent management of carbon bound energy.

1.1.4 Neurodegenerative disorders

Similar to the protective role of SIRT1 in the pathology of type-2 diabetes, SIRT1 function has also been implicated in protecting against neurodegenerative disorders such as Parkinson's and Alzheimer's disease. The accumulation of β-amyloid and hyper-phosphorylated tau in these diseases is suppressed by the activity of SIRT1 (Donmez et al. 2010; Min et al. 2010). SIRT1 is able to genetically upregulate the enzyme ADAM10 and the Notch signalling pathway, which suppresses β-amyloid production (Donmez et al. 2010) and directly deacetylates the tau protein, suppressing its aggregation (Min et al. 2010). Crucially, in both of these studies suppression of SIRT1 correlated with increased disease severity in mouse models. This indicates the opportunity to activate SIRT1 as a potential method to treat these common neurodegenerative disorders.

1.1.5 Ischemia

SIRT1 is expressed in endothelial cells and is important in the response to localised reduced oxygen availability, termed ischemia (Potente et al. 2007; Hsu et al. 2010; Nadtochiy et al. 2011). In endothelial cells SIRT1 activity promotes resistance to ischemia and regenerative neovascularisation following an ischemic event. SIRT1 activity may therefore be protective against damage from stroke following brain ischemia, and could protect against cardiac ischemia associated with myocardial infarction.

As well as type 2 diabetes, neurodegeneration and ischemia, SIRT1 has been linked to further disease states such as aberrant inflammation and in the regulation of kidney function (reviewed by Donmez and Guarente 2010; Hao and Haase 2010). Together this highlights the diverse range of diseases in which SIRT1 has been implicated. However, chief among these diseases is cancer. This is the context in which SIRT1 is analysed in this work.

1.2 *SIRT1 and cancer*

The role of SIRT1 in cancer has been the source of much debate, with apparently conflicting reports as to whether SIRT1 promotes or suppresses tumour growth and formation. Interestingly, the answer appears to be both, with SIRT1 having pleiotropic effects depending on context.

1.2.1 Cancer cell survival

The first indication that SIRT1 has a role in cancer came with the observation that SIRT1 deacetylates the tumour suppressor protein p53 (Luo et al. 2001; Vaziri et al. 2001). The importance of p53 in protecting against cancer formation is demonstrated in its mutation in 50% of cancers, with suppressive misregulation of the protein hypothesised in the remaining 50% (Vogelstein et al. 2000; Olivier et al. 2010; Goh et al. 2011). Thus, constitutive suppression of p53 appears to be essential for cancer formation.

Interestingly for the role of SIRT1, the acetylation status of p53 is linked to its tumour suppressive activity, with acetylation promoting sequence specific DNA binding (Gu and Roeder 1997). More recently acetylation of p53 has been described as 'indispensible' for p53 activation (Tang et al. 2008). In the 'Tang Model' for p53 activation, acetylation of lysine allows activation of p53, while mutant p53 that cannot be acetylated is unable to transactivate p53 target genes involved in tumour suppression (Figure 1.1).

According to the Tang Model the reversible acetylation and deacetylation of p53 will have a determining effect upon p53 activity (Figure 1.1). SIRT1 deacetylates p53, thus promoting its inactivation (Luo et al. 2001; Vaziri et al. 2001). Given the role of p53 as a tumour suppressor and 'guardian of the genome' (Lane 1992), inactivation was hypothesised to promote cancer cell survival. This was found to be the case, with suppression of SIRT1 correlating with cancer cell arrest and apoptosis (programmed cell death), with an associated increase in p53 acetylation (Ford et al. 2005). Furthermore, the increase in p53 acetylation observed following SIRT1 suppression belies a constitutive cycle of acetylation and deacetylation (Figure 1.1). Accordingly, perturbation of SIRT1-mediated deacetylation results in

constitutive acetylation of p53, due to the constitutive activity of the acetyl-transferase enzymes opposing SIRT1 activity (Ford et al. 2005).

The role of SIRT1 as a regulator of tumour suppression was further enhanced by the discovery that it can also deacetylate and suppress the FOXO family of tumour suppressor transcription factors (Brunet et al. 2004; Motta et al. 2004). Thus, SIRT1 is able to promote cancer cell growth by suppressing the pro-apoptotic and anti-proliferative signalling of p53 and the FOXO proteins. Importantly, despite being able to suppress both p53 and the FOXO proteins, SIRT1-mediated cancer cell survival does not require the expression of p53 or FOXO3 in colorectal adenocarcinoma cell lines (Ford et al. 2005). However, SIRT1 mediated suppression of cancer cell apoptosis *does* require the expression of FOXO4.

Thus, Ford et al identified that SIRT1 suppresses cancer cell apoptosis independent of p53 and FOXO3, but dependent upon FOXO4 (2005). This highlights the role of SIRT1 in suppression of FOXO4, or stated differently, FOXO4 is a cancer cell 'executioner' with SIRT1 suppressing the activity of this executioner. It is important to stress that SIRT1 *does* deacetylate and suppress p53, but that this was not essential for cancer cell survival in this study. This is an important mechanistic observation that is drawn upon during the analysis of SIRT1 regulation in this project.

SIRT1 has been termed a cancer cell survival factor, based on its ability to suppress cancer cell arrest and apoptosis (Ford et al. 2005). SIRT1 promotion of cancer cell survival via protein deacetylation appears to be conserved in many types of cancer, most recently studied in gastric cancer (Bou Kheir et al. 2011), hepatocellular carcinomas (Chen et al. 2011a) and pancreatic cancer (Zhao et al. 2011). SIRT1 has also been linked with the epigenetic suppression of tumour suppressor genes in cancer, presumably dependent upon histone deacetylation (Pruitt et al. 2006). Together this indicates that SIRT1 has a range of mechanisms to suppress cancer cell death.

Importantly for potential anti-cancer therapeutic inhibition, SIRT1 is *not* required for non-cancer cell line survival (Ford et al. 2005). Thus, SIRT1 is not only

a cancer cell survival factor but a *specific* cancer cell survival factor. However, the role of SIRT1 in non-cancer cells has recently been questioned. Evidence suggests that despite being redundant for survival, SIRT1 may have an important role in tumour suppression.

1.2.2 Non-cancer cell tumour suppression

The manipulation of the *SIRT1* gene in mice has presented a role in tumour suppression. The first indication that SIRT1 suppresses tumour formation was in transgenic mice genetically predisposed to cancer where the *SIRT1* gene was over-expressed (Firestein et al. 2008). Mice engineered to over-express *SIRT1* specifically in gastro-intestinal villi were crossed with mice expressing low levels of the *APC* gene, which are predisposed to intestinal cancer. In this mouse model, over-expression of *SIRT1* reduced the incidence of colon cancer compared to mice with normal *SIRT1* expression. Thus, the presence of SIRT1 protected against tumour formation.

The mechanism by which SIRT1 suppresses tumour formation was later linked to the maintenance of genomic stability in $SIRT1^{+/-}$ haploinsufficient mice (Wang et al. 2008b). Reduced SIRT1 expression correlated with increased tumourigenesis, which was reduced by chemical activation of SIRT1 activity. The inverse experiment in an alternative mouse model of SIRT1 overexpression resulted in decreased incidence of aging associated cancers (Oberdoerffer et al. 2008). Together the manipulation of the *SIRT1* gene in the mouse provides strong evidence that SIRT1 acts as a tumour suppressor.

Although a role as a tumour suppressor appears to contradict SIRT1 being a cancer cell survival factor, the consensus in the field is that SIRT1 acts as *both* a tumour suppressor and cancer cell survival factor. A key parameter for SIRT1 function appears to be context. Thus, in normal cells SIRT1 protects against the formation of tumours, likely via a mechanism involving genomic stability (Oberdoerffer et al. 2008; Wang et al. 2008b), but following the formation of cancer SIRT1 acts as a survival factor for cancer cells (Ford et al. 2005).

This pleiotropy for SIRT1 function has implications for direct inhibition of the protein as an anti-cancer strategy. Suppressing SIRT1 may induce cancer cell death but could also subvert normal SIRT1 function in tumour suppression in non-cancerous tissue. To address this issue novel methods of modulating SIRT1 activity in cancer are being sought, which may allow specific targeting in cancer, leaving functions in non-cancer cells unaffected. This draws upon the expanding field of SIRT1 regulation (see below).

1.2.3 SIRT1 expression in cancer

SIRT1 expression is commonly increased in cancer, consistent with its role as a cancer cell survival factor (see above). Over-expression of SIRT1 protein has been reported in human cancer cell lines compared to non-cancer cells (Ford et al. 2008; Wang et al. 2011a), as well as in two studies of primary prostate cancer samples compared to samples of non-cancerous origin (Huffman et al. 2007; Zhao et al. 2011). Furthermore, overexpression of SIRT1 protein, but not mRNA, has been reported in hepatocellular carcinomas (Chen et al. 2011a). This suggests that post-translational regulation of SIRT1 expression in cancer is important. Post-translational regulation may also explain the observation that *SIRT1* mRNA was expressed at a *lower* level in a study of human colorectal tumours compared to parallel normal specimens (Ozdag et al. 2006). Importantly, this study did not analyse SIRT1 protein, which may still have been expressed at a higher level and able to act as a cancer cell survival factor.

Thus, regulation of SIRT1 protein appears to be important in cancer, and will potentially influence cancer cell survival via the SIRT1-mediated suppression of cancer cell apoptosis and arrest (Ford et al. 2005). Regulation of SIRT1 protein may also negate the requirement for increased expression from the *SIRT1* gene, which appears to be varied. Two mechanisms of regulation of SIRT1 protein are analysed in this project, via a direct SIRT1 binding partner called AROS, and via the metabolic enzyme LDH-A.

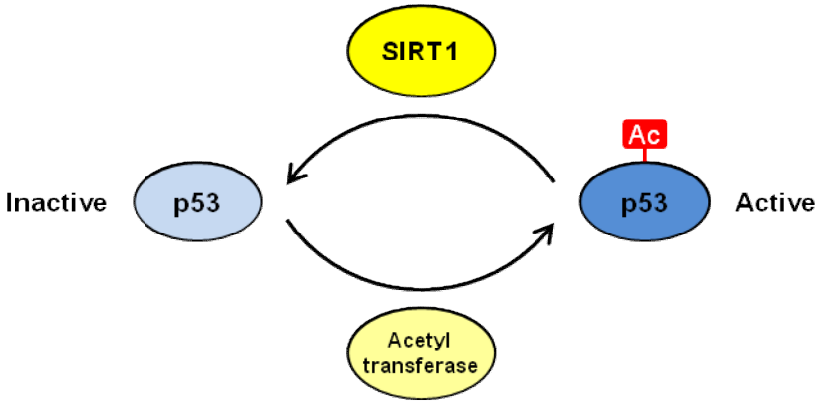

Figure 1.1: SIRT1 and the Tang Model of p53 activation

Deacetylated p53 (left) is inactive, whereas acetylated p53 (right) is active as a transcription factor. The role of SIRT1, other deacetylase enzymes and the acetyl-transferases that catalyse the reversible acetylation of p53 is thus extremely important. SIRT1 deacetylates p53 at lysine 382 promoting inactivation of p53. This contributes to a constitutive cycle of acetylation and deacetylation. Suppression of SIRT1 activates p53 via increased acetylation.

1.3 *Regulation of SIRT1 transcription*

SIRT1 is subject to regulation at the transcriptional, post-transcriptional and post-translational level. The final expression of SIRT1 protein may influence its function, as will SIRT1 subcellular localisation and crucially the availability of the SIRT1 co-enzyme NAD^+. The multiple methods of SIRT1 regulation are outlined below, with a focus on how this may contribute to increased SIRT1 function in cancer cells. In many cases the upregulation of SIRT1 can be cited as further evidence for SIRT1 acting as a cancer cell survival factor due to the cancer association of many of the regulators described herein.

The *SIRT1* gene is located on the 'q' arm of chromosome 10. It is subject to regulation by a number of transcription factors, detailed below. Most of these factors form autoregulatory feedback loops via SIRT1 protein, which are hypothesised to limit SIRT1 expression under normal conditions. However, these autoregulatory loops may be aberrant in cancer to contribute to SIRT1 overexpression. Regulation of *SIRT1* transcription is summarised in Figure 1.2.

1.3.1 Hypoxia inducible factors (HIFs)

The hypoxia inducible factors, HIF1 and HIF2, are transcription factors that both promote *SIRT1* gene expression (Chen et al. 2011b). Both HIF complexes are in turn subject to regulation by SIRT1-mediated deacetylation, which promotes HIF target gene transcription (Dioum et al. 2009; Lim et al. 2010). This creates positive feedback loops for *SIRT1* expression, dependent upon HIF activity. These loops may modulate the metabolic response to hypoxic stress. However, HIF activity is commonly increased in hypoxic tumours, which may induce increased expression of *SIRT1*. This could contribute to the role of SIRT1 as a cancer cell survival factor, which would be responsive to the physical environment of tumours (Knight and Milner 2011).

1.3.2 Cyclic-AMP and Carbohydrate Responsive-Element-Binding proteins (CREB and ChREBP)

SIRT1 mRNA and protein expression can be modulated by nutrient availability. SIRT1 expression is modulated by two transcription factors in response

to the availability of nutrients in the liver, adipose and muscle (Noriega et al. 2011). CREB is activated during low nutrient availability in order to release stored nutrients to meet organism energy demand. Inversely, ChREBP ensures energy is stored when available, also via transcriptional regulation. SIRT1 expression is promoted by CREB and suppressed by ChREBP, providing two additive mechanisms that activate SIRT1 in low nutrient conditions and suppress SIRT1 in high nutrient conditions (Noriega et al. 2011).

As well as expression from the *SIRT1* gene responding to nutrient availability, SIRT1 activity can be modulated more rapidly via alterations in the availability of NAD^+. The kinase AMPK responds to ATP abundance and modulates NAD^+ availability via activation of mitochondria (Canto et al. 2009). Fasting or activation of AMPK increases NAD^+ availability and thus SIRT1 activity in response to nutrient deprivation. This appears to correlate with the genetic modulation of SIRT1 via CREB and ChREBP in response to nutrients (Noriega et al. 2011), with these together presumably allowing SIRT to be modulated both acutely (via AMPK) and then maintained for a greater period of time (via CREB/ChREBP).

Importantly, cancerous tissue is often poorly vascularised, leading to poor nutrient supply to tumours (reviewed by Hanahan and Weinberg 2011). As a result, many cancer cells experience nutrient stress. In light of the evidence above, nutrient deprivation may support SIRT1 expression and function in cancer, although these studies were in non-cancerous cells. Intriguingly, these mechanisms provide a further example of modulation of SIRT1 expression being linked to the tumour environment.

1.3.3 Hypermethylated in cancer (HIC1)

The *HIC1* gene is commonly down-regulated in cancer by hypermethylation of its promoter (Wales et al. 1995). Consistent with SIRT1 overexpression in cancer, the HIC1 protein acts as a transcriptional suppressor at the *SIRT1* gene (Chen et al. 2005). As such, reduced HIC1 expression due to cancer associated hypermethylation may result in increased SIRT1 expression. Interestingly, to suppress the *SIRT1* gene, HIC1 complexes with SIRT1 protein, forming an autoregulatory loop in the process.

This autoregulation would be lost following HIC1 suppression in cancer, potentially allowing SIRT1 expression to increase above normal levels.

1.3.4 c-Myc

c-Myc is an endogenous regulator of cell proliferation but is also a proto-oncogene able to drive the transformation of normal cells into cancerous cells following aberrant upregulation (reviewed by Soucek and Evan 2010). SIRT1 forms a negative autoregulatory feedback loop with c-Myc (Yuan et al. 2009). Within this loop, c-Myc promotes *SIRT1* transcription, and is in turn suppressed by SIRT1 deacetylation. Aberrant increased activity of c-Myc contributes to cancerous growth and it has become a putative therapeutic target (Soucek and Evan 2010). Together, this evidence suggests that upregulation of *SIRT1* may participate in aberrant c-Myc driven cancers.

1.3.5 E2F transcription factor 1 (E2F1)

The transcription factor E2F1 promotes *SIRT1* transcription, in a process suppressed by interaction between the SIRT1 and E2F1 proteins (Wang et al. 2006). Thus, SIRT1 protein suppresses transcription of its own gene via E2F1 in a negative autoregulatory loop. E2F1 is a downstream target of the Rb tumour suppressor and is commonly deregulated in cancer, leading to increased expression (Wu et al. 2009). Similar to the mechanism above for c-Myc, increased E2F1 activity in cancer may lead to increased *SIRT1* expression, associated with cancer cell survival.

1.3.6 p53

p53 promotes *SIRT1* gene transcription (Nemoto et al. 2004), and is in turn suppressed via SIRT1 mediated deacetylation (Luo et al. 2001; Vaziri et al. 2001). This creates a negative feedback loop for *SIRT1* expression controlled by a key tumour suppressor. Wild-type p53 protein expression is lost in 50% of tumours and the protein is believed to be misregulated in many of the remaining cases (Vogelstein et al. 2000; Olivier et al. 2010; Goh et al. 2011). This may reduce SIRT1 expression in cancer, and thus appears to contradict SIRT1 overexpression. However, it is possible that regulation of *SIRT1* by p53 may be secondary to regulation by other

factors, allowing SIRT1 overexpression. Indeed the upregulation of gene expression by other factors is likely to counteract loss of upregulation from p53.

1.3.7 Breast cancer type 1 susceptibility protein (BRCA1)

BRCA1, commonly mutated in breast cancer, directly promotes *SIRT1* transcription (Wang et al. 2008a). No autoregulatory feedback loop has been discussed between SIRT1 and BRCA1, although this does not rule out its existence. Like p53 above, BRCA1 is a tumour suppressor, suggesting that SIRT1 expression would be reduced following its mutation in cancer. However, as with p53, this may be counteracted by regulation of SIRT1 by alternative transcription factors known to modulate *SIRT1* expression.

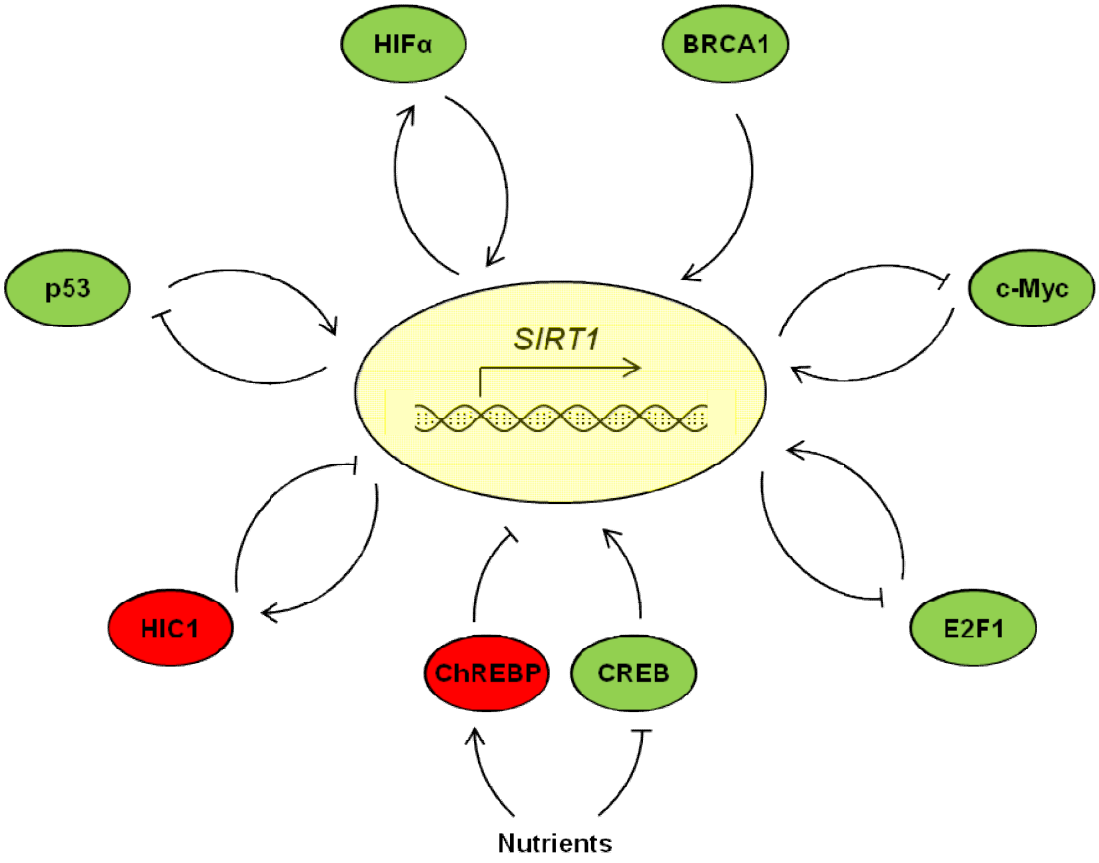

Figure 1.2: Regulation of *SIRT1* gene expression

Modes of regulation of the *SIRT1* gene. Transcription factors in red suppress *SIRT1* transcription, whereas factors in green promote *SIRT1* mRNA production. Factors that have a feedback loop with SIRT1 are identified by the arrows. ChREBP and CREB respond to nutrient availability ('Nutrients') to regulate *SIRT1* expression.

1.4 *Translational regulation of SIRT1*

SIRT1 mRNA is subject to regulation by interaction with small regulatory RNAs and proteins. *SIRT1* mRNA is bound by the RNA binding protein HuR (Abdelmohsen et al. 2007b). HuR stabilises *SIRT1* mRNA via this direct interaction, upregulating protein expression. Interestingly, HuR regulates a number of anti-apoptotic factors, suggesting that *SIRT1* mRNA is stabilised as part of a wider network to promote cell survival (Abdelmohsen et al. 2007a). This may play a role in cancer-associated upregulation of SIRT1, but has not been formally assessed.

microRNAs target *SIRT1* mRNA for degradation, with this loss of SIRT1 protein having negative effects on cancer cell viability and growth. This provides further evidence for the survival promoting function of SIRT1 in cancer. The first microRNA characterised to target *SIRT1* mRNA was miR-34a, which promotes colon cancer cell apoptosis via suppression of *SIRT1* (Yamakuchi et al. 2008). Similarly, microRNAs that target SIRT1 induce breast cancer cell senescence, miR-22, and reduce gastric cancer cell proliferation, miR-449, via direct suppression of *SIRT1* mRNA (Bou Kheir et al. 2011; Xu et al. 2011). Thus, to correlate with SIRT1 overexpression in cancer it appears that the microRNAs targeting *SIRT1* are likely to be suppressed in cancer. Consistent with this, the SIRT1 targeting microRNA miR-200a is expressed at low levels in breast cancer cells, which inversely correlates with SIRT1 expression (Eades et al. 2011).

1.5 *Post-translational modification of SIRT1*

SIRT1 protein is subject to regulation via reversible covalent modification, direct interaction with other proteins and the provision of its essential coenzyme NAD^+. Reversible covalent modification takes the form of phosphorylation and SUMOylation as outlined below, although there is also evidence for SIRT1 methylation, also discussed. There is likely to be interplay between post-translational modification and regulation by direct protein binding to fine tune SIRT1 activity.

SIRT1 is subject to phosphorylation by at least 7 cellular kinases, which modulate SIRT1 activity, stability and localisation. This can promote or suppress SIRT1 activity and may contribute to increased SIRT1 function in cancer cells.

1.5.1 c-Jun N-terminal Kinases (JNKs)

Phosphorylation of SIRT1 by JNK2 at serine 27 (S27) increases SIRT1 protein stability, in a mechanism linked to increased SIRT1 expression in cancer cell lines (Ford et al. 2008). The JNK2 homologue, JNK1 is also able to directly phosphorylate SIRT1 protein at S27, as well as S47 and threonine 530 (T530) (Nasrin et al. 2009). This enhances SIRT1 activity and increases nuclear localisation in human and mouse non-cancer cells. The JNK proteins are responsive to stress and participate in apoptotic signalling (Dhanasekaran and Reddy 2008; Ahmed and Milner 2009). Interplay between JNK and SIRT1 may represent coordination of apoptotic signalling pathways.

1.5.2 Dual-specificity tyrosine phosphorylation regulated kinases (DYRKs)

Two pro-survival kinases from the DYRK family (DYRK1a and DYRK3) directly phosphorylate SIRT1 at T522 (Guo et al. 2010b). In accordance with the pro-survival role of SIRT1, this increases SIRT1 activity and reduces apoptosis. Further, SIRT1 phosphorylation is shown to be required for DYRK promotion of cell survival. Thus, in the form of the JNK and DYRK proteins 4 kinases promote SIRT1 activity and prolong cell survival in the process. However, kinases also suppress SIRT1 activity.

1.5.3 Mammalian Target of Rapamycin (mTOR)

mTOR regulates cellular metabolism, longevity and has been implicated in cancer survival signalling (reviewed by Yecies and Manning 2011). In many ways mTOR and SIRT1 are extremely similar. Interestingly, the two appear to form a regulatory loop via reciprocal repression. The mTOR complex has kinase activity and regulates SIRT1 by phosphorylation of serine 47 (Back et al. 2011). Phosphorylation decreases SIRT1 activity and sensitises cancer cells to enter apoptosis in response to DNA damage. In reciprocal, SIRT1 is able to suppress mTOR via interaction with the TSC2 protein, a component of an inhibitory-complex upstream of mTOR (Ghosh et al. 2010). Thus, SIRT1 and mTOR repress reciprocal activity. This may be linked to their similar roles in regulating metabolism and longevity, requiring each to keep the reciprocal protein in check.

Interestingly, serine 47 phosphorylation was associated with SIRT1 activation by JNK1 in cells of non-cancerous origin (Nasrin et al. 2009), as opposed to SIRT1 suppression by mTOR in cancer cells under stress (Back et al. 2011). This implies that phosphorylation may have specific effects according to cell type and may differ between non-cancer and cancer cells.

1.5.4 Mammalian Sterile 20-like kinase 1 (MST1)

MST1 directly phosphorylates the SIRT1 carboxyl terminal region (Yuan et al. 2011). This phosphorylation inhibits SIRT1 activity, indicated by loss of SIRT1-mediated suppression of p53. Suppression of SIRT1 by MST1 is consistent with a proposed tumour suppressor function for MST1 (Pan 2010).

1.5.5 Casein Kinase II (CK2)

Phosphorylation of SIRT1 by the CK2 protein has also been reported, but with no functional significance (Zschoernig and Mahlknecht 2009). Importantly for the study of SIRT1 phosphorylation, no phosphatase has been identified that counteracts the function of the kinases detailed above. With phosphorylation able to promote or suppress SIRT1 activity it is clear that phosphatases will also be able to modulate SIRT1 function.

1.5.6 SUMOylation

SIRT1 is SUMOylated in the carboxyl terminus of the protein at lysine 734 in a reaction that is opposed by the de-SUMOylation enzyme SENP1 (Yang et al. 2007). SUMOylation increases SIRT1 activity, promoting human cancer cell survival. The enzyme responsible for SUMOylation of SIRT1 has yet to be identified but is likely, together with SENP1, to have an important role in regulating SIRT1 activity.

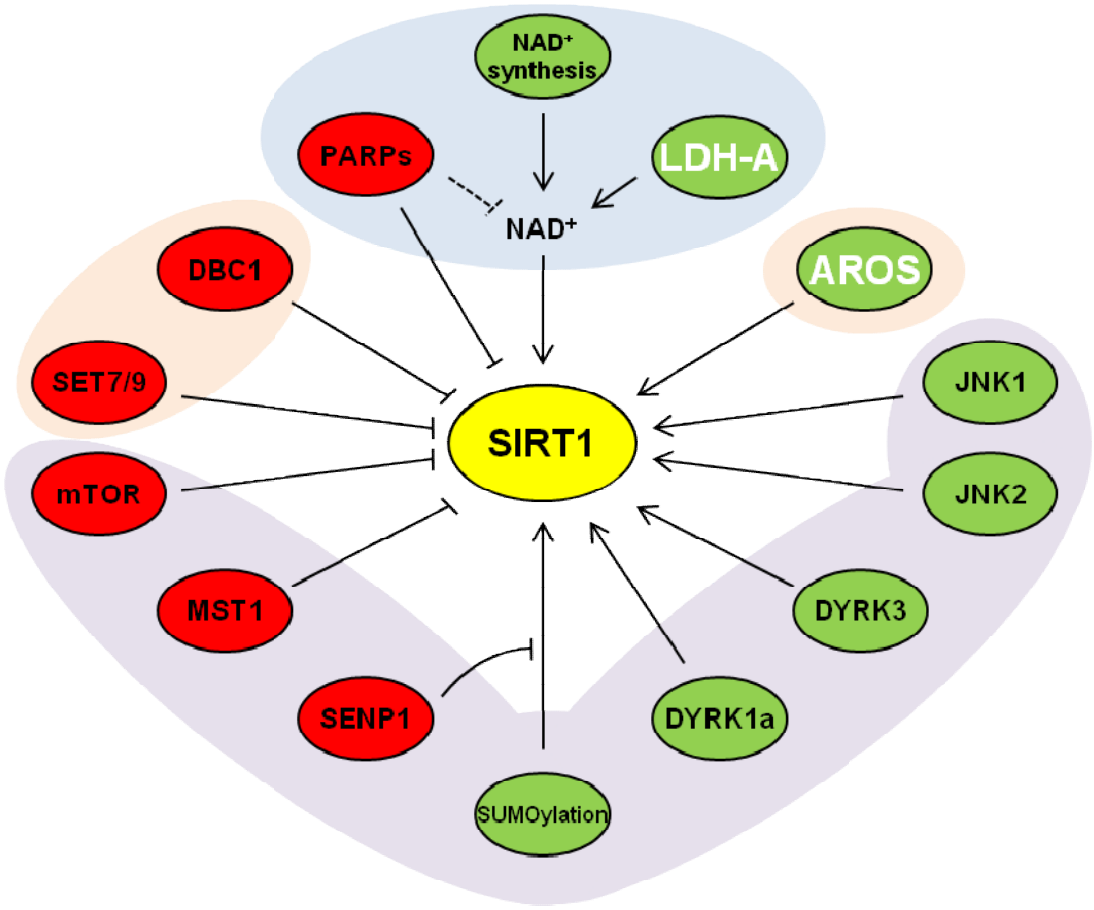

Figure 1.3: Post-translational regulation of SIRT1

SIRT1 protein is subject to both positive (shown in green) and negative regulation (shown in red). This can occur via regulation of NAD^+ availability (enclosed in light blue), direct interaction with other proteins (enclosed in light orange) or post-translational modification (enclosed in light purple). LDH-A and AROS are highlighted in white lettering as the proteins studied within this work. PARP-2 acts via suppression of SIRT1 gene expression, but has been included here together with PARP-1 under the bracket of 'PARPs.'

1.6 *Regulation of SIRT1 by direct interaction*

Modulation by post-translational modification requires direct interaction of the modifying enzyme with SIRT1. However, SIRT1 is also subject to modulation by interaction with proteins independent of reversible modification. Protein association can promote or suppress SIRT1 activity. The first direct modulator of SIRT1 to be identified was a protein termed AROS, for Active Regulator Of SIRT1 (Kim et al. 2007). AROS is a major focus of the analysis in this project and is thus discussed in greater detail below (Section 1.8). Here the regulation of SIRT1 by other direct interactions is outlined.

1.6.1 Deleted in breast cancer 1 (DBC1)

DBC1 directly interacts with SIRT1 and suppresses its deacetylase activity (Kim et al. 2008; Zhao et al. 2008). The interaction with DBC1 is mediated by the SIRT1 catalytic domain (Kim et al. 2008), suggesting that DBC1 binding occludes the association of substrates with SIRT1. At the functional level, suppression of DBC1 results in increased SIRT1 activity towards p53, and subsequent suppression of p53-dependent apoptosis (Zhao et al. 2008). As suggested by the nomenclature of DBC1, it is located in a region of the genome that is commonly lost in breast cancers (Hamaguchi et al. 2002). Loss of an endogenous suppressor of SIRT1 in cancer correlates well with the role of SIRT1 in promoting cancer cell survival detailed above.

1.6.2 Internal peptide sequence

SIRT1 activity is regulated by an intra-molecular interaction between the catalytic core domain and a 25 amino acid sequence in the carboxyl terminus of SIRT1 (Kang et al. 2011). This peptide sequence, termed the ESA region – Essential for SIRT1 Activity region – is highly conserved and may facilitate the interaction of SIRT1 with substrates. SIRT1 activity is inhibited by deletion or mutation of the ESA sequence. Interestingly, the ESA region appears to directly compete with DBC1 for autoregulatory binding to the SIRT1 catalytic core, giving mechanistic insight into how DBC1 suppresses SIRT1 activity. The interaction also presents the possibility to modulate SIRT1 activity with ESA region mimetics.

1.6.3 Set domain containing 7/9 (Set7/9)

Set7/9 is a histone methyltransferase important for facilitating transcription by orchestrating epigenetic modification of histones (Nishioka et al. 2002). Set7/9 has also been implicated in the regulation of p53 localisation and stability, promoting a longer half life for nuclear p53 protein (Chuikov et al. 2004). As well as directly regulating p53, Set7/9 has recently been implicated in the regulation of p53 via modulation of SIRT1 activity (Liu et al. 2011). Set7/9 directly associates with SIRT1 and suppresses the ability of SIRT1 to bind and deacetylate p53. Set7/9 is included under the bracket of regulation by interaction as, despite the observation that SIRT1 can be methylated, Set7/9 appears to suppress SIRT1 activity independent of methyltransferase function (Liu et al. 2011).

The effect Set7/9 has on SIRT1 functions other than suppression of p53 has not been formally assessed. This highlights one of the main areas for expansion in the field of SIRT1 regulation – analysis of the effect of each modulator on a greater number of SIRT1 substrates than the classical target p53. This is one area addressed in relation to the chosen SIRT1 regulators in this project.

1.7 *Regulation of SIRT1 by NAD^+ availability*

SIRT1 enzymatic activity is entirely dependent upon NAD^+ as a co-enzyme for every deacetylation event (Imai et al. 2000; Landry et al. 2000; Smith et al. 2000). Furthermore, SIRT1 activity is modulated by NAD^+ in response to nutrient availability (Canto et al. 2009). The ability to target SIRT1 via modulation of NAD^+ has been postulated ever since the discovery that SIRT1 is dependent upon the redox metabolite, but has only recently been analysed functionally (reviewed by Cantó and Auwerx 2011; Imai 2011). The avenues that have currently been explored are via modulation of NAD^+ synthesis or the NAD^+ consuming PARP enzymes. It is also likely that the other sirtuins compete with SIRT1 for NAD^+, but this has not been addressed experimentally.

1.7.1 NAD^+ synthesis

NAD^+ can be synthesised *de novo* or recycled after use as a co-enzyme via a salvage pathway (reviewed by Yang and Sauve 2006; Ying 2008). SIRT1 produces Nicotinamide (NAM) from NAD^+ during deacetylation, which can inhibit SIRT1 activity at high concentrations. NAM is converted back into NAD^+ via two reactions catalysed by two enzymes. Firstly, the Nicotinamide Mononucleotide Adenylyl Transferase enzyme (NMNAT) converts NAM into Nicotinamide Mononucleotide (NMN) by the addition of phospho-ribose. NMN is then converted into NAD^+ by the ligation of adenine to the phosphate group creating the dinucelotide structure of NAD^+. The second reaction is catalysed by the enzyme Nicotinamide Phosphoribosyltransferase (NAMPT). This salvage pathway has the ability to promote SIRT1 activity by providing further NAD^+ and also by reducing potential inhibition by NAM. NAD^+ synthesis is summarised in Figure 1.4.

Interestingly, NMNAT co-localises to gene promoters with SIRT1, enhancing transcription of genes regulated by SIRT1 (Zhang et al. 2009). Suppression of NMNAT function reduced SIRT1 activity, suggesting that NMNAT is required at gene promoters to process NAM to perpetuate SIRT1 activity. Interestingly, in the same study suppression of NAMPT also affected SIRT1-mediated gene transcription, but this was not localised at promoters. This identifies

NMNAT as a potent local regulator of SIRT1 function, likely via the removal of NAM and perhaps provision of NAD^+ via NAMPT.

Upregulation of NAMPT was observed to be sufficient to increase NAD^+ availability and SIRT1 deacetylation activity in murine fibroblast cells (Revollo et al. 2004). From this, NAMPT activity was proposed as the rate limiting step in the NAD^+ salvage pathway, giving NAMPT a crucial role in controlling SIRT1 function. Despite not having the same effect on NAD^+ or SIRT1 in the same study, the role of NMNAT is undoubtedly essential for NAD^+ synthesis in this pathway. Perhaps consistent with the rate limiting role for NAMPT, overexpression of the enzyme has been reported in prostate cancer cell lines (Wang et al. 2011a). This was linked to cancer cell survival in the same study, as overexpression of NAMPT permitted the SIRT1-dependent survival of prostate cancer cells in response to stress.

Thus, NMNAT and NAMPT appear to be important for the provision of NAD^+ to perpetuate SIRT1 activity, in a mechanism that is potentially upregulated in cancer. Unfortunately, inhibition of NAMPT in an anti-cancer clinical trial resulted in side effects ranging from vomiting and nausea to alterations in the cellular constitution of patient blood (von Heideman et al. 2010). These side effects may be attributable to an essential role of NAMPT in non-cancer cells. Thus, NAMPT does not appear to be a cancer specific survival factor.

1.7.2 Poly-ADP ribose polymerases (PARPs)

The family of PARP proteins are also NAD^+-dependent, catalysing the ligation of ADP-ribose to a range of substrates to modulate their function (Schreiber et al. 2006; Krishnakumar and Kraus 2010). The dominant function of the PARP enzymes appears to be in the orchestration of the DNA damage response following genotoxic stress. Due to the NAD^+ dependence of the PARP proteins they are believed to compete with SIRT1 for NAD^+. The potential to modulate SIRT1 activity via PARP family members was analysed in *PARP-1* and *PARP-2* knockout mice (Bai et al. 2011a; Bai et al. 2011b).

Knockout of *PARP-1* gave an increase in NAD^+ levels, presumably due to reduced NAD^+ expenditure by the PARP-1 enzyme, and a correlative increase in

SIRT1 activity (Bai et al. 2011b). However, the study also noted an increase in SIRT1 expression in the absence of PARP-1, indicative of a negative effect on SIRT1 protein turnover, which may explain the decrease in SIRT1 activity. A parallel study following knockout of the PARP-2 enzyme also increased SIRT1 activity, but this occurred via upregulation of SIRT1 protein and mRNA levels (Bai et al. 2011a). This was achieved by PARP-2 suppressing *SIRT1* gene transcription directly at the *SIRT1* promoter.

In these studies, modulation of both PARP-1 and PARP-2 was hypothesised to alter SIRT1 activity and promote mitochondria biogenesis. The clinical application of this was discussed in relation to type-2 diabetes and obesity. However, inhibition of the PARP proteins may leave cells susceptible to DNA damage, due to the role of the PARPs in orchestrating DNA repair. Thus, modulation of SIRT1 via the PARP proteins may risk genomic instability (Knight and Milner 2011).

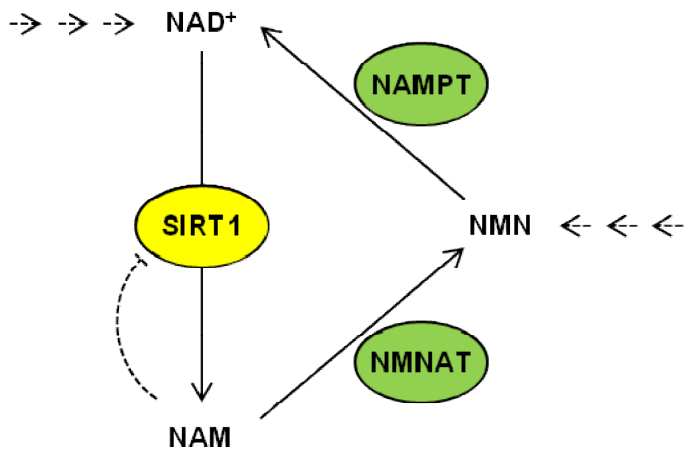

Figure 1.4: The process of NAD^+ synthesis via the salvage pathway

NAD^+ is synthesised from NAM via the salvage pathway. NAM is converted into NMN by the action of NMNAT, then converted into NAD^+ by NAMPT (Yang and Sauve 2006; Ying 2008). The dotted arrows indicate where the NAD^+ *de novo* synthesis pathways enter. NAM inhibits the activity of SIRT1 by competing with NAD^+ for its active site.

1.8 *Regulation of SIRT1 in this work*

The publication dates on many of the citations above, evinces that the regulation of SIRT1 is an emerging field. At the undertaking of the project two potential post-translational positive regulators of SIRT1 activity were identified for analysis, LDH-A and AROS. These act via distinct mechanisms which potentially integrate with cancer cell metabolism and ribosome biogenesis respectively.

1.8.1 Lactate Dehydrogenase A (LDH-A)

LDH-A is an enzyme that, along with its isoenzyme LDH-B, catalyses the interconversion of pyruvate and NADH to lactate and NAD^+ (Baumberger et al. 1933). LDH-A favours the production of NAD^+, which is known to facilitate SIRT1 activity (Figure 1.3). It is for this reason that LDH-A is studied in this work. LDH-A has also been implicated in cancer and the alteration in metabolism associated with transformation (Le et al. 2010). There may be an increased requirement for LDH-A to process cytoplasmic pyruvate and permit the Aerobic Glycolysis cycle in cancer cells. The role of LDH-A in cancer metabolism and how this integrates with SIRT1 activity in cancer cell survival is introduced and analysed in *Chapter 3*.

1.8.2 Active Regulator Of SIRT1 (AROS)

AROS directly binds to SIRT1 in a region towards the amino terminus from the core catalytic domain (Kim et al. 2007). Via this interaction AROS increases SIRT1 activity towards p53 in human cancer cells (Figure 1.3). AROS specifically interacts with SIRT1 over other sirtuins and was linked to cancer cell survival in the same study by Kim and colleagues (2007). AROS is believed to increase SIRT1 activity by inducing an allosteric alteration in the SIRT1 active site, increasing SIRT1 catalytic capacity compared to non-AROS bound SIRT1 (Autiero et al. 2009). AROS is analysed in relation to its role in SIRT1 activation in *Chapter 4* and *Chapter 5*, focusing on the effect upon p53 and FOXO4 as example SIRT1 targets with relevance to cancer. The regulation of SIRT1 by AROS in non-cancer cells is also analysed, which has not been previously reported.

The work undertaken also encompassed analysis of ribosome biogenesis, where a role for AROS is hypothesised and tested. This is based on the observation that AROS interacts the ribosomal protein RPS19, which is known to be required for the synthesis of 40S small ribosomal subunits (Maeda et al. 2006; Choesmel et al. 2007; Flygare et al. 2007; Idol et al. 2007). Analysis of AROS in ribosome biogenesis and how this integrates with cancer cell survival and the *SIRT1* gene forms the work presented in *Chapter 6*, *Chapter 7* and *Chapter 8*. For clarity, the premise of the analysis of ribosome biogenesis is introduced with reference to the current literature during these *Chapters*. Proteins, processes and hypotheses are introduced throughout the progression of the *Thesis* building from chapter to chapter. As such, formal introduction to AROS and the other factors studied are confined to each relevant *Results Chapter*.

1.9 *Aims of project*

The overall aim of this *Thesis* is to identify and characterise novel anti-cancer therapeutic targets that specifically promote cancer cell survival via post-translational modulation of SIRT1. The possibility to target cancer cells via SIRT1 is based on the role of SIRT1 as a cancer specific survival factor and draws from the currently expanding field of SIRT1 regulation. As discussed above, direct targeting of SIRT1 for therapeutic gain may be problematic due to a role of SIRT1 as a tumour suppressor in non-cancer cells. Thus, the ability to target SIRT1 specifically in cancer cells, leaving its activity in non-cancer cells unaffected, would be advantageous. For this reason both cancer and non-cancer cell lines are analysed throughout the *Thesis*.

The chosen targets for the experimental work, LDH-A and AROS, have been implicated in aberrant cancer metabolism and ribosome biogenesis respectively. This is explained in detail as each protein is introduced in respective *Results Chapters*. As such, a second broad aim of the *Thesis* is to uncover potential links between the cancer cell survival function of SIRT1, the role of LDH-A in cancer metabolism and the putative function of AROS in ribosome biogenesis (Figure 1.5).

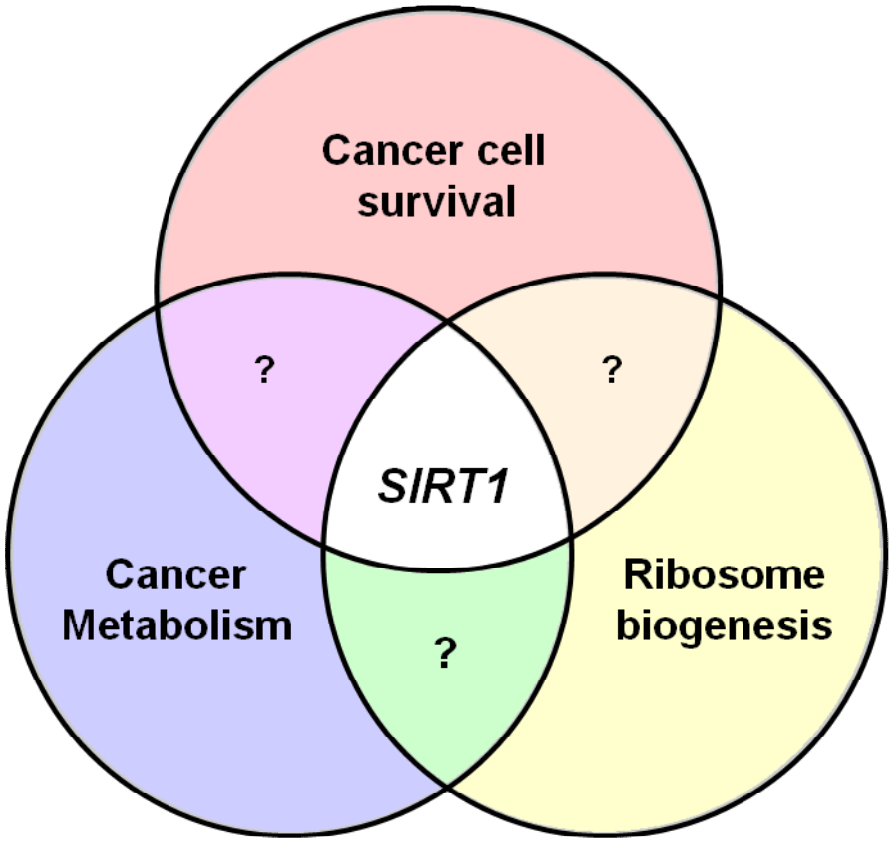

Figure 1.5: SIRT1, cancer metabolism and ribosome biogenesis

A Venn diagram depicting the putative link between the *SIRT1* gene and regulation of cancer cell survival, cancer metabolism and the biogenesis of ribosomes.

2 Materials and Methods

2.1 *Human cell culture*

2.1.1 General cell culture methods

All cell lines were grown at 37°C and 5% CO_2 in sterile uncoated plastic-ware (Corning). Prior to use all media and supplements were warmed to 37°C. All handling of cell lines was contained within laminar flow tissue culture hoods to maintain sterility. Aseptic technique was maintained throughout using ethanol and Barrycidal 36 (Interchem Hygiene). All cells were routinely cultured in the absence of antibiotics within growth medium.

2.1.2 Subcultivation of cells

Cell lines were maintained in appropriate media, as indicated in Table 2.1 and Table 2.2. Cell passage was by trypsinisation. Growth media was aspirated and cells washed briefly with 1x phosphate buffered saline (PBS) (Roche). Typically 3-5mLs trypsin-EDTA (Gibco) per T75 flask was added and cells returned to 37°C and 5% CO_2 and monitored to ensure optimum trypsinisation time. Trypsin was quenched with excess serum proteins in complete media, which was subsequently aspirated from cells following centrifugation at 150g for 3 minutes. For passage of MCF10A cells, trypsin was quenched using an equal volume of trypsin inhibitor (Cascade Biologics), due to lack of serum proteins in the MCF10A growth media. Cells were resuspended into a single cell suspension and cultivated into fresh growth media and flasks. The frequency and ratio of each split was cell line specific (See Table 2.1 and Table 2.2). Flasks were briefly agitated in a diagonal fashion to ensure even coverage of cells across the growth surface. Cells were not subcultivated for more than 8 passages or 4 weeks.

Name (ATCC)	***Origin, cell type and mutations***	***Media formulation***	***Subcultivation regime***
HCT116† (**CCL-247)**	Adult male patient Epithelial colorectal carcinoma Mutated *RAS* proto-oncogene	DMEM (Gibco) plus 10% foetal calf serum (FCS) (Autogen Bioclear) and 2mM L-glutamine (Gibco)	Passage at 1:15 to 1:25 every 3 or 4 days
HCT116 $p53^{-/-}$ †	Isogenic clone of HCT116 Directed knockout of both p53 alleles	DMEM plus 10% FCS and 2mM L-glutamine	Passage at 1:10 to 1:20 every 3 or 4 days
MCF7 (**HTB-22)**	69 year old Caucasian female Epithelial mammary gland adenocarcinoma	MEM (Gibco) plus 10% FCS, 2mM L-glutamine, 1mM sodium pyruvate and 0.1mM Non-essential amino acids (all Gibco).	Passage at 1:5 to 1:15 every 3 to 4 days
DLD1 **(CCL-221)**	Adult male patient Epithelial colorectal adenocarcinoma. Mutant p53 S241F	RMPI 1640 (ATCC) plus 10% FCS , 2mM L-Glutamine and 1mM sodium pyruvate	Passage at 1:5 to 1:15 every 3 to 4 days
LoVo **(CCL-229)**	56 year old male Epithelial colorectal adenocarcinoma	DMEM plus 10% FCS and 2mM L-glutamine	Passage at 1:2 to 1:4 every 3 to 4 days

Table 2.1: Information on cell lines of cancerous origin

† - A kind gift from Professor Bert Vogelstein, John Hopkins University.

Name	***Origin, cell type and mutations***	***Media formulation***	***Subcultivation regime***
ARPE19 **(CRL-2302)**	19 year old male head trauma fatality Retinal pigmented epithelium	DMEM:F12 (Gibco) plus 10% FCS (Autogen Bioclear), 2mM L-Glutamine (Gibco)	Passage at 1:3 to 1:5 every 3 to 4 days
WI38 **(CCL-75)**	3 month gestation Caucasian female foetus Lung fibroblast	MEM (Gibco) plus 10% FCS, 2mM L-glutamine, 1mM sodium pyruvate, 0.1mM NEAA (all Gibco).	Passage at 1:3 to 1:5 every 3 to 4 days
MCF10A	36 year old Caucasian female with fibrocystic disease Mammary gland epithelium	MEBM plus recombinant hEGF, insulin, bovine pituitary extract, hydrocortisone (as instructed by supplier – Lonza) plus 100ng/mL cholera toxin (Sigma)	Passage at 1:5 to 1:15 every 3 to 4 days

Table 2.2: Information on cell lines of non-cancerous origin

2.1.3 Freezing of cells for storage

Cells were routinely frozen at lower than passage 3 for future revival to ensure the use of low passage cells throughout the *Thesis*. Cells were trpysinised as outlined previously (Section 2.1.2), then resuspended out of trypsin in freeze media comprising 30% normal growth media (See Table 2.1 and Table 2.2), 60% foetal calf serum (Autogen Bioclear) and 10% DMSO (Sigma). Cells were frozen at 70% confluency while still in the log growth phase. 1mL aliquots were frozen at -80°C in cryovials (Nunc), prior to transfer to liquid nitrogen for long term storage. Cells were revived out of liquid nitrogen by thawing in a water bath at 37°C and cultivated into fresh pre-warmed growth media in sterile flasks.

2.1.4 Seeding of cells into six well plates

Cells were trypsinised as outlined previously (Section 2.1.2) and resuspended to a single cell suspension in an appropriate volume of growth media. From this volume 10µL was applied to a haematocytometer (Neubauer) for cell counting. Two independent readings were taken and the total cell number calculated. This was used to ensure seeding at the desired density for each cell line as outlined in Table 2.3. Uncoated plastic six well plates (Corning) were briefly agitated in a diagonal fashion to ensure even coverage of cells across the growth surface.

Cell line	***Cells per mL***
HCT116	7.0×10^4
HCT116 $p53^{-/-}$	7.0×10^4
MCF7	5.0×10^4
DLD-1	6.0×10^4
LoVo	6.5×10^4
ARPE19	3.0×10^4
WI38	4.0×10^4
MCF10A	7.0×10^4

Table 2.3: Seeding densities for siRNA transfection by cell line

2.1.5 Transient transfection of cells with siRNA

Transfection of cells with synthetic siRNA was carried 24 hours after seeding of cells at the densities shown in Table 2.3. Cells were monitored to ensure successful even plating across the growth surface. The desired density for transfection varied between cell lines, but was in the region of 50%. Once this was assured, siRNA (Dharmacon) was transfected in liposomal vesicles (Oligofectamine – Invitrogen) at a standard concentration of 200nM per well. For further information on siRNA design see Section 2.2.1 and Table 2.5.

Low serum media Opti-MEM (Gibco) was used during liposome and siRNA complex formation as high serum content can disrupt complex formation and lead to low transfection efficiency. Liposomal vesicles were produced according to the suppliers guidelines (Invitrogen), diluted with Opti-MEM. siRNA for transfection was diluted in Opti-MEM to the desired concentration and combined with the oligofectamine dilution for 30 minutes. Cells in 6 well plates were washed in Opti-MEM then supplied with 800µL of Opti-MEM media per well. Cells were handled quickly and direct pipetting onto the cells was avoided to reduce mechanical dislodging. 200µL of the combined siRNA and Oligofectamine was evenly added drop-wise followed by mixing of the contents by gentle agitation.

Four hours after transfection, cells were supplemented with 0.5mLs feed media containing 3x the supplements of the appropriate normal media. MCF10A cells were fed with an equal volume (1mL) normal growth media due to the restrictions of the media supplements provided by the supplier.

Cotransfection of siRNA to selectively silence multiple targets followed the same protocol as above, with the total siRNA used not exceeding the 200nM limit. For example, to silence two targets individual siRNAs were used at 100nM to give a total siRNA concentration of 200nM.

2.1.6 Validation of basal RNAi

The Milner laboratory has previously shown that RNAi is achievable without inducing the cell stress response pathway (Ford et al. 2005; Ahmed and Milner

2009). For verification here, HCT116 colorectal adenocarcinoma cells were plated and then transfected following the standard Mock treatment used throughout the *Thesis*. This involves transfection with active liposomal vesicles in the absence of siRNA. As detailed above, Mock transfected cells were fed at 4 hours post-transfection.

Two further treatments were analysed in parallel: cells treated with a media change at the point of cell feeding, and entirely untreated cells. Untreated cells were plated in parallel to the other treatments but not treated any further from this point. Prior to harvesting, cell phenotypes appeared similar between the conditions (Figure 2.1A). The cells were mostly adherent with a comparable density and appearance to cells in routine cell culture.

Protein samples from each condition were analysed. Induction of a cell stress response would manifest as an increase in total p53 levels. This did not occur, as p53 expression was comparable between all three conditions (Figure 2.1B). The levels of SIRT1, AROS and RPS19 were also not greatly altered by the manipulation of the cells. The Mock treatment shown here is the same as that used in RNAi transfection throughout the *Thesis.* The treatment does not alter cell phenotype or expression of the proteins of interest compared to untreated cells, making Mock treatment a valid comparison for functional RNAi.

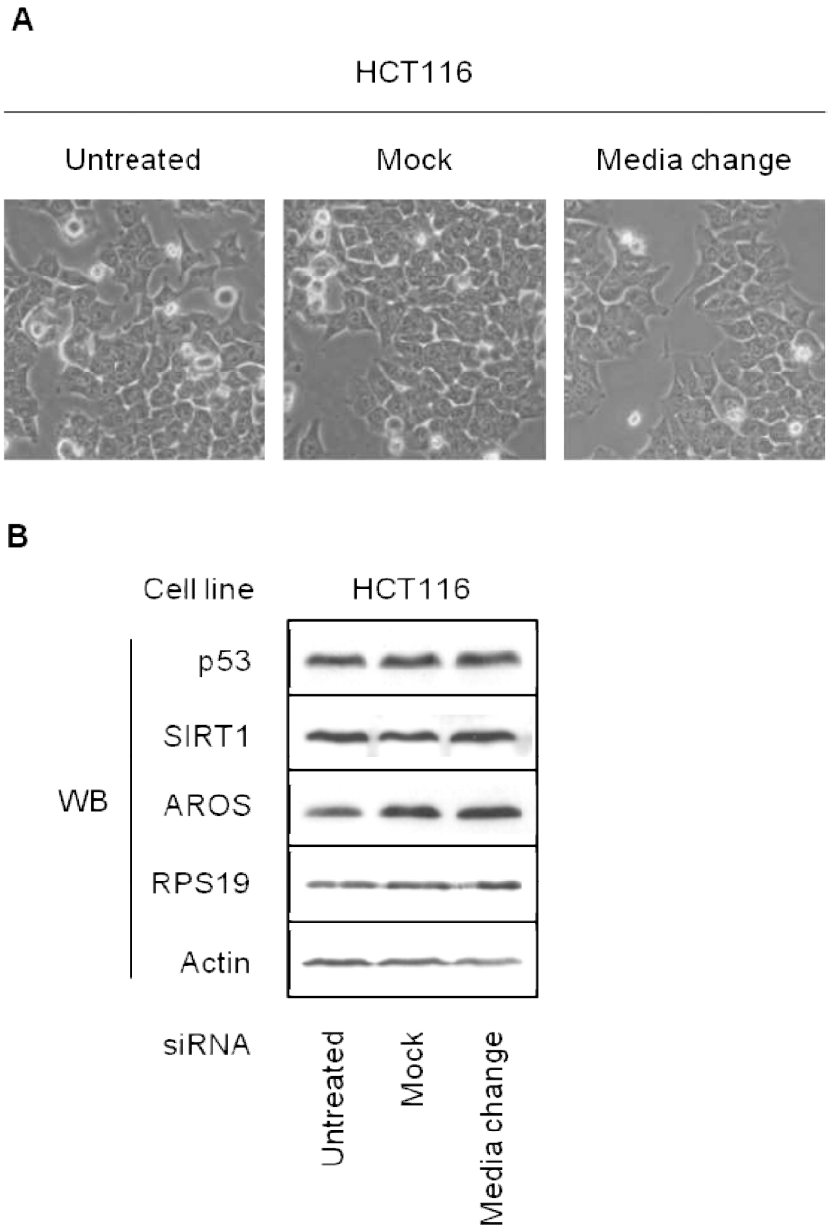

Figure 2.1: Validation of RNAi controls under basal conditions

(A) Phase contrast micrographs of HCT116 cells treated as indicated. Untreated cells were undisturbed between plating for transfection and harvesting. Mock cells were treated with Opti-MEM and Oligofectamine as for all Mock transfections herein. Media change cells were treated with new media on transfection day, in parallel to Mock treatment. Cells were harvested 48 hours after Mock treatment. **(B)** Protein samples from cells shown in (A) were analysed by SDS-PAGE and Western blotting for the abundance of proteins indicated. Equivalent protein was loaded by mass.

2.1.7 Transient transfection of cells with DNA plasmids

Transfection of cells with cDNA encoding proteins for exogenous expression under control of a constitutive human promoter followed a similar protocol to siRNA transfection. Cells were seeded 24 hours before transfection in six well plates at twice the density of siRNA transfection detailed above. This allowed transfection at a higher density (~70%) 24 hours later and the harvesting of cells a further 24 hours later for subsequent analysis.

Transfection was in liposomal vesicles (Lipofectamine – Invitrogen) diluted in low serum Opti-MEM according to the suppliers guidelines. Low serum Opti-MEM was used to ensure unhindered liposomal complex formation. Liposomes formed after 30 minute incubation. cDNA was diluted in Opti-MEM then combined with the liposomal formulation and incubated for a further 30 minutes. The administered concentration of DNA did not exceed 1µg per well to avoid potential cytotoxicity. For cotransfection of multiple plasmids, DNA was pooled and mixed, ensuring the total concentration did not exceed 1µg per well. Details of the cDNAs used are shown in Table 2.4.

Cells were transfected as for siRNA transfection in Section 2.1.5; in 800µL low serum Opti-MEM, plus 200µL cDNA/liposome, pipetted drop-wise evenly across each well and the plates agitated gently to ensure even distribution of liposomes. Over-expression of protein occurred under control of the constitutive cytomegalovirus promoter for all cDNAs detailed in Table 2.4. Over-expression was seen within 24 hours of transfection in human cells.

Open reading frame	***Plasmid vector***	***Bacterial selection***	***Typical use in HCT116***	***Source or reference***
Flag-AROS	pcDNA3	Ampicillin at 100µg/mL	400ng per well	(Kim et al. 2007)
Myc-Flag-RPS19	pCMV6	Kanamycin at 25µg/mL	400ng per well	Origene TrueORF
Myc-His-SIRT1-FL	pcDNA3.1	Ampicillin at 100µg/mL	500ng per well	(Lynch et al. 2010)
Myc-His-SIRT1-Δ8	pcDNA3.1	Ampicillin at 100µg/mL	500ng per well	(Lynch et al. 2010)

Table 2.4: Details of cDNAs used during the project

The Flag-AROS pcDNA3 vector was a kind gift from Eun-Joo Kim and Soo-Jong Um, Sejong University, South Korea. The Myc-Flag-RPS19 pCMV6 construct was purchased from Origene TrueORF. The Myc-His-SIRT1-FL and Myc-His-SIRT1-Δ8 pcDNA3.1 vectors were produced in the YCR p53 Research Unit by Dr Zahid Shah. Expression of all ORFs is under the control of the constitutive cytomegalovirus (CMV) promoter. Kanamycin and Ampicillin were purchased from Sigma.

2.1.8 Application of ultraviolet irradiation

Prior to treatment media was aspirated from cells to ensure radiation was not absorbed. Cells were washed in PBS to remove remaining media. Cells were positioned perpendicular to the ultraviolet source within growth plates and exposed to radiation as indicated at a fluency of $2J/m^2/s$. Growth plate lids were removed during irradiation. Cells were then grown in normal growth media prior to harvesting at the stated time post UV exposure.

2.1.9 Application of soluble drug treatments

Media was aspirated from cells. Cells were then washed in pre-warmed PBS. Soluble drugs were applied to cells at the indicated concentrations premixed within normal growth media. Cells were returned to 37°C for the stated duration prior to harvesting.

2.1.10 Harvesting of cells

Directly prior to harvesting cell phenotypes were recorded by phase contrast light microscopy using an Olympus CKX41 compact inverted microscope at 200x zoom. A representative area was chosen for each condition and recorded using an Olympus C-7070 digital camera. Micrographs were adjusted for optimum contrast in greyscale and cropped using Corel PhotoPaint X3.

Cells were harvested by trypsinisation. Harvesting of cells from flasks followed the same protocol as for subcultivation (2.1.2). Prior to trypsinisation cells were washed in PBS to remove all growth media (unless stated in specific protocols).Growth media and PBS from pre-trypsin washes was retained in harvested material. Harvesting from six well plates used 0.5 – 1.0mLs trypsin per well, incubated at 37°C and 5% CO_2 until cells became detached, followed by quenching and pooling of cells from multiple wells where appropriate. Media was removed by centrifugation and cells were washed twice with ice cold PBS, allowing final resuspension in desired medium.

2.2 *Preparation of material for transfection*

2.2.1 Custom siRNA design and preparation

The design of custom siRNAs allowed specificity to produce target specific mRNA knock down. In all cases knockdown was verified at both the mRNA and protein level (See Sections 2.6.4and 2.5.5). However, in some cases issues with antibody availability did not permit protein level analysis. The target sequence for all siRNAs was 19 nucleotides long with two deoxythymidine (dT) bases at the 3' end, making 21 nucleotides overall. The 19 nucleotide sequence is complementary to the mRNA sequence to be silenced. The 'dTdT' addition is important for siRNA stability in mammalian cells.

Sequences of mRNA targets were attained from public databases, such as FASTA and GENBANK. Sequences were viewed using the bioinformatics software Vector NTI (Invitrogen). 19 nucleotide sequences were analysed within this mRNA sequence to meet three criteria: 1) a 'GC%' value of between 40% and 60%; 2) no repeats of the same nucleotide for more than 3 bases; 3) minimal formation of dimeric or hairpin structures. Failure to meet these criteria is predicted to result in siRNAs that remain annealed or form non-duplexed structures. As such, these criteria were should ensure efficacy of the custom siRNA.

Sequences meeting these criteria were then analysed for homology to other human mRNA sequences. This was a crucial step to ensure specific knock down of the desired mRNA. For this the online 'Basic Local Alignment Search Tool' (BLAST) was used (available at the National Centre for Biotechnology Information website). A nucleotide BLAST homology search of human mRNA sequences was carried out and any significant (>60%) homology to other mRNAs was generally considered unacceptable.

Targeting of specific splice variants of genes is possible, but leaves few options for target sequence. Specific variants lacking a single exon were targeted at the relevant exon-exon boundary to ensure specificity. For example, for SIRT1-Δ8, which lacks exon 8, the 7 to 9 exon boundary was targeted by siRNA. During the project siRNA sequences were also used that had been previously published. In these

cases the siRNA sequence was checked using the same criteria as above to ensure that it met the standard required. A list of all the siRNA sequences used is shown in Table 2.5.

Custom siRNAs were ordered from Dharmacon as a desalted and duplexed precipitated solid. These were stored at -80°C as solid until required. siRNA was dissolved in siRNA buffer (Dharmacon – containing 300mM KCl, 30mM HEPES, 1.0mM magnesium chloride at pH 7.5). Solutions were briefly mixed by pipette then placed on an orbital shaker for 30 minutes. To break up aggregates from the drying process, siRNA was heated to 95°C for 2 minutes then slowly cooled to 37°C for 1 hour. Repeated freeze-thaw cycles of siRNAs were avoided. This procedure was implemented to decrease the possibility of non-duplexed siRNA, important to attain knockdown of target mRNA.

Target mRNA	***siRNA sense sequence***
AROS (1)	5'-CCGUGUUC ACCGAGGAAGA-(dTdT)-3'
AROS (2)	5'-GACCACCUCAGAGUAAACC-(dTdT)-3'
FOXO3 †	5'-GCACAGAGUUGGAUGAAGU-(dTdT)-3'
FOXO4 †	5'-AGAAGCCGAUAUGUGGACC-(dTdT)-3'
LDH-A	5'-CCAGCCGUGAUAAUGACCA-(dTdT)-3'
LDH-B	5'-ACUUAAUCCAAUAGCCCAG-(dTdT)-3'
RPS19 †	5'-AGAGCUUGCUCCCUACGAU(dTdT)-3'
SIRT1-FL †	5'-ACUUUGCUGUAACCCUGUA-(dTdT)-3'
SIRT1-Δ8 †	5'-UAAUUCCAAGUAAUCAGUA-(dTdT)-3'
TP53 †	5'-CAGCAUCUUAUCCGAGUGG-(dTdT)-3'

Table 2.5: List of validated siRNA sequences used

(†) denotes previously published as indicated: *RPS19 (1)* - (Choesmel et al. 2007), *SIRT1-FL*, *FOXO4*, *FOXO3* - (Ford et al. 2005), *SIRT1-Δ8, TP53* - (Lynch et al. 2010)

2.2.2 Amplification of expression plasmids in bacterial cells

All work with bacteria was carried out on an ethanol sterilised lab bench under a blue Bunsen flame. XL10 Gold ultra-competent *Escherichia Coli* cells (Stratagene) were cultured in liquid broth and on agar plates. Liquid broth was made by the litre, consisting of 10g sodium chloride, 10g tryptone and 5g yeast extract at pH 7.0, sterilised by autoclave. Agar plates (Sterilin) were cast with 1.6% weight-by-volume agar dissolved in liquid broth. To ensure antibiotic activity, antibiotics were added below 55°C at a concentration of 25µg/mL (Kanamycin) and 100µg/mL (Ampicillin).

cDNA plasmids were amplified by transformation into XL10 Gold bacterial cells. Once transformed cDNA plasmids were subject to replication from SV40 origins of replication. Transformation was by heat shock of *E. Coli* incubated with cDNA for 30 seconds at 42°C. Bacteria were then cultured at 37°C on an orbital shaker at 200rpm. This was in the absence of selection antibiotics to allow initial expression of the resistance gene. After 1 hour, 200µL of the cultured cells were spread onto agar plates containing selection antibiotic. Plates were incubated at 37°C overnight. Antibiotics used for each expression plasmid are shown in Table 2.4.

Individual colonies were picked using a pipette tip and transferred to liquid broth containing selection antibiotic. Cells were grown at 37°C on an orbital shaker at 200rpm for 8 hours, or until broth had become cloudy. Cells were then transferred into a larger volume of liquid broth (25mL) containing antibiotic for overnight (minimum 16 hours) incubation.

Following incubation, bacterial cells were pelleted from liquid broth by centrifugation at 14,000g for 15 minutes at 4°C. Purification of plasmid DNA followed the QIAGEN plasmid purification protocol according to the manufacturer's protocol. Final cDNA resuspension was in QIAGEN elution buffer (10mM TrisCl at pH 8.5). Plasmid cDNA was quantified by OD260nm reading (See Section 2.6.2) and purity by analysis of the protein content at OD280nm. cDNA was diluted in RNase / DNase free water (Gibco) to appropriate dilutions for transfection.

2.3 *Analysis of whole cells*

2.3.1 Determination of apoptosis by Annexin-V and propidium iodide staining

This technique worked with live cells, and was thus carried out at room temperature. All media, trypsin and PBS were used at room temperature throughout, as were all centrifugation techniques. Great care was taken throughout to produce a single cell suspension, to ensure cells enter the fluorescence activated cell sorter (FACS) machine individually. Other than these modifications cells were harvested following the protocol in Section 2.1.8.

Final resuspension of cells was in *'Incubation buffer'* provided in Annexin-V-FLUOS Staining Kit (Roche), supplemented with a 1:50 dilution of Annexin-V-Fluorescein and propidium iodide (PI) (as provided in kit). Cells were incubated at room temperature for 10 minutes with periodic agitation to maintain suspension of cells. Cells were then transferred to FACS falcon tubes (Beckton Dickinson) and diluted in *'Incubation buffer'* as appropriate. After a further 5 minute incubation cells were analysed by FACS on a FACSCalibur machine with CellQuest interface (Beckton Dickinson).

Both Annexin-V-Fluorescein and PI were excited at 488nm. Annexin-V-Fluorescein emission was read in the 'FL-1 channel' at 518nm and PI in the 'FL-2 channel' at 617nm, according to suppliers guidelines (Roche). Forward-scatter and side-scatter attributes were routinely analysed to confirm efficacy of single cell suspension techniques. 10,000 events were read for each condition and conditions read as independent duplicates.

For analysis of apoptosis a scatter plot of FL-1 (Annexin-V-Fluorescein) against FL-2 (propidium iodide) was drawn. Early apoptotic cells stain positive for Annexin-V-Fluorescein due to the presence of phosphatidylserine on the outer leaflet of the cell membrane; phosphatidylserine is usually maintained on the inner leaflet only. PI is a DNA intercalator unable to freely cross phospholipid membranes. The membrane integrity maintained by apoptotic cells ensures that they stain negative for PI, allowing differentiation from cells undergoing necrosis which stain positive for both Annexin-V-Fluorescein and PI.

The open access software WinMDI (The Scripps Research Institute) was used for quantification of apoptosis from raw scatter plots. Figure 2.2A shows a representation of the data and the quadrant based gating used. The number of early apoptotic cells was expressed as a percentage of the total cell number. Mock treated cells were then set to a value of 1, and other conditions compared against this – giving a fold change in apoptosis. This data is presented in graph format in the *Results* chapters (SigmaPlot). The error bars shown on these graphs are the standard deviation between replicates, standardised to the fold change. Statistical analysis was carried out using Student's t-test. A value of less than 0.05 was considered to be statistically significant, as indicated. Raw scatter plots are presented in the *Appendices*.

2.3.2 Cell cycle distribution analysis by propidium iodide staining

Cells were harvested following the protocol in Section 2.1.8 and fixed in solution in ice cold ethanol. The final resuspension after trypsinisation was in 1mL of ice cold PBS. To this 4mL of ice cold 90% ethanol (Fisher) was pipetted drop-wise whilst vortexing. The final ethanol percentage for fixation was 72%. Fixed cells were kept on wet ice for 1.5 hours then maintained at 4°C until staining with propidium iodide. Fixed cells were not left for longer than one week before analysis.

For staining, cells were spun out of 72% ethanol at 4°C at 150g for 5 minutes then washed twice in 10mL ice cold PBS. The centrifugations out of PBS were at 600g. Cells were resuspended in 500µL PBS containing 50 U/mL RNase A (QIAGEN) and incubated at 37°C for 15 minutes. An equal volume of 60µg/mL propidium iodide solution was added and thoroughly mixed by pipette. Staining occurred for 30 minutes at room temperature.

The fluorescent properties of the DNA intercalator propidium iodide (excited at 488nm and read at 617nm) were exploited to allow cell cycle phase to be analysed using a FACSCalibur machine with CellQuest interface (Beckton Dickinson). This allowed the separation and quantification of cells according to stage in the cell cycle. Propidium iodide (PI) fluorescence (in the FL-2 channel) was plotted against the number of events to produce a histogram. Strict gating of cells was essential during

FACS due to the tendency for cells to aggregate during the fixation process. Cells were gated from the total population to an experimental population of cells according to forward-scatter and side-scatter. This was to reduce the number of aggregated cells entering the analysis. Aggregated cells were visualised in the FL-2 channel due to the appearance of large numbers of 'cells' containing 8n or more copies of DNA. These were deemed to represent aggregations in the most part, not polyploid cells. Gating was deemed sufficient when the aggregated population was low, after which experimental readings were taken for 10,000 cells in duplicate.

PI intercalates with cellular DNA in a proportional manner, allowing the elucidation of G1, S and G2/M population. A representation of the raw data gained from this analysis is shown in Figure 2.2B. The open access software Cylchred (Cardiff University) was used to analyse the data from CellQuest. G1, S and G2/M phase populations were designated within the overall histogram, defining the S phase population between the G1 and G2/M peaks. The software produced values for the percentage of cells in each population, allowing these values to be plotted as stacked histograms (SigmaPlot).

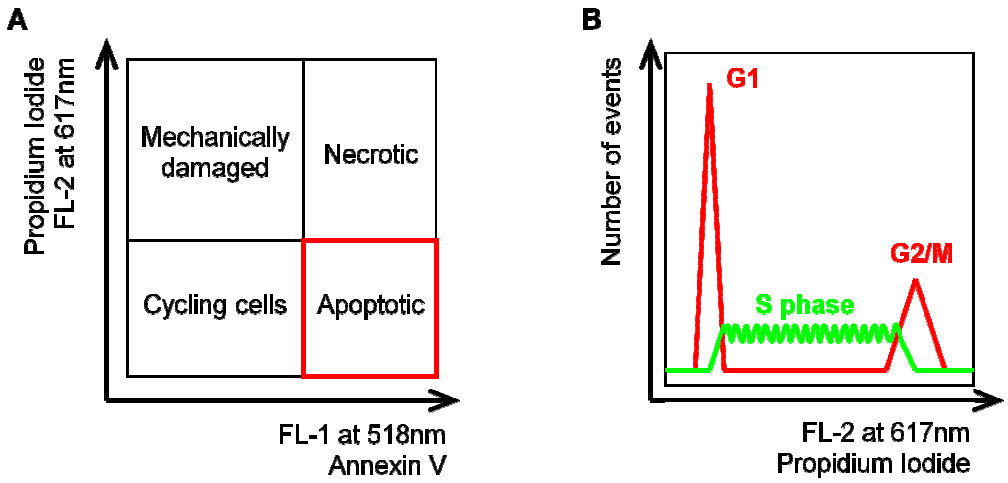

Figure 2.2: Representative data for whole cell analysis techniques

(A) Apoptotic cells were determined as cells staining positive for Annexin-V-Fluorescein but negative for propidium iodide, as depicted in a scatter plot. The lower right quadrant was defined as apoptotic and data gathered in duplicate using WinMDI. **(B)** Cells in G1 stain with the lowest intensity for propidium iodide due to the lower copy number of DNA. After replication of DNA cells in G2/M phase have twice the DNA content of G1 cells and thus stain more intensely for propidium iodide. Cells passing through S phase have a DNA content between that of G1 and G2/M cells, giving a continuum of intensities between the two. The Cylchred software is able to define and distinguish between S phase and the peaks either side, presenting the data as shown here. Values for the percentage of cells in each phase were gathered by this method.

2.4 *Fractionation of cells for subcellular analysis*

2.4.1 Sucrose gradient ultra-centrifugation for analysis of ribosomes

Sucrose density ultra-centrifugation was based on recently published protocols (Choesmel et al. 2007; Guo et al. 2010a). The protocol is summarised diagrammatically in Figure 2.3. Sucrose was dissolved in gradient buffer containing 20mM TrisHCl, 80mM sodium chloride, 5mM magnesium chloride, 2mM DTT and 20U/mL RNase inhibitor (SUPERase – Ambion) at pH 7.4. 50% and 10% sucrose weight-by-volume solutions were made and maintained at 4°C. 24 hours prior to use an equal volume of 10% sucrose solution was layered above 50% sucrose solution in UltraClear 12.5mL open top centrifuge tubes (Beckman). The tube tops were sealed using parafilm and carefully tilted to horizontal and kept at 4°C for 6.5 hours. Tubes were then returned to the vertical and maintained at 4°C overnight until use.

Cells were treated with 100µg/mL cycloheximide for 10 minutes then harvested by trypsinisation. Lysis at 4°C used lysis buffer containing 10mM TRIS-HCl, 5mM magnesium chloride, 10mM potassium chloride, 2mM DTT, 500U/mL RNase inhibitor, 2% Triton X-100 supplemented with protease inhibitor cocktail (Roche) at pH 7.4. Cell membranes were disrupted by gentle pipetting and nuclei pelleted by centrifugation at 8,000g for 5 minutes at 4°C. The cytoplasmic fraction was removed and protein content estimated (Section 2.5.1) to standardise the protein concentration between experimental conditions. Samples were subjected to 160,000g for 2 hours at 4°C under a vacuum using an Ultra Beckman 100XP centrifuge in a SW41Ti swing out rotor (Beckman).

After ultra-centrifugation, samples were kept on ice within centrifuge buckets. Fractions (~400µL each) were removed from the gradient by pipette, starting from the top, and stored at -20°C. Optical density at 260nm (OD260nm) was used to quantify RNA (Section 2.6.2). Readings were taken in duplicate and data aligned using SigmaPlot into spline-curve joined graphs. Samples were also analysed by SDS-PAGE as detailed in Section 2.5.4.

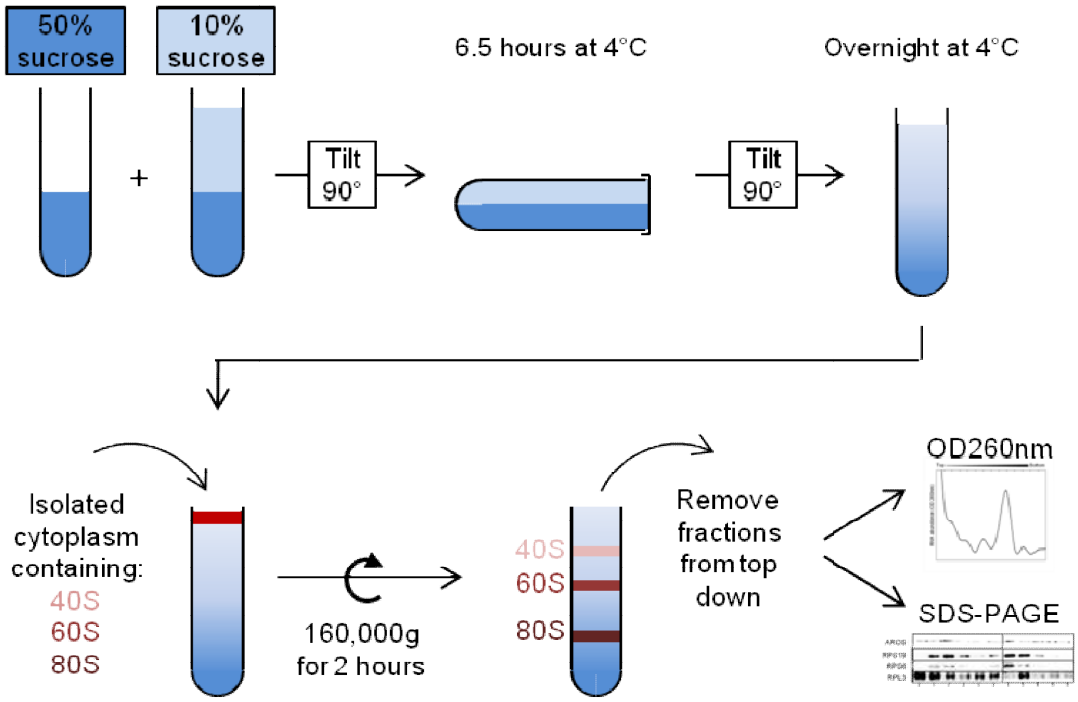

Figure 2.3: Summary of sucrose density ultra-centrifugation protocol

Sucrose gradients were layered 24 hours prior to use. Equal volumes of 50% and 10% sucrose in gradient buffer were layered and allowed to form a gradient during horizontal incubation at 4°C, then incubation in the vertical position overnight at 4°C. Isolated cytoplasm was loaded onto the gradient and ultra-centrifuged at 160,000g for 2 hours. Fractions were then removed and analysed for their separated ribosomal subunits.

2.4.2 Subcellular fractionation for protein analysis

The protocol follows that of the supplier (NE-PER kit – Pierce) for the fractionation of cells into cytoplasmic protein, nuclear soluble protein and nuclear insoluble protein. In brief, cells were harvested and resuspension in ice cold CER I and CER II buffers supplemented with protease inhibitor cocktail (Roche). After incubation to lyse the cell membrane nuclei were pelleted by centrifugation at 14,000g for 5 minutes at 4°C. The supernatant was removed as the cytoplasmic fraction, and the nuclei were lysed in NER I buffer supplemented with protease inhibitor cocktail (Roche). Following a further incubation nuclear insoluble protein was pelleted by centrifugation at 14,000g for 10 minutes at 4°C. The supernatant was removed as the nuclear soluble fraction and the remaining protein treated with lysis buffer containing 140mM sodium chloride, 10mM TrisBase, 2mM calcium chloride, 0.5% v/v NP-40 at pH 8.0, supplemented with protease inhibitor cocktail (Roche) and 5 U/mL micrococcal nuclease (Sigma). After incubation for 5 minutes at room temperature all samples were frozen at -80°C prior to analysis by SDS-PAGE (Section 2.5.4).

This method was modified and extended to allow immunoprecipitation of exogenous Flag-tagged nuclear proteins. The cytoplasmic fraction was removed as detailed here, and then the nuclear pellet was used in place of the total cell lysate for immunoprecipitation as detailed in Section 2.5.2.

2.4.3 Subcellular fractionation for RNA analysis

This protocol was similar to that above for protein analysis, allowing the separation of cells and isolation of cytoplasmic and nuclear RNA. Again, buffers were used as provided by the supplier (Pierce) supplemented with protease inhibitor cocktail and RNase inhibitor (Ambion) to prevent degradation of proteins and RNAs. Cytoplasm was removed as previously then nuclei were lysed in buffer containing 140mM sodium chloride, 10mM TrisBase, 0.5% v/v NP-40 at pH 8.0, supplemented protease inhibitor cocktail, 1,000 U/mL RNase inhibitor and 65 U/mL DNase I with RDD buffer (QIAGEN). All fractions were immediately used for RNA purification, as detailed in Section 2.6.1.

2.5 *Molecular biological analyses of proteins*

2.5.1 Determination of protein concentration

The protocol is based on the bicinchoninic acid (BCA) method as supplied by Pierce. The technique quantifies protein concentration in samples against a standard curve of the spectrophotometric change at 562nm from bovine serum albumin standard solutions of known concentrations. Standards were read in quadruplicate from 96 well plates (Nunc) using a FluoSTAR Omega plate reader (BMG Labtech) and a standard curve was drawn using the attached software. Samples were also read in quadruplicate. Any outlying readings were omitted and the average protein concentration (in mg/mL) was attained for each protein sample. This value allowed the accurate dilution of protein for various techniques.

2.5.2 Immunoprecipitation of exogenous Flag-tagged proteins

Cells were harvested following the protocol in Section 2.1.8. Final resuspension of cells was in *'Lysis buffer'* supplied by Sigma (150mM sodium chloride, 1% v/v Triton X-100, 50mM TrisHCl, 1mM EDTA) supplemented with protease inhibitor cocktail (Roche). Cells were sonicated at 2.5 microns for 10 seconds three times in total, kept on wet ice for 30 seconds between pulses (Soniprep 150 – MSE). Cell debris was pelleted at 10,000g for 5 minutes at 4°C then discarded.

The protein content of the lysate was assayed following protocol 2.5.1. Protein quantity (500 - 1500µg) was matched between conditions and a negative control was included with *'Lysis buffer'* only, termed the 'No lysate' control. Remaining Input protein was stored at -80°C. Lysate was incubated on SigmaPrep spin columns with 60µL Anti-Flag M2-Agarose affinity beads (Sigma) for 2 hours at 4°C on an inversion wheel. Anti-Flag M2-Agarose affinity beads were pre-washed 4 times with *'Wash buffer'* supplied by Sigma (50mM TrisHCl, 150mM sodium chloride at pH 7.4). During incubation, the Anti-Flag M2-Agarose affinity beads bound the exogenously expressed Flag-tagged protein of interest.

After incubation, the *'Immunodepletion'* was removed by centrifugation at 5,000g for 1 minute through the spin column. Bound proteins were then washed four

times in ice cold *'Wash buffer'* supplemented with protease inhibitor cocktail (Roche). Samples were washed on an inversion wheel for 2 minutes at 4°C after each wash and separated by centrifugation at 5,000g for 1 minute. These washing steps reduced the amount of non-specific binding of protein to the agarose beads.

After the final wash, bound protein was eluted by addition of excess Flag-peptide (Sigma) to compete for the Anti-Flag M2-Agarose affinity beads. 15µg Flag-peptide was added to the beads in a low volume of *'Wash buffer'* and mixed on an orbital shaker for 1 hour. *'Elution'* was collected by centrifugation at 5,000g for 2 minutes and termed the 'Flag-IP'. Samples were stored at -80°C. Figure 2.4A summarises the Flag immunoprecipitation protocol in a flow diagram.

Samples were analysed by SDS-PAGE and Western blotting to detect proteins of interest using specific antibodies. 'Input' protein was loaded as a fraction of the original 'Input' loaded into each immunoprecipitation. This fraction represented 1/*Y* amount of immunoprecipitation 'Input'. Thus, upon analysis the 'Flag-IP' samples are equivalent to a *Y*-fold excess of protein compared to respective 'Input' samples. This allows the quantification of the proportion of total protein that is immunoprecipitated in the analysis. The scheme for loading of SDS-PAGEs for analysis of immunoprecipitation samples is shown in Figure 2.4B.

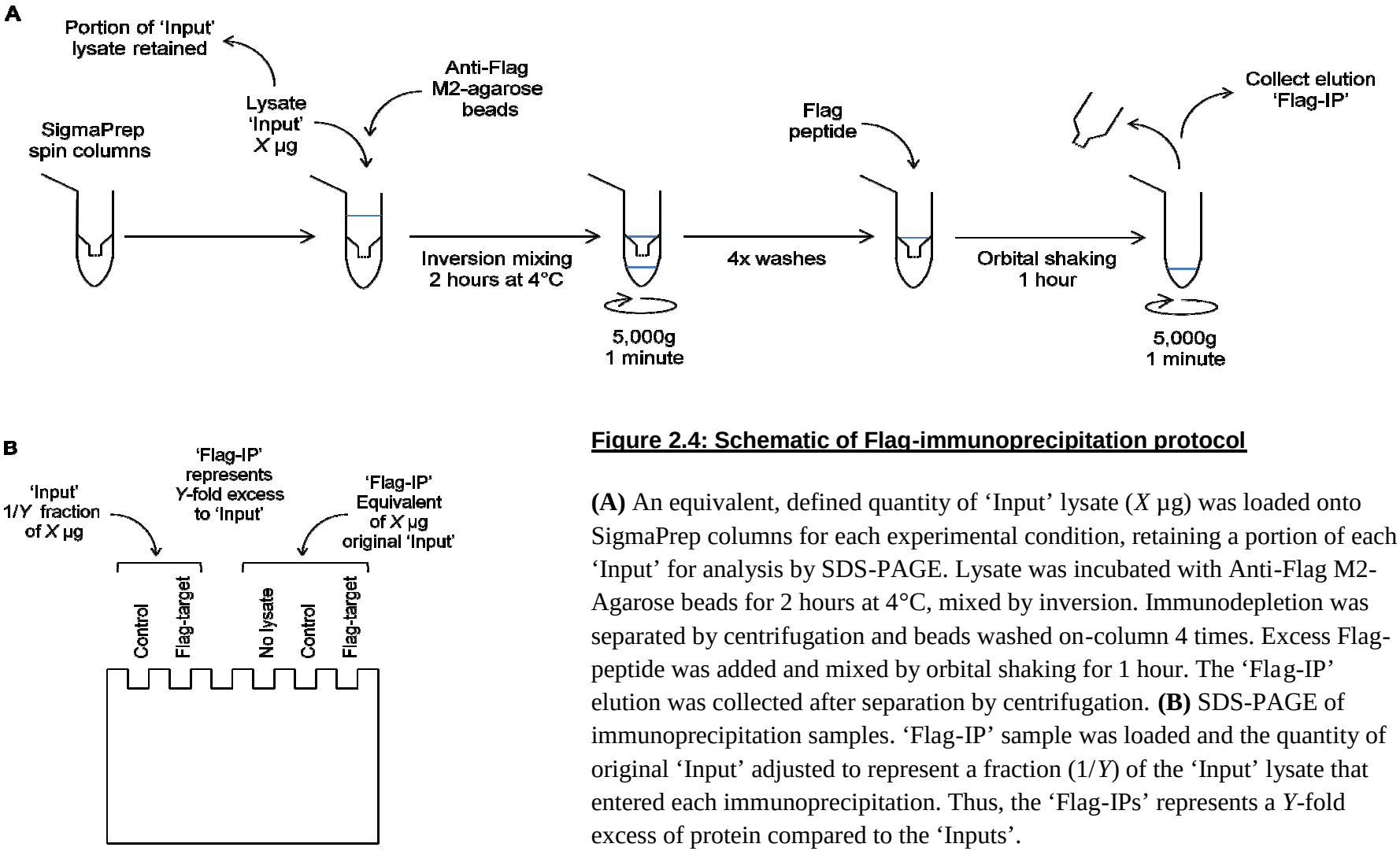

Figure 2.4: Schematic of Flag-immunoprecipitation protocol

(A) An equivalent, defined quantity of 'Input' lysate (*X* µg) was loaded onto SigmaPrep columns for each experimental condition, retaining a portion of each 'Input' for analysis by SDS-PAGE. Lysate was incubated with Anti-Flag M2-Agarose beads for 2 hours at 4°C, mixed by inversion. Immunodepletion was separated by centrifugation and beads washed on-column 4 times. Excess Flag-peptide was added and mixed by orbital shaking for 1 hour. The 'Flag-IP' elution was collected after separation by centrifugation. **(B)** SDS-PAGE of immunoprecipitation samples. 'Flag-IP' sample was loaded and the quantity of original 'Input' adjusted to represent a fraction (1/*Y*) of the 'Input' lysate that entered each immunoprecipitation. Thus, the 'Flag-IPs' represents a *Y*-fold excess of protein compared to the 'Inputs'.

2.5.3 Lysis of cells for total protein

Cells were harvested following the protocol in Section 2.1.8, then resuspended in ice cold lysis buffer containing 140mM sodium chloride, 10mM TrisBase, 2mM calcium chloride, 0.5% v/v NP-40 at pH 8.0, supplemented with protease inhibitor cocktail (Roche) and 5 U/mL micrococcal nuclease (Sigma). This was incubated at room temperature for 5 minutes for nuclease digest. After digestion samples were used for protein estimation (Section 2.5.1) and SDS-PAGE (Section 2.5.4).

2.5.4 SDS-PAGE

Samples were prepared for SDS-PAGE by addition of SDS-loading buffer. This was made at a six fold concentration consisting of 12% w/v sodium dodecyl sulphate, 300mM TrisBase, 35% v/v glycerol, a few crystals of bromophenol blue, 6% v/v β-mercaptoethanol, then added to sample to a final 1x concentration. Samples were then placed at 95°C for 3 minutes and allowed to cool to room temperature before use. Protein lysates were also stored at -80°C under these conditions.

Poly-acrylamide gels were used for electrophoretic separation of proteins by molecular mass under denaturing conditions provided by sodium dodecyl sulphate. The poly-acrylamide resolving gels were poured at either 10 or 15% v/v acrylamide and allowed to set at room temperature for 30 minutes under a layer of distilled water. Once set, the distilled water was removed and the appropriate stacking gel (4% acrylamide for 10% resolver, 5% acrylamide for 15% resolver) was poured with wells created using a comb. Gels were cast using the Mini Protean II gel assembly apparatus (BioRad). Gel electrophoresis was applied at 90 volts for 2.5 hours in running buffer containing 250mM glycine, 25mM TrisBase and 0.1% w/v SDS. A PageRuler pre-stained protein ladder was used to visualise the separation of proteins on the gel (Fermentas). Following SDS-PAGE gels were taken into the protocol for Westerns blotting below.

2.5.5 Western blotting

Proteins separated by SDS-PAGE were transferred to nitrocellulose membranes (Whatman) by overnight transfer at 35 mAmps. The Mini Trans-Blot Electrophoretic Transfer Cell (BioRad) was used as instructed by the supplier, with transfer buffer containing 200mM glycine, 25mM TrisBase, 0.1% w/v SDS and 20% v/v methanol.

For immunoblotting the standard buffer used was TBST consisting of 200mM TrisBase, 250mM sodium chloride and 0.1% Tween-20 at pH 7.5. An alternative buffer was used for antibodies provided by *Cell Signalling Technology*, termed CST-TBST. This was made following the supplier's recommendations, consisting of 20mM TrisBase, 135mM sodium chloride and 0.1% Tween-20 at pH 7.6. Buffers were 0.22µm filter sterilised prior to use (Millipore).

Following overnight transfer, membranes were washed for 5 minutes in TBST or CST-TBST then blocked for 1 hour at room temperature in 5% w/v low fat dried milk (Marvell). All washes and incubations were carried out with rotational agitation of membranes. Membranes were then placed into appropriate dilution of primary antibody in blocking buffer and incubated overnight at 4°C. *Cell Signalling Technology* antibodies were diluted in 5% w/v bovine serum albumin (Sigma) in CST-TBST and incubated overnight at 4°C. CST membranes were washed three times for 5 minutes between milk block and application of antibody in CST-TBST. A list of primary antibodies used is shown in Table 2.6.

Membranes were washed after primary antibody incubation with three 5 minute washes in appropriate TBST. The appropriate species-matched horse radish peroxidise conjugated secondary antibody was applied in 5% low fat dried milk blocking buffer for all antibodies and incubated at room temperature for a minimum of 1 hour. A list of secondary antibodies used is shown in Table 2.7. Membranes were washed three times for 5 minutes to remove excess secondary antibody.

Immuno-detection of bound antibodies was achieved using the electrochemiluminescence method. Membranes were incubated in POD reagent

(Roche) for 1 minute then exposed to Hyperfilm (GE Healthcare) within light safe cassettes. Films were developed using a Xograph X2.

Hyperfilms were scanned to picture files for presentation of results. Images were altered and cropped to show optimal results using Corel PhotoPaint X3. Densitometry from these files was calculated using Quantity One software (BioRad) and presented as histograms created with SigmaPlot.

Protein target	***Species and isoform***	***Clone and supplier***	***Typical dilution range***
Actin	Mouse IgG1κ	C4 monoclonal Millipore	1:5,000 to 1:10,000
AROS	Rabbit Not specified	AT135 polyclonal Alexis	1:500 to 1:2,000
c-Myc	Mouse IgG1	9E10 monoclonal Santa Cruz	1:500 to 1:2,000
HDM2	Mouse IgG	4B2 monoclonal Produced in house	1:3 to 1:5
Lamin AC	Mouse IgG2b	636 monoclonal Santa Cruz	1:1000 to 1:4000
LDH	Rabbit IgG	1563Y monoclonal Epitomics	1:2,000 to 1:5,000
p53	Mouse IgG2a	DO-1 monoclonal Santa Cruz	1:1,000 to 1:4,000
p53 K382Ac (1)	Rabbit IgG	2525 polyclonal Cell Signalling	1:500 to 1:2,000
p53 K382Ac (2)	Rabbit IgG	356(2) monoclonal Epitomics	1:500 to 1:2,000
RPL3	Rabbit IgG	C-14 polyclonal Santa Cruz	1:1,000 to 1:4,000

Protein target	***Species and isoform***	***Clone and supplier***	***Typical dilution range***
RPS19	Mouse IgG2b	3C6 monoclonal AbCam	1:2,000 to 1:5,000
RPS6	Rabbit IgG	5G10 monoclonal Cell Signalling	1:2,000 to 1:5,000
SIRT1	Rabbit IgG	H-300 polyclonal Santa Cruz	1:1,000 to 1:4,000

Table 2.6: List of primary antibodies

Protein target	***Species and isoform***	***Clone and supplier***	***Typical dilution range***
HRP-conjugated anti-mouse	Rabbit Mainly IgG	P-0260 polyclonal DakoCytomation	1:1,000 to 1:10,000
HRP-conjugated anti-rabbit	Goat Mainly IgG	P-0449 polyclonal DakoCytomation	1:1,000 to 1:10,000

Table 2.7: List of secondary antibodies

2.6 *Molecular biological analyses of RNAs*

2.6.1 Isolation of RNA

This protocol followed the RNeasy method (QIAGEN). Cell or nuclear pellets (from Section 2.4.3) were lysed in the recommended volume of RLT buffer containing 1% v/v β-mercaptoethanol (Sigma). Lysates were applied to a QIAShredder homogeniser at 10,000 g for 2 minutes. The lysate was then supplemented with an equal volume of 70% ethanol, applied to an RNeasy column and centrifuged at 10,000 g for 15 seconds.

The column contents were washed with buffer RW1 and an on-column DNase I digest was carried out. 25 units of DNase I was diluted in buffer RDD (both QIAGEN) and incubated on column for 15 minutes. This removed genomic DNA from subsequent analyses of RNA. Samples were then washed with buffer RW1. Samples were finally washed twice in buffer RPE (made from concentrate by addition of ethanol) and RNA was eluted using RNase free distilled water. Samples were stored at -80°C and freeze-thaw cycles were avoided.

2.6.2 Quantification of RNA

This technique allowed the determination of RNA concentration by exploitation of the spectrophotometric properties of nucleotides at 260nm. From the values attained, accurate dilution of RNA was carried out to ensure equal loading of template in polymerase chain reactions (Sections 2.6.3 and 2.6.4), or to provide an accurate reading of the quantity of ribosomal RNA separated by sucrose density ultra-centrifugation (Section 2.4.1). RNA was quantified using a GeneSpec V spectrophotometer (Hitachi) and associated computer software. A volume of 2µL was used in a quartz micro-cuvette (Hitachi) with a pathlength of 1mm. The apparatus was blanked using RNase / DNase free water (Gibco) and the cuvette cleaned between samples using 100% ethanol and RNase / DNase free water.

This technique was also applied for the quantification of DNA, with the apparatus able to detect DNA using an alternate set of parameters defined in the computer software. The protocol carried out was otherwise identical.

2.6.3 Reverse transcription PCR

This technique synthesised cDNA from isolated RNA by reverse transcription. Subsequent polymerase chain reaction amplification of cDNA on a Dyad DNA Engine (MJ Research) was followed by analysis of products by agarose gel electrophoresis (Section 2.6.5). The protocol followed the OneStep RT-PCR Kit (QIAGEN) and made use of the primers detailed in Section 2.6.6.

A master mix containing reverse transcription and Taq polymerase enzymes, appropriate buffers and forward and reverse primers was made and aliquoted across purified RNA to be analysed. The primers for amplification were used at 750nM (detailed in Table 2.9). 50ng of total RNA was routinely used for amplification of mRNA targets and 5ng of total RNA for rRNA targets. In all cases a reaction lacking template was analysed, termed the blank. Amplification in the blank sample was monitored to ensure no contamination of reagents. Typical thermal cycling followed the steps shown in Table 2.8.

2.6.4 Quantitative Real Time RT-PCR

This protocol is essentially identical to that outlined for RT-PCR above but employs the QuantiTect SYBR Green kit (QIAGEN). This allows the quantification of cDNA as it is synthesised, by detecting the fluorescence from SYBR Green bound to DNA on an Opticon Monitor 2 machine (BioRad). The thermal cycling used was the same as that used for RT-PCRs, with the addition of a 'read' step at a designated temperature during which the fluorescence was recorded (See Table 2.8). The primers were used at 400nM and are shown in Table 2.9.

A standard curve of RNA dilutions was created to facilitate the plotting of a graph depicting RNA quantity against cycle number of amplification. This standard curve was created by serial dilution and designed to cover the range of data to be produced from the PCR. The relative quantities of RNA were intercepted from the standard curve and an average of at least three independent polymerase chain reactions taken (i.e. $n \geq 3$). These were standardised against one sample allotted the mRNA content of '100%.'

Data were plotted as histograms with standard deviation error bars using SigmaPlot. Housekeeping gene mRNAs were used as indicated to standardise the mRNA quantities between samples. For statistical analysis the Student t-test was used with a P value less than 0.05 considered significant. This method of data analysis is in accordance with the Larionov-Krause-Miller Method (Larionov et al. 2005).

Step	***Temperature***	***Time***	***Purpose***
1	50°C	30 m	Reverse transcription
2	94°C	15 m	Taq polymerase activation
3	94°C	30 s	Denaturing of DNA
4	50-65°C *	30 s	Annealing of primers
5	72°C	30-60 s	Extension of DNA
6	Repeat 3 to5	25 to 40 times †	Amplification
7	72°C	10 m	Final extension of DNA

Table 2.8: Thermal cycling used in RT-PCR

* - Annealing temperature depended on the melting temperature of the primers used for amplification. Typically the annealing temperature was 5°C below the lowest melting temperature of the primers.

† - The number of repeated cycles depended on the abundance of the RNA target. Low abundance targets required more cycles, whereas higher abundance targets required fewer.

N.B. Thermal cycling for qRT-PCR analysis was identical, except for the addition of a step between 5 and 6 where the Opticon Monitor 2 carried out a plate read of SYBR Green fluorescence at a designated temperature.

2.6.5 Agarose gel electrophoresis

This technique allowed the separation of cDNA according to size. This was used to verify the expected size of PCR products as shown in Table 2.9 and the *Appendices*. 1-1.5% weight-by-volume of agarose was dissolved in TAE supplemented with 170µg/mL ethidium bromide (Amresco) and cast into gels.

6x DNA loading dye (Fermentas) was added to PCR primer products to a final concentration of 1x. TAE was used as the electrophoresis running buffer for electrophoresis at 90V for a minimum of 30 minutes (Flowgen Bioscience). Intercalated ethidium bromide was visualised by ultra-violet transillumination. Data was recorded using Canon PowerShot G10 digital camera mounted to a CSL-MICRODOC System (Wolf Laboratories). Images were processed using Corel PhotoPaint X3 to optimise contrast.

2.6.6 Design and production of DNA primers

Primers were designed to ensure specific amplification of cDNA in polymerase chain reactions. The sequences of some primer pairs were designed and verified by other laboratory members, where indicated. RNA sequences were retrieved from public access databases such as FASTA and GENBANK and analysed using Vector NTI (Invitrogen).

Primer sequences were selected which fulfil the following three criteria in the *'Thermodynamic properties'* in Vector NTI; 1) 50-60% GC content, with no repeated bases more than 3 bases long, 2) a melting temperature above 50°C and within 5°C of the relevant primer partner, 3) no predicted stem loop or dimeric structures. These parameters were chosen to reduce the possibility of primer dimer or secondary structure formation. Sequences were between 19 and 24 base pairs long and were selected to have less than 60% BLAST homology to other human RNAs. Where appropriate, primers were designed to amplify only the splice variant of interest. Primers were ordered from Sigma and diluted in RNase / DNase free water (Gibco). All primers designed not previously verified were analysed by agarose gel electrophoresis to ensure correct cDNA product size (see Appendices).

mRNA	***Primers sequences***	***Product size***
18S rRNA	Fd: 5'-GGACACGGACAGGATTGACAG-3' Rvs: 5'-GCTTATGACCCGCACTTACTCG-3'	395bps
28S rRNA[†]	Fd: 5'-CGTGGAATGCGAGTGCCTAG-3' Rvs: 5'-TTGATTCGGCAGGTGAGTTG-3'	199bps
Actin (ACTG1)[†]	Fd: 5'-GCCAACAGAGAGAAGATGAC-3' Rvs: 5'-CGCAAGATTCCATACCCAGG-3'	477bps
AROS	Fd: 5'-GGAAGACGAAGGCAATTCAGGC-3' Rvs: 5'-TCCTCGGTGAACACGGTGCC-3'	261bps
BIM L[†]	Fd: 5'-ACCAGGCGGACAATGTAACGTAA-3' Rvs: 5'-CCACAAACAGGAGCCCAGCA-3'	281bps
FOXO4[†]	Fd: 5'-GCAGGATGGAAGAACTCGAT-3' Rvs: 5'-ACTGCTGACTGAAGCTGGTA-3'	432bps
GAPDH[†]	Fd: 5'-CGGAGTCAACGGATTTGGTCGTAT-3' Rvs: 5'-AGCCTTCTCCATGGTGGTGAAGAC-	307bps
Lamin AC[†]	Fd: 5'-AAGCAGCGTGAGTTTGAGAGC-3' Rvs: 5'-AGGGTGAACTTTGGTGGGAAC-3'	770bps
LDH-A	Fd: 5'-TTGGTCCAGCGTAACGTGAAC-3' Rvs: 5'-CCAGGATGTGTAGCCTTTGAG-3'	426bps
LDH-B	Fd: 5'-CTGGGAAAGTCTCTGGCTGATG-3' Rvs: 5'-CACTCCACACAGCCACACTTGA-3'	489bps
RPS19	Fd: 5'-ACCAGCAGGAGTTCGTCAGAGC-3' Rvs: 5'-CCACCTGTCCGGCGATTCTG-3'	386bps

mRNA	*Primers sequences*	*Product size*
SIRT1-FL[†]	Fd: 5'-TCAGTGTCATGGTTCCTTTGC-3' Rvs: 5'-AATCTGCTCCTTTGCCACTCT-3'	820bps
SIRT1-Δ8[†]	Fd: 5'-GGGATGGTATTTATGCTCGC-3' Rvs: 5'-AACAGATACTGATTACTTGGA-3'	547bps

Table 2.9: List of primers used for amplification of RNA

(†) - Designed and verified by other members of the YCR p53 Research Unit.

Dr Jack Ford – *FOXO4, GAPDH, Lamin AC, SIRT1-FL.*

Dr Cian Lynch – *SIRT1-Δ8.*

Dr Shafiq Ahmed – *28S rRNA, Actin, BIM-L.*

3 Regulation of SIRT1 activity by LDH-A

3.1 *Overview*

In this *Chapter* the role of lactate dehydrogenase A (LDH-A) in facilitating SIRT1 activity is assessed. Selective RNAi was employed to silence LDH-A, as well as its isoenzyme LDH-B, providing a case study for the specificity of RNAi. Cell phenotypes and fate for cancer and non-cancer cells were analysed, giving encouraging data for potential future cancer therapy. Molecular biological analyses further explored the consequences of LDH-A knockdown in cancer and non-cancer cells.

The premise of this analysis draws on two factors: first the requirement SIRT1 has upon the metabolite NAD^+, the levels of which are managed by LDH-A, and second the common metabolic switch in cancer cells from Oxidative Phosphorylation to using the Aerobic Glycolysis Cycle, which relies upon an increase in LDH-A activity. The broader aim of the *Thesis* is maintained with the characterisation of a target that positively regulates SIRT1 activity.

3.2 *Introduction*

3.2.1 Nicotinamide adenine dinucleotide

Nicotinamide adenine dinucleotide is a dinucleotide consisting of one adenine and one nicotinamide base. The nicotinamide base can exist in two stable forms according to oxidation status (Warburg and Christian 1936). The oxidised form, NAD^+, is able to accept two electrons and a hydrogen ion to become the reduced form, NADH. NADH can then be oxidised back into NAD^+ when required. This interconversion is coupled to substrate oxidation and reduction during carbon catabolism, allowing the energy of electrons to be harnessed and linked to the generation of ATP (see below). NAD^+ is also an essential co-enzyme for SIRT1 (Imai et al. 2000; Landry et al. 2000; Smith et al. 2000).

3.2.2 Carbon catabolism and energy production

The controlled release of energy bound in glucose into the manageable unit of cellular energy, ATP, was principally investigated in the early 20th century. The forerunner in the field was Otto Meyerhof, for which he was recognised by the Nobel Prize in Physiology and Medicine in 1922. Along with collaborators, Meyerhof described the multistep process and intermediates of the biologically ubiquitous pathway of glycolysis – which for a time was called the Embden-Meyerhof pathway. Another seminal discovery of Meyerhof's was the investigation of the increase in glucose consumption under oxygen limiting conditions. This was termed the Pasteur-Meyerhof Effect and is now known as the Anaerobic Glycolysis Cycle. The work of Meyerhof is well summarised in a review of his career published in 2005, containing reference to his original research papers and that of his colleagues (Kresge et al. 2005).

Further release of energy from carbon occurs via mitochondrial Oxidative Phosphorylation. Mitochondrial carbon metabolism utilises the Citric Acid Cycle, detailed by Albert Szent-Györgyi and Hans Krebs in the early 20th century. The chemiosmotic mechanism of ATP production parallel to this pathway was first proposed by Peter Mitchell in 1961 (Mitchell 1961). A very brief summary of these pathways is presented to set the scene for the analysis undertaken.

Glucose is oxidised to pyruvate during glycolysis. The oxidative potential for glycolysis is provided by NAD^+, which is reduced to NADH. Glycolysis yields two molecules of ATP per molecule of glucose oxidised (Figure 3.1A – left panel). This occurs by substrate level phosphorylation of ADP.

Pyruvate is further oxidised by mitochondrial Oxidative Phosphorylation, again using the oxidative potential of NAD^+. The final products of Oxidative Phosphorylation are CO_2 and NADH (Figure 3.1A – left panel). The electrons stored in this NADH, and NADH from glycolysis, are then used in the electron transport chain. This is coupled to the production of ATP by ATP-synthase (Mitchell 1961), yielding a further thirty-four molecules of ATP for each glucose molecule that entered glycolysis. Importantly, donation of electrons from NADH oxidises it to NAD^+, allowing further glycolysis and Oxidative Phosphorylation to occur.

Glycolysis and subsequent Oxidative Phosphorylation are the dominant metabolic pathways used by non-cancer cells (Figure 3.1A). However, under anaerobic conditions Oxidative Phosphorylation cannot occur. ATP production is maintained by glycolysis. Without Oxidative Phosphorylation to consume pyruvate and NADH these products accumulate. Anaerobic cells also become deficient for the oxidative potential of NAD^+, which is no longer regenerated by Oxidative Phosphorylation. To overcome this, an alternative metabolic pathway is engaged, which requires lactate dehydrogenase (LDH).

3.2.3 LDH – decision maker in carbon catabolism

LDH catalyses the interconversion of pyruvate and NADH to lactate and NAD^+ (Baumberger et al. 1933). The ability to regenerate NAD^+ from NADH enables cells to continue glycolysis, with the NAD^+ used for further glucose oxidation. This is termed the Anaerobic Glycolysis Cycle (Figure 3.1A – right panel). Lactate from this reaction is excreted from the cell. Importantly, LDH catalyses the reaction in both directions, allowing either NADH and pyruvate or NAD^+ and lactate to be favoured (Baumberger et al. 1933) (Figure 3.1B). This gives LDH power as a decision maker at the end of glycolysis – with either Oxidative Phosphorylation or the Anaerobic Glycolysis Cycle the prospective pathways.

LDH is a tetrameric enzyme encoded by different genes; *LDH-A*, *LDH-B* and *LDH-C* (Markert et al. 1975). *LDH-C* expression is confined to the testis (Hintz and Goldberg 1977; Goldberg et al. 2010). *LDH-C* can be aberrantly expressed in cancer, but there is no evidence for this in the cell lines used here (Koslowski et al. 2002). Therefore, this analysis has focussed on the more common *LDH-A* and *LDH-B*. The relative expression of each isoenzyme is believed to determine function (Read et al. 2001). LDH-A favours the conversion of NADH and pyruvate into NAD^+ and lactate, whereas LDH-B favours the opposite reaction, NAD^+ and lactate conversion into NADH and pyruvate (Figure 3.1B). This is due to amino acid charge differences in non-catalytic surface residues between the two isoenzymes. As such, the LDH isoenzymes play an important role in deciding the direction of carbon catabolism. Dominant LDH-A would favour the Anaerobic Glycolysis Cycle, whereas dominant LDH-B would promote Oxidative Phosphorylation.

3.2.4 Metabolic alterations in cancer cells

The production of ATP from carbon catabolism is essential for the survival of all cells. However, cancer cells have a high rate of proliferation, giving a higher metabolic requirement for ATP. In contrast the majority of non-cancer cells do not have high metabolic activity due to a slower rate of proliferation. This difference presents an opportunity to specifically target energy production as a means to selectively eliminate cancer cells. One of the earliest characterisations of cancer cell biology was increased release of lactate, even under aerobic conditions (Warburg 1956). This was the first indication that not only the metabolic requirements of cancer cells are altered, but also the means employed to meet these requirements.

Consistent with increased release of lactate, cancer cells commonly undergo a metabolic shift towards the Anaerobic Glycolysis Cycle, even in the presence of adequate oxygen (Figure 3.1A – right panel) – leading to the definition of this form of cancer metabolism as ‘Aerobic Glycolysis’ (Warburg 1956). Later, in recognition of the work of Otto Warburg in the field, this was termed The Warburg Effect. Despite its early observation The Warburg Effect has only recently been studied with great intensity, leading to ‘altered metabolism’ being designated status as an

emerging hallmark of cancer (Hanahan and Weinberg 2011). Increasing knowledge of the mechanisms and enzymes behind The Warburg Effect has earned this status.

Of note among these enzymes is LDH-A. As discussed, LDH-A promotes carbon catabolism through the Anaerobic Glycolysis Cycle, in opposition to its isoenzyme LDH-B (Read et al. 2001). With this metabolic phenotype favoured in cancer cells, LDH-A has been analysed as the potential culprit for the altered metabolism of cancer cells. Evidence in support of this comes from expression studies for *LDH-A* and targeting of LDH-A *in vivo*.

3.2.5 *LDH-A* expression in cancer

LDH-A is expressed at higher levels in human tumour tissues compared to paired non-cancerous tissue (Goldman et al. 1964). This early observation has been supplemented by molecular biological analyses into the mechanisms behind this overexpression, which have revealed that *LDH-A* is upregulated by two important tumour-related transcription factors: c-Myc and HIF1 (hypoxia inducible factor 1).

c-Myc orchestrates cell proliferation by transactivating a wide range of genes (Vita and Henriksson 2006). In malignancy c-Myc acts as an oncogene, able to aberrantly promote the proliferation of cancer cells. c-Myc transactivates the *LDH-A* promoter, with overexpression of c-Myc resulting in a 6-fold increase in *LDH-A* mRNA (Lewis et al. 1997). Adding further to a role for LDH-A in cancer, LDH-A is required for c-Myc regulated transformation (Shim et al. 1997). These data illustrate the potential overexpression of LDH-A in cancer and implicate the enzyme in the c-Myc driven progression of cells to a cancerous state.

LDH-A mRNA expression increases 2-fold under hypoxia, due to the tumour-related HIF1 hetero-dimer binding to elements in the *LDH-A* promoter (Firth et al. 1995). Hypoxia commonly occurs in tumours, resulting in the derepression of HIF1α (Majmundar et al. 2010). HIF1α then hetero-dimerises with the HIFβ subunit to function as a selective transcription factor. HIF1 transactivates genes to promote hypoxic cell survival, a facet cancer cells are able to exploit (Majmundar et al. 2010). The transactivation of the *LDH-A* gene by HIF1 is indicative of a role in hypoxic tumour maintenance. HIF1 targeting for anti-cancer therapeutic gain is a

popular concept (Semenza 2003). Targeting the genes activated by HIF1 may also represent a means to reduce hypoxic cancer growth, with *LDH-A* a putative target among these.

Interestingly the activation of *LDH-A* by c-Myc and HIF1 is not evident for the *LDH-B* isoenzyme. Indeed the *LDH-B* isoenzyme is a target for promoter hypermethylation and epigenetic silencing in prostate cancer (Leiblich et al. 2006). Together these data indicate that LDH-A expression may be dominant over LDH-B expression in cancer. This correlates with The Warburg Effect where LDH-A is predicted to be required to favour the Aerobic Glycolysis Cyclic (Figure 3.1A). This putative dependence upon overexpression of LDH-A identifies it as a potential anti-cancer therapeutic target.

3.2.6 Targeting LDH-A in tumours

LDH-A is required for tumour maintenance in a mouse tumour model (Fantin et al. 2006). Targeting LDH-A in tumours results in a switch to Oxidative Phosphorylation for energy production, consistent with the hypothesis that LDH determines the direction of carbon catabolism, and that LDH-A favours the Aerobic Glycolysis Cycle. Interestingly, targeting LDH-A also reduces tumour growth capacity under hypoxia, indicating that LDH-A promotes tumour cell viability.

In an independent *in vivo* analysis, LDH-A targeting reduced tumour initiation and expansion (Le et al. 2010). Targeting of LDH-A in this study reduced cellular NAD^+ levels, and simultaneous targeting of LDH-A and NAD^+ synthesis enhanced cancer cell death. This strongly implicates the maintenance of NAD^+ levels by LDH-A as the mechanism promoting cancer cell survival. The requirement for NAD^+ is presumably to enable the Aerobic Glycolysis Cycle outlined above (Figure 3.1A – right panel). However, there is the possibility that reduced NAD^+ availability could impact on other essential enzymes that require NAD^+.

3.2.7 NAD^+ as a facilitator of SIRT1 activity

SIRT1 has a strict requirement for NAD^+ as a coenzyme for all deacetylase activity (Imai et al. 2000; Landry et al. 2000; Smith et al. 2000). SIRT1 removes the

acetyl group from target lysine residues, transferring it to NAD^+, which is cleaved during the process to nicotinamide and a novel substrate, O-acetyl-ADP-ribose (Tanner et al. 2000). Without NAD^+, SIRT1 cannot function.

SIRT1 is overexpressed in many cancers and has a strong role in maintaining cancer cell viability (see *Chapter 1*). LDH-A is important for the production of NAD^+ in cancer cells, which appears to be essential for their viability, although the exact mechanism is unclear (Le et al. 2010). One possibility is that NAD^+ generated by LDH-A drives the cancer-related pro-survival functions of SIRT1 (Ford et al. 2005). This could expand the emerging pro-survival role of LDH-A in cancer, beyond altered metabolism, to also include anti-apoptotic signalling. Indeed, there is the potential for LDH-A *linking* the altered metabolic phenotype to the activation of SIRT1 in cancer. The analysis of these hypotheses forms this *Chapter*.

3.2.8 Hypotheses

1. LDH-A, but not LDH-B, is essential for the survival of human cancer cells.
2. LDH-A sustains the deacetylase and cancer related anti-apoptotic activities of SIRT1.

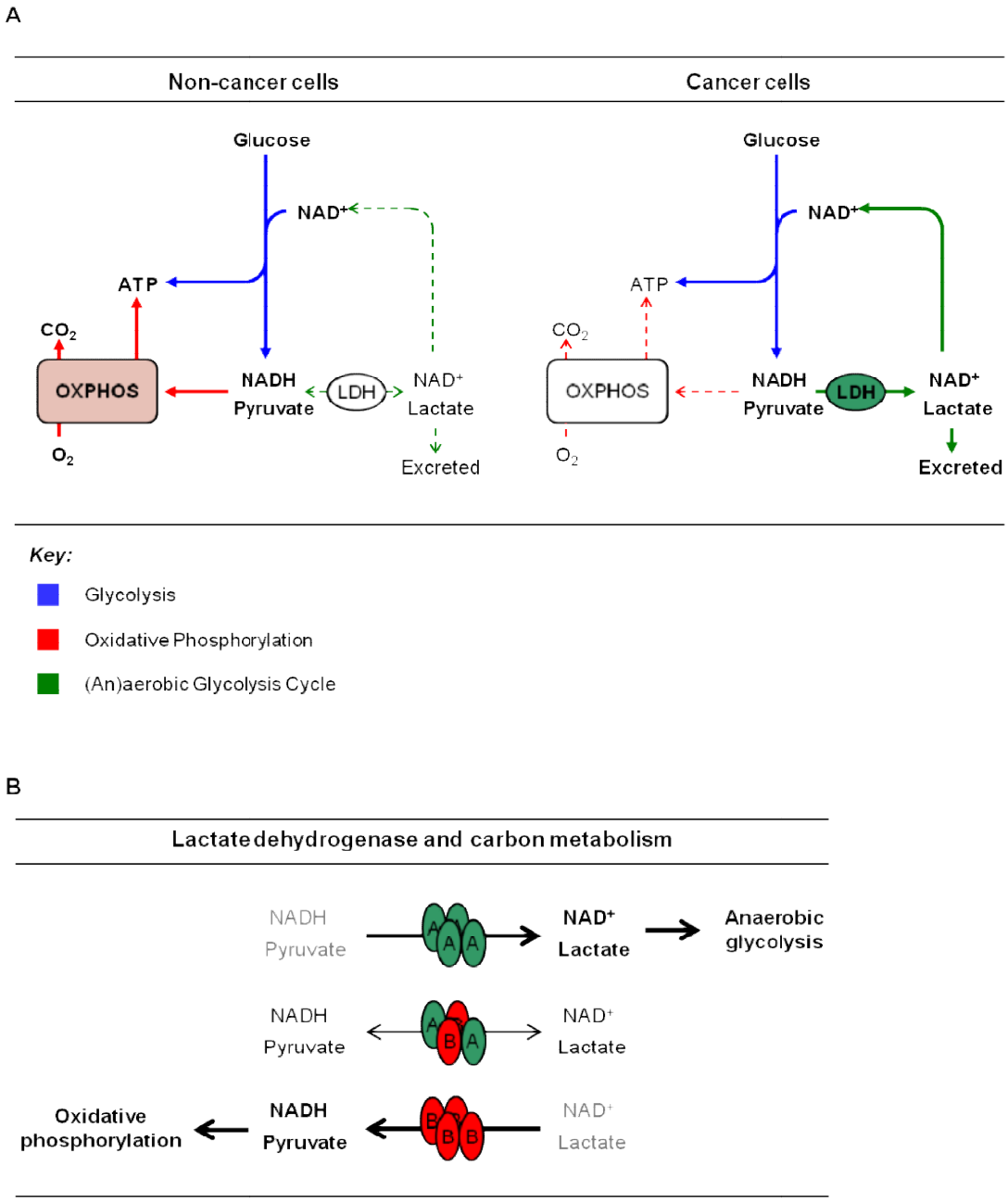

Figure 3.1: Metabolism of non-cancer and cancer cells

(A) Schematic of the energy-yielding glucose metabolism pathways in non-cancer cells (left) and cancer cells (right). OXPHOS = Oxidative Phosphorylation. Dashed lines indicate suppressed pathways and filled lines active pathways. Oxidative Phosphorylation is favoured in non-cancer cells, whereas some cancer cells alter their metabolism towards the (An)aerobic Glycolysis Cycle (See Text). **(B)** Representation of the control that the LDH isoenzyme tetramer has over carbon catabolism. LDH-A is shown in green and favours the (An)aerobic Glycolysis Cycle. LDH-B, in red, favours Oxidative Phosphorylation.

3.3 *Specific silencing of LDH isoenzymes by RNAi*

3.3.1 A note on specific siRNA and primer design

LDH-A and LDH-B have amino acid sequence identity of 75% (Read et al. 2001). This is also the case for the mRNA sequences (68% identity), necessitating careful design of specific siRNAs and DNA primers for each isoenzyme. The sequences are shown in Figure 3.2, with annotation of siRNA and primer positions. Specificity was paramount to the analysis, requiring low sequence identity to the alternate mRNA for each target mRNA. The identity of the LDH-A siRNA to *LDH-B* mRNA was 57.9%, and the identity of the LDH-B siRNA to *LDH-A* mRNA was 78.9%. Specificity of knockdown was determined by qRT-PCR using the primers shown as detailed herein.

3.3.2 Knockdown of *LDH-A*

Initial investigation focussed on LDH-A, with LDH-B analysed in later experiments. RNAi against *LDH-A* was carried out in parallel to *Lamin AC* silencing, which acted a positive control for RNAi. Silencing of *LDH-A* mRNA was achieved in a panel of four cell lines: three cancer cell lines, HCT116 (wild-type p53), DLD1 (mutant p53) and HCT116 $p53^{-/-}$ (null for p53); and a non-cancer cell line, ARPE19 (Figure 3.3A-D). *LDH-A* mRNA was significantly reduced compared to Mock transfected cells in all four lines.

A rabbit monoclonal antibody detected LDH-A and LDH-B proteins by western blot. LDH-A has a molecular weight of ~35kDa, running below LDH-B at ~36kDa (Read et al. 2001) . RNAi against *LDH-A* reduced in the lower band (representing LDH-A) in all four cell lines analysed compared to Mock or Lamin AC siRNA treatments (Figure 3.3A-D). This is consistent with the silencing seen at the mRNA level. The effect of LDH-A silencing on the upper band, representing LDH-B, was negligible in all four cell lines, exemplary of the selectivity of RNAi.

Control Lamin AC siRNA transfection significantly reduced *Lamin AC* mRNA in all four cell lines (Figure 3.3A-D). Lamin AC protein levels were also efficiently

reduced by RNAi in all four cell lines compared to Mock treated cells (Figure 3.4A-D).

3.3.3 Knockdown of *LDH-B*

To further validate the specificity of the siRNAs against *LDH-A* and *LDH-B* before progressing to analyse cell phenotypes, parallel transfection of each siRNA was undertaken in the HCT116 cancer and ARPE19 non-cancer cell lines. LDH-A and LDH-B cosilencing was also performed in the analysis.

LDH-B mRNA was significantly reduced compared to Mock transfection in both cell lines following LDH-B siRNA transfection (Figure 3.5A). *LDH-A* silencing was again efficient, consistent with the initial observations in Figure 3.4. Cosilencing of both isoenzymes resulted in a reduction of both target mRNAs compared to Mock. The extent of silencing was similar to or lower than that of the individual silencing carried out in parallel. This supports isoenzyme selectivity in the RNAi, as the use of both siRNAs did not give an additive silencing compared to single siRNA usage.

The selective silencing of LDH-A and LDH-B is shown at the protein level (Figure 3.5B). This is the case for both cell lines but is perhaps best seen for the HCT116 cells due to a more favourable ratio of LDH-A to LDH-B. LDH-A protein is reduced compared to Mock treatment in lanes 2, 4, 6 and 8, where LDH-A siRNA was used. LDH-B protein is reduced in lanes 3, 4, 7 and 8 where LDH-B siRNA was used. The specificity of this was high. There is potentially a reduction in LDH-A protein following LDH-B silencing in the HCT116 cell line (lane 3), but this is not evident at the RNA level (Figure 3.5A).

These initial experiments in Section 3.3 indicate that targeting of *LDH-A* or *LDH-B* by RNAi gives a robust reduction in target mRNA and that this translates to the protein level. The specificity of RNAi silencing for both isoenzymes allows further analysis of the cellular and molecular effects of silencing of LDH-A or LDH-B, which can be done with confidence of isoenzyme selectivity.

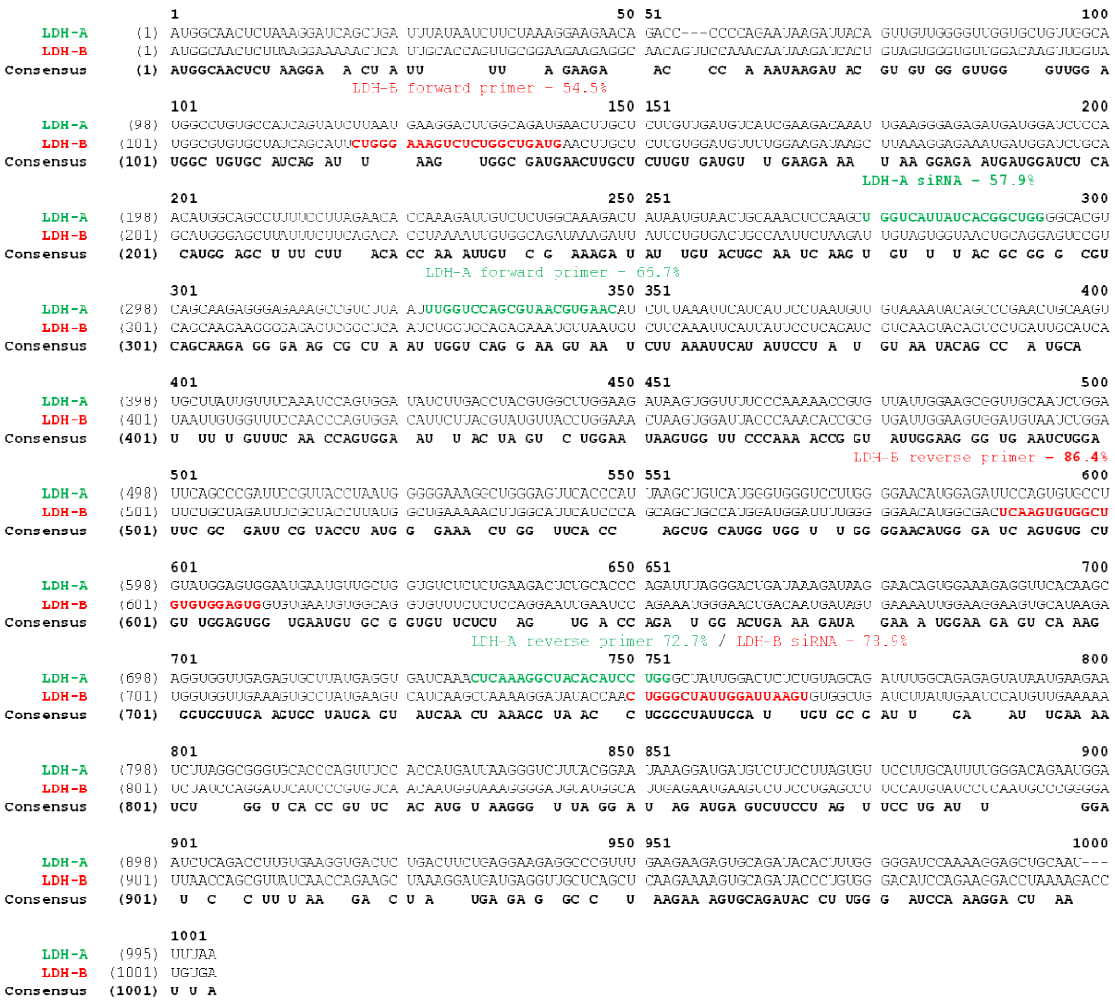

Figure 3.2: Comparison of LDH isoenzyme mRNA sequences

Aligned coding mRNA sequences for the human LDH isoenzymes A and B. Total sequence identity of the isoenzymes is 68.1%. Highlighted regions indicate siRNAs and DNA primers used – *LDH-A* is shown in green and *LDH-B* in red.

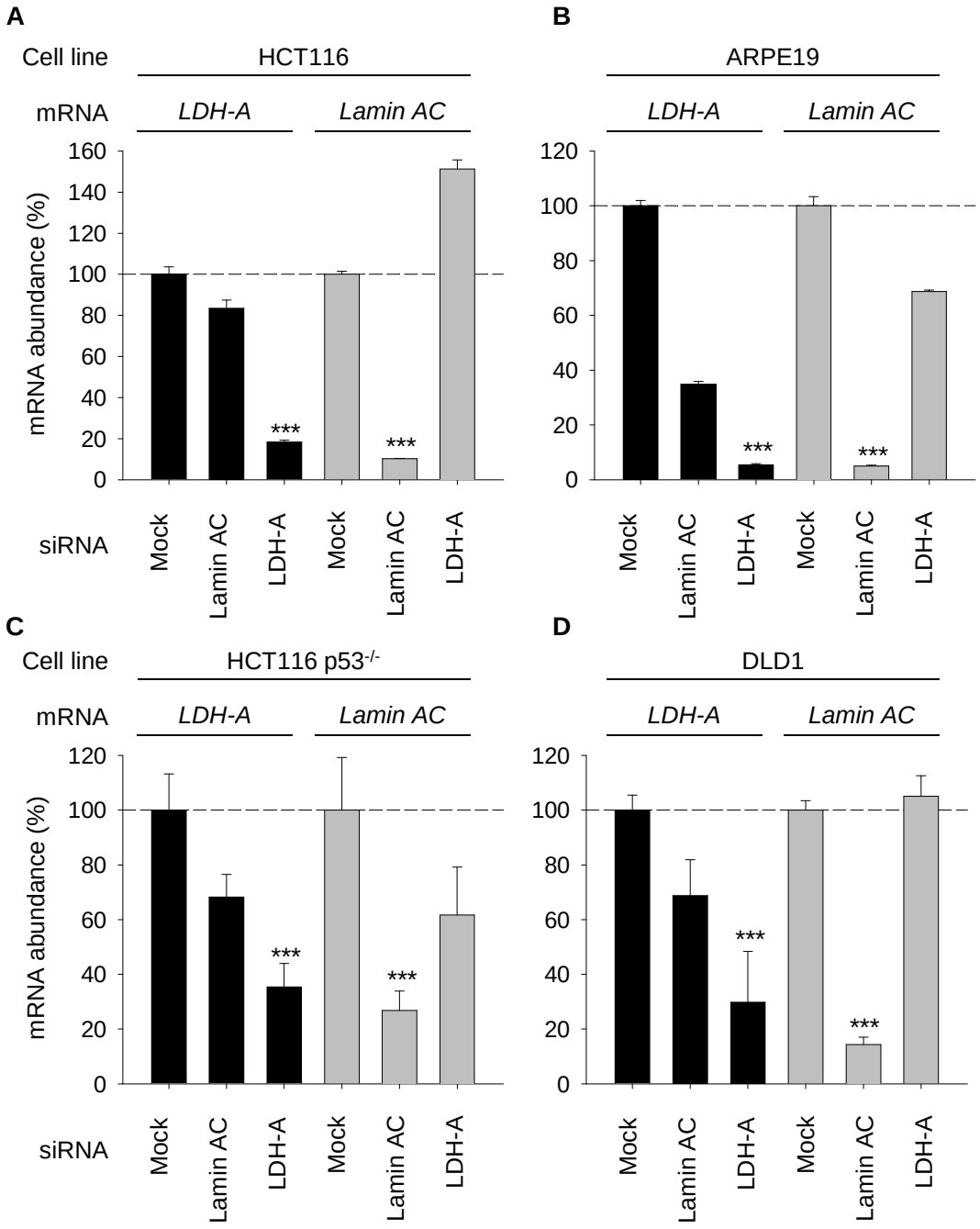

Figure 3.3: Targeting *LDH-A* mRNA by RNAi

(A) Quantification of *LDH-A* and *Lamin AC* mRNAs following specific RNAi against each target in the HCT116 cancer cell line. Cells were transfected with siRNA as indicated, harvested 48 hours post-transfection. RNA was isolated by RNeasy method and qRT-PCR carried out as indicated (See Methods). **(B)** Data as for (A) for the ARPE19 non-cancer cell line. Harvesting of cells was at 72 hours post-transfection. **(C)** Data as for (A) for the HCT116 $p53^{-/-}$ cancer cell line. Harvesting of cells was at 72 hours post-transfection. **(D)** Data as for (A) for the DLD1 cancer cell line. Harvesting of cells was at 72 hours post-transfection. *** $P<0.001$.

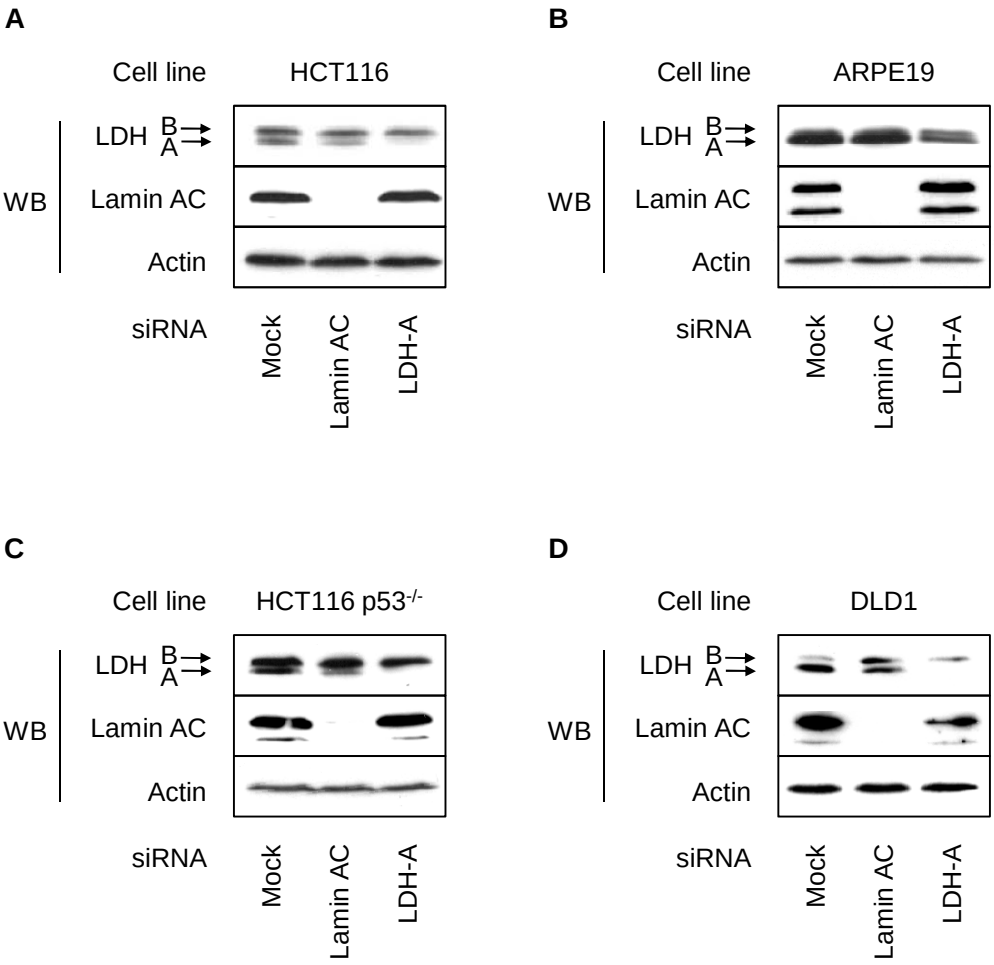

Figure 3.4: Targeting LDH-A protein by RNAi

(A) Analysis of LDH isoenzyme and Lamin AC expression following targeting by RNAi in HCT116 cells. Actin is used as a loading control. Cells were transfected with siRNA as indicated, harvested 48 hours post-transfection and lysed in protein lysis buffer (see Methods). Equivalent protein was loaded by calculated mass. **(B)** Data as for (A) for the ARPE19 cell line. Harvesting of cells was at 72 hours post-transfection. **(C)** Data as for (A) for the HCT116 $p53^{-/-}$ cell line. Harvesting of cells was at 72 hours post-transfection. **(D)** Data as for (A) for the DLD1 cell line. Harvesting of cells was at 72 hours post-transfection.

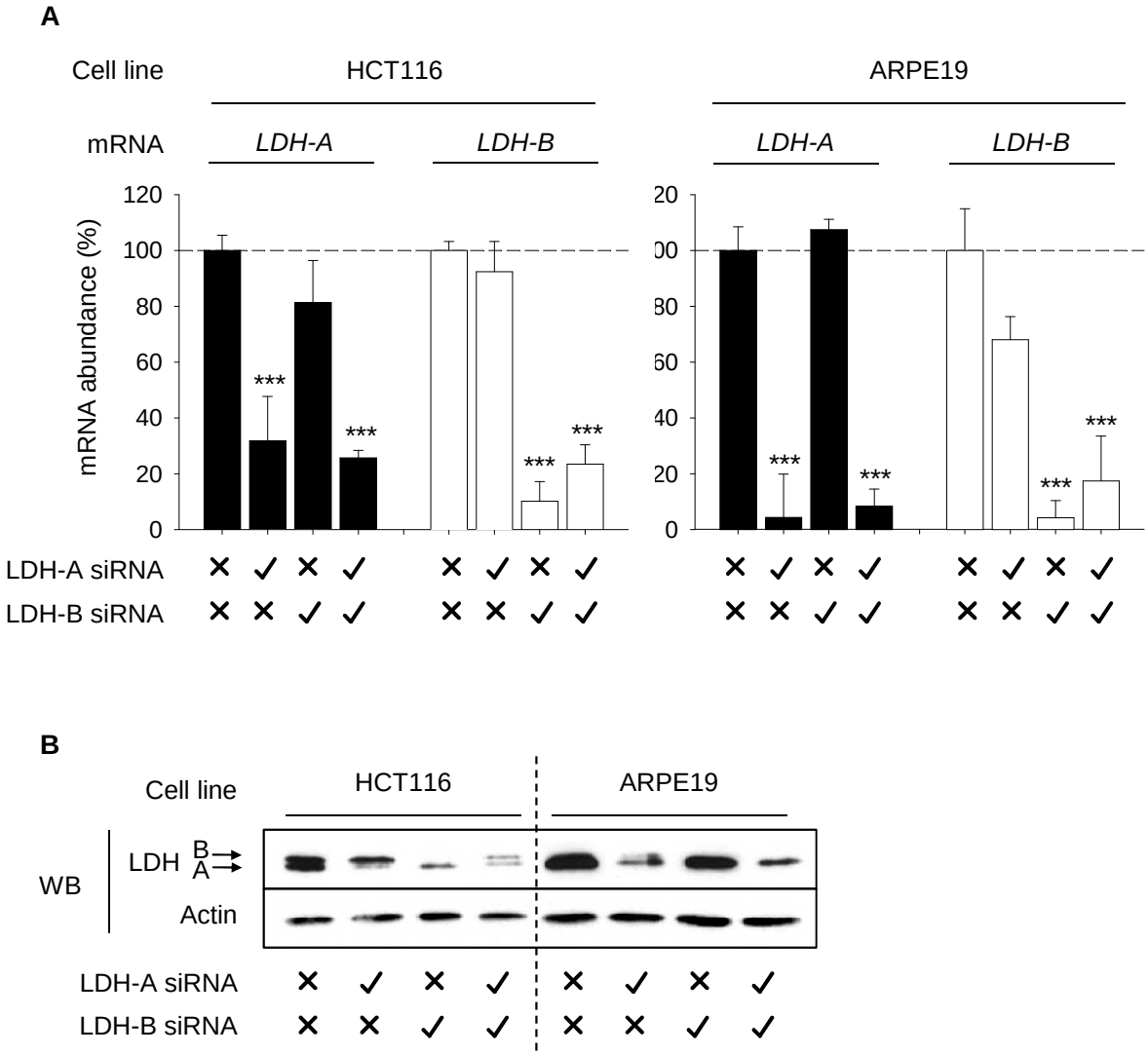

Figure 3.5: Targeting LDH-B by RNAi

(A) Parallel independent silencing and cosilencing of *LDH-A* and *LDH-B* as indicated. RNA was purified by RNeasy method and quantified by qRT-PCR (see *Methods*) using specific primers detailed in Figure 3.2. Cells were harvested at 48 hours (HCT116) or 72 hours (ARPE19). **(B)** Analysis of LDH isoenzyme expression following the same independent silencing and cosilencing in (A). Actin is used as a loading control. *** P<0.001.

3.4 *Characterisation of cell phenotype following LDH isoenzyme silencing*

3.4.1 Cancer cell lines

Phase contrast microscopy of the cancer cell lines HCT116 (Figure 3.6Ai) HCT116 $p53^{-/-}$ (Figure 3.6Aii) and MCF7 (Figure 3.6Aiii) revealed little difference in phenotype between Mock treatment and LDH-B silenced cells. The majority of cells remained adhered to the surface and appeared at a similar density to Mock treatment. Following RNAi against LDH-A in each line there was an increase in cell detachment and more cells were refringent under microscopy. There appeared to be concomitant reduction in the adhered population. Following cosilencing of both LDH-A and LDH-B in the HCT116 and HCT116 $p53^{-/-}$ cell lines, the phenotype was similar to that of the LDH-A silenced cells – an increase in detached, refringent cells and a reduction in adhered cell density.

The use of the LDH-A siRNA, with or without LDH-B cosilencing, produced a phenotype consistent with an induction of apoptosis. This was confirmed by quantification of apoptosis by flow cytometry (see *Methods*). In the HCT116, HCT116 $p53^{-/-}$ and MCF7 cell lines, LDH-A silencing induced a significant induction in apoptosis (Figure 3.7A-C). Apoptotic induction is greater in the p53 wild-type cell lines (HCT116 and MCF7) than the null cell line (HCT116 $p53^{-/-}$). This suggests that p53 is important in LDH-A suppressed apoptosis. However, this phenomenon may be attributable to apoptosis occurring over a longer period in the HCT116 $p53^{-/-}$ cell line than the HCT116.

The apoptotic detection method used quantifies cells in early apoptosis (see *Methods*). HCT117 $p53^{-/-}$ cells appeared to enter apoptosis over a longer period of time (from 48 to 72 hours and beyond), in contrast to HCT116 cells which appeared to peak in their early apoptotic quantity at 48 hours then have reduced apoptotic numbers thereafter. As such, p53 is not required for apoptosis (as evidenced by HCT116 $p53^{-/-}$ cell death) but may play a facilitating role in allowing faster induction of apoptosis (as illustrated by greater induction at a specific early time point in p53 wild-type over null cells).

LDH-B silencing did not greatly alter the scored number of apoptotic cells in the three lines, compared to Mock (Figure 3.7A-C). Further, cosilencing of LDH-A and LDH-B in the HCT116 and HCT116 $p53^{-/-}$ cell lines resulted in a significant induction of apoptosis (Figure 3.7A and B). This is consistent with the micrographs in Figure 3.6A, and a correlation between LDH-A silencing and induction of apoptosis.

The post-silencing phenotypes of the LoVo cell line were broadly consistent with those above (Figure 3.6Aiv); LDH-B siRNA treatment caused little alteration compared to Mock, whereas LDH-A siRNA treatment caused a reduction in adhered cell density. There was also an increase in the number of refringent cells following LDH-A siRNA treatment, although few cells appeared to have detached. This is again consistent with an induction of apoptosis following RNAi against LDH-A in this cancer cell line.

LDH-A was also targeted in the DLD1 cancer cell line, but not in parallel with LDH-B silencing (Figure 3.6B). *Lamin AC* was targeted as a positive control for RNAi with no effect on cell phenotype, and did not induce apoptosis (Figure 3.7D). LDH-A silencing resulted in an increase in detached cells compared to Mock treatment. This phenotype is consistent with the induction of apoptosis, which was again confirmed by flow cytometry (Figure 3.7D).

3.4.2 Non-cancer cell line

The data in Section 3.4.1 indicate that LDH-A has a role in promoting the survival of five cancer cell lines. The effect of silencing LDH-A in non-cancer cell lines will therefore allow an analysis of the cancer specificity of this effect. For this the ARPE19 epithelial cell line was used as a representative line of non-cancerous origin.

Silencing of each LDH isoenzyme individually did not greatly alter the phenotype or density of the cell line compared to Mock treatment (Figure 3.8A). LDH-B depleted cells appeared more rounded than Mock transfected cells. Following LDH-A siRNA transfection there was a potential increase in refringent

cells, but these remained attached to the plate. The phenotypes were not consistent with an induction of apoptosis.

In agreement with this, silencing of LDH-A or LDH-B did not greatly alter the number of apoptotic cells compared to Mock treatment, as is the case for cosilencing of the two isoenzymes (Figure 3.8B). All four conditions analysed returned an apoptotic cell count of ~1% of the total population, with no significant deviation from Mock with any of the specific siRNA treatments. This indicates that neither LDH-A or LDH-B are required for ARPE19 cell survival, which may be representative of non-cancer cells in general.

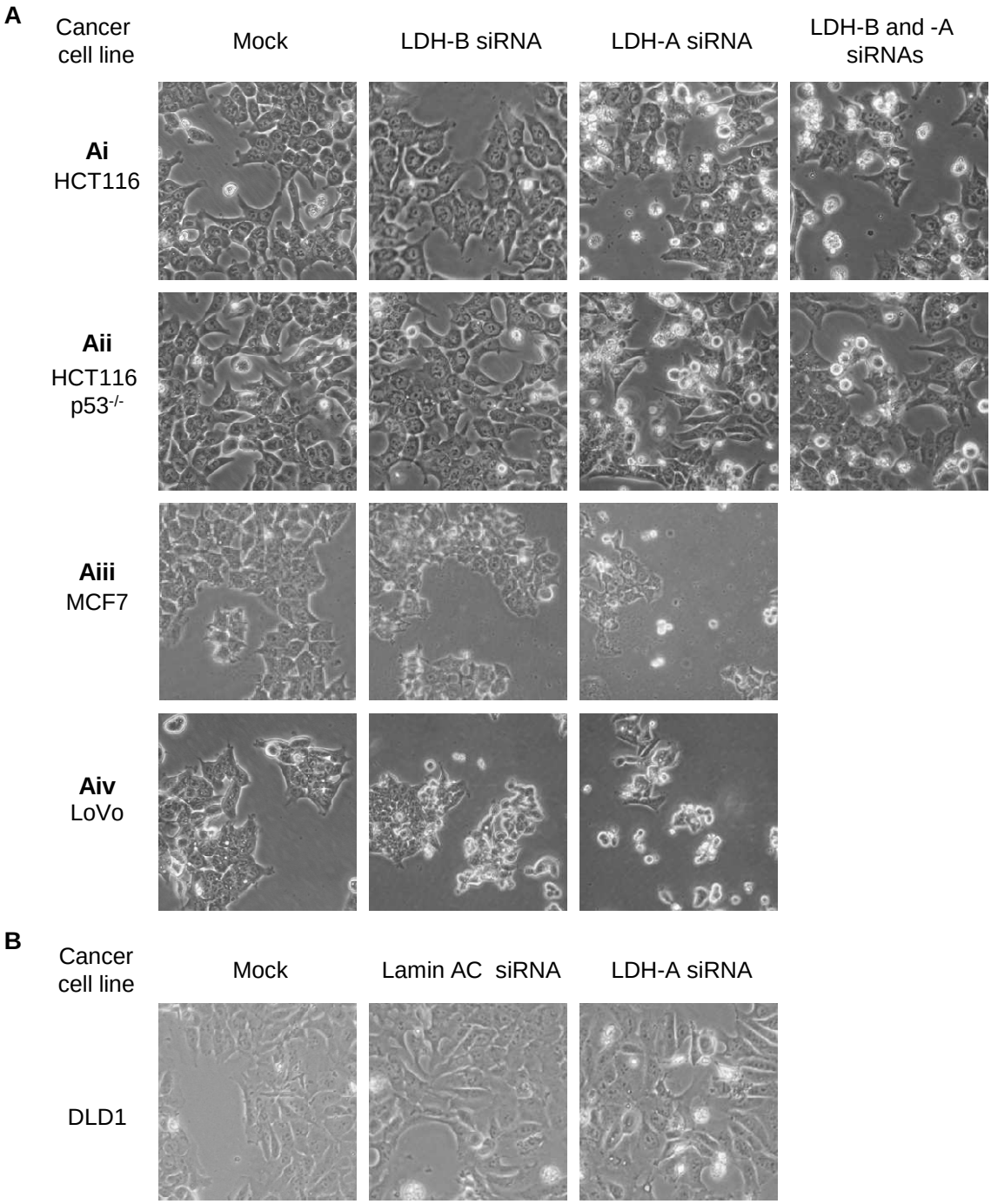

Figure 3.6: The effect of LDH isoenzyme silencing on cancer cell phenotype

(A) Phase contrast microscopy at 200x magnification of four cancer cell lines (HCT116, HCT116 p53$^{-/-}$, MCF7 and LoVo) following silencing of LDH-A or LDH-B and, for the HCT116 and HCT116 p53$^{-/-}$, cosilencing of the isoenzymes together. Micrographs were recorded 48 hours (HCT116, MCF7, LoVo) or 72 hours (HCT116 p53$^{-/-}$) post siRNA transfection in all cases. **(B)** Images as in (A) for the DLD1 cell line following LDH-A silencing and Lamin AC silencing as a control. Harvesting of cells was at 72 hours.

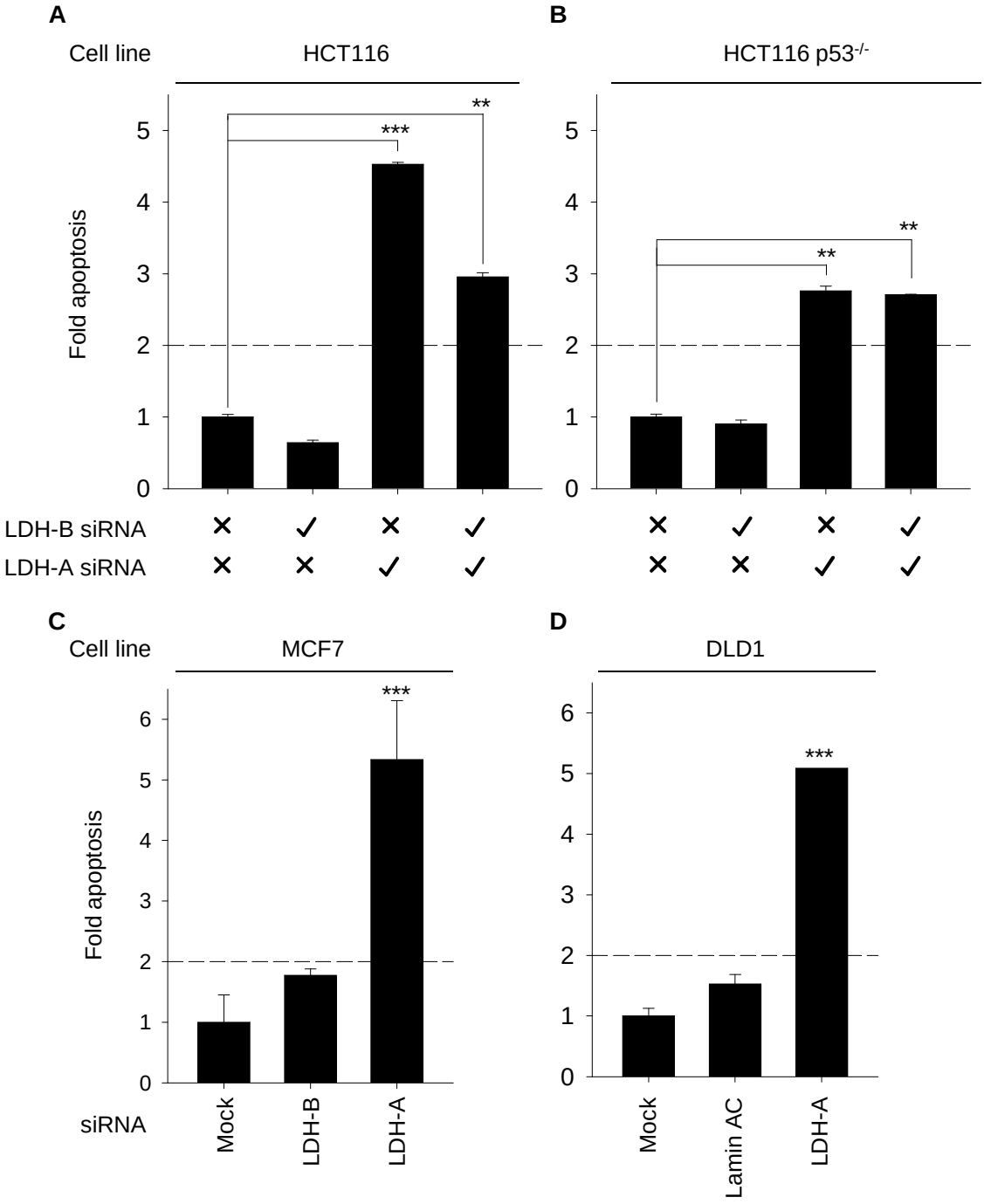

Figure 3.7: The effect of LDH isoenzyme silencing on cancer cell apoptosis

(A) Fold apoptosis induction compared to Mock siRNA treated cells following individual LDH isoenzyme silencing and cosilencing of both isoenzymes, in the HCT116 cell line. Cells were treated with siRNA for 48 hours post-transfection and analysed by Annexin V staining and flow cytometry (See Methods). **(B)** Data as in (A) for the HCT116 $p53^{-/-}$ cell line at 72 hours post-transfection. **(C)** Data as in (A) for the MCF7 cell line following individual silencing of LDH-A and LDH-B. **(D)** Data as in (A) following Lamin AC and LDH-A silencing in the DLD1 cell line at 72 hours post-transfection. *** P<0.001, ** P<0.01.

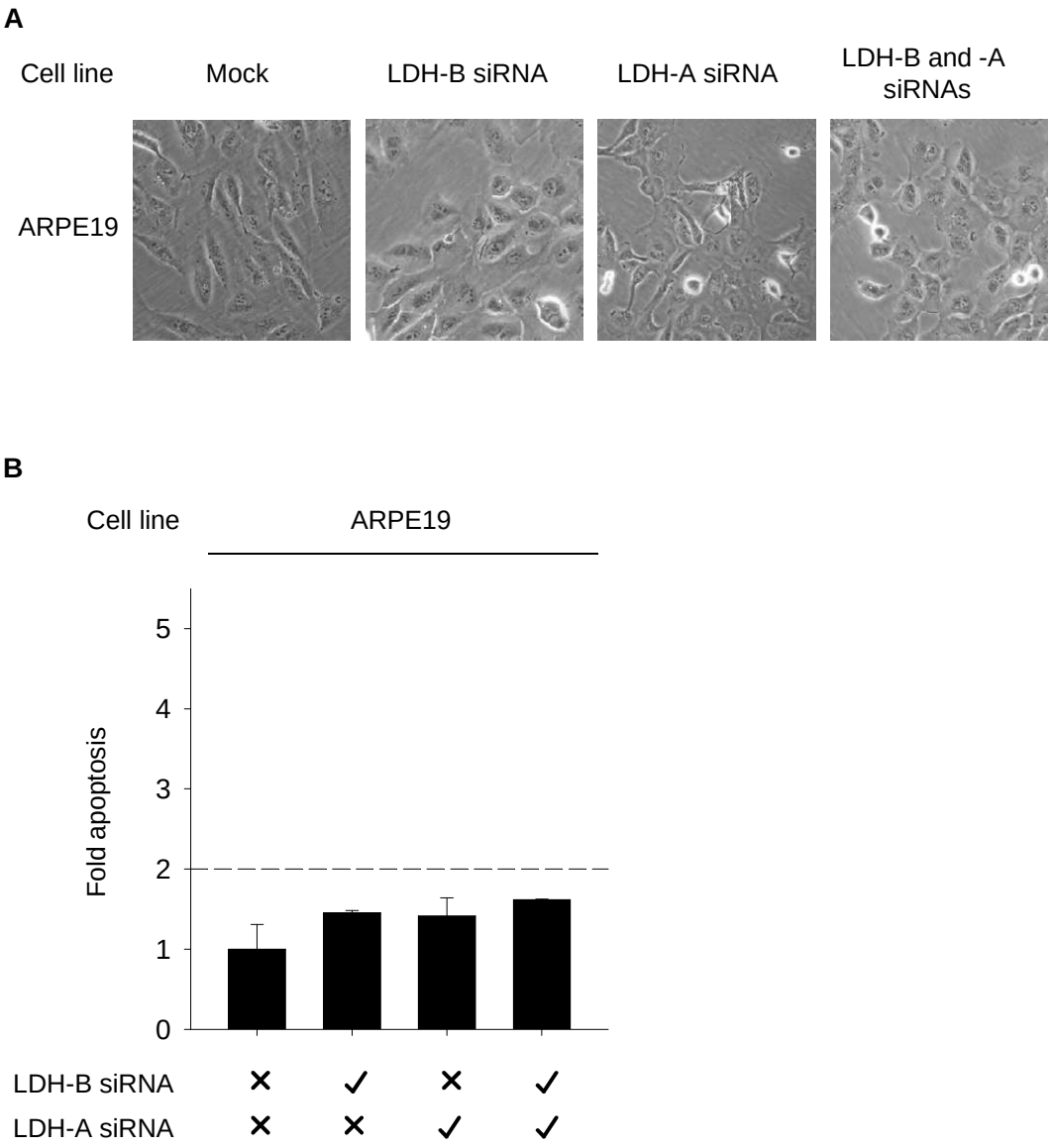

Figure 3.8: The effect of LDH isoenzyme silencing on non-cancer cell apoptosis

(A) Phase contrast microscopy at 200x magnification of the ARPE19 non-cancer cell line following independent silencing of LDH-A and LDH-B and cosilencing of the isoenzymes together. Micrographs were recorded 72 hours post siRNA transfection in all cases. **(B)** Fold apoptosis induction compared to Mock siRNA treated cells following individual LDH isoenzyme silencing and cosilencing of both isoenzymes in the ARPE19 cell line. Cells were treated with siRNA for 72 hours post-transfection and analysed by Annexin V staining and flow cytometry (See Methods).

3.5 *Influence of LDH-A silencing on SIRT1 activity*

The data so far agree with hypothesis 1, that '*LDH-A, but not LDH-B, is essential for the survival of human cancer cells'*. To understand the cellular events contributing to the apoptotic phenotype in cancer cells depleted of LDH-A, the effect on SIRT1 activity was analysed, the second hypothesis being that *'LDH-A promotes the deacetylase and cancer related anti-apoptotic activities of SIRT1'*.

3.5.1 LDH-A and acetylation of p53

SIRT1 deacetylates the tumour suppressor p53 at lysine 382, resulting in attenuation of p53 activity (Luo et al. 2001; Vaziri et al. 2001). This contributes to a constitutive cycle of acetylation and deacetylation (see *Chapter 1* and Ford et al. 2005). Silencing of SIRT1 by RNAi increases p53 acetylation as the cycle is broken and constitutive acetylation dominates. If LDH-A sustains SIRT1 activity, LDH-A silencing will manifest as an increase in p53 acetylation at lysine 382, without alteration in SIRT1 protein levels.

Silencing of LDH-A in the HCT116 and DLD1 cell lines resulted in an increase in p53 acetylation at lysine 382 compared to control and Lamin AC siRNA treated cells (Figure 3.9A and D). Total p53 levels were unchanged by LDH-A knockdown, making this a post-translation modification specific effect. Importantly, there was no effect on the expression of SIRT1 protein following LDH-A silencing. These data are consistent with LDH-A sustaining the constitutive activity of SIRT1 towards p53 protein acetylated at lysine 382.

In the non-cancer ARPE19 cell line, the silencing of LDH-A may have altered the acetylation of p53 at lysine 382 (Figure 3.9B). In comparison to the cancer cell lines, basal acetylation of p53 is low in the ARPE19 cells. A band is visible for the LDH-A lane but may or may not be present in the Mock lane given the proximity of non-specific bands above and below the band of interest. Thus, commenting on the acetylation status of p53 in the ARPE19 cell line is difficult. The effect of LDH-A silencing on p53 expression is negligible.

Lamin AC silencing reduced total and acetyl-p53 expression in the HCT116 and ARPE19 cell lines (Figure 3.9A and B). This was unexpected but is not inconsistent with the use of Lamin AC siRNA as a positive control, and lack of p53 induction under these conditions. Western blots for total p53 and acetylated p53 in the HCT116 $p53^{-/-}$ cell line returned negative as expected for this p53 null cell line.

3.5.2 Regulation of p53 target genes

p53 acts as a transcription factor, modulating gene expression. p53 promotes the expression of its own ubiquitin ligase HDM2 (Momand et al. 1992; Barak et al. 1993). The acetylation of p53 is essential for transcriptional activation of p53 tumour suppressive target genes (Tang et al. 2008). Given that p53 acetylation increases following LDH-A silencing in the HCT116, DLD1 and potentially ARPE19 cell lines, the expression of HDM2 protein was analysed.

HDM2 protein was elevated compared to Mock treatment following LDH-A silencing in both the HCT116 and ARPE19 cell lines (Figure 3.9A and B). This is consistent with an increase in p53 transcriptional activity. Importantly the induction of HDM2 was not seen in either p53 null (HCT116 $p53^{-/-}$ – Figure 3.9C) or mutant (DLD1 – Figure 3.9D) cell lines. This is a strong indication that the elevation of HDM2 expression following LDH-A silencing requires wild-type, functional p53.

The p53 expressed in the DLD1 cell line carries a mutation in the DNA-binding domain (S241F) predicted to disrupt p53 tertiary structure and reduce transactivation of target genes (Rippin et al. 2002). The results here support this. p53 in the DLD1 cell line is hyper-acetylated following LDH-A silencing (Figure 3.9C) but HDM2 protein levels are unchanged.

Together the data from Figure 3.9 indicate that 1) LDH-A suppresses p53 acetylation, but not SIRT1 protein expression, and 2) p53 acetylation correlates with HDM2 protein expression, but only in a p53 wild-type background.

3.5.3 Regulation of FOXO4 pro-apoptotic function

SIRT1 is required for survival of cancer cells with wild-type, mutant and null p53 status (Ford et al. 2005). As such, p53 is not an essential apoptotic mediator following reduction of SIRT1 activity by RNAi. The data for LDH-A presented in Section 3.4 correlates well with this published role of SIRT1; LDH-A silencing induces apoptosis in cancer cell lines of wild-type, mutant and null p53 status and is consistent with a role for LDH-A in sustaining SIRT1 activity in these cancer cell lines.

Despite an independence from p53 for the induction of apoptosis, SIRT1 silencing requires the expression of the pro-apoptotic factor FOXO4 to initiate apoptosis. Cosilencing of FOXO4 rescues apoptosis induced by SIRT1 silencing alone (Ford et al. 2005). From this, constitutive suppression of FOXO4 by SIRT1 has been inferred. To further test the hypothesis that *'LDH-A sustains the deacetylase and cancer related anti-apoptotic activities of SIRT1'*, cell fate following cosilencing of LDH-A and FOXO4 was analysed. LDH-A silencing should correlate with SIRT1 silencing in its requirement for FOXO4 expression to induce apoptosis.

Silencing of LDH-A, as previously carried out in Section 3.4, resulted in an increase in detached and refringent HCT116 cancer cells compared to Mock treated cells (Figure 3.10A). There was also a slight reduction in the number of adhered cells. The number of apoptotic cells scored by flow cytometry after LDH-A silencing increased compared to Mock treatment (Figure 3.10B), consistent with previous data in this *Chapter* (Figure 3.7A).

Following cosilencing of LDH-A and FOXO4 the number of detached and refringent cells appeared to fall slightly (Figure 3.10A). Cosilencing reduced the fold induction of apoptosis compared to Mock treatment (Figure 3.10B). This constituted a significant 1.8-fold reduction in apoptosis for cosilencing with FOXO4 compared to LDH-A silencing alone. These data support the hypothesis that *'LDH-A sustains the deacetylase and cancer related anti-apoptotic activities of SIRT1'*.

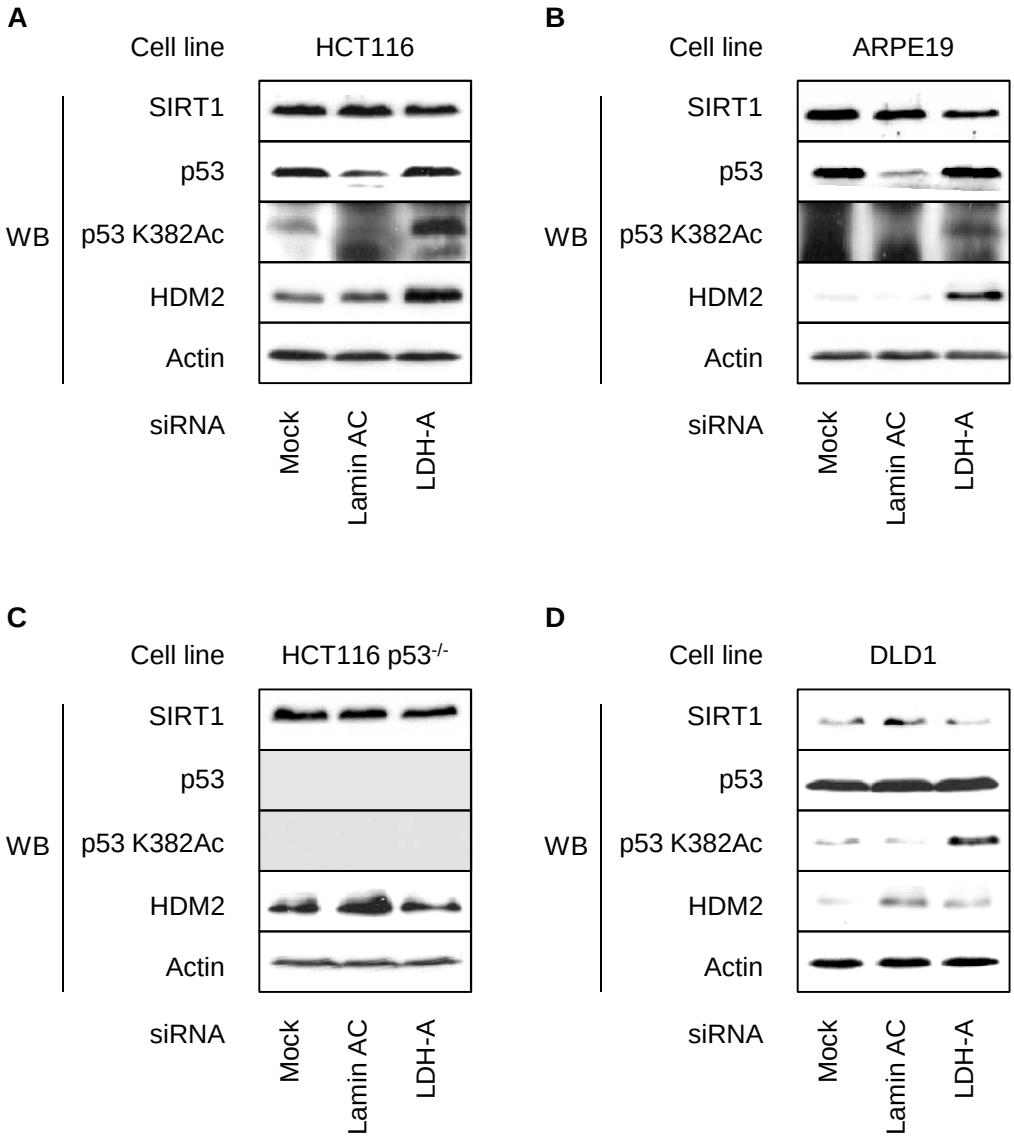

Figure 3.9: The effect of LDH-A silencing on SIRT1 and p53 protein

(A) Analysis of protein abundance by western blot following silencing of LDH-A, using Lamin AC as a positive control siRNA in the HCT116 cell lines. RNAi was carried out 48 hours prior to harvesting of cells and lysis for total protein. Protein was loaded for SDS-PAGE with equivalent mass of protein (See Methods). Actin expression was used as a loading control. **(B)** Data as for (A) for the ARPE19 cell line, harvested at 72 hours post-transfection. **(C)** Data as for (A) for the HCT116 $p53^{-/-}$ cell line, harvested at 72 hours post-transfection. **(D)** Data as for (A) for the DLD1 cell line, harvested at 72 hours post-transfection.

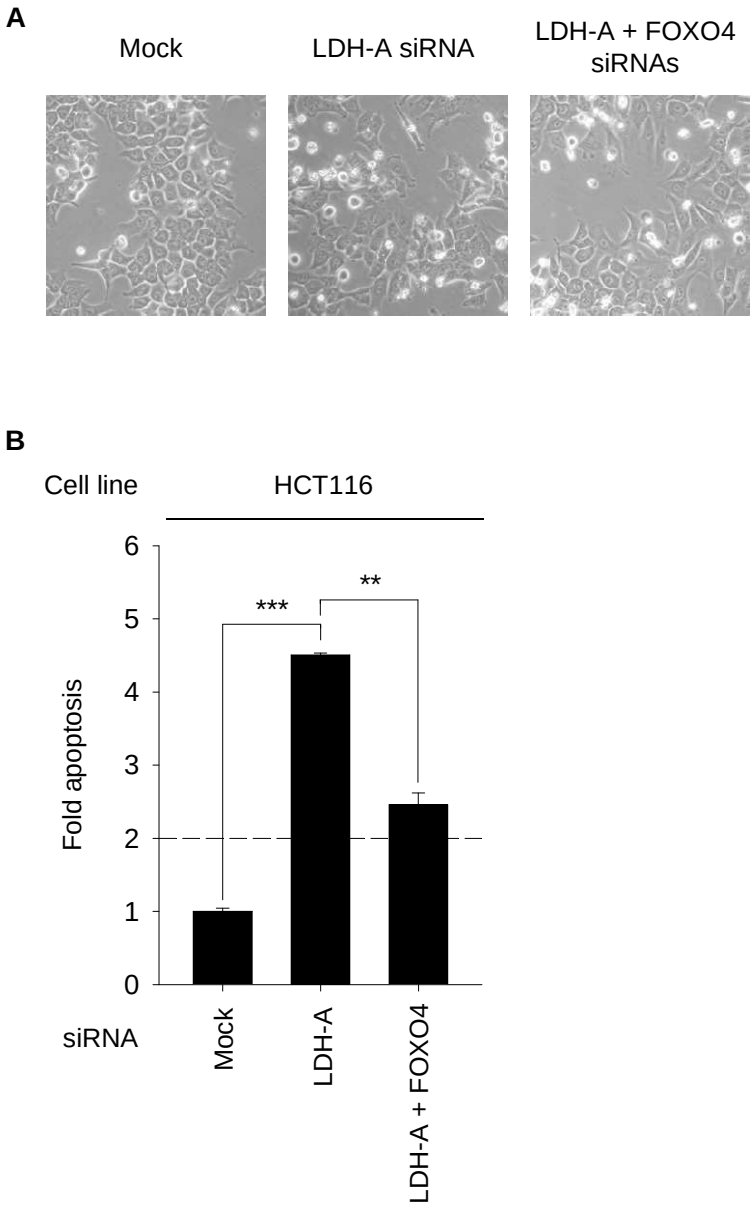

Figure 3.10: LDH-A silencing induced apoptosis is suppressed by FOXO4 silencing

(A) Phase contrast micrographs at 200x magnification of HCT116 cancer cells following silencing of LDH-A and cosilencing of LDH-A with FOXO4. Cells treated with siRNA were harvested 48 hours later and analysed by Annexin V staining and flow cytometry (See Methods). **(B)** Fold induction of apoptosis compared to Mock treated cells following the same silencing conditions in (A). *** $P<0.001$, ** $P<0.01$.

3.6 *Discussion*

3.6.1 Relative expression of the LDH isoenzymes

The literature suggests that LDH-A is the dominant isoenzyme in cancer cells (Goldman et al. 1964; Leiblich et al. 2006). The LDH antibody used here detects both isoenzymes, inviting comparison of expression levels. However, this may not be possible as the avidity of the antibody for each target may differ such that one form is favoured. This would bias the binding of one isoenzyme over the other, increasing its apparent expression. As a result, this analysis has not been carried out.

In Figure 3.5B samples from the HCT116 cancer and ARPE19 non-cancer cell lines were analysed side-by-side by western blot. This allows comparison of the relative levels of each isoenzyme between the two cell lines. Expression of LDH-A is higher in the ARPE19 cell line, and expression of LDH-B is higher in the HCT116 cell line – the inverse of the predicted expression levels for cancer and non-cancer cells. However, these are only two cell lines; a wider analysis of further cancer and non-cancer cell lines may correlate better with the literature.

In the HCT116 cell line, silencing of LDH-B reduces the protein level of LDH-A (Figure 3.5B). The effect occurs at the protein level, but not the mRNA level (Figure 3.7A). LDH forms tetramers containing both A and B isoenzymes (Markert et al. 1975). The impact of reducing one isoenzyme on the other is not known. The data presented here suggest a potential impact on isoenzyme stability with silencing of the alternate isoenzyme. Following this line of investigation fell outside the scope of the work so was not pursued.

3.6.2 LDH isoenzymes and cancer therapy

LDH-A may be a cancer specific survival factor; silencing LDH-A in five cancer cell lines induced apoptotic phenotypes, confirmed by flow cytometry in four of these lines (Figure 3.6 and Figure 3.8). In contrast, in the ARPE19 non-cancer cell line apoptosis was not recorded (Figure 3.8). Cancer cell apoptosis is specific for the LDH-A isoenzyme as silencing of the LDH-B form does not induce apoptosis in the four cell lines analysed, including both cancer and non-cancer cells. This is

consistent with the hypothesis that *'LDH-A, but not LDH-B, is essential for the survival of cancer cells'*. The role of LDH-A in promoting tumour growth and progression is well known (Shim et al. 1997; Fantin et al. 2006; Le et al. 2010), but this is the first comparison to the role of LDH-B.

The tumour suppressor p53 is lost or mutated in 50% of all tumours, and believed to be misregulated in the remaining tumours (Vogelstein et al. 2000; Olivier et al. 2010; Goh et al. 2011). Thus the independence from p53 expression for the induction of cell death is desirable for an anti-cancer therapeutic. This is the first assessment of the requirement for p53 as a pro-apoptotic mediator following LDH-A repression. The data here indicate that LDH-A targeting induced apoptosis in cancer cell lines with wild-type, mutant and null *TP53* genotypes. This adds significantly to the field and supports the anti-cancer targeting of LDH-A.

Despite this, it is difficult to definitively conclude as to cancer specificity for LDH-A survival function from the data presented here. Expansion of the non-cancer cohort of the analysis to a similar level acquired for AROS silencing in *Chapter 4* would be required for more confidence in a conclusion of cancer specificity. Nevertheless these observations are consistent with published data demonstrating that LDH-A targeting reduced tumour initiation and growth in the mouse (Fantin et al. 2006; Le et al. 2010). Importantly these reports indicated no side effects from LDH-A repression.

Furthermore, deficiency in LDH-A has been documented in the human population (Kanno et al. 1988). The genotype manifests as an exertional myopathy; patients suffer during exercise due to a build up of pyruvate, consistent with reduced LDH-A activity in promoting the Anaerobic Glycolysis Cycle. Other than this, patients lead unhindered lifestyles. The existence of LDH-A deficiency in the human population suggests that targeting the function of the protein would not cause negative side effects.

3.6.3 LDH-A and SIRT1 activity

The novel data here add to the expanding analysis of LDH-A as a therapeutic target for cancer, where it may be specific and p53 independent. The mechanism of

LDH-A tumour promotion has been linked to its role in carbon catabolism (Fantin et al. 2006), and also in the provision of NAD^+ (Le et al. 2010). Adequate NAD^+ would potentiate the Aerobic Glycolysis Cycle, but may also sustain the activity of the NAD^+-dependent enzyme SIRT1. The data here represents the first observation of a potential reduction in SIRT1 activity following LDH-A silencing.

LDH-A silencing resulted in an increase in p53 acetylation in two of the three p53-expressing cell lines analysed, with the third difficult to interpret (Figure 3.9). In each of these cell lines the levels of SIRT1 protein were unaltered. This supports the mechanism outlined in the hypothesis, where LDH-A sustains SIRT1 cancer related function. This is summarised diagrammatically in Figure 3.11. Further to this, targeting of LDH-A appears to effect p53 function. The Tang Model details increased p53 target gene transactivation potential as a result of increased acetylation (Tang et al. 2008). Increased acetylation of p53 following LDH-A silencing correlated with increased expression of the known p53 target HDM2 (Momand et al. 1992; Barak et al. 1993) (Figure 3.9). Importantly this did not occur in p53 null cells, or in p53 mutant cells, where LDH-A silencing did not correlate with increase HDM2 expression (Figure 3.11).

However The Tang Model explicitly does not apply to *HDM2* transactivation, making the data appear contradictory (Tang et al. 2008). However, the model describes p53-mediated *HDM2* transcription as being independent of acetylation (i.e. able to occur in the absence of acetylation) but does not rule out an increase upon acetylation. Indeed with p53 transactivation potential increased by acetylation it is likely that all p53 target gene transcription would be elevated upon acetylation – supporting the increase in HDM2 protein seen here.

As further evidence for a role in sustaining SIRT1 activity, LDH-A suppresses the pro-apoptotic signalling of FOXO4 in cancer cells (Figure 3.10), summarised in Figure 3.11. This is a well documented cancer related function of SIRT1 (Ford et al. 2005). This correlation in function between SIRT1 and LDH-A, and the observation that LDH-A suppresses p53 acetylation, supports the hypothesis that '*LDH-A sustains the deacetylase and cancer related anti-apoptotic activities of SIRT1'*.

3.6.4 Mechanisms of LDH-A promotion of cancer cell survival

LDH-A is required for cancer cell survival, with evidence here suggests suggesting that this may occur via facilitation of SIRT1 activity. However, the data do not exclude LDH-A promoting cancer cell survival via alternative mechanisms. The metabolism of cancer cells is commonly altered, such that LDH-A is crucial for the regeneration of NAD^+ to potentiate Aerobic Glycolysis (Figure 3.1A – right panel). Knockdown of LDH-A may therefore render cancer cells unable to generate sufficient ATP, which would undoubtedly be detrimental to their viability. LDH-A inhibition may provide a means to target the metabolic phenotype of cancer as well as the aberrant signalling pathways promoted by SIRT1.

It is possible that LDH-A sustains other non-glycolytic NAD^+-dependent enzymes to promote cancer cell survival. Of the known non-glycolytic NAD^+-dependent enzymes few have known biological roles in humans. The sirtuins and the poly(ADP)-ribose polymerase enzymes represent the two well characterised groups of NAD^+-dependent enzymes. Of the sirtuins, SIRT1 in cancer is well documented (See *Chapter 1*). However, the other sirtuins, SIRT2-7, are all NAD^+-dependent (Landry et al. 2000), and will probably be modulated by NAD^+ availability. The broad role of the sirtuins in cancer and longevity has been previously discussed (Saunders and Verdin 2007). Sirtuins 2, 4, 5 and 7 have documented roles in a range of biological activities, but with little implication in cancer beyond reports of chromosomal abnormalities at their loci in certain malignancies (Alhazzazi et al. 2011). However, SIRT3 and SIRT6 have been implicated, particularly in the context of cancer metabolism.

3.6.4.1 SIRT3:

SIRT3 has been implicated as both a tumour suppressor and promoter, according to cancer type and context (Alhazzazi et al. 2011). Functionally, SIRT3 is the dominant deacetylase in mitochondria (Lombard et al. 2007), regulating mitochondrial carbon metabolism and energy production. Despite evidence that SIRT3 suppresses mitochondrial p53 function (Li et al. 2010), strong evidence indicates that SIRT3 *promotes* apoptotic signalling pathways (Allison and Milner 2007). Further to this, SIRT3 suppresses metabolic reprogramming in cancer via

negative regulation of HIF1α (Finley et al. 2011). *LDH-A* is a target of HIF1 (Firth et al. 1995), meaning SIRT3 may suppress *LDH-A* transcription. These data suggest that, although not formally analysed, it is unlikely that SIRT3 is sustained by LDH-A to promote cancer cell survival.

3.6.4.2 SIRT6:

SIRT6 has also been implicated in the choice between Oxidative Phosphorylation and the Glycolysis Cycle (Zhong and Mostoslavsky 2010). Of note in this putative model, SIRT6 influences HIF1 in the transactivation of the *LDH-A* gene. This is based on upregulation of *LDH-A* expression in SIRT6 knockout embryonic stem cells (Zhong et al. 2010). However, this is non-specific as the *LDH-B* gene is also upregulated in the same analysis, by an unknown mechanism. Thus the role of SIRT6 in regulating carbon metabolism remains unclear, as does a role in the altered metabolism of cancer.

SIRT6 regulates histone 3 by deacetylation of lysine 9 (Michishita et al. 2008). This activity maintains chromosomal integrity at telomeres, and suppresses ageing-related NF-κB signalling (Michishita et al. 2008; Kawahara et al. 2009), potentially contributing to genomic instability and premature aging in SIRT6 knockout mice (Mostoslavsky et al. 2006). However, SIRT6 has not been implicated in pro- or anti-apoptotic signalling. As for SIRT3, this makes it unlikely that LDH-A sustaining SIRT6 function promotes cancer cell survival. This brings greater significance to the data here relating to the role of LDH-A in sustaining SIRT1 activity.

3.6.4.3 Poly(ADP)-ribose polymerases:

The poly(ADP)-ribose polymerase (PARP) enzymes, of which 18 have been discovered by sequence homology analysis (Schreiber et al. 2006), are also NAD^+-dependent enzymes. PARP-1 and PARP-2 participate in the DNA damage response, promoting DNA repair and the induction of apoptosis when appropriate (Krishnakumar and Kraus 2010). A role for PARP-3 in DNA repair has also emerged, suggesting that the PARP enzymes may specialise in DNA repair (Boehler et al. 2011). The effect of the postulated reduction in NAD^+ availability following

LDH-A silencing would be a reduction in the pro-apoptotic activity of the PARP proteins. This is contradictory to the data here where LDH-A has an anti-apoptotic role. As such, it seems unlikely that LDH-A suppression of apoptosis occurs via the PARP enzymes.

The published data for these NAD^+-dependent enzymes adds to the hypothesis that *'LDH-A sustains the deacetylase and cancer related anti-apoptotic activities of SIRT1',* and not other NAD^+-dependent enzymes. The roles of SIRT3 and SIRT6 in carbon metabolism have parallels with emerging roles for SIRT1.

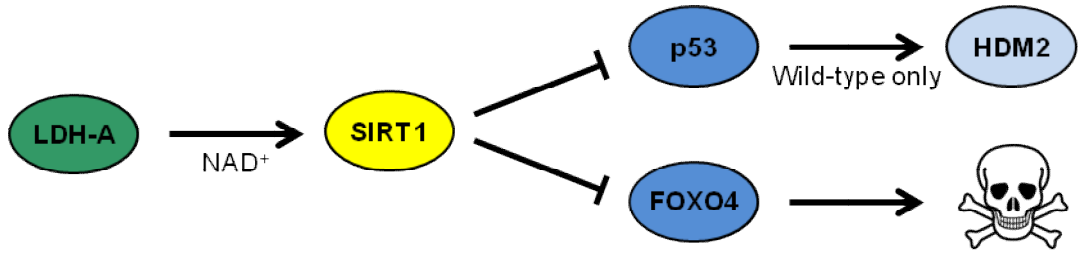

Figure 3.11: Schematic of the role of LDH-A in sustaining SIRT1 activity

LDH-A sustains SIRT1 activity in cancer cells. LDH-A silencing removes the suppression of p53 acetylation, resulting in p53 hyper-acetylation. Wild-type p53 expression results in increased HDM2 protein expression. FOXO4 pro-apoptotic activity is suppressed by SIRT1. LDH-A also suppresses FOXO4, consistent with LDH-A sustaining this function of SIRT1.

3.7 *Conclusions*

1. LDH-A is required for the survival of a panel of cancer cell lines but not for a non-cancer cell line.
2. LDH-A suppresses apoptosis in cancer cell lines independent of p53 status – wild-type, mutant or null.
3. LDH-B is *not* required for survival of any of the cell lines analysed, cancerous or non-cancerous.
4. LDH-A appears to sustain SIRT1 activity in cancer cells:
    a. p53 acetylation increases following LDH-A silencing, consistent with decreased constitutive deacetylation by SIRT1.
    b. Increased p53 acetylation correlates with an increase in the p53 target gene product HDM2, in the presence of wild-type p53.
    c. LDH-A suppresses FOXO4 pro-apoptotic signalling, correlative with SIRT1 suppression of FOXO4.

4 Regulation of SIRT1 activity by AROS

4.1 *Overview*

This *Chapter* describes the initial investigations of the protein AROS. The expression and conservation of AROS is detailed and targeting of AROS by selective RNAi is achieved. Differences in the role of AROS are revealed between basal and stress conditions, suggesting that the AROS-SIRT1 interaction is more complicated than obligate activation. Multiple cell lines are used throughout the *Thesis*, which are each analysed within this *Chapter*. This allowed the comparison of data between the lines, revealing further differences in the role of AROS in SIRT1 activation.

The *Chapter* also introduces the work undertaken and the methodologies used. Conclusions are drawn regarding the role of AROS in SIRT1 activation, specifically in the suppression of p53. This links to *Chapter 5*, which extends the data presented here to analyse cell phenotype following AROS silencing, and considers FOXO4 as a further target of SIRT1.

4.2 *Introduction*

4.2.1 Active Regulator Of SIRT1

AROS was first identified in a yeast two hybrid screen as a protein that interacts with the ribosomal protein RPS19 (Maeda et al. 2006). This was observed in murine cells and the interaction was mapped to residues 81 to 142 of murine AROS (Figure 4.1). In this context AROS was termed RPS19 binding protein 1, or RPS19BP1. For clarity it shall be referred to as AROS throughout this work. AROS was expressed in all tissues analysed and localised to the nucleus of Cos-7 cells (Maeda et al. 2006). AROS has also been observed in the nuclei of human cells (Kim et al. 2007). Further, in some cells AROS localised to foci within the nuclei, which were speculated to be nucleoli by the authors (Maeda et al. 2006; Kim et al. 2007).

No function has been attributed to the interaction between AROS and RPS19. However, a later analysis of RPS19 phosphorylation revealed modulation of the AROS-RPS19 interaction by CaM kinase Iα (Maeda et al. 2009). Phosphorylation of RPS19 at serines 59 and 90 promoted the interaction with AROS in rat and human cells (Figure 4.1). Human AROS is a relatively small protein at 136 amino acids in length and only 15.4kDa. It was first characterised in relation to the function of SIRT1.

4.2.2 AROS and SIRT1

AROS was termed Active Regulator Of SIRT1 due to its functional interaction with the NAD^+-deacetylase SIRT1 (Kim et al. 2007). This interaction is specific for SIRT1 protein, with no interaction observed between AROS and the other 6 human sirtuins. The AROS binding site was mapped to a region distal to the SIRT1 active site (Figure 4.1). A subsequent *in silico* structural analysis predicted this location for the AROS interaction, and suggested that AROS causes a conformational change in SIRT1 protein upon binding (Figure 3.1 and Autiero et al. 2009).

The AROS-SIRT1 interaction and associated allosteric alteration in SIRT1 suggest that AROS influences SIRT1 activity. Among other targets, SIRT1

deacetylates lysine residue 382 of the tumour suppressor p53 (Luo et al. 2001; Vaziri et al. 2001). This occurs as part of a constitutive cycle of acetylation and deacetylation, such that loss of SIRT1 results in hyper-acetylation of p53 (Ford et al. 2005). By assaying the activity of SIRT1 as inversely proportional to the acetylation of p53 at lysine 382, AROS was identified as an activator of SIRT1 activity (Kim et al. 2007). This observation was used to identify AROS as the first protein-level regulator of SIRT1 activity; however the full extent of regulation of SIRT1 by AROS required further investigation. This is the purpose of *Chapters 4 and 5* here where a more detailed investigation of the AROS-SIRT1 relationship was undertaken.

AROS was identified as a positive regulator of SIRT1 via analysis of the acetylation status of SIRT1 targets, namely p53 (Kim et al. 2007). The acetylation status of p53 was assumed to be inversely correlative with SIRT1 activity. Thus, overexpression of AROS reduced p53 acetylation, but only in the presence of SIRT1. However, it is important to note that the conclusion that AROS activates SIRT1 was based on experimental data where human cells were subjected to applied stress in the form of etoposide and trichostatin A drug treatment (Kim et al. 2007) . These chemical agents induce DNA-damage and increase p53 acetylation respectively (Chen et al. 1984; Yoshida et al. 1990). As such, the conditions where AROS was identified as an activator of SIRT1 activity cannot be considered physiological. Furthermore, these conditions are likely to have induced acetylation of p53, which may be regulated differently by AROS than under normal physiological conditions. Thus, an initial aim of the analyses was to clarify the role of AROS in SIRT1 activation under physiological/basal conditions. For this, transient RNAi against AROS was used, which is possible under basal conditions (See *Methods* and Ford et al. 2005; Ahmed and Milner 2009).

A further line of investigation was identified as the regulation of SIRT1 targets other than p53. SIRT1 regulates a diverse range of proteins via deacetylation at specific lysine residues (for a recent review see Knight and Milner 2011). AROS has been characterised in its suppression of p53 acetylation via SIRT1 (Kim et al. 2007), however whether AROS regulates further SIRT1 targets is not know. This raises the possibility that AROS is not an obligate activator of SIRT1, perhaps acting

to specifically promote SIRT1 function towards specific targets such as p53. To this end, AROS regulation of FOXO4 is analysed as a second target of SIRT1 in *Chapter 5*.

To gain a wider appreciation of the role of AROS in suppression of p53 a range of cell lines of both cancer and non-cancer origin (see *Methods* for full details) were analysed following silencing of AROS. This was carried out under basal conditions, as well as following the application of both drug and irradiation induced stress.

4.2.3 Hypotheses

1. The *AROS* gene is widely expressed in humans and has orthologues in other species.
2. The regulation of SIRT1 by AROS is complex. This will be analysed in terms of:
    a. cell line dependent effects,
    b. cell context dependent effects.

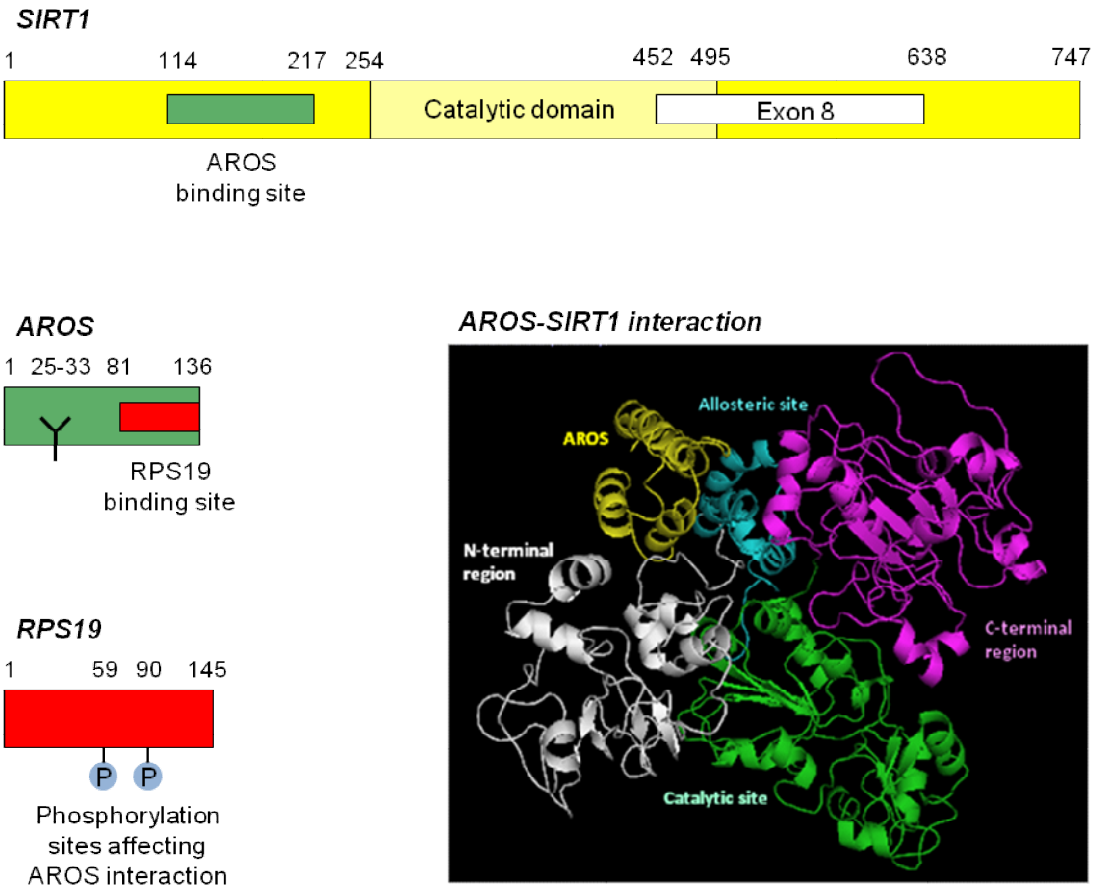

Figure 4.1: Schematics of SIRT1, AROS and RPS19 proteins

To scale annotated schematic representations of the SIRT1, AROS and RPS19 protein primary sequences. SIRT1 shows the mapped AROS binding site (114-217), the conserved catalytic core (254-495) and position of Exon 8 (452-638) which is important for later *Chapters* (Lynch et al. 2010). The AROS sequence shows the residues recognised by the Kim et al antibody (2007), and those required for interaction with RPS19 (Maeda et al. 2006). RPS19 shows the serine residues (S59, S90) which augment the AROS-RPS19 interaction upon phosphorylation (Maeda et al. 2009). Inset shows the predicted interaction between AROS and SIRT1. AROS is in yellow, with SIRT1 domains annotated in white, green and magenta. Turquoise represents the AROS-interacting allosteric site of SIRT1 (Autiero et al. 2009).

4.3 *Initial analyses of AROS*

4.3.1 Conservation of AROS in animalia

The AROS protein is conserved across animalia, with high levels of conservation between closely related species (Figure 4.2). Most striking is the 100% sequence identity between the human and chimpanzee forms of the protein. Human AROS retains almost 75% identity to all mammalian forms of the protein analysed, with lower sequence identity seen to AROS orthologues from other animal kingdoms. Also of note is the 87.4% identity between the mouse and rat orthologues of AROS.

Database searches found AROS in all vertebrate branches of the animal kingdom; birds, reptiles, fish, amphibians and marsupials (Figure 4.2). An AROS orthologue was found in the species *Brachiostoma floridiae*, one of the simplest vertebrates known and a model organism for chordate development (Yu et al. 2007). This organism is believed to represent the earliest divergence of vertebrates from invertebrates, and shares sequence identity with many invertebrate genes. AROS also has orthologues in invertebrate species, such as the pea aphid (*Acyrthosiphon pisum*), suggesting that AROS is conserved in invertebrates as well as vertebrates (Figure 4.2).

Interestingly, no orthologue of AROS could be found outside the animal kingdom. Fellow eukaryotes, the fungi and plants do not have an AROS orthologue, neither do any species of bacteria or archaea analysed. This indicates that AROS is a conserved protein only among animalia.

Sirtuin orthologues are found in eukaryotes, most archaea and bacteria species (Greiss and Gartner 2009). However, specific SIRT1 orthologues are only found in animalia and some fungi – no SIRT1 orthologues were reported in plants, archaea or bacteria. *SIRT1* conservation in animalia is thus similar to the status of *AROS*, however the *SIRT1* gene may appear in the absence of *AROS* in some species of fungi. Animal species outnumber fungal species by around 10:1 (Blackwell 2011). This implies that the majority of species with a *SIRT1* orthologue also bear an *AROS* gene and indicates the potential for co-evolution of the two genes in animalia.

4.3.2 Human homologues of AROS

AROS is not a member of a gene family. Sequence identity searches for the *AROS* mRNA returns only three human genes above 50% identity (Figure 4.3). This identity is modular based on regions of the alternative gene that have identity to the full *AROS* sequence. These 3 genes have no unifying function, although two (REV3 and Spinophilin) are both subunits of larger enzymatic machines. This has partial parallels to the role of AROS as a regulator of SIRT1 activity; although it seems likely that this similarity is coincidental.

4.3.3 Expression of *AROS* mRNA and protein

AROS was ubiquitously expressed across a representative panel of human tissues (Figure 4.4A). Expression was comparable between tissues with no large variation between samples. Consistent with wide expression, searching the online gene expression database 'RefExA' revealed expression in all cell lines and tissues analysed (http://www.lsbm.org). *RPS19* was also expressed in all of the tissues analysed, both here (Figure 4.4A) and in the 'RefExA' database. This is consistent with its role as an essential ribosomal protein gene. *SIRT1-FL*expression has been reported in the same panel (Lynch et al. 2010), similar to the expression of *AROS*.

With wide RNA expression of *AROS* the relative levels of the protein were analysed in a panel of human cell lines from the colorectal epithelium (HCT116, DLD1, LoVo), mammary gland epithelium (MCF10A, MCF7), retinal pigmented epithelium (ARPE19) and lung fibroblast (WI38). AROS was expressed in all eight cell lines analysed, but with high variability (Figure 4.4B). Expression was lowest in the WI38 line, being undetectable in these images. However AROS was detected in WI38 cells in later experiments (Figure 4.9). AROS expression was also low in the MCF10A and MCF7 cell lines. AROS protein expression was greatest in the HCT116 and ARPE19 cell lines. These two cell lines form the basis of experiments in the *Thesis*, with the other six cell lines analysed where appropriate.

Despite the varied expression of AROS this could not be correlated with the expression of its two known binding partners. SIRT1 was expressed in each of the cell lines (Figure 4.4B), with expression highest in the five cancer cell lines (Lanes

4-8) and lower in the three non-cancer cell lines (Lanes 1 to 3). This correlates well with the role of SIRT1 as a cancer cell survival factor (see *Chapter 1* and Ford et al. 2005), but does not correlate with the expression of AROS across the panel of cell lines. Similarly, RPS19 protein was expressed across all cell lines analysed (Figure 4.4B). RPS19 expression was similar in each cell line and did not correlate with the expression of AROS.

Expression of p53 was extremely variable between cell lines (Figure 4.4B). As expected no p53 protein was observed in the HCT116 $p53^{-/-}$ cell line where the p53 gene is disrupted (Bunz et al. 1998). The p53 protein expressed in the DLD1 cell line carries a mutation leading to substitution of serine 241 to a phenylalanine (Rippin et al. 2002). Despite this p53 is expressed at a similar level to cell lines from colorectal adenocarcinomas. Indeed p53 expression was high in the three colorectal adenocarcinoma cell lines – HCT116, DLD1 and LoVo – (Lanes 4, 7 and 8) with lower expression seen in the cell lines from other origins. The variable expression of p53 did not correlate with the variability in AROS expression.

	Acyrthosiphon pisum	*Branchiostoma floridae*	*Xenopus laevis*	*Anolis carolinensis*	*Danio rerio*	*Gallus gallus*	*Ornithorhynchus anatinus*	*Mus musculus*	*Rattus norvegicus*	*Macaca mulatta*	*Pan troglodytes*
Homo sapiens	22.9	28.0	31.3	42.1	33.4	45.7	19.0	74.8	75.2	95.6	100.0
Pan troglodytes	22.9	28.0	31.3	42.1	33.4	45.7	19.0	74.8	75.2	95.6	
Macaca mulatta	23.4	27.8	31.1	42.5	32.6	46.1	19.7	72.7	73.0		
Rattus norvegicus	23.1	26.1	32.0	43.9	31.7	47.6	19.5	87.4			
Mus musculus	19.5	27.7	29.7	42.7	31.3	47.6	19.4				
Ornithorhynchus anatinus	9.2	13.4	18.0	20.3	11.5	22.7					
Gallus gallus	25.0	32.5	35.6	52.1	30.9						
Danio rerio	20.8	24.8	28.2	31.3							
Anolis carolinensis	25.5	34.0	39.5								
Xenopus laevis	22.0	36.4									
Branchiostoma floridae	20.5										

Figure 4.2: Conservation of AROS protein

The sequence of human AROS (NP_919307) was used in a BLAST search against all published sequences. Sequences annotated as orthologous to AROS were used for alignment in Vector NTI to generate percentage sequence identity data shown in the table. Mammalian species were: *Homo sapiens* (Human), *Pan troglodytes* (Chimpanzee), *Macaca mulatta* (Rhesus macaque), *Rattus norvegicus* (Laboratory rat) and *Mus musculus* (Laboratory mouse). Marsupial species: *Ornithorhynchus anatinus* (Platypus). Bird species: *Gallus gallus* (Domesticated chicken). Fish species: *Danio rerio* (Zebrafish), Reptile species: *Anolis carolinensis* (Carolina anole lizard). Amphibian species: *Xenopus laevis* (African clawed frog). Invertebrate species: *Acyrthosiphon pisum* (Pea aphid). *Branchiostoma floridae* (Lancelet) as discussed.

Protein	*Identity to AROS*	*Function*
REV3	79.0%	Catalytic subunit of DNA polymerase zeta subunit
Mat3Bb homologue	71.0%	Regulator of cell cycle progression
Spinophilin	55.0%	Regulatory subunit of protein phosphatase 1

Figure 4.3: Homologues of AROS mRNA

(B) The sequence of human *AROS* (NM_194326) was used in a BLAST search against all human mRNAs. The table lists the 3 genes which returned sequence identity higher than 50% and a brief description of gene function.

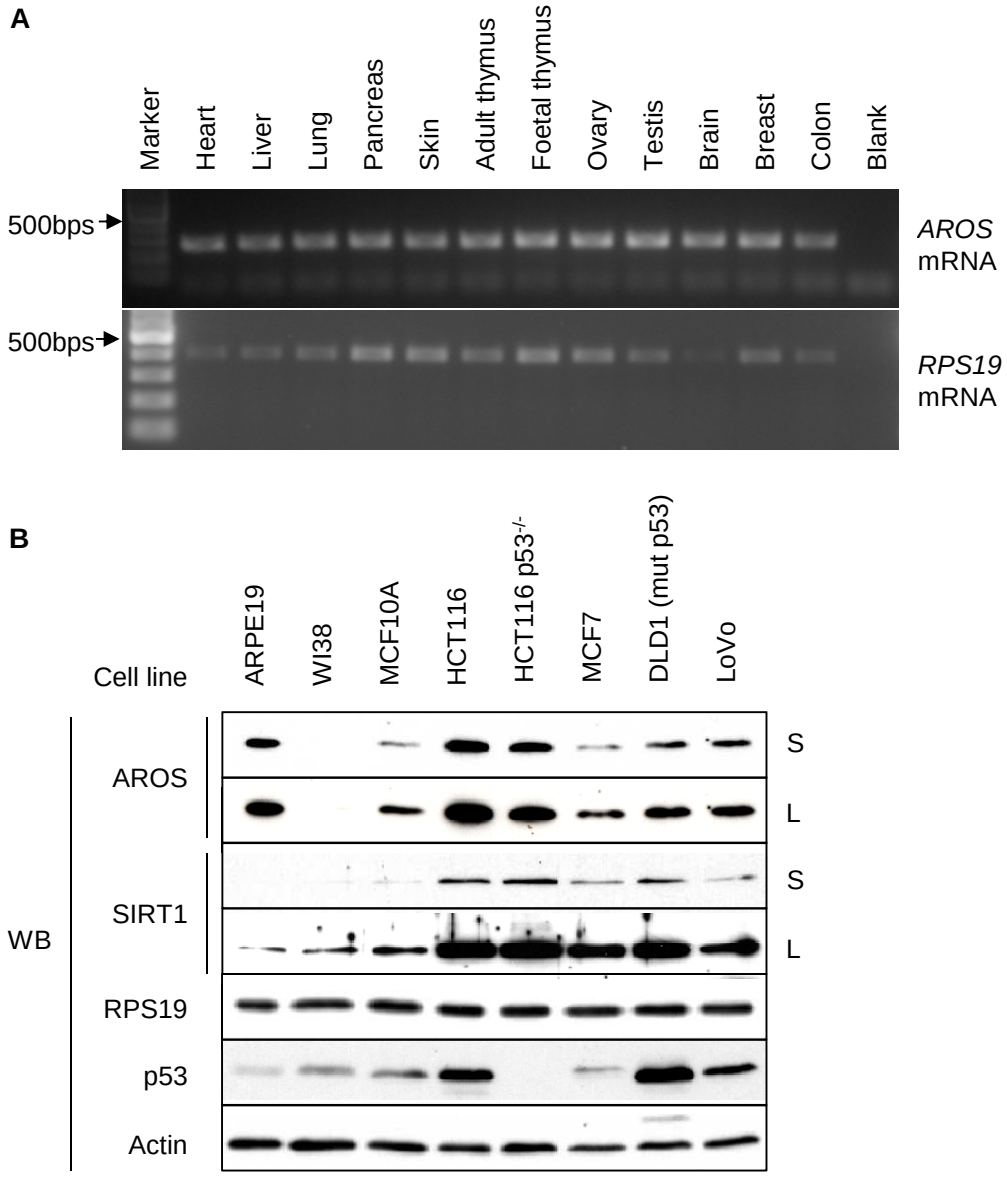

Figure 4.4: Expression of human AROS mRNA and protein

(A) Expression of *AROS* and *RPS19* mRNAs across a representative panel of human cell lines (AMS Biotechnology). Data represents agarose gel separated cDNA from RT-PCR using specific primers against each mRNA (see *Methods*). Visualisation was by transillumination of ethidium bromide intercalated into the cDNA. 'Blank' represents RT-PCR in the absence of template RNA. **(B)** Expression of proteins across a panel of human cell lines. All samples were Mock treated in siRNA transfection and harvested at either 48 or 72 hours post-transfection. The ARPE19, WI38 and MCF10A represent non-cancer cell lines, whereas the HCT116, HCT116 $p53^{-/-}$, MCF7, DLD1 and LoVo cell lines are all of cancerous origin. Equivalent protein was loaded by mass, as calculated by the Pierce BCA method. 'Blank' represents RT-PCR in the absence of template RNA.

4.4 *Targeting of AROS by RNAi*

Silencing of *AROS* mRNA was achieved in the HCT116 and ARPE19 cell lines using two independent siRNAs (Figure 4.5). Both siRNAs reduced *AROS* mRNA expression to below 15% of Mock expression. In both cell lines AROS siRNA 1 was more effective. Parallel RNAi against *SIRT1* specifically reduced *SIRT1* mRNA levels, as did transfection of the positive control siRNA against *Lamin AC*, reducing *Lamin AC* mRNA. Importantly the silencing in all cases was specific, with the expression of each mRNA only reduced by transfection of the complementary siRNA.

Silencing of SIRT1 and Lamin AC translated to the protein level in the HCT116 cells (Figure 4.6A). However, total AROS protein levels were not reduced by RNAi with either independent siRNA. Total AROS protein expression may have been partially reduced but not to the extent seen for Lamin AC or SIRT1, or the extent expected given the efficient mRNA silencing seen in Figure 4.5A. This Subcellular fractionation of the HCT116 cells was used to analyse the effect of AROS siRNA 1 within different fractions of the cells. AROS siRNA 1 treatment reduced the expression of nuclear AROS but had little effect on AROS present in the cytoplasmic fraction (Figure 4.6B). It appears likely that the cytoplasmic fraction contributed to the persistence of total AROS protein. Cytoplasmic localisation of AROS has not been previously reported, making this a novel population of the protein to the field.

Similar to the HCT116 cell line, targeting of Lamin AC, SIRT1 and AROS (with siRNA 1) in the ARPE19 non-cancer cell line specifically reduced target protein expression (Figure 4.6C). AROS siRNA 2 did not reduce AROS protein expression, again despite efficient mRNA knockdown (Figure 4.5B). Subcellular fractionation following AROS siRNA 1 transfection confirms that all fractions of AROS are reduced by RNAi, giving the total protein level loss observed (Figure 4.6D). This fractionation also indicates that the novel cytoplasmic population of AROS is present in high quantity in the ARPE19 cell line.

The reason for greater efficacy of AROS siRNA 1 compared to siRNA 2 is not known. The two siRNAs target regions just 128bps apart within *AROS* mRNA. The siRNAs target neighbouring exons, exon 3 (siRNA 2) and exon 4 (siRNA 1). It is possible that the differential in efficiency is attributable to protection of *AROS* mRNA either by nucleotide base pairing or mRNA-protein interactions. Nevertheless, with AROS siRNA 1 appearing the most effective at silencing AROS, at least at the mRNA level, this was used throughout the analyses in the *Thesis*.

Targeting of AROS did not alter the protein abundance of SIRT1 in the HCT116 cancer, or ARPE19 non-cancer cell lines, and vice versa (A and C). This is consistent with the reported role of AROS in regulation of SIRT1 (Kim et al. 2007), and indicates that any effect AROS has upon SIRT1 activity is not due to alterations in SIRT1 endogenous protein level. With this noted the effect of AROS upon SIRT1 activity was analysed, using p53 acetylation status as an assay.

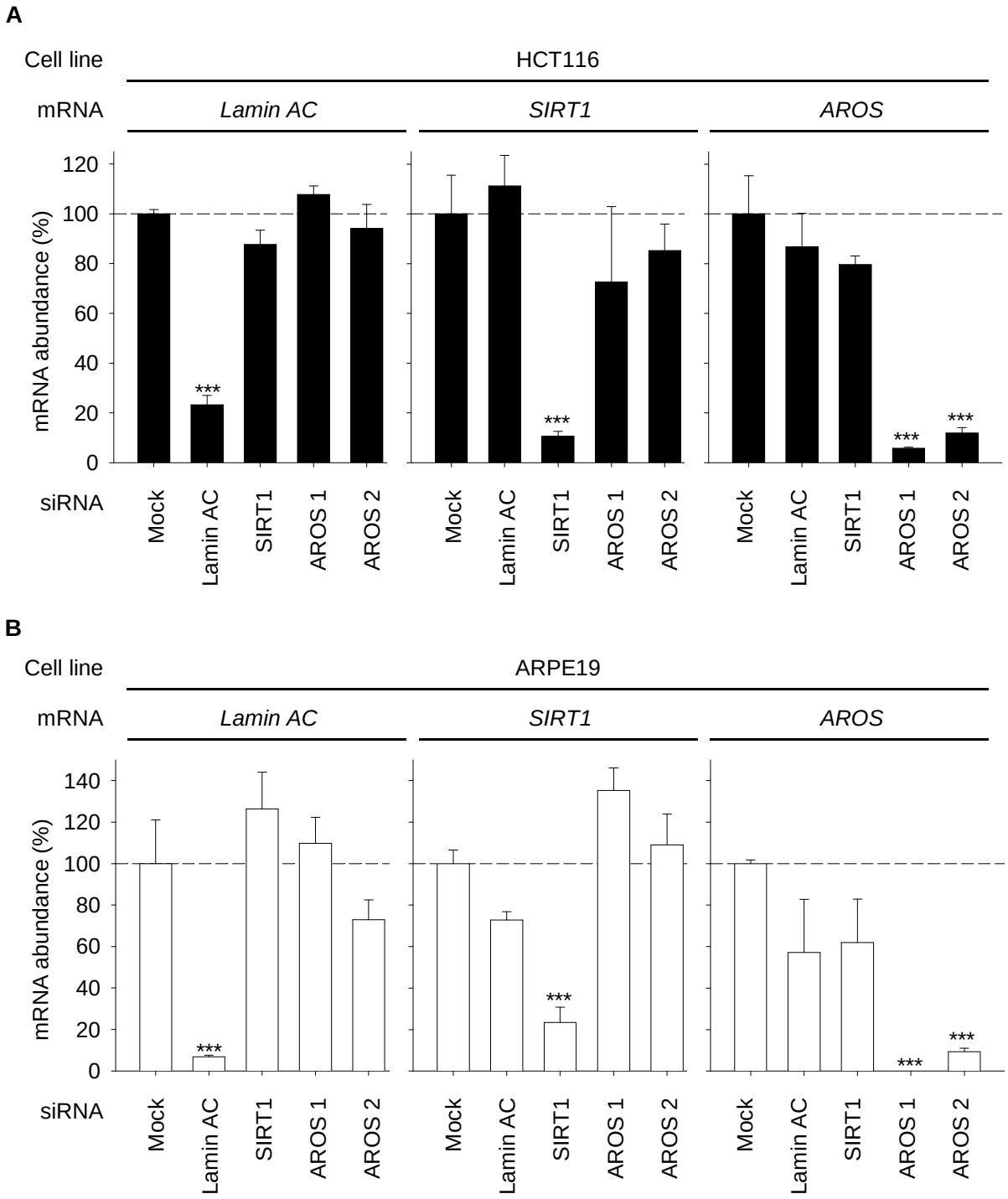

Figure 4.5: RNAi against AROS mRNA

(A) Quantification of mRNA following RNAi against Lamin AC, SIRT1 or AROS (2 independent siRNAs). HCT116 cancer cells were transfected with siRNA as indicated, harvested 48 hours post-transfection. RNA was isolated by RNeasy method and qRT-PCR carried out as indicated (See *Methods*). **(B)** Quantification of mRNA as in (A). ARPE19 non-cancer cells were harvested 72 hours post-transfection. *** P<0.001

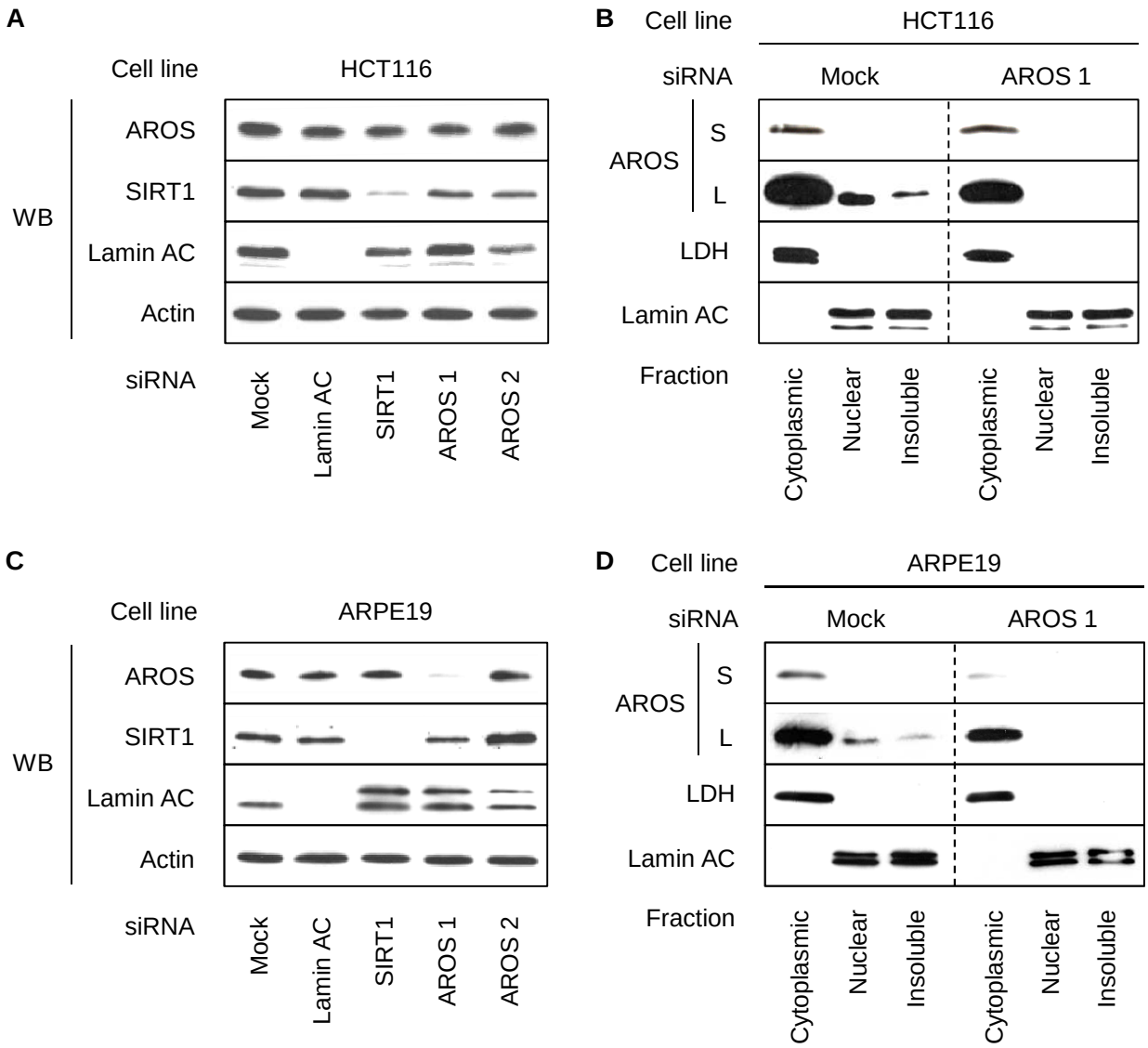

Figure 4.6: AROS protein knockdown following RNAi

(A) Analysis of target protein abundance following RNAi in HCT116 cancer cells. Cells were transfected with siRNA as indicated, harvested 48 hours post-transfection and lysed in protein lysis buffer (see *Methods*). Equivalent protein by mass was analysed and Actin expression used as a loading control. **(B)** Subcellular localisation of AROS protein following fractionation of HCT116 cancer cells according to Pierce protocol (see *Methods*). Cells were treated with siRNA for 48 hours prior to harvesting. LDH is used as a cytoplasmic marker protein, and Lamin AC as a nuclear marker protein. **(C)** Analysis of protein abundance from RNAi analysis as in (A) for the ARPE19 non-cancer cell line, harvested at 72 hours post-transfection. **(D)** Subcellular localisation of AROS and the effect of AROS siRNA as in (B) for the ARPE19 cell line, harvested 72 hours post-transfection.

4.5 *The effect of AROS on SIRT1 activity*

4.5.1 AROS suppression of p53

Under basal conditions in the HCT116 cancer cell line SIRT1 is known to constitutively suppress p53 acetylation (Ford et al. 2005). This result was repeated here, with silencing of SIRT1 resulting in an increase in p53 acetylation and total p53 levels (Figure 4.7A). In contrast, parallel use of AROS siRNA in the HCT116 cells did not stabilise either total or acetylated p53 compared to Mock treatment (Figure 4.7A). This appears to disagree with the previously published role of AROS as an activator of SIRT1 activity (Kim et al. 2007) and is the first indication that *'the regulation of SIRT1 by AROS is complex'*. As outlined in the *Introduction*, the reason for this disparity may be different cellular contexts used. Here under basal conditions AROS does not appear to be required for SIRT1 activity, whereas in the original analysis AROS was required following the application of stress.

AROS silencing in the ARPE19 non-cancer cell line gave inconclusive results regarding the modulation of p53 acetylation (Figure 4.7B). Acetylation of p53 in this non-cancer cell line is constitutively low, especially under these basal conditions. Thus, although bands could be detected upon long exposure these are difficult to interpret with confidence. Taking the lower band as acetylated p53 the trend appears to be an increase in acetylation following silencing of either SIRT1 or AROS compared to Mock treatment (Figure 4.7B). Partly consistent with this, total p53 protein levels appeared to increase following AROS silencing but not SIRT1 silencing. This may indicate that in the ARPE19 cell line under basal conditions that AROS suppresses p53, presumably via activation of SIRT1. This is in agreement with the work of Kim and colleagues (2007).

The potential for complexity in the regulation of p53 by AROS lead to the combinatorial silencing of SIRT1 and AROS in the HCT116 cell line (Figure 4.7C). SIRT1 protein was depleted by both individual (lane 2) and combinatorial (lane 4) siRNA application. AROS protein exhibited partial resistance to siRNA treatment where used (lanes 3 and 4) as reported above. Individual silencing of SIRT1 again increased the total and acetylated levels of p53 compared to Mock, whereas individual targeting of AROS had little effect on p53 (Figure 4.7C). This agrees with

the data in Figure 4.7A. Interestingly, combinatorial silencing of SIRT1 and AROS appeared to have a reduced effect on p53 acetylation compared to SIRT1 silencing alone, despite similarly efficient reduction in SIRT1 protein expression (Figure 4.7C). This is consistent with the regulation of AROS by SIRT1 being more complex than originally reported.

Densitometry standardised against actin expression from two independent biological replicates allowed statistical analysis of the difference in p53 acetylation shown in Figure 4.7C. Densitometry quantified the increase in p53 acetylation following SIRT1 knock down as greater than 2.5-fold (Figure 4.7D). In contrast targeting of AROS had no significant effect upon acetylation of p53. Interestingly, densitometry indicated that the cosilencing of AROS with SIRT1 did not result in the stabilisation of p53 acetylation (Figure 4.7D). This is in contrast to the effect of single SIRT1 silencing and the reported role for AROS as an activator of SIRT1 (Kim et al. 2007). Furthermore, this result suggests that AROS does not suppress p53 acetylation, but conversely that it may actively promote acetylation, potentially in opposition to SIRT1 (see *Discussion*).

The acetylation of p53 may have been suppressed by AROS in the ARPE19 cell line but was not in the HCT116 cell line. This suggests that the AROS-SIRT1 relationship is more complex than obligate activation. Apparent cell line specific effects prompted analysis of five further cell lines for the effect of silencing AROS on p53. The validation of silencing was also carried out in each cell line, important for the analysis of resulting phenotypes in *Chapter 5*.

4.5.2 Silencing of AROS in further cell lines

4.5.2.1 MCF7

Silencing of AROS was apparent at the total protein level in the MCF7 mammary gland epithelial cancer cell line (Figure 4.8A – lane 1 compared to lane 2). SIRT1 was silenced at both the mRNA and protein level but this did not modulate p53 levels (lane 1 compared to lane 3); total p53 levels did not appear to be affected and acetylated p53 remained undetectable. In contrast AROS silencing appeared to increase total p53 levels compared to Mock, but again acetylated p53 was

undetectable. This increase in total p53 following AROS silencing implies that AROS suppresses p53 in the MCF7 cell line. Furthermore, this may be independent of SIRT1, which did not affect p53 upon knock down. This is a further indication *'the regulation of SIRT1 by AROS is complex'*.

Interestingly, AROS protein was also reduced by SIRT1 silencing (lane 1 compared to lane 3). This is likely via a post-transcriptional mechanism as the abundance of *AROS* mRNA was not reduced beyond control *Actin* mRNA levels by SIRT1 silencing (Figure 4.8B). This represents a subset of conditions where SIRT1 was seen to effect AROS abundance (discussed herein).

4.5.2.2 DLD1

Targeting of AROS in the DLD1 colorectal adenocarcinoma cell line did not greatly diminish AROS protein expression (Figure 4.8C – lane 1 compared to lane 3). However, *AROS* mRNA expression was significantly reduced compared to Mock treatment (Figure 4.8D). This is similar to the data for the HCT116 colorectal cancer cell line (Figure 4.6A), and as such AROS may be selectively silenced in the nuclear fractions of DLD1 cells. SIRT1 was efficiently silenced at both the mRNA and protein level (Figure 4.8C and D).

DLD1 cells express mutant p53 protein, with an amino acid alteration from serine 241 to phenylalanine (Rippin et al. 2002). Nevertheless this p53 protein appears to be subject to regulation by post-translational modification as acetylation of p53 was detected by Western blot (Figure 4.8C). This appeared to increase following silencing of SIRT1 compared to Mock (lane 2 compared to lane 1) and silencing of AROS (lane 3 compared to lane 1). The increase was greater following SIRT1 silencing. Following silencing of either SIRT1 or AROS the total level of p53 protein also appeared to increase compared to Mock. This implies that both SIRT1 and AROS have the same effect on the mutant p53 in DLD1 cells, suppressing acetylation and total protein levels. This is consistent with AROS promoting SIRT1 activity.

4.5.2.3 LoVo

Similar to the silencing of AROS in the HCT116 and DLD1 cell lines, targeting of AROS in the LoVo colorectal adenocarcinoma cell line did not result in a reduction in AROS protein (Figure 4.8E – lane 4 compared to lane 1). This was despite a significant reduction in *AROS* mRNA (Figure 4.8F). Silencing of Lamin AC and SIRT1 was efficient at both the mRNA and protein levels. Lamin AC siRNA treatment did not appear to effect p53 expression, consistent with its use as a positive control for RNAi under basal conditions.

Targeting of AROS by siRNA appeared to stabilise total p53 levels and increase the acetylation of p53 (Figure 4.8E – lane 4 compared to lane 1). Interestingly, this was in contrast to silencing of SIRT1, which did not appear to affect either total or acetylated p53 levels (Figure 4.8E – lane 3 compared to lane 1). This implies that, AROS may be able to suppress p53 under conditions where SIRT1 does not. This difference adds further support to the hypothesis that *'the regulation of SIRT1 by AROS is complex'*.

4.5.2.4 WI38

AROS was targeted in cell lines of non-cancerous origin, firstly the WI38 lung fibroblast line. Expression of AROS was low in the WI38 cell line compared to the other cell lines analysed (Figure 4.4B). This is seen in Figure 4.9A where AROS expression was close to the threshold of detection. Knockdown of AROS may have occurred at the protein level in this cell line but the data is open for interpretation. *AROS* was selectively silenced at the mRNA level by siRNA treatment (Figure 4.9B). Silencing of both Lamin AC and SIRT1 was efficient at the protein level in this cell line (Figure 4.9A).

Silencing of both AROS and SIRT1 in the WI38 line induced a large increase in total p53 protein (Figure 4.9A). There also appeared to be an increase in the acetylation of p53 under both silencing conditions. This suggests that AROS and SIRT1 have the same effect on p53 in this cell line. This presumably involves AROS promoting SIRT1 activity towards acetylated p53 as identified in the original characterisation of AROS (Kim et al. 2007).

Interestingly, SIRT1 knockdown appeared to result in an increase in AROS protein, suggesting that SIRT1 suppresses AROS expression in the WI38 cell line (Figure 4.9C). *AROS* mRNA was not affected by SIRT1 silencing, suggestive of post-transcriptional modulation of AROS by SIRT1. This represents an example of SIRT1 effecting AROS levels, which forms part of the *Discussion*.

4.5.2.5 MCF10A

AROS was also targeted in the MCF10A mammary gland epithelium line, which is of non-cancerous origin. AROS was selectively silenced in the MCF10A cell line at both the mRNA and protein level (Figure 4.9C and D). Knockdown of both Lamin AC and SIRT1 was also efficient at both the mRNA and protein level.

Total p53 levels were slightly increase by silencing of AROS or SIRT1 in the MCF10A non-cancer cell line (Figure 4.9C). Unfortunately, acetylated p53 was not analysed in this line due to lack of sample. However the trend shown by total p53 levels suggests that AROS and SIRT1 both suppress p53 stabilisation.

Interestingly, the knockdown of SIRT1 appeared to effect AROS protein expression in this non-cancer cell line (Figure 4.9A). This is despite no effect on *AROS* mRNA with SIRT1 siRNA (Figure 4.9B). SIRT1 appears to promote AROS protein in the MCF10A cell line (Figure 4.9C), similar to the effect seen previously in the MCF7 cell line (Figure 4.8A). These two lines are both from the mammary gland epithelium, indicating that this may be a conserved effect in this tissue.

4.5.2.6 HCT116 p53$^{-/-}$

AROS was successfully targeted by RNAi in the HCT116 p53$^{-/-}$ cell line. This was carried out in parallel to silencing of Lamin AC and SIRT1. Depletion of target mRNA was significant and specific (Figure 4.10A), and this translated to the protein level for each of the 3 targets (Figure 4.10B). p53 is not expressed in this null cell line, making analysis of p53 protein levels void. However, the cell line is a useful tool for analysis of p53-depenendency. This confirmation of knockdown will allow analysis of the resulting phenotype in *Chapter 5*. Also of note, is that SIRT1 silencing did not appear to effect AROS protein expression in this cell line.

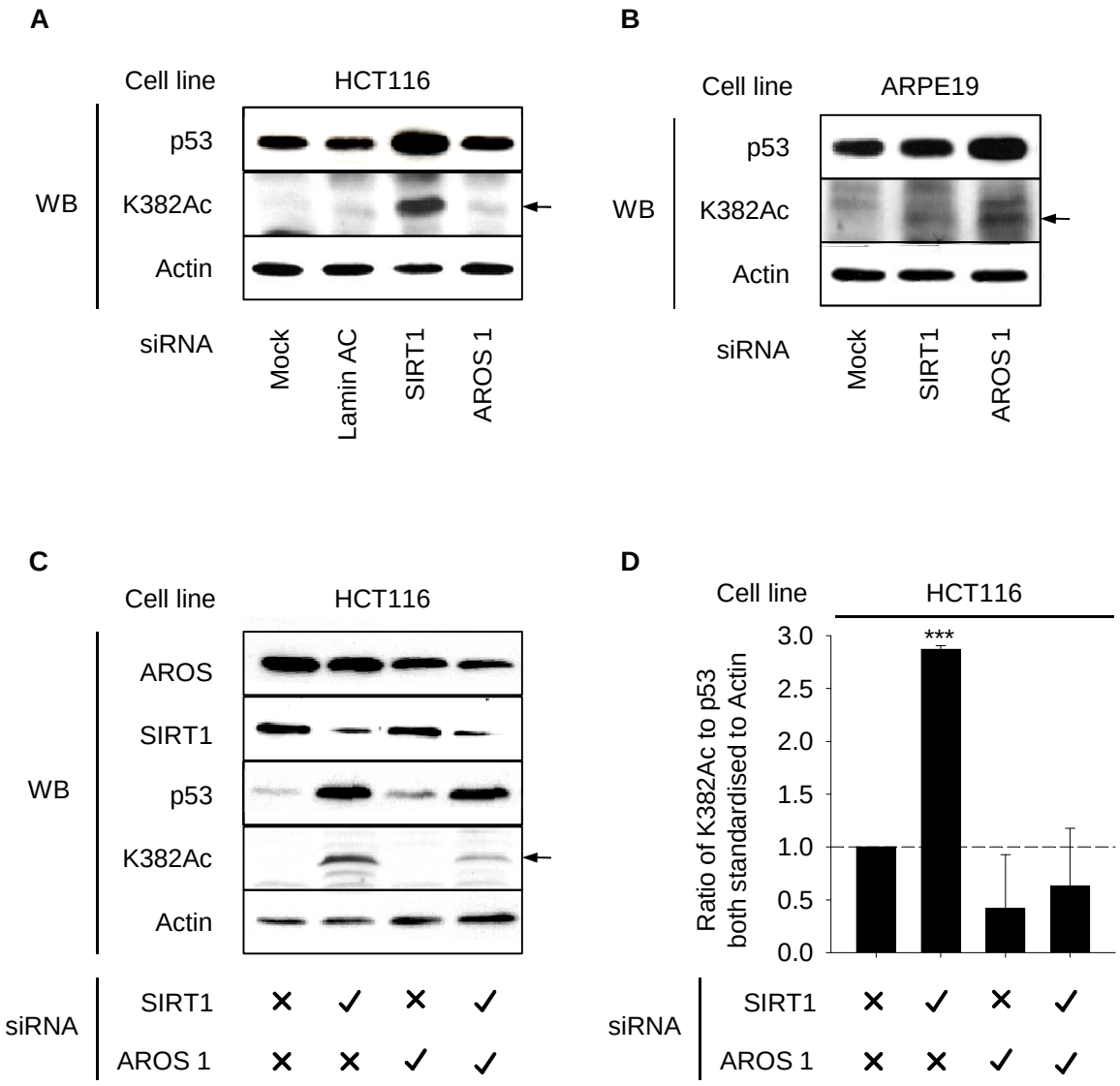

Figure 4.7: AROS has a variable effect on p53 acetylation

(A) Analysis of the effect of SIRT1 and AROS RNAi on total and acetylated p53 levels by Western blot. HCT116 cells here were those analysed in Figure 5.5A. Actin is used as a loading control. **(B)** Analysis of ARPE19 cells as in Figure 5.5C for total and acetylated p53 levels. **(C)** The effect of SIRT1 and AROS individual and combined silencing on total and acetylated p53 levels. HCT116 cells were transfected with siRNA and harvested 48 hours later in protein lysis buffer (see *Methods*). Protein was loaded by equivalent mass and separated by SDS-PAGE followed by Western blotting with antibodies as indicated. **(D)** Quantification of data from (C). Quantity One software was used to quantify total and acetylated p53 levels. These values were standardised to Actin and expressed as a ratio. Values here represent two independent experiments with error bars as standard deviation. *** P<0.001

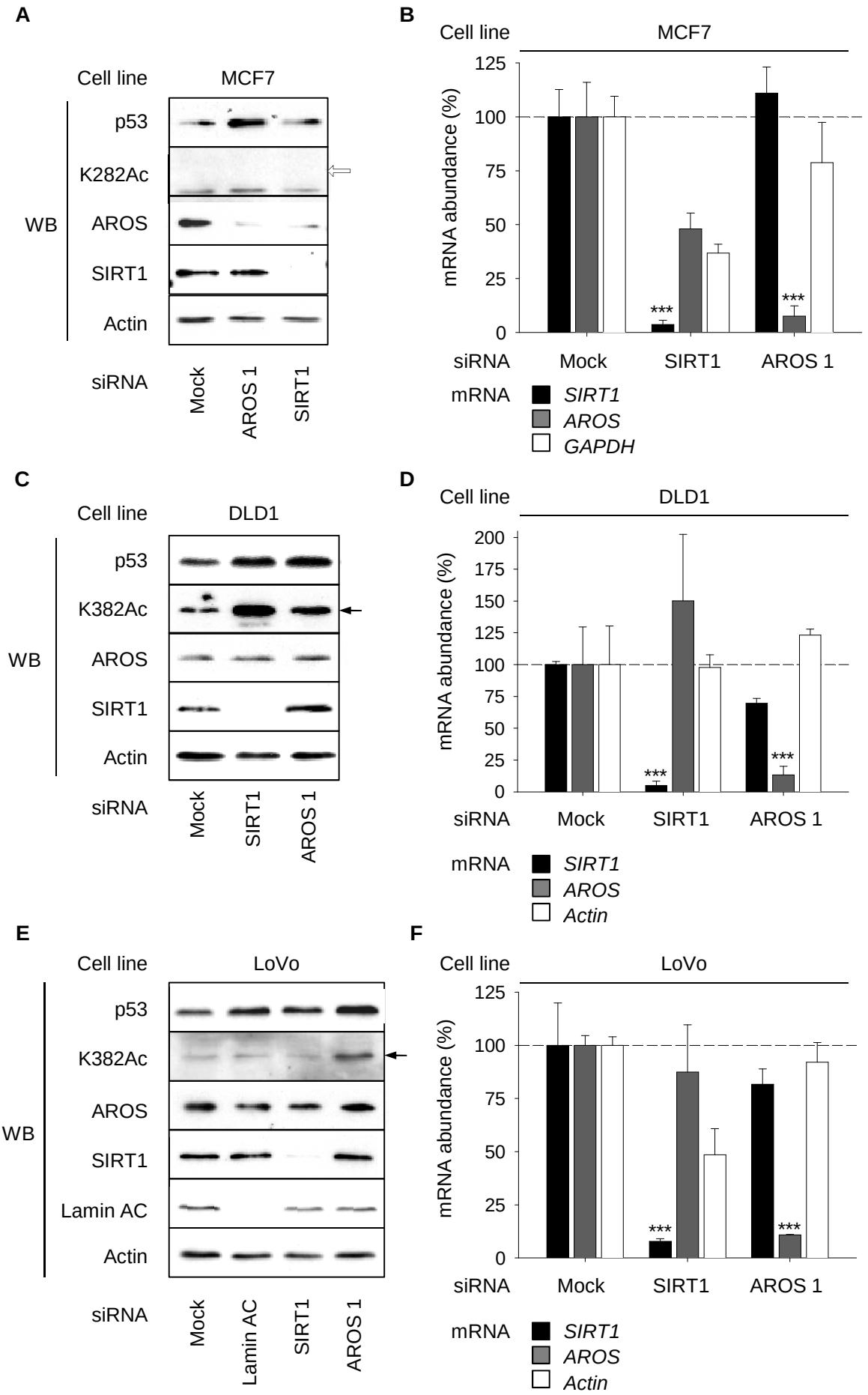
A
Cell line
MCF7
p53
K282Ac
AROS
SIRT1
Actin
WB
siRNA
Mock
AROS 1
SIRT1
B
Cell line
MCF7
mRNA abundance (%)
125
100
75
50
25
0
***
***
siRNA
Mock
SIRT1
AROS 1
mRNA
SIRT1
AROS
GAPDH
C
Cell line
DLD1
p53
K382Ac
AROS
SIRT1
Actin
WB
siRNA
Mock
SIRT1
AROS 1
D
Cell line
DLD1
mRNA abundance (%)
200
175
150
125
100
75
50
25
0
***
***
siRNA
Mock
SIRT1
AROS 1
mRNA
SIRT1
AROS
Actin
E
Cell line
LoVo
p53
K382Ac
AROS
SIRT1
Lamin AC
Actin
WB
siRNA
Mock
Lamin AC
SIRT1
AROS 1
F
Cell line
LoVo
mRNA abundance (%)
125
100
75
50
25
0
***
***
siRNA
Mock
SIRT1
AROS 1
mRNA
SIRT1
AROS
Actin

Figure 4.8: RNAi against AROS by cell line (I) – cancer cells

(A) Protein abundance following RNAi against AROS and SIRT1 in the MCF7 mammary gland epithelial cancer cell line. Cells were transfected with siRNA and harvested 48 hours later by lysis in protein lysis buffer (see *Methods*). Protein was analysed by SDS-PAGE and Western blotting with protein loaded according to equivalent mass. Empty arrow indicates expected position of relevant protein. **(B)** Quantification of mRNAs following RNAi against AROS and SIRT1 from same experiment as in (A). RNA was isolated by the RNeasy method and analysed by qRT-PCR. **(C)** Protein abundance by Western blot of target proteins and p53 following silencing of SIRT1 and AROS in the DLD1 colorectal adenocarcinoma cell line. Cells were treated and harvested as in (A). **(D)** Quantification of mRNAs as carried out in (B) for the DLD1 cell line, harvested in parallel to protein samples shown in (C). **(E)** p53 and target protein abundance following RNAi in the LoVo colorectal carcinoma cell line harvested 48 hours post-transfection. For all Western blotting Actin was used as a loading control. **(F)** Quantification of mRNAs as carried out in (B) for the LoVo cell line, harvested in parallel to protein samples shown in (E). *** $P<0.001$.

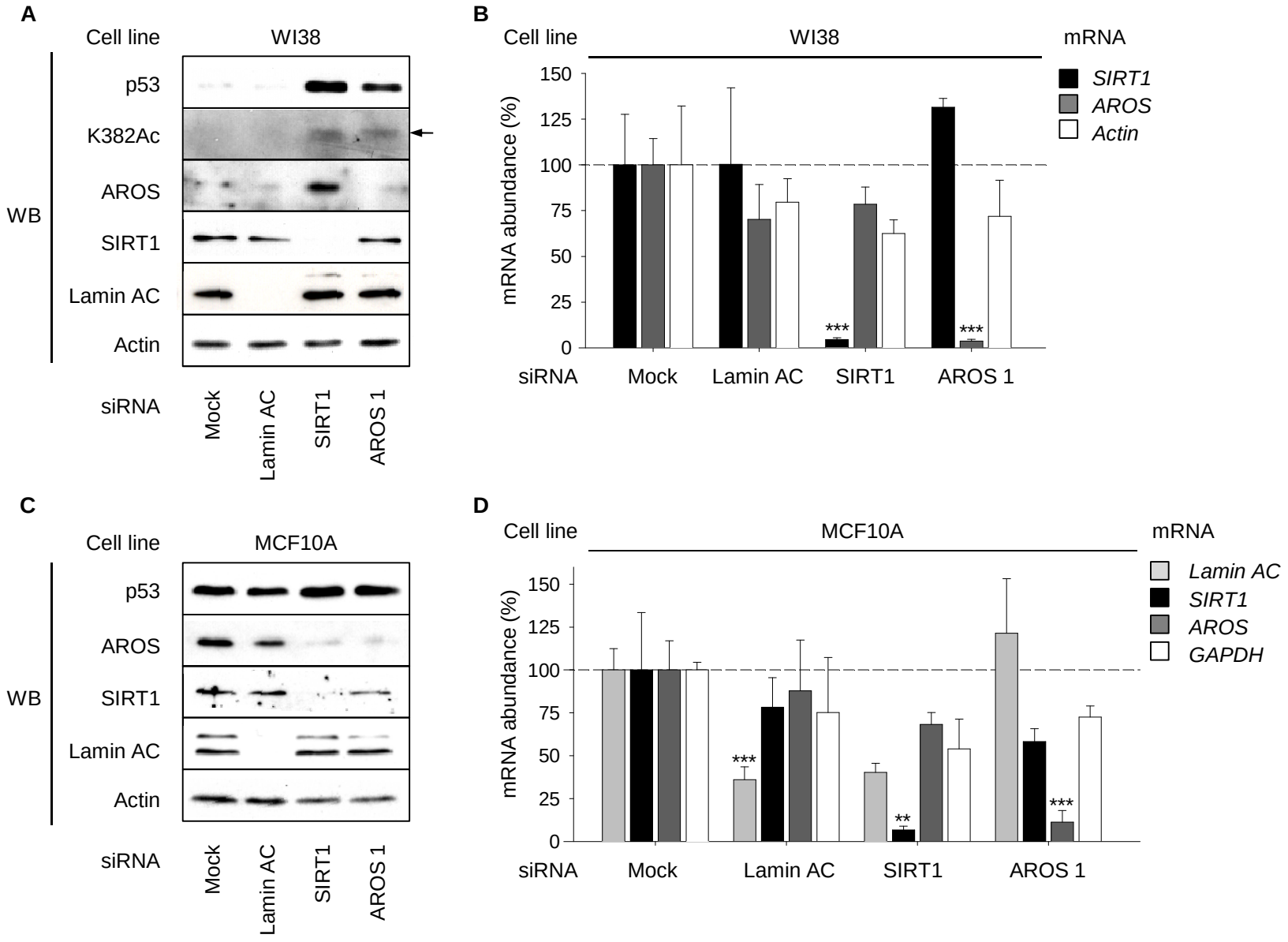
A
Cell line
WI38
WB
p53
K382Ac
AROS
SIRT1
Lamin AC
Actin
siRNA
Mock
Lamin AC
SIRT1
AROS 1
B
Cell line
WI38
mRNA
SIRT1
AROS
Actin
mRNA abundance (%)
150
125
100
75
50
25
0
***
***
siRNA
Mock
Lamin AC
SIRT1
AROS 1
C
Cell line
MCF10A
WB
p53
AROS
SIRT1
Lamin AC
Actin
siRNA
Mock
Lamin AC
SIRT1
AROS 1
D
Cell line
MCF10A
mRNA
Lamin AC
SIRT1
AROS
GAPDH
mRNA abundance (%)
150
125
100
75
50
25
0
***
**
***
siRNA
Mock
Lamin AC
SIRT1
AROS 1

Figure 4.9: RNAi against AROS by cell line (II) – non-cancer cells

(A) Abundance of target proteins and p53 following RNAi against *AROS*, *SIRT1* and *Lamin AC* mRNAs. WI38 lung fibroblast cells were harvested 72 hours post siRNA transfection and lysed for total protein content. Equivalent mass of protein was analysed by Western blotting following separation by SDS-PAGE. **(B)** Quantification of mRNA abundances harvested in parallel to protein analysis in (A). RNA isolated by RNeasy method and analysed by qRT-PCR. **(C)** Analysis of relative protein abundance in the MCF10A mammary gland epithelial cell line following RNAi as indicated. Cells treated as in (A). **(D)** mRNA quantification by qRT-PCR from parallel RNA isolation in parallel to protein data in (C). ** $P<0.01$, *** $P<0.001$.

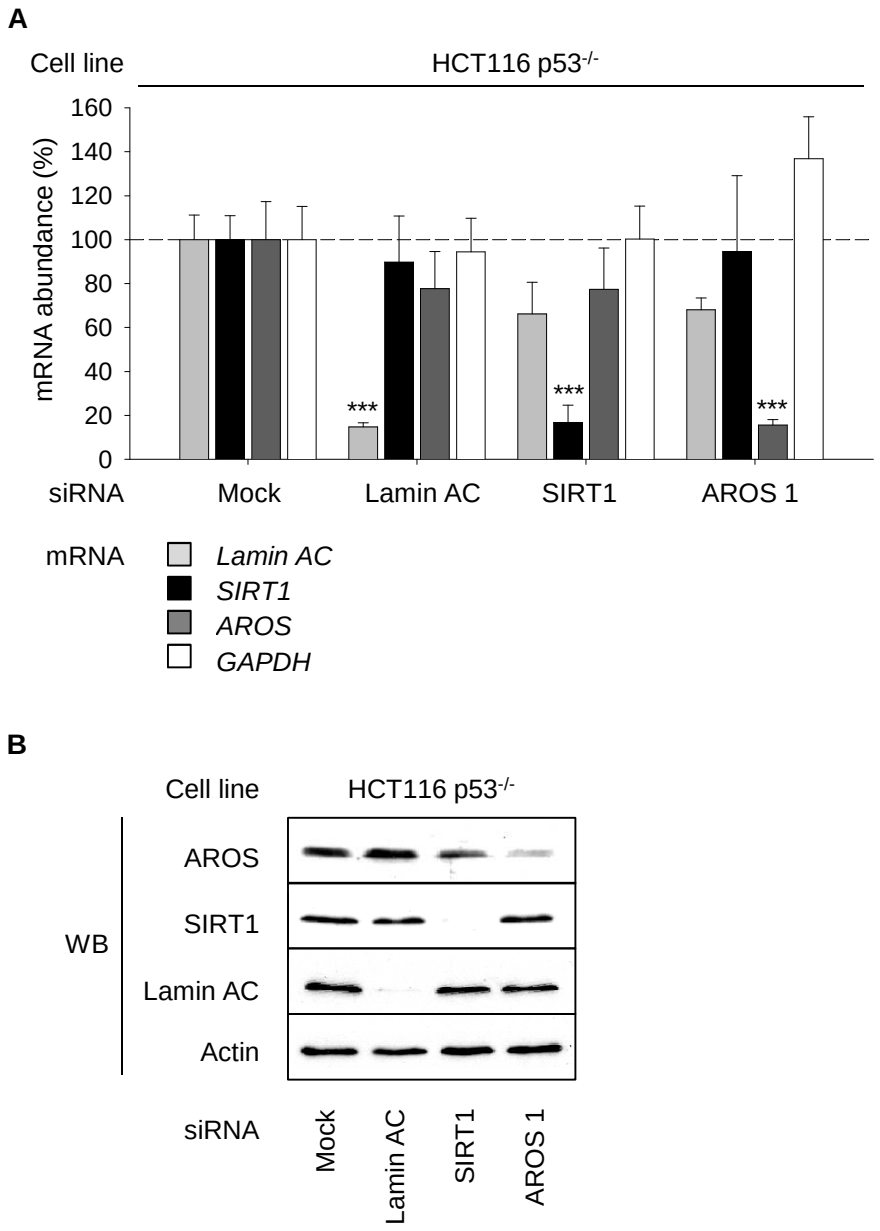

Figure 4.10: RNAi against AROS by cell line (III) – HCT116 p53$^{-/-}$

(A) Quantification of mRNA in the HCT116 p53$^{-/-}$ cell line following RNAi. Total RNA was harvested 72 hours post-transfection by the RNeasy method and used in qRT-PCR (see *Methods*). GAPDH mRNA is used as a loading control. *** P<0.001. **(B)** Protein abundance from protein samples harvested in parallel to total RNA samples analysed in (A).

4.6 *The role of AROS following stress*

4.6.1 Etoposide and Trichostatin A

Etoposide is an inhibitor of the topoisomerase II enzyme, with administration resulting in DNA damage during DNA replication (Chen et al. 1984). Trichostatin A (TSA) is an inhibitor of all histone deacetylases, except the sirtuins (Yoshida et al. 1990; Barlow et al. 2001). These cytotoxic drugs were used in combination during the original characterisation of AROS (Kim et al. 2007). Under these conditions silencing of AROS by shRNA induced an increase in p53 acetylation. The effect of AROS upon p53 acetylation is variable under basal conditions (see above). The potential for differences between basal and stress conditions was analysed, initially using the same cytotoxic drug regime employed by Kim and colleagues (2007).

Administration of etoposide and TSA markedly increased p53 protein levels, both total and acetylated (Figure 4.11). This was seen in both the HCT116 and ARPE19 cell lines. Given the effect of the drugs this was not unexpected. DNA damage resulting from etoposide treatment activates the p53 stress response pathway; and inhibition of non-sirtuin deacetylation by TSA increases p53 acetylation.

The effect of silencing SIRT1 and AROS was assessed under these stress conditions. Application of etoposide and TSA did not significantly alter the expression of the mRNAs analysed, and silencing of *AROS* and *SIRT1* was efficient and specific at the mRNA level in the HCT116 cells (Figure 4.12). SIRT1 protein was depleted by SIRT1 siRNA, but AROS protein was not greatly reduced in the HCT116 cell line (Figure 4.11). This is similar to the results following AROS silencing under basal conditions (Figure 4.6).

Silencing of SIRT1 stabilised p53 acetylation, compared to Mock siRNA in drug treated HCT116 cells (Figure 4.11). In contrast, AROS siRNA treatment did not alter the acetylation of p53 under these stress conditions. This is consistent with the data from the earlier basal experiments where SIRT1, but not AROS, was seen to suppress p53 acetylation. The data appear to contradict the role of AROS reported under these stress conditions (Kim et al. 2007). However, this may be attributable to

cell line specific effects. Thus analysis of the role of AROS in the ARPE19 cells was undertaken.

Silencing of SIRT1 and AROS was efficient at both the mRNA and protein levels in the ARPE19 cell line under these stress conditions (Figure 4.11 and Figure 4.12). p53 acetylation was increased by SIRT1 silencing compared to Mock silencing. However, AROS silencing did not stabilise p53 acetylation. Interestingly, this may be contrary to basal conditions where both SIRT1 and AROS may have suppressed p53 acetylation (Figure 4.7B). This suggests that not only is the role of AROS in p53 suppression different by cell line but also perhaps different according to cell context – basal versus stress. This supports the hypothesis that *'the regulation of SIRT1 by AROS is complex'*.

Interestingly AROS silencing in both the HCT116 and ARPE19 cell lines appeared to result in a loss of SIRT1 protein (Figure 4.11). This was not seen under any other condition analysed. This loss of SIRT1 might be expected to impact on SIRT1 activity. However, as outlined above, AROS silencing did not alter p53 acetylation under these conditions. Furthermore, this suggests a role of AROS in promoting the expression of SIRT1, not merely its activity. Again this is supportive of a more complex AROS-SIRT1 relationship than originally outlined by Kim and colleagues (2007).

4.6.2 Ultraviolet irradiation

Irradiation by ultraviolet light (UV) damages DNA, evoking the DNA damage response which stabilises p53 protein expression. To this end, exposure to UV was used as a second method of inducing cellular stress. This was carried out in the HCT116 cell line to assess the effect on p53 acetylation. Protein level knockdown of AROS and SIRT1 was also validated in the HCT116 $p53^{-/-}$, important for phenotype analyses in *Chapter 5*.

Application of UV stress appeared to increase the level of total and acetylated p53 protein, consistent with the induction of a stress response (Figure 4.13Ai). Silencing of both AROS and SIRT1 protein was seen in both the p53 wild-type and null cell lines (Figure 4.13A). Interestingly, an apparent reduction in AROS

expression was seen following SIRT1 silencing in both cell lines under these conditions, which was not due to a significant loss of *AROS* mRNA in the HCT116 cell line this (Figure 4.13B). This represents another condition where SIRT1 appeared to modulate AROS expression.

Consistent with the known role of SIRT1, silencing of the deacetylase stabilised total and acetylated p53 under these stress conditions (Figure 4.13Ai). In contrast to the previous data following AROS silencing in the HCT116 line, in UV treated cells total and acetylated p53 levels were stabilised following AROS RNAi. This has parallels to the potential disparity between basal and etoposide / TSA treated ARPE19 cells. Together these data indicate that the role of AROS in suppression of p53 is context dependent. This provides more evidence supporting the hypothesis that *'the regulation of SIRT1 by AROS is complex'*.

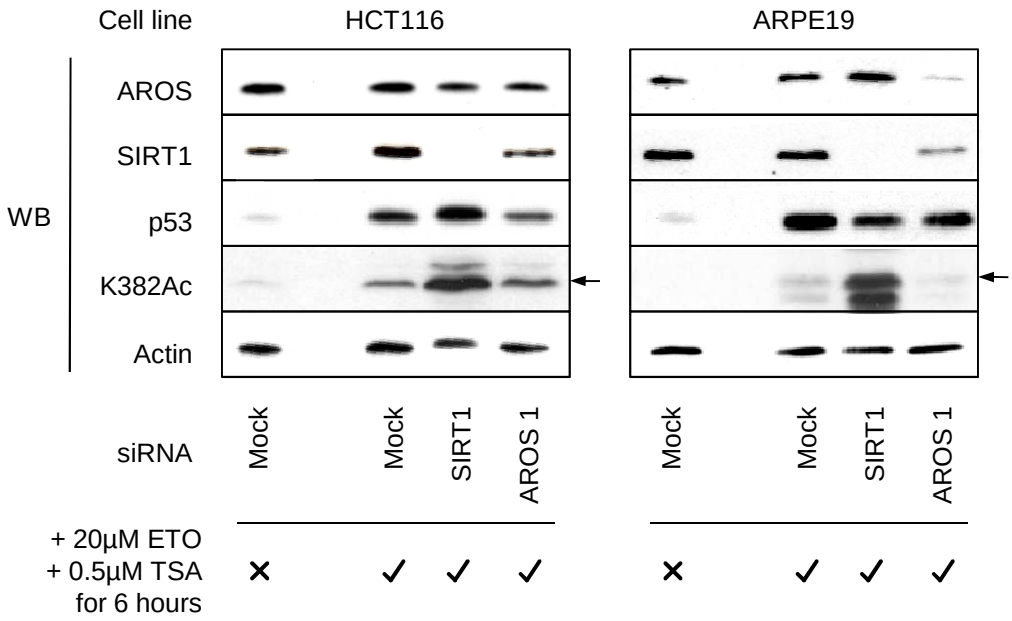

Figure 4.11: The role of AROS under stress (I) – cytotoxic drugs

Protein abundance following combined RNAi and cytotoxic drug treatment. RNAi was carried out as previously and etoposide (ETO) and trichostatin A (TSA) administered for 6 hours directly prior to harvesting as indicated. Non-drug treated controls are included for comparison. HCT116 cells were treated with siRNA for 48 hours and ARPE19 cells for 72 hours.

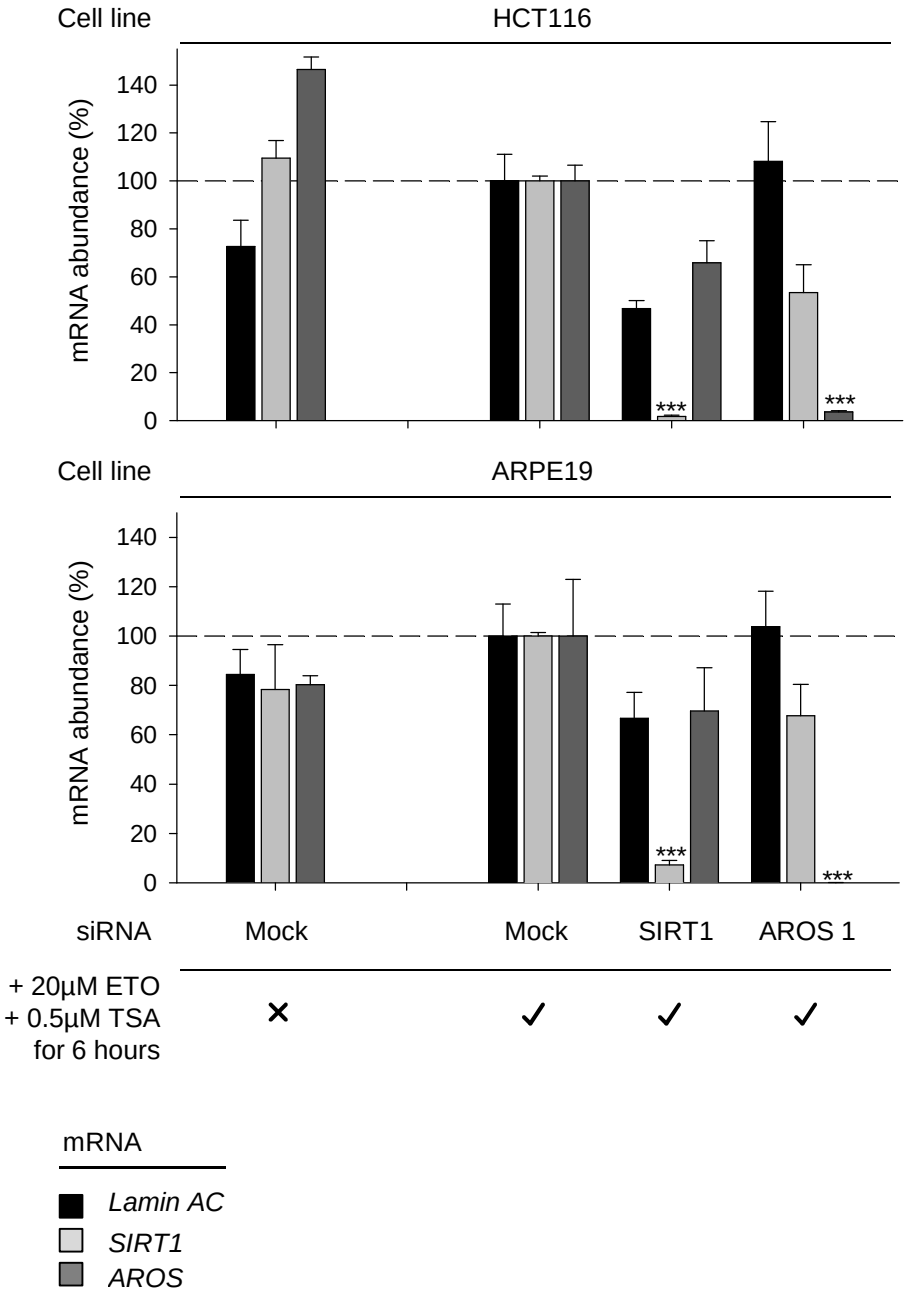

Figure 4.12: The role of AROS under stress (I) – cytotoxic drugs

mRNA quantification following total RNA isolation from cells transfected and drug treated in parallel to those in Figure 4.11. Data standardised against Mock transfected, drug treated cells. *** P<0.001.

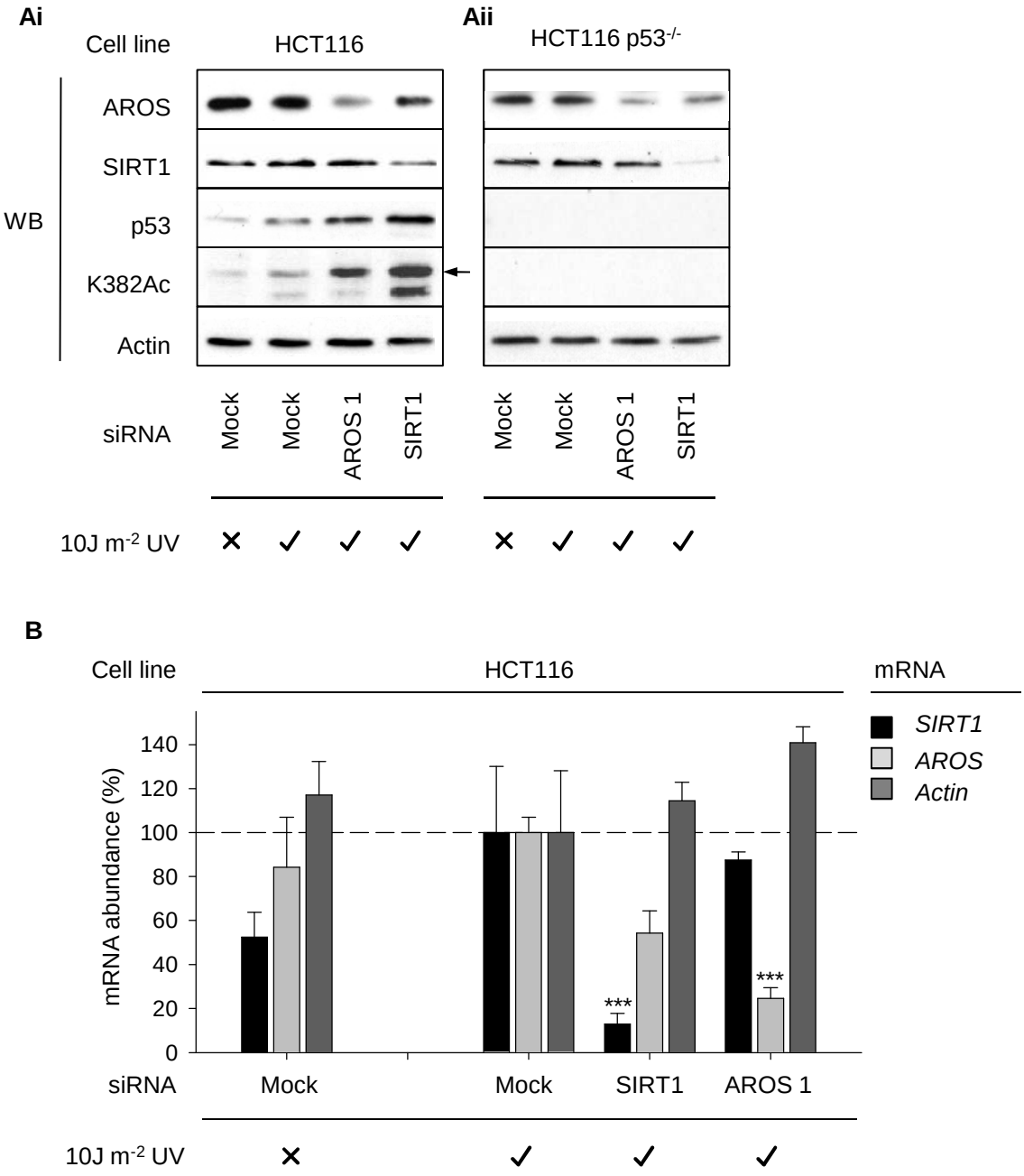

Figure 4.13: The role of AROS under stress (II) – UV radiation

(A) Target protein and p53 abundance following combined RNAi and ultraviolet (UV) radiation treatment. UV radiation was administered at the indicated dosage 24 hours prior to harvesting (see *Methods*). Total protein samples was isolated by lysis of cells in protein lysis buffer and analysed by equivalent protein mass. HCT116 cells were harvested 48 hours after siRNA transfection **(Ai)** and HCT116 p53$^{-/-}$ cells 72 hours post-transfection **(Aii)**. **(B)** mRNA quantification by qRT-PCR following RNAi. HCT116 cells were harvested for total RNA in parallel to protein samples shown in (Ai). Data standardised against Mock transfected, UV irradiated cells. *** P<0.001.

4.7 *Discussion*

4.7.1 Subcellular localisation of AROS

AROS has been reported as a nuclear protein, with expression in the cytoplasm unspecified (Maeda et al. 2006; Kim et al. 2007). Here, subcellular fractionation reveals a large proportion of AROS in the cytoplasm of the HCT116 cancer and ARPE19 non-cancer epithelial cells (Figure 4.6B and D). A smaller fraction of AROS appears to be expressed in the nucleus of both cell lines. Online tools allow the prediction of nuclear localisation sequences (NLSs) and nuclear export signals (NESs) within the primary sequences of proteins (la Cour et al. 2004; Brameier et al. 2007). Analysis of AROS protein reveals conserved NLS and NES regions, which suggests that AROS can be imported *and* exported from the nucleus. This appears to be consistent with expression of AROS in both the nucleus and the cytoplasm.

The Western blotting data indicates that the dominant population of AROS is the cytoplasmic fraction and provokes the question, why was it not observed previously? AROS was previously visualised in the nucleus by immunofluorescence (Maeda et al. 2006; Kim et al. 2007). This technique relies on a cumulative signal to identify protein localisation within individual cells. This can be focused within nuclei but dispersed across the cytoplasm. Here, subcellular fractionation does not rely on local protein concentrations for visualisation, accumulating the total expression of protein from multiple cells into the analysis. As such disperse cytoplasmic protein may explain the cytoplasmic AROS reported here escaping previous characterisation.

Another possibility is the difference in antibodies used to detect human AROS between the studies. In this *Chapter*, a polyclonal antibody raised against the full length of AROS was used for immuno-detection, whereas Kim and colleagues used a monoclonal antibody raised against residues 25-33 of AROS (Kim et al. 2007). This presents the possibility that the epitope detected by the Kim et al antibody is occluded in the cytoplasm, and thus AROS was not detected in this fraction of human cells. Whereas in the nucleus the epitope is not occluded, allowing

detection. In contrast, the polyclonal antibody used in this characterisation is able to detect AROS regardless of localisation or occlusion of individual epitopes.

This observation also asks what significance does the cytoplasmic localisation of AROS carry? SIRT1 is known to shuttle between the nucleus and the cytoplasm, with expression of the protein reported in each compartment (Tanno et al. 2007). Localisation of AROS in both compartments suggests that AROS may be able to modulate SIRT1 throughout the cell. AROS also interacts with the protein RPS19, which is a structural component of the small ribosomal subunit (Maeda et al. 2006; Ben-Shem et al. 2010; Rabl et al. 2011). Ribosomes are cytoplasmic ribonucleoprotein complexes required for the synthesis of proteins. They are present at high abundance in the cytoplasm and synthesised in the subnuclear structure the nucleolus. Interestingly, AROS may localise to nucleoli, suggesting a role in ribosome synthesis (Maeda et al. 2006; Kim et al. 2007). AROS is analysed in the context of the ribosome in *Chapter 8*. This is partly based on the observation here that populations of AROS appear to reside in the cytoplasm and the nucleolus.

4.7.2 AROS and p53 – a variable suppression

p53 acetylation is essential for its transactivation of pro-apoptotic genes (Tang et al. 2008). SIRT1 constitutively deacetylates and suppresses p53 activity (Luo et al. 2001; Vaziri et al. 2001; Ford et al. 2005). The original characterisation of AROS described a role in activation of SIRT1, seen as suppression of p53 acetylation and function (Kim et al. 2007). AROS activated SIRT1 deacetylation of p53 thus suppressing p53 acetylation in the HCT116 human cancer cell line. However, these analyses applied stress in the form of the cytotoxic drugs etoposide and TSA.

The cumulative data in this *Chapter* suggests that AROS does not always suppress p53. This was apparent under physiological conditions in the HCT116 cells, the cell line used in the original analysis by Kim et al (Figure 4.7A). Interestingly, applying the same drug regime as Kim and colleagues in this system did not appear to alter the role of AROS – AROS still did not suppress p53 (Figure 4.11). However under an alternative stress treatment, UV irradiation, AROS *was* found to suppress

p53 in HCT116 cells (Figure 4.13A). This suggests that within the same cell line AROS has different effects on p53 according to context.

It must be noted that the silencing of AROS protein was most successful in the UV irradiated cells, compared to the basal and etoposide / TSA treated cells. However, an extent of knockdown was seen under all conditions, which would be predicted to effect SIRT1 deacetylation of p53. Similar context variability in p53 suppression may occur for the ARPE19 cell line where knockdown of AROS was comparable between contexts (Figure 4.7B and Figure 4.11). These data are summarised in Table 4.1 and together suggest differentials in the role of AROS in response to external stress stimulation of the cell. The observation is consistent with the hypothesis that *'the regulation of SIRT1 by AROS is complex'*.

The effect of AROS and SIRT1 upon p53 acetylation was determined under seven different conditions, either by cell line or context. In three of these conditions the effect of AROS silencing correlated with that of SIRT1 silencing (Table 4.1). However, in the other four conditions AROS appeared to have a different effect on p53 acetylation than SIRT1 (Table 4.1). This took both possible forms; SIRT1 having an effect on p53 and AROS not (HCT116 – basal and etoposide / TSA, ARPE19 – etoposide / TSA), or the inverse; AROS having an effect on p53 and SIRT1 not (LoVo). The implication of this is that SIRT1 does not always require AROS for deacetylation of p53. In the case of the LoVo cells, AROS may be able to suppress p53 independent of SIRT1. This again agrees with the hypothesis of a more complex relationship between AROS and SIRT1 than originally characterised.

The mechanism behind these discrete differences is unknown. It is likely that between stress and basal conditions and between cell lines there are differences in regulators of both AROS and SIRT1. For example, following stress many endogenous kinases become activated, which may modify the functional interaction between AROS and SIRT1. Similarly the expression of such regulators is likely to differ between cell lines. It is important to consider the multitude of pathways likely intersecting upon AROS and SIRT1, which will differ greatly between systems. This suggests a dynamic AROS-SIRT1 relationship responding to both internal and

external stimuli. This is far from the original characterisation of AROS as an obligate activator of SIRT1.

Perhaps the most interesting evidence presented here as to the complexity of the AROS-SIRT1 relationship is the effect of combinatorial silencing. Given the identified role of AROS in SIRT1 activation, this could be expected to result in additive suppression on p53 acetylation. However, under basal conditions in the HCT116 cell line this did not appear to be the case (Figure 4.7C and D). Silencing of AROS with SIRT1 appeared to negate the stabilisation of p53 acetylation seen with SIRT1 silencing alone. This suggests that AROS actively *opposes* SIRT1 suppression of p53 acetylation in this context. How this may occur is unknown, but the theory that AROS is a mere obligate activator of SIRT1 is significantly diminished by this observation. This adds greatly to the hypothesis that *'the regulation of SIRT1 by AROS is complex'*.

4.7.3 AROS and SIRT1

AROS and SIRT1 form a direct interaction (Kim et al. 2007; Autiero et al. 2009). This association has been verified in *Chapter 7*. The interaction was previously reported to influence SIRT1 activity (Kim et al. 2007). Importantly, no effect on the expression of either protein was reported following modulation of the other. Here, in a subset of cell lines and under specific conditions the AROS and SIRT1 interaction appears to extend to influence reciprocal protein abundance.

AROS appeared to promote SIRT1 protein abundance in the HCT116 and ARPE19 cell lines following administration of etoposide and TSA (Figure 4.11). This was the only condition analysed where AROS influenced SIRT1 protein abundance. This decrease in SIRT1 expression did not correlate with a greater effect on SIRT1 activity, assayed as p53 acetylation. Indeed, under these conditions AROS silencing did not affect p53 in either cell line, despite the reduction in SIRT1 expression. Why AROS may promote SIRT1 expression under these conditions but not others is unclear.

SIRT1 silencing appeared to influence AROS protein expression on various occasions throughout the *Chapter*. These are summarised in Table 4.1 – Column 5.

In four separate experiments silencing of SIRT1 reduced the protein abundance of AROS. These could be correlated into two distinct groups. Firstly, SIRT1 appeared to promote AROS expression in two cell lines originating from the mammary gland epithelium (MCF7 - Figure 4.8A and MCF10A - Figure 4.9C). SIRT1 also appeared to promote AROS expression in the two colorectal adenocarcinoma cell lines (HCT116 and HCT116 $p53^{-/-}$) treated with UV irradiation stress (Figure 4.13A). Correlation to this cell origin and stress condition is striking. However, the reason for this specific effect is unknown. It may relate to the complexity of the AROS-SIRT1 interaction and unknown cell line and context specific effects.

The modulation of AROS expression by SIRT1 appears to occur both positively and negatively. In the WI38 cell line silencing of SIRT1 appeared to significantly increase the expression of AROS, suggesting that SIRT1 suppresses AROS expression (Figure 4.9A). This is the only cell line analysed from a non-epithelial origin, WI38 cells being fibroblastic. In later *Chapters* further functions of AROS are uncovered where the data presented here will be discussed in the context of SIRT1 influencing these new functions.

4.7.4 AROS protein stability

Reduction in AROS protein abundance following AROS siRNA treatment varied between cell lines. In non-cancer cells (ARPE19, MCF10A and potentially WI38) AROS silencing at the protein level appeared to be efficient (Figure 4.6C and Figure 4.9). This was also the case for the MCF7 mammary gland epithelium cancer cell line (Figure 4.8A) and the p53 null colorectal adenocarcinoma cell line, the HCT116 $p53^{-/-}$ (Figure 4.10).

However, in 3 further colorectal adenocarcinoma cell lines with wild-type p53 (HCT116 – Figure 4.6A, LoVo –Figure 4.8A) and mutant p53 (DLD1 –Figure 4.8C) AROS protein did not appear to be greatly reduced compared to Mock treatment by AROS siRNA. In each case this was despite efficient reduction in *AROS* mRNA. Furthermore, the stability of AROS did not correlate with the higher expression of AROS in these cell lines over lines where AROS was efficiently

silenced (Figure 4.4B). This implies that the AROS resistance to depletion by siRNA is a post-transcriptional event. This is likely a result of increased protein stability.

Thus there appears to be heightened AROS protein stability in colorectal adenocarcinoma cells, with the exception being the HCT116 $p53^{-/-}$ cell lines. This has some important possible implications. Firstly, the increased level of AROS in these cancer cell types may indicate an important function of AROS within these cells. Whether this is an important function in colorectal adenocarcinoma cells, or colorectal epithelial cells in general is unclear, as the expression of AROS in non-cancerous colorectal epithelial cells was not carried out. If the case, increased stability of AROS in colorectal adenocarcinoma cells may be useful biomarker.

AROS protein stability also appears to rely on the expression of p53 – wild-type or mutant. This is based on the effective silencing of AROS protein observed in the HCT116 $p53^{-/-}$ cell line (Figure 4.10B), compared to the otherwise isogenic HCT116 cell line. As such, p53 may promote AROS stability and resistance to siRNA mediated knockdown. In the context of using AROS as a biomarker, this may also allow the status of the p53 gene to be inferred from the protein stability of AROS.

The stability of AROS protein can be attributed to the cytoplasmic fraction of the protein in HCT116 cells (Figure 4.6B), with this also a possibility for the other colorectal adenocarcinoma cell lines. This allows speculation as to how the stability is achieved. AROS is known to interact with the ribosomal protein RPS19 (Maeda et al. 2006). A variety of proteins bind the ribosome in the cytoplasm. Thus, with AROS expressed and stable in the cytoplasm it is possible that AROS interacts with ribosomes via RPS19 and that this contributes to the stability of AROS protein. This possibility is analysed and discussed further in *Chapter 8*.

Cell line	***Condition***	***Stabilisation of p53***	***Identity to SIRT1 effect***	***SIRT1 effect on AROS***
HCT116	Basal	✗	✗	~
	Eto+TSA	✗	✗	~
	UV	✓	✓	↑
HCT116 p53$^{-/-}$	Basal	-	-	~
	UV	-	-	↑
DLD1	Basal	✓	✓	~
LoVo	Basal	✓	✗	~
MCF7	Basal	[✓]	[✗]	↑
ARPE19	Basal	[✓]	[✓]	~
	Eto+TSA	✗	✗	~
MCF10A	Basal	-	-	↑
WI38	Basal	✓	✓	↓

Table 4.1: Summary of data from AROS RNAi experiments

This Table collates the data presented in the *Chapter*. Cell lines are listed as described in the text. 'Basal' refers to the application of RNAi as validated in the *Methods*. 'Eto+TSA' represents etoposide and TSA treatment. 'UV' represents ultraviolet light irradiation. Stabilisation of p53 acetylation following AROS knockdown is indicated by a 'tick' in Column 3. No effect is indicated by a 'cross'. Comparison of the effect of AROS (listed in Column 3) and SIRT1 is indicated by a 'tick' or 'cross' in Column 4. Dashes indicate no data available. Square brackets indicate an inferred result from total p53 levels. The effect of SIRT1 on AROS protein stability is shown in Column 5 – an upward arrow indicates a positive effect, '~' indicates no effect and a downward arrow indicates a negative effect.

4.8 *Conclusions*

1. AROS is conserved among animalia and widely expressed in human cell lines and tissues.
2. AROS is present in both the cytoplasm (a previously unreported population) and the nucleus of two human cell lines.
3. AROS does not always suppress p53. This alters according to:
    a. cell line,
    b. and potentially cell context – basal compared to stress.
4. SIRT1 and AROS can modulate reciprocal protein abundance in a subset of cell lines and conditions.

Together *Conclusions 3 and 4* suggest that the AROS-SIRT1 relationship is more complex than obligate activation. Thus, perhaps a more accurate description of the relationship is: AROS and SIRT1 form a variable relationship, which appears to be able to suppress p53, but this is dependent on cell line and condition.

5 The influence of AROS on cell fate

5.1 *Overview*

In *Chapter 4* the molecular effects of silencing AROS were compared to the silencing of SIRT1 across a range of cancer and non-cancer cell lines. This was carried out under both basal and stress conditions. The results highlighted differences in the role of AROS compared to SIRT1, as well as differences in the role of AROS between cell lines and context.

SIRT1 has been extensively studied as a cancer specific survival factor (*Chapter 1*). Such a role for AROS has not been as extensively studied. In this *Chapter*, the role of AROS in cell viability for both cancer and non-cancer cell lines is outlined. This continues to highlight a dichotomy of function between AROS and SIRT1 in the regulation of p53. However, a unified role is seen in the regulation of FOXO4, which carries importance in the regulation of cancer cell apoptosis.

5.2 *Introduction*

5.2.1 p53 tumour suppression

More than half of all cancerous growth correlates with mutation in the *TP53* tumour suppressor gene, with misregulation of wild-type p53 protein believed to contribute to the remaining tumours (Vogelstein et al. 2000; Olivier et al. 2010; Goh et al. 2011). p53 expression is responsive to DNA damage, allowing it to react to mutagenic events by attenuating cell proliferation or viability, earning p53 the moniker of "guardian of the genome" (Lane 1992). Perturbation of p53 protein function following mutation or misregulation constitutively removes this suppression of proliferation and viability. p53 function can be suppressed to result in the same outcome. This gives great power to the factors which control p53 activity.

p53 has a short half-life under basal conditions due to rapid turnover mediated by poly-ubiquitin ligation. p53 is targeted for degradation by a variety of ubiquitin ligases (reviewed in Lee and Gu 2010). The first and best characterised of these is the MDM2 protein. MDM2 acts in a comparable manner to many of the other ubiquitin ligases in regulating p53 turnover, which ultimately leads to p53 degradation.

MDM2 poly-ubiquitinylates lysine residues of p53, then remains bound in a p53-MDM2 complex (Haupt et al. 1997; Kubbutat et al. 1997). This complex is labelled for degradation, during which both p53 and MDM2 are degraded, due to auto-ubiquitinylation of MDM2 (Fang et al. 2000; Honda and Yasuda 2000). The p53-MDM2 complex is exported to the cytoplasm, negating p53 transcription factor activity (Roth et al. 1998; Tao and Levine 1999), and is ultimately silenced by proteasomal degradation (Honda et al. 1997). MDM2 also represses p53 by a degradation independent mechanism by forming a complex at target gene promoters, inhibiting p53 transactivation (Ohkubo et al. 2006; Tang et al. 2008). p53 promotes MDM2 transcription, initiating a negative feedback loop that limits p53 activity under basal conditions (Momand et al. 1992; Barak et al. 1993; Wu et al. 1993); p53 increases MDM2 expression, which in turn mediates the degradation of both parties.

Negative feedback suppresses the inhibitory effects of p53 on proliferating cells but permits the rapid activation of p53 when required. Activation of p53 is achieved by increasing protein abundance, which is classically achieved by disruption of the pathways leading to p53 degradation, such as the p53-MDM2 pathway. This can occur, for example, through post-translational modification, competitive interaction or sequestration of MDM2. For example, MDM2 can be modified by ATM, inhibited by RPL11 and sequestered by ARF (Weber et al. 1999; Lohrum et al. 2000; Maya et al. 2001).

p53 protein is subject to considerable post-translational modification, including reversible lysine acetylation (Brooks and Gu 2011). This modification of p53 protein leads to stabilisation due to decreased MDM2-mediated degradation, which in turn increases p53 transcription factor activity. The gene targets of p53 promote cell cycle arrest and apoptosis, resulting in reduced cell viability. This is the mode of p53 tumour suppression, blocking individual cell viability where appropriate for overall survival.

5.2.2 FOXO tumour suppression

The forkhead box O (FOXO) family of transcription factors are capable of targeting a range of genes involved in cell cycle arrest and apoptosis (van der Vos and Coffer 2011). The array of genes the FOXOs transactivate has similarities to those regulated by p53, promoting cell cycle arrest and apoptosis. This highlights the role of the FOXOs in tumour suppression. There are four human FOXO family members, FOXO1, FOXO3, FOXO4 and FOXO6, which bind to consensus regions as monomers to activate gene transcription.

FOXO proteins are regulated by post-translational modification. This again has similarity to p53. The 14-3-3 proteins are the key regulators of the FOXOs, acting similarly to MDM2 in the p53-MDM2 relationship. 14-3-3 proteins target FOXOs for nuclear export in response to phosphorylation by proto-oncogenic kinases, such as Akt (Brunet et al. 2002). Disruption of the FOXO-14-3-3 interaction and subsequent gene activation can be achieved by modification of either protein. For example, JNK-mediated phosphorylation of 14-3-3 reduces its association with

FOXO3 (Sunayama et al. 2005). FOXO4 is also a target for JNK phosphorylation in response to stress, resulting in dissociation from the 14-3-3 proteins and increased gene transcription (Essers et al. 2004). All FOXO proteins are subject to acetylation and deacetylation, the latter process being mediated by SIRT1 (reviewed in Calnan and Brunet 2008). Removal of acetyl groups from the FOXO proteins reduces their transactivation potential, giving SIRT1 a similar role in regulation of FOXO tumour suppression to its role in p53 tumour suppression.

5.2.3 Deacetylation and cell fate

Reversible acetylation is a key regulatory mechanism for both p53 and the FOXO proteins. p53 is acetylated by TIP60/MOF, PCAF and p300/CBP (reviewed in Brooks and Gu 2011). Deacetylation and subsequent down-regulation of p53 involves either of two identified deacetylases, one of which is a complex containing the class I deacetylase HDAC1 (Luo et al. 2000). Over-expression of components of this complex reduces p53 acetylation and p53-dependent apoptosis. Secondly, SIRT1 deacetylates p53, reducing the apoptotic capacity of cells and favouring proliferation (Luo et al. 2001; Vaziri et al. 2001). Deacetylation by SIRT1 contributes to a basal constitutive cycle, such that removal of SIRT1 results in stabilisation of acetyl-lysine p53, due to continued acetylation (Ford et al. 2005).

According to the ‘Tang Model’, acetylation of p53 is essential for transactivation (Tang et al. 2008). Thus removal of acetyl groups from p53 by HDAC1 and SIRT1 will suppress p53 function. Given the role of p53 in suppressing cell proliferation, deacetylation of p53 promotes cell survival. Further to this, ubiquitinylation can only target non-acetylated p53, indicating a correlation between deacetylation activity and subsequent MDM2-mediated degradation of p53 (Li et al. 2002). Together, this predicts that suppression of deacetylation would promote p53 activity and potentially lead to cell cycle arrest or apoptosis.

Acetylation is also important for regulation of the FOXO proteins, reportedly enhancing their role as tumour suppressors. This is based on observations following suppression of deacetylation. SIRT1 deacetylates all FOXO proteins, suppressing transcription of pro-apoptotic genes (Brunet et al. 2004; Motta et al. 2004; Calnan

and Brunet 2008). With striking similarity to the regulation of p53, deacetylation of FOXOs promotes cell survival. The *BIM* gene has a FOXO binding element in its promoter and can be regulated by the FOXOs. BIM protein is expressed *de novo* when required and promotes mitochondrial apoptosis by sequestering anti-apoptotic members of the Bcl-2 family of proteins (reviewed by Gillings et al. 2009). BIM is a pro-apoptotic target of the FOXOs, potentially important for tumour suppression. Consistent with this, FOXO promotion at the *BIM* promoter leads to apoptosis (Gilley et al. 2003). Interestingly, of the FOXOs analysed, FOXO4 acetylation has been linked to *BIM* transactivation; *BIM* gene expression is diminished by deacetylation of FOXO4 by SIRT1 (Motta et al. 2004).

AROS was proposed as an obligate activator of SIRT1 activity (Kim et al. 2007). As indicated in *Chapter 4*, this may not always be true for SIRT1 suppression of p53. The role of AROS in suppression of FOXO4 has not been analysed. Given the strong evidence for a direct interaction between AROS and SIRT1, any suppression of the FOXOs by AROS is likely to occur via SIRT1. In the context of cancer, FOXO4 is known to be essential for apoptosis following suppression of SIRT1 (Ford et al. 2005). Analyses similar to those presented by Ford and colleagues (2005) were carried out following AROS silencing for comparison of the role of AROS to that of SIRT1.

5.2.4 AROS and cell fate

The role of AROS has been reported for human cancer cells (Kim et al. 2007). Importantly, cells from non-cancerous origin were not analysed. Knockdown of AROS resulted in an increase in cell death following etoposide and trichostatin A treatment in this study. This correlates with the role of SIRT1 in promoting cancer cell survival (Ford et al. 2005), and was attributed to AROS promoting SIRT1 activity. Importantly, SIRT1 is known to suppress cancer cell apoptosis under basal conditions. The role of AROS under these conditions is not known. Furthermore, SIRT1 is not required for non-cancer cell survival under these basal conditions. AROS has not been studied in non-cancer cells, presenting the possibility that AROS, like SIRT1, is a specific cancer cell survival factor.

The data here represent the phenotypic characterisation following RNAi against AROS and SIRT1 as validated in *Chapter 4*. Details of the silencing of each target in the cell lines analysed are given in *Chapter 4*. Interestingly, the data suggested that silencing of AROS had different molecular effects to the silencing of SIRT1. This led to the conclusion that the AROS-SIRT1 relationship is more complex than obligate activation. Whether this manifests as differences in the effect on cell phenotype will be addressed in this *Chapter*.

5.2.5 Hypotheses

1. AROS is required for cancer cell survival under physiological and stress conditions.
2. AROS is not required for non-cancer cell survival.
3. AROS and SIRT1 have different effects on cell phenotype, consistent with different molecular effects.
4. AROS is required for SIRT1 suppression of FOXO4.

5.3 *Characterisation of cell phenotype following AROS silencing*

5.3.1 Cancer cell lines - apoptosis

Lamin AC was targeted as a positive control gene which can be successfully knocked down without altering cell fate. The data here are consistent with this. Lamin AC silencing did not appear to alter the phenotypes of the HCT116, HCT116 $p53^{-/-}$ or MCF7 cancer cell lines compared to Mock transfection (Figure 5.1). Consistent with these micrographs, Lamin AC siRNA did not cause a significant induction of apoptosis in any of these three cell lines (Figure 5.2A).

In the DLD1 cell line Lamin AC silencing was carried out as described in *Chapter 3*, revealing no alteration in phenotype following knockdown (Figure 3.6B). The targeting of *Lamin AC* in the LoVo colorectal adenocarcinoma cell line caused an alteration in cell phenotype compared to control (Figure 5.1). The cells were aggregated and refringent under phase contrast microscopy. This cell line is able to grow both adhered and free in the media (Drewinko et al. 1976), and the observed phenotype may represent a shift from adherent growth towards growth in the media. In support of this, the apoptotic phenotype of LoVo cells (and all cell lines used in this study) appeared to be individual refringent cells. This is based on the increase in the number of these cells following silencing of SIRT1 (Figure 5.1), which is known to be anti-apoptotic in cancer cells (Ford et al. 2005).

SIRT1 siRNA also induced an increase in unadhered, refringent cells in the HCT116, HCT116 $p53^{-/-}$, MCF7 and DLD1 cell lines (Figure 5.1). This phenotype is consistent with an induction of apoptosis. An induction of apoptosis was confirmed in the HCT116, HCT116 $p53^{-/-}$ and MCF7 cell lines by Annexin V staining and FACS analysis (Figure 5.2A). Thus, in five cancer cell lines SIRT1 silencing resulted in a phenotype consistent with apoptosis, which was confirmed by flow cytometry in three of those cell lines. This agrees with the published role of SIRT1 in promoting tumour cell viability (see *Chapter 1*).

AROS was analysed in parallel to SIRT1 under these basal conditions, allowing comparison of silencing. Differences between the molecular roles of AROS and SIRT1 detailed in *Chapter 4* suggested that the phenotypes following silencing

may also differ. However, this was not the case. An increase in individual refringent cells was apparent following silencing of AROS in the HCT116, HCT116 $p53^{-/-}$, MCF7, DLD1 and LoVo lines (Figure 5.1).

In the HCT116 cancer cell line, two independent siRNAs against AROS appeared to induce the same apoptotic phenotype (Figure 5.1). Significant induction of apoptosis following use of AROS siRNA 1 was recorded in the HCT116, HCT116 $p53^{-/-}$ and MCF7 cell lines after 48 hours (Figure 5.2A). Both AROS siRNA 1 and 2 resulted in a significant fold increase in apoptosis compared to Mock in the HCT116 cell line after 72 hours (Figure 5.2B). Interestingly, the fold induction of apoptosis was almost identical when comparing SIRT1 siRNA and AROS siRNA 1 treated cells in all cases. The fold induction of apoptosis with AROS siRNA 2 was lower, perhaps related to the less effective knockdown achieved with this siRNA (*Chapter 4*).

These data suggest that AROS is required for cancer cell survival. This appears to be independent of p53 status, as apoptosis was induced in the p53 null HCT116 $p53^{-/-}$ cell line following AROS silencing. SIRT1 acts independently of p53 to suppress apoptosis, promoting viability of p53 null cancer cells (This work and Ford et al. 2005). Interestingly, AROS and SIRT1 had different molecular effects on p53 under basal conditions, characterised in *Chapter 4*. SIRT1 suppressed p53 acetylation, but this did not appear to be required for suppression of apoptosis. AROS did not appear to suppress p53 acetylation under these conditions, which is consistent with independence from p53 in suppression of apoptosis.

The absolute induction of apoptosis differed between p53 wild-type and p53 null cells, which were otherwise isogenic (Figure 5.2A). This may suggest that p53 is important in AROS suppressed apoptosis. However, this phenomenon may be attributable to apoptosis occurring over a longer period in the HCT116 $p53^{-/-}$ cell line than in HCT116 cells, as discussed in *Chapter 3*.

5.3.2 Cancer cell lines - cell cycle

Silencing of SIRT1 appeared to reduce the adhered cell density compared to Mock in each of the cancer cell lines (Figure 5.1). In contrast, AROS silencing did

not appear to reduce the adhered cell density to such an extent, despite an increase in refringent unadhered cells. This suggests that SIRT1 and AROS have different effects on cell cycle progression, which manifested here as differences in cell density.

Cell cycle distribution analysis appeared to agree with the phenotypes. In the HCT116 cell line, SIRT1 silencing resulted in a reduction in the population of cells in S phase (Figure 5.3A). A reduced S phase population is likely to affect the cell cycle progression of these cells. AROS silencing appeared to have no effect compared to control in the HCT116 cell line, suggesting a difference between AROS silencing and SIRT1 silencing. AROS silencing had a slight effect in the HCT116 $p53^{-/-}$ cell line, with an increase in the G2/M and S phase populations and concomitant reduction in the G1 population (Figure 5.3B). These differences are slight and not inconsistent with the maintenance of cell density in

Figure 5.1. In contrast, following SIRT1 silencing there was a decrease in cells in G1 and a large increase in G2/M cells. This resulted in a decrease in the S phase population, which is likely to impinge on cell cycle progression.

These differences in cell cycle distribution may correlate with differences in the molecular effect of silencing AROS and SIRT1. SIRT1 silencing induced an increase in p53 acetylation in the HCT116 cell line, whereas silencing of AROS did not (*Chapter 4*). Here, SIRT1 silencing caused apoptosis and cell cycle arrest in the HCT116 cell line, whereas AROS siRNA only induced apoptosis (Figure 5.2A and Figure 5.3A).

p53 is known to promote both apoptosis and cell cycle arrest following acetylation (Tang et al. 2008). The data here correlate with stabilised p53 acetylation resulting in cell cycle arrest following SIRT1 silencing, and no arrest following AROS silencing due to no stabilisation of p53 acetylation. This is an attractive theory to correlate phenotype to molecular alterations. However, there is likely to be multiple factors involved in correlating molecular alterations to phenotype. This is suggested by the HCT116 $p53^{-/-}$ cell line, where SIRT1 silencing induces cell cycle arrest, in the absence of p53. Despite this, the arrest phenotypes are different

between the HCT116 and HCT116 $p53^{-/-}$ cell lines and the influence of other factors cannot be ruled out. As such, the data are consistent with a potential phenotypic manifestation of the AROS-SIRT1 relationship being more complex than obligate activation.

The analysis of AROS in five cancer cell lines suggests that it is required for evasion of apoptosis, but is perhaps redundant for promoting cell cycle progression. These data agree with the hypothesis that *'AROS is required for cancer cell survival under physiological conditions'*. Interestingly, the role of AROS on the fate of non-cancer cell lines has not been analysed. Redundancy for viability in non-cancer cell lines would present AROS as a potential anti-cancer therapeutic target.

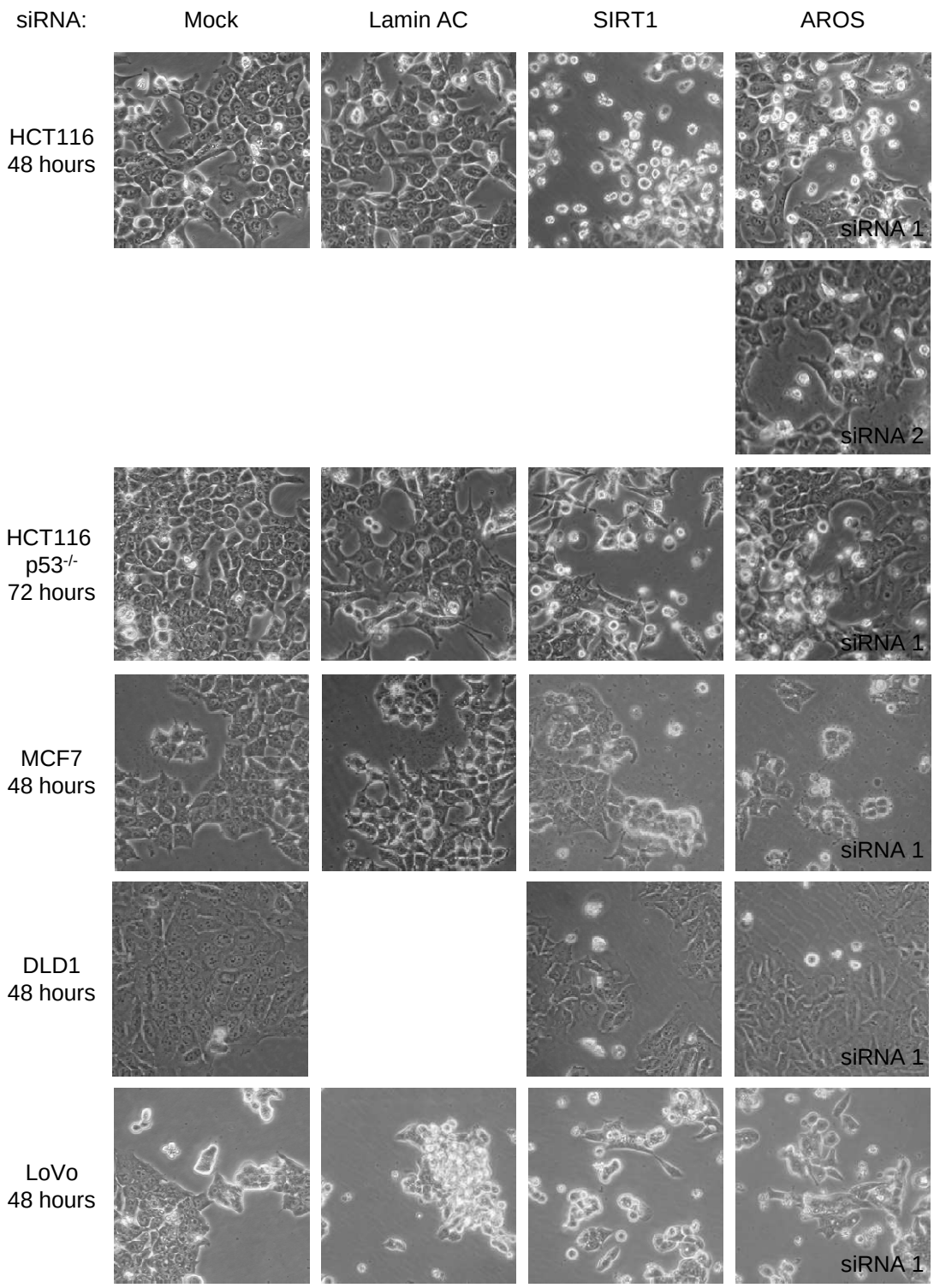
siRNA:
Mock
Lamin AC
SIRT1
AROS
HCT116
48 hours
siRNA 1
siRNA 2
HCT116
p53-/-
72 hours
siRNA 1
MCF7
48 hours
siRNA 1
DLD1
48 hours
siRNA 1
LoVo
48 hours
siRNA 1

Figure 5.1: Cancer cell phenotype following siRNA transfection

Phase contrast micrographs of cancer cell lines following transfection of siRNA as indicated. Cells were treated with siRNA and phenotype recorded at the time point shown. AROS siRNA refers to siRNA 1, apart from transfection of siRNA 2 in the HCT116 cell line.

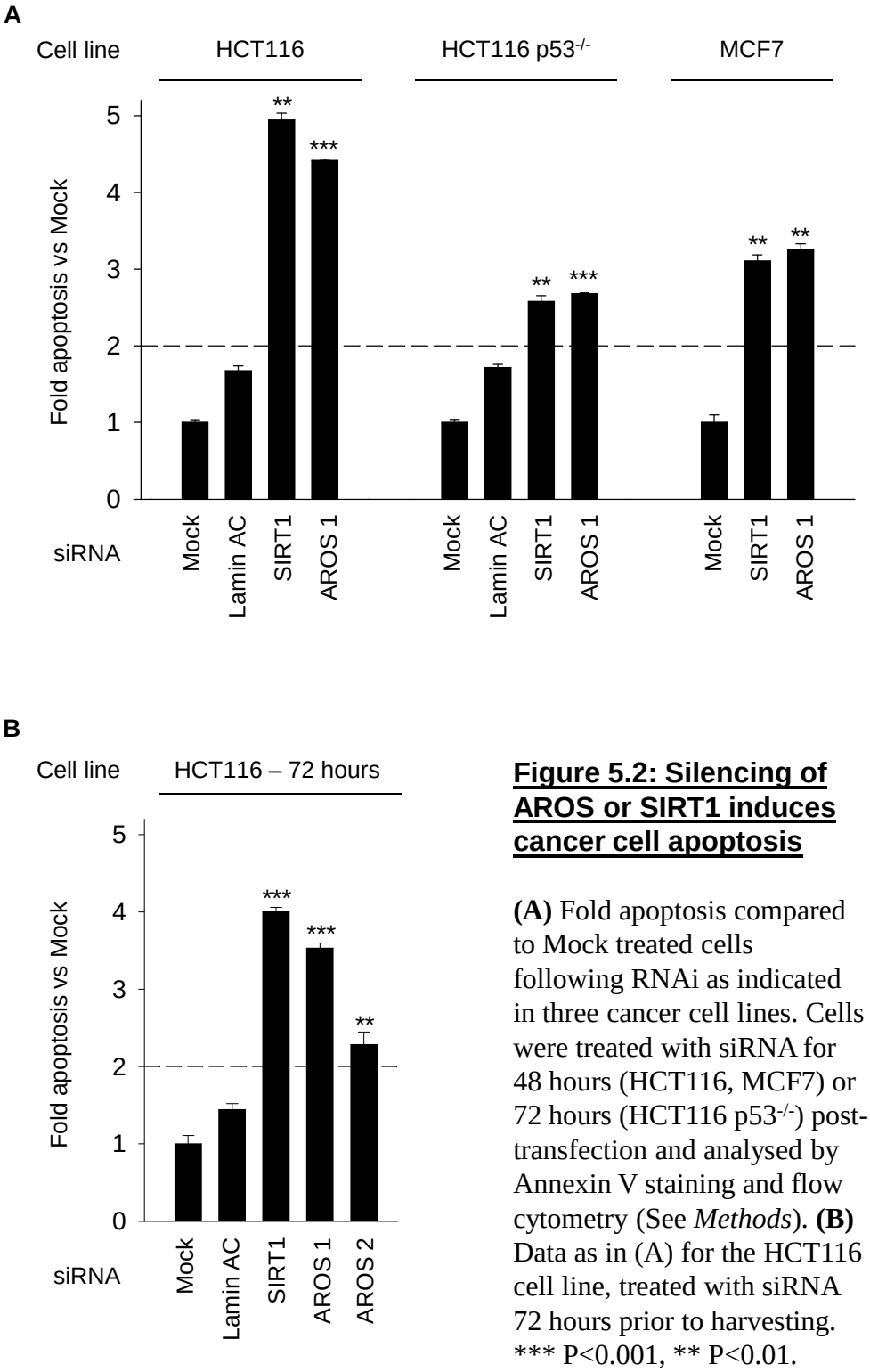

Figure 5.2: Silencing of AROS or SIRT1 induces cancer cell apoptosis

(A) Fold apoptosis compared to Mock treated cells following RNAi as indicated in three cancer cell lines. Cells were treated with siRNA for 48 hours (HCT116, MCF7) or 72 hours (HCT116 p53$^{-/-}$) post-transfection and analysed by Annexin V staining and flow cytometry (See *Methods*). **(B)** Data as in (A) for the HCT116 cell line, treated with siRNA 72 hours prior to harvesting. *** P<0.001, ** P<0.01.

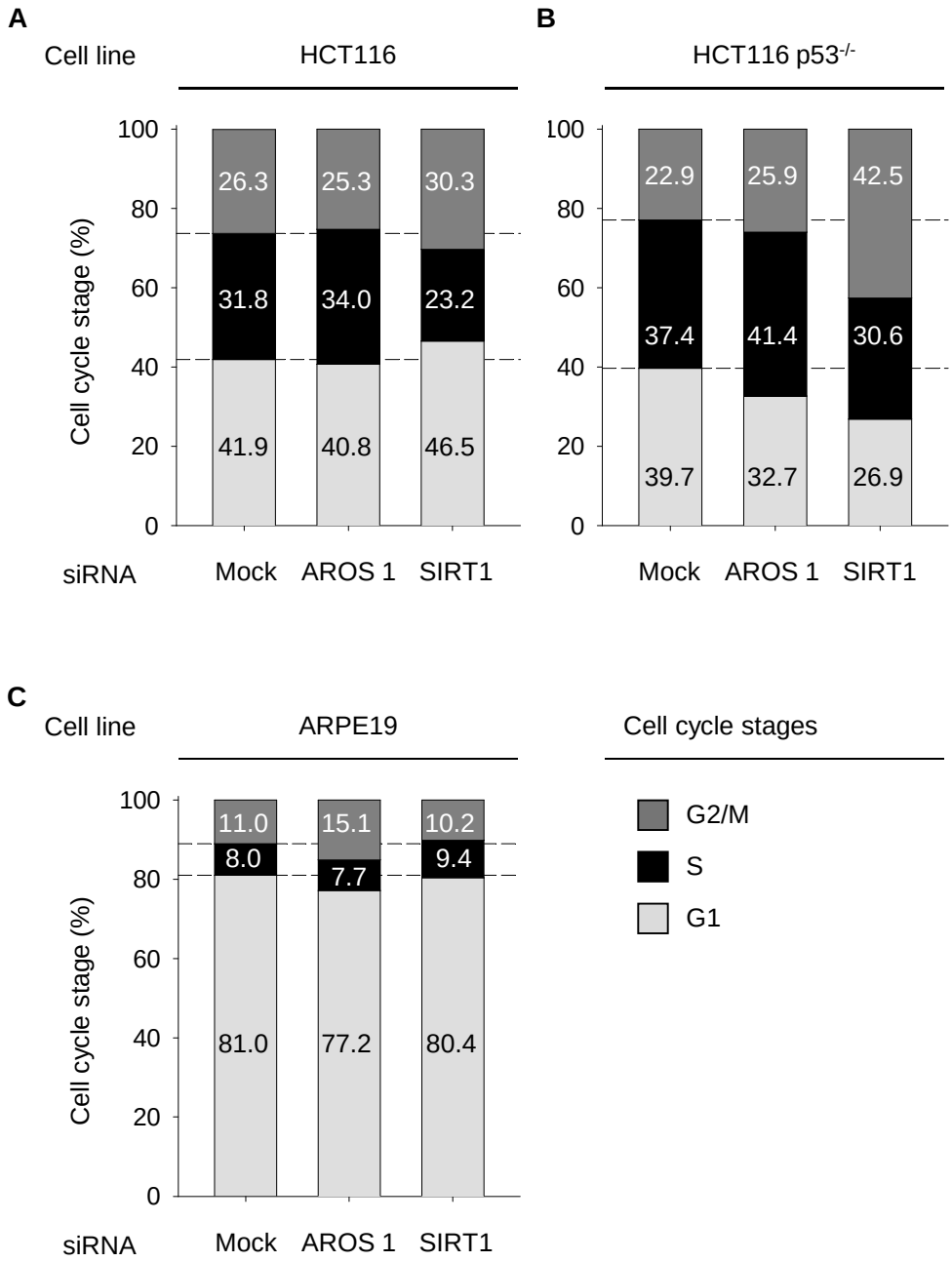

Figure 5.3: AROS and SIRT1 affect cell cycle differently

(A) Cell cycle distribution according to propidium iodide intercalation and flow cytometry, presented as a percentage of cells for each condition (see *Methods*). HCT116 cells were treated with siRNA as indicated and harvested 48 hours later. **(B)** Data presented as in (A) for the HCT116 p53$^{-/-}$ cell line harvested 72 hours post-transfection. **(C)** Data presented as in (A) for the ARPE19 cell line harvested 72 hours post-transfection.

5.3.3 Non-cancer cell lines

Knockdown of AROS in three cell lines of non-cancerous origin did not greatly alter cell phenotype compared to Mock or Lamin AC siRNA treated cells (Figure 5.4). Silencing of AROS in the ARPE19 retinal epithelial cell line resulted in a slight change in morphology, with cells appearing more rounded than Mock transfected cells and resembling Lamin AC siRNA treated more than Mock treated cells. Silencing of SIRT1 in this cell line causes a distinct morphological change, with the cells becoming refringent and elongated. This has been attributed to differentiation of the ARPE19 cells into neuronal cells and has been an independent parallel project within the laboratory. AROS siRNA 2 also had little effect on the phenotype of the ARPE19 cells (Figure 5.4). This difference is consistent with the hypothesis that '*AROS and SIRT1 have different effects on cell phenotype*'.

These phenotypes are not indicative of apoptosis in the ARPE19 cell line. This was confirmed in Figure 5.5B, where knockdown of Lamin AC, SIRT1 or AROS did not result in a significant induction of apoptosis under basal conditions. Silencing of AROS or SIRT1 also had little effect on cell cycle distribution (Figure 5.3C). Slight variation in the fraction of cells in G2/M or G1 occurred, but the number of cells in S phase was comparable between conditions. This suggests that non-cancer cell cycle progression was not affected by silencing of AROS or SIRT1.

The phenotype of the WI38 lung fibroblast cell line was unaltered from Mock by Lamin AC, SIRT1 or AROS siRNA. Similarly, silencing of all three targets in the MCF10A mammary gland epithelium cell line had little effect on phenotype. This is consistent with Lamin AC, SIRT1 and AROS not being essential for either WI38 or MCF10A viability. Consistent with this, silencing of SIRT1 and AROS in both cell lines did not induce an increase of apoptosis compared to Mock (Figure 5.5).

Together the phenotypes of these three non-cancer cell lines suggest that *'AROS is not required for non-cancer cell survival'*. SIRT1 is a cancer specific survival factor (Ford et al. 2005), and the data for AROS are highly correlative with this function of SIRT1. The data also indicate that AROS may be an effective anti-cancer therapeutic target under these basal conditions.

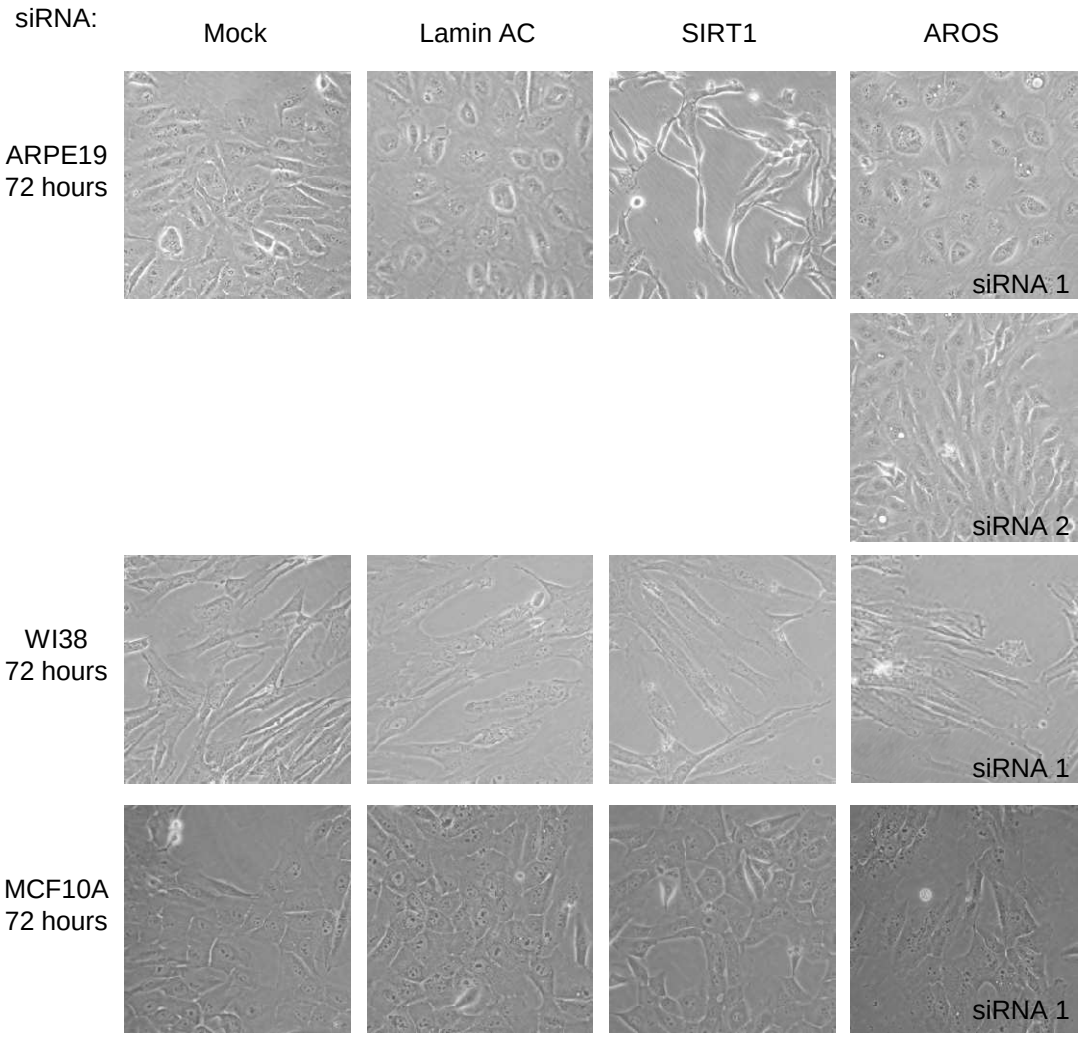

Figure 5.4: AROS has little effect on non-cancer cell phenotype

Phase contrast micrographs of non-cancer cell lines following transfection of siRNA as indicated. Cells were treated with siRNA and phenotype recorded at 72 hours post-transfection. AROS siRNA refers to siRNA 1, apart from transfection of siRNA 2 in the ARPE19 cell line.

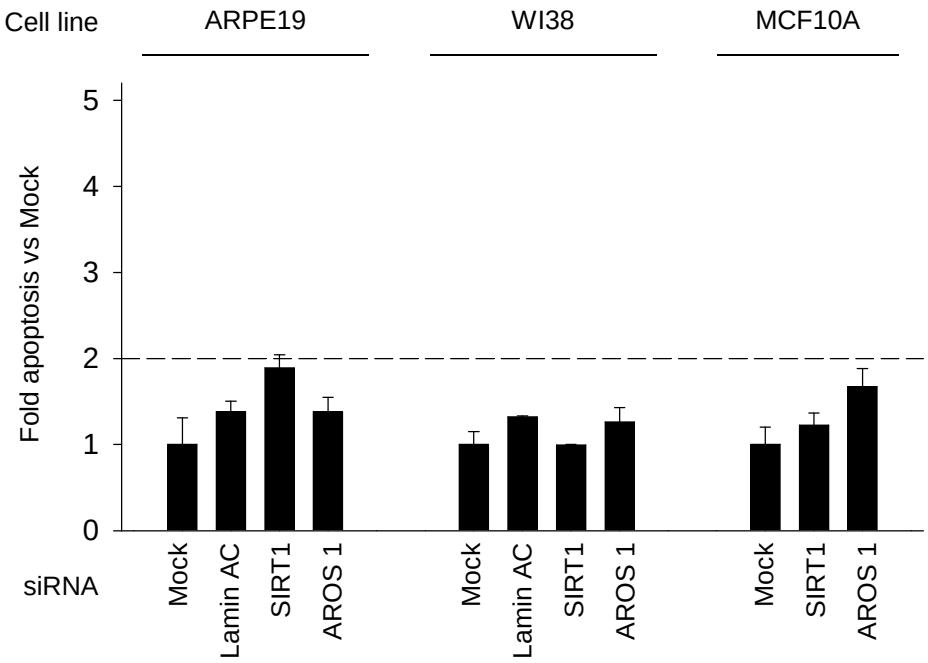

Figure 5.5: AROS silencing does not induce non-cancer cell apoptosis

Fold apoptosis compared to Mock treated cells following RNAi as indicated in three non-cancer cell lines. Cells were treated with siRNA 72 hours prior to harvesting and analysis by Annexin V staining and flow cytometry (See *Methods*).

5.4 *Cell fate following applied stress*

5.4.1 Etoposide and trichostatin A

As discussed in *Chapter 4*, application of etoposide and trichostatin A (TSA) results in cell stress, indicated by an increase in p53 protein abundance. This drug treatment was used during the original characterisation of AROS, where knockdown was seen to stabilise p53 acetylation and induce cancer cell death (Kim et al. 2007). However, as shown in *Chapter 4*, silencing of AROS in combination with etoposide and TSA did not induce stabilisation of p53 acetylation. This was performed in two separate cell lines – the HCT116 colorectal adenocarcinoma line and the ARPE19 retinal epithelium line, of non-cancerous origin. The effect of silencing and drug treatment on cell phenotype is more consistent with the original report and a role for AROS in specific cancer cell survival.

Etoposide and TSA stress in the HCT116 cell line appeared to increase the number of apoptotic cells compared to non-drug treated cells (Figure 5.6A). Consistent with this a slight increase in apoptosis was seen following application of etoposide and TSA (Figure 5.6B). Silencing of SIRT1 or AROS combined with drug treatment appeared to give an even greater increase in apoptosis seen by phase contrast microscopy (Figure 5.6A). This was confirmed as increased apoptosis by flow cytometry (Figure 5.6B). As previously seen in cancer cells under basal conditions, the values for the fold induction of apoptosis are almost identical for SIRT1 and AROS silencing.

Etoposide and TSA treatment of the non-cancer ARPE19 cell line did not appear to alter the phenotype of the cells (Figure 5.6A). This is consistent with no increase in apoptosis following the drug treatment (Figure 5.6B). Silencing of AROS combined with etoposide and TSA treatment did not result in an altered phenotype or induction of apoptosis compared to Mock siRNA and drug treated cells. In contrast, SIRT1 silencing resulted in an increase in detached refringent cells and an alteration in adhered morphology (Figure 5.6A). This alteration is similar to morphology under basal conditions, which represents a neuronal differentiation. However, despite an increase in apoptotic cells, this was not significant compared to Mock siRNA and drug treated cells (Figure 5.6B).

5.4.2 Ultraviolet irradiation

Ultraviolet (UV) irradiation was used as an alternative means to induce cell stress, and analyse molecular effects, as described in *Chapter 4*. Under these conditions, AROS appeared to suppress p53 acetylation. This was consistent with AROS promoting the activity of SIRT1, which was seen to suppress p53 acetylation in parallel. Silencing was efficiently carried out in the HCT116 and HCT116 $p53^{-/-}$ cell lines. The phenotype of silencing both AROS and SIRT1 was predicted to be similar, given the similarities in molecular alterations.

UV irradiation of Mock treated HCT116 cells produced an increase in apoptotic cells with a concomitant reduction in the adhered cell population compared to non-irradiated cells (Figure 5.8A). Apoptosis was confirmed by Annexin V staining and FACS analysis (Figure 5.8B). Silencing of both SIRT1 and AROS resulted in a comparable phenotype by phase contrast microscopy (Figure 5.8A); HCT116 cells appeared at a lower density than Mock irradiated cells, with the majority of cells apparently unadhered and refringent. This suggests an induction of apoptosis, as well as alterations in the cell cycle following silencing of each target. A significant induction of apoptosis was seen compared to Mock irradiated cells, with both SIRT1 and AROS silencing achieving a greater than 7-fold induction (Figure 5.8B). Again consistent with the phenotype, silencing of AROS or SIRT1 altered cell cycle distribution (Figure 5.8C). An increase in G1 cells and reduction in G2/M cells was observed following silencing of AROS or SIRT1. The population of cells in S phase appeared similar to Mock treated, UV irradiated cells. Interestingly, the alteration in cell cycle distribution was almost identical between AROS and SIRT1 siRNA treated cells.

The data here suggest that in the HCT116 cell line following UV irradiation, silencing of SIRT1 or AROS has highly similar effects on cell phenotype, apoptotic induction and cell cycle distribution. This is in contrast to the seemingly different roles of SIRT1 and AROS under basal conditions and following etoposide / TSA treatment (see above). The previous differences in cell phenotype correlate with differences in suppression of p53 – SIRT1 did suppress p53, whereas AROS did not. Following UV irradiation here, both SIRT1 and AROS *did* appear to suppress p53

acetylation (*Chapter 4*). Interestingly, this correlation in molecular function also correlates with phenotype. Silencing of SIRT1 or AROS only appeared to alter cell cycle distribution under conditions where p53 acetylation was stabilised. This suggests that p53 is important for cell cycle distribution following silencing of AROS or SIRT1.

To further analyse this, silencing was carried out in the HCT116 $p53^{-/-}$ cell line following UV irradiation. Should p53 play an important role in cell cycle distribution following AROS or SIRT1 silencing, this cell line would not be expected to experience such alterations. Following AROS silencing and UV irradiation in the HCT116 $p53^{-/-}$ cell line, cell cycle distribution appears almost identical to the distribution for Mock siRNA and UV irradiated cells (Figure 5.9C). There is perhaps a slight reduction in the S phase population, but this may not be significant. In contrast, silencing of SIRT1 induces a reduction in the S phase population, due to a large increase in cells in the G2/M phase (Figure 5.9C). These data for SIRT1 silencing following UV stress are comparable to the effect recorded under basal conditions (Figure 5.3B).

Together, the cell cycle analyses following AROS silencing reveal a potential correlation between molecular effects and cellular outcome. AROS appeared to only suppress p53 acetylation following the application of UV irradiation, and this correlated with the only incidence of alterations in cell cycle distribution following AROS silencing. As such, AROS appears to be required for stabilisation of p53 acetylation in response to UV stress, and associated suppression of alterations in the cell cycle. Consistent with this, cell cycle distribution was not altered in the HCT116 $p53^{-/-}$ cell line, even with the application of UV irradiation. This is highly indicative that the cell cycle arrest induced by AROS is dependent upon p53. The reliance upon UV irradiation to allow AROS to influence p53 acetylation and cell cycle distribution is indicative of an unknown factor altering the relationship between AROS, SIRT1 and p53. This could be one of the factors themselves and/or an external contributor, potentially activated by the UV irradiation process.

This section demonstrates a divergence from the heterogeneity between SIRT1 and AROS function, with only subtle differences seen following UV

irradiation. Interestingly, these differences seem to involve p53 regulation and potentially subsequent function in controlling cell cycle progression. The data here conclude the analysis of p53 regulation by SIRT1 and AROS. For the remainder of the *Chapter* the regulation of the FOXO proteins is the focus.

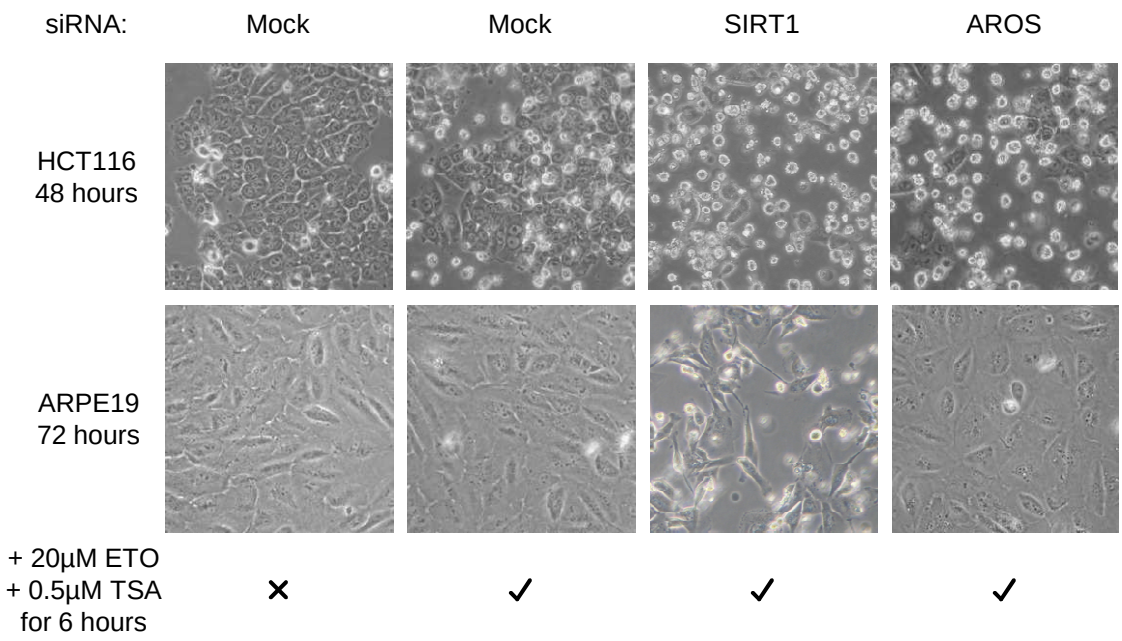

Figure 5.6: The role of AROS in cell viability after stress - etoposide and TSA (I)

Phase contrast micrographs of HCT116 and ARPE19 cells following transfection with siRNA for the indicated time and administration of etoposide (ETO) and trichostatin A (TSA) as shown. Non-drug treated cells are included as a control.

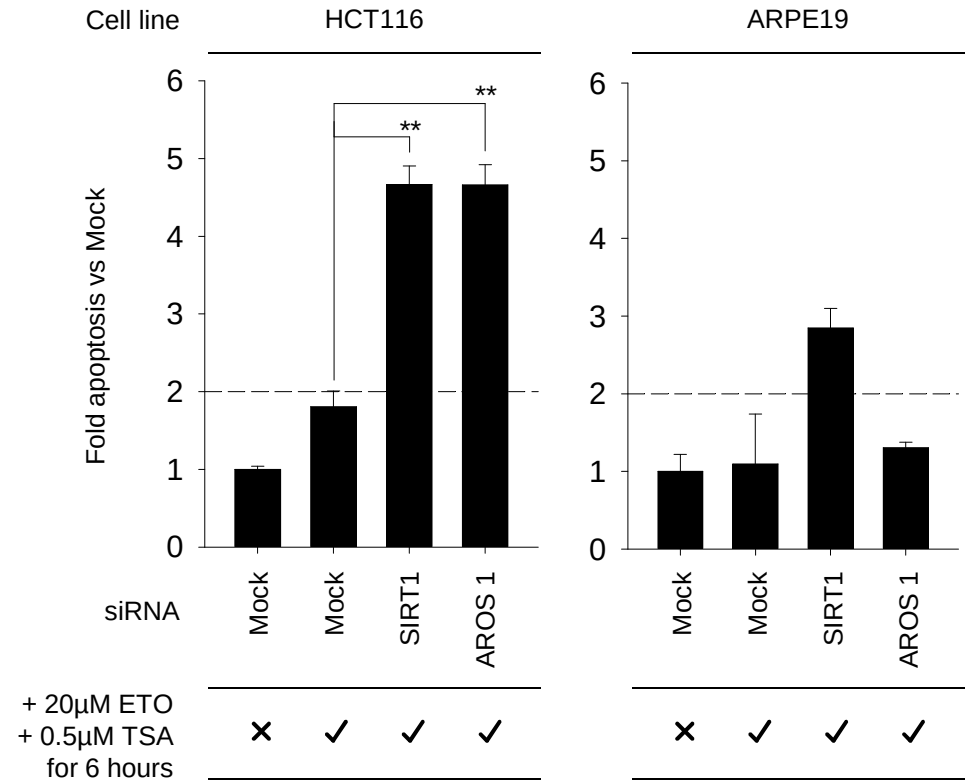

Figure 5.7: The role of AROS in cell viability after stress - etoposide and TSA (II)

Values represent fold apoptosis following siRNA transfection compared to Mock transfected, non-drug treated cells in the cell lines from Figure 5.6. Cells were treated with siRNA as indicated and analysed by Annexin V staining and flow cytometry (See *Methods*). ** P<0.01.

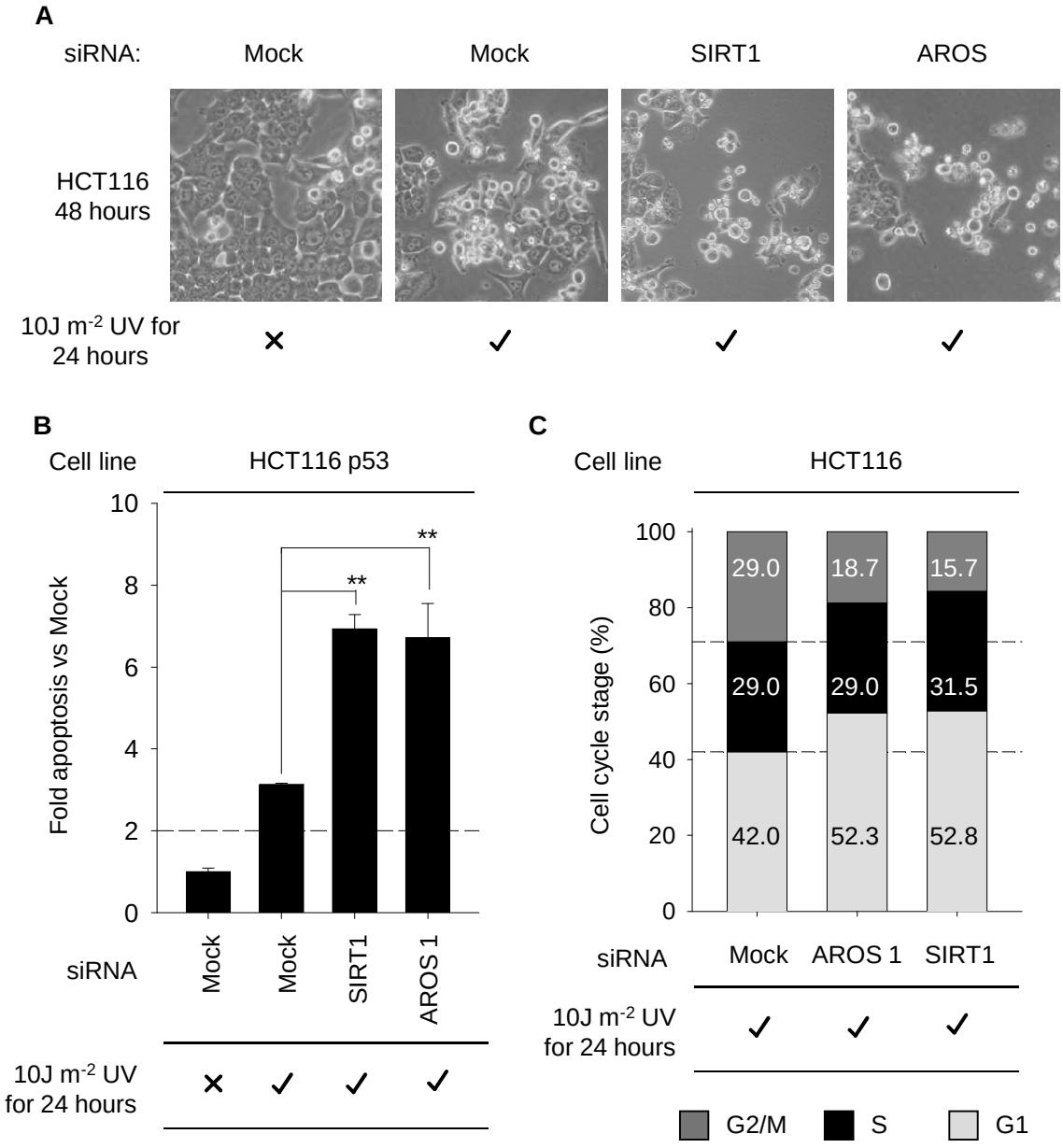

Figure 5.8: The role of AROS in cell viability after stress - UV irradiation

(A) Micrographs from phase contrast microscopy of HCT116 colorectal adenocarcinoma cells following transfection and UV irradiation as indicated. Cells were transfected with siRNA 48 hours prior to harvesting, and irradiated with UV 24 hours prior to harvesting. **(B)** Apoptosis quantified by Annexin V staining and flow cytometry, represented as fold change compared to non-irradiated Mock in the HCT116 cells treated as in (A). ** P<0.01. **(C)** Cell cycle distribution as a percentage of total cells analysed following transfection and UV irradiation as detailed in (A). Cell cycle stages were determined by propidium iodide intercalation and flow cytometry (see *Methods*).

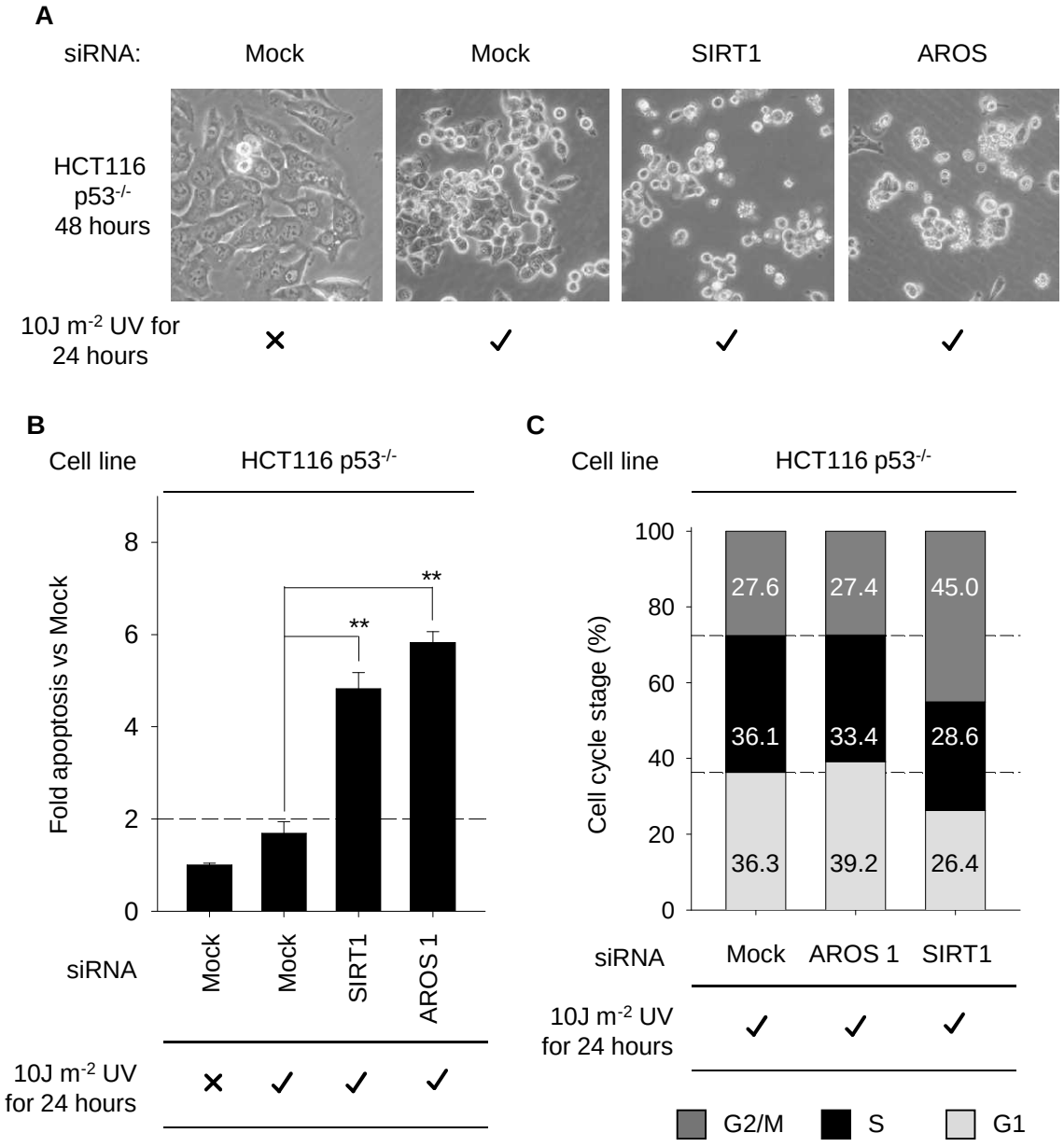

Figure 5.9 The role of AROS in cell viability after stress - UV irradiation without p53

(A) Phase contrast micrographs of HCT116 p53$^{-/-}$ cell phenotype 72 hours following siRNA transfection, and 24 hours following UV irradiation as indicated. **(B)** Apoptotic cell death following treatment as in (A) quantified by Annexin V staining and flow cytometry. Data represent fold change compared to Mock siRNA treated non-irradiated cells. ** P<0.01. **(C)** Percentage of total cells within each stage of the cell cycle, determined by flow cytometry of propidium iodide intercalation (see *Methods*). Cells were treated with siRNA and UV irradiation as in (A).

5.5 *Suppression of FOXO4 by AROS*

5.5.1 FOXO4 promotes apoptosis downstream of AROS

AROS has been characterised as a p53 independent suppressor of apoptosis (see above). This has parallels with the published role of SIRT1 and prompted further analysis of potential continuing parallels (Ford et al. 2005). SIRT1 deacetylates and suppresses the pro-apoptotic function of the FOXO proteins (Brunet et al. 2004; Motta et al. 2004). Importantly the basal anti-apoptotic function of SIRT1 is specifically dependent upon FOXO4 expression; cosilencing of SIRT1 and FOXO4 resulted in complete rescue of apoptosis induced by SIRT1 silencing alone (Ford et al. 2005). Interestingly, cosilencing of SIRT1 and FOXO3 did not rescue the apoptotic phenotype. With this considered, cosilencing of AROS was carried out with both FOXO4 and FOXO3. Individual silencing of each FOXO protein was also undertaken to analyse the basal roles of these tumour suppressors.

Silencing of AROS in the HCT116 colorectal adenocarcinoma cell line resulted in a phenotype consistent with previous experiments and the induction of apoptosis, confirmed by flow cytometry (Figure 5.10A and B). Cosilencing of AROS with FOXO4 resulted in a phenotype comparable to Mock transfected cells, more cells were adhered and fewer were refringent than with AROS silencing alone (Figure 5.10A). This suggests that FOXO4 silencing rescues apoptosis suppressed by AROS. In agreement with this, flow cytometric analysis of AROS and FOXO4 cosilencing resulted in a significant reduction in apoptosis compared to AROS silencing alone. The level of apoptosis was similar to that following Mock transfection. This correlates with the role of SIRT1 in regulation of FOXO4 and supports the hypothesis that *'AROS is required for SIRT1 suppression of FOXO4'*.

As mentioned, SIRT1 does not suppress apoptosis via FOXO3 (Ford et al. 2005). Cosilencing of AROS and FOXO3 parallels this result, with no alteration in the fold increase in apoptosis compared to AROS silencing alone (Figure 5.10). Thus, AROS suppresses apoptosis via FOXO4, but independently of FOXO3. Silencing of FOXO4 and FOXO3 individually resulted in a modest increase in apoptotic HCT116 cells, but this did not constitute a significant induction of apoptosis (Figure 5.10).

Cancer associated SIRT1 suppression of FOXO4 occurs in both the presence and absence of p53 (Ford et al. 2005). This is consistent with SIRT1 suppressing apoptosis independently of p53 expression. FOXO4 appears to be a highly important tumour suppressor for suppression by SIRT1. Silencing of AROS alongside cosilencing of AROS with both FOXO4 and FOXO3 in the HCT116 $p53^{-/-}$ cell line resulted in similar phenotypes and apoptotic induction compared to the HCT116 cell line (Figure 5.11). The extent of rescue with FOXO4 cosilencing appears to be reduced but is significant, supporting a p53 independent role for AROS in suppression of FOXO4. , This correlation is consistent with the hypothesis that *'AROS is required for SIRT1 suppression of FOXO4'*.

Silencing of *AROS* and *FOXO4* was verified at the mRNA level by qRT-PCR for both HCT116 and HCT116 $p53^{-/-}$ cells (Figure 5.12A). Silencing was achieved individually as well as by cosilencing of each target. Protein level silencing of AROS was previously verified on multiple occasions (*Chapter 4*). Protein silencing of FOXO4 was not verified due to the lack of a reliable antibody for this purpose. However, the reduction in *FOXO4* mRNA and the strong phenotypic effect of cosilencing with AROS are highly suggestive of a reduction in the functional FOXO4 protein.

5.5.2 AROS and SIRT1 suppress FOXO4 target gene transactivation

The pro-apoptotic Bcl-2 family protein BIM is a target for genetic transactivation by the FOXO proteins (Gilley et al. 2003). Furthermore, reduced SIRT1 activity has been linked to FOXO4 dependent induction of *BIM* transcription (Motta et al. 2004). Consistent with this, silencing of SIRT1 in HCT116 cells resulted in a significant increase in *BIM-L* mRNA compared to Mock treated cells (Figure 5.12B). *BIM-L* is one of three specific splice variants derived from the *BIM* gene, which is able to induce apoptosis upon overexpression (O'Connor et al. 1998). Upregulation of *BIM-L* following SIRT1 silencing suggests increased transactivation by FOXO4.

Given the similarities between SIRT1 and AROS in their suppression of the pro-apoptotic activity of FOXO4, the effect of AROS silencing on *BIM-L* mRNA

was also analysed. Silencing of AROS also induced a significant increase in *BIM-L* mRNA expression compared to control, with levels of induction almost identical to those for SIRT1 silencing (Figure 5.12B). This suggests that AROS is required for SIRT1 suppression of FOXO4 mediated apoptosis, which is at least in part promoted by BIM-L.

To test this further, the level of *BIM-L* mRNA following cosilencing of FOXO4 with either SIRT1 or AROS would be required. This would indicate whether FOXO4 is the key intermediary in the regulation of *BIM-L* by SIRT1 and AROS. It would also be possible to co-silence AROS or SIRT1 with BIM-L in HCT116 cancer cells. This would demonstrate if *BIM-L* is a crucial pro-apoptotic gene suppressed by SIRT1 and AROS. Unfortunately, in this analysis only single silencing was analysed due to time constraints, but these experiments represent possibilities for the future.

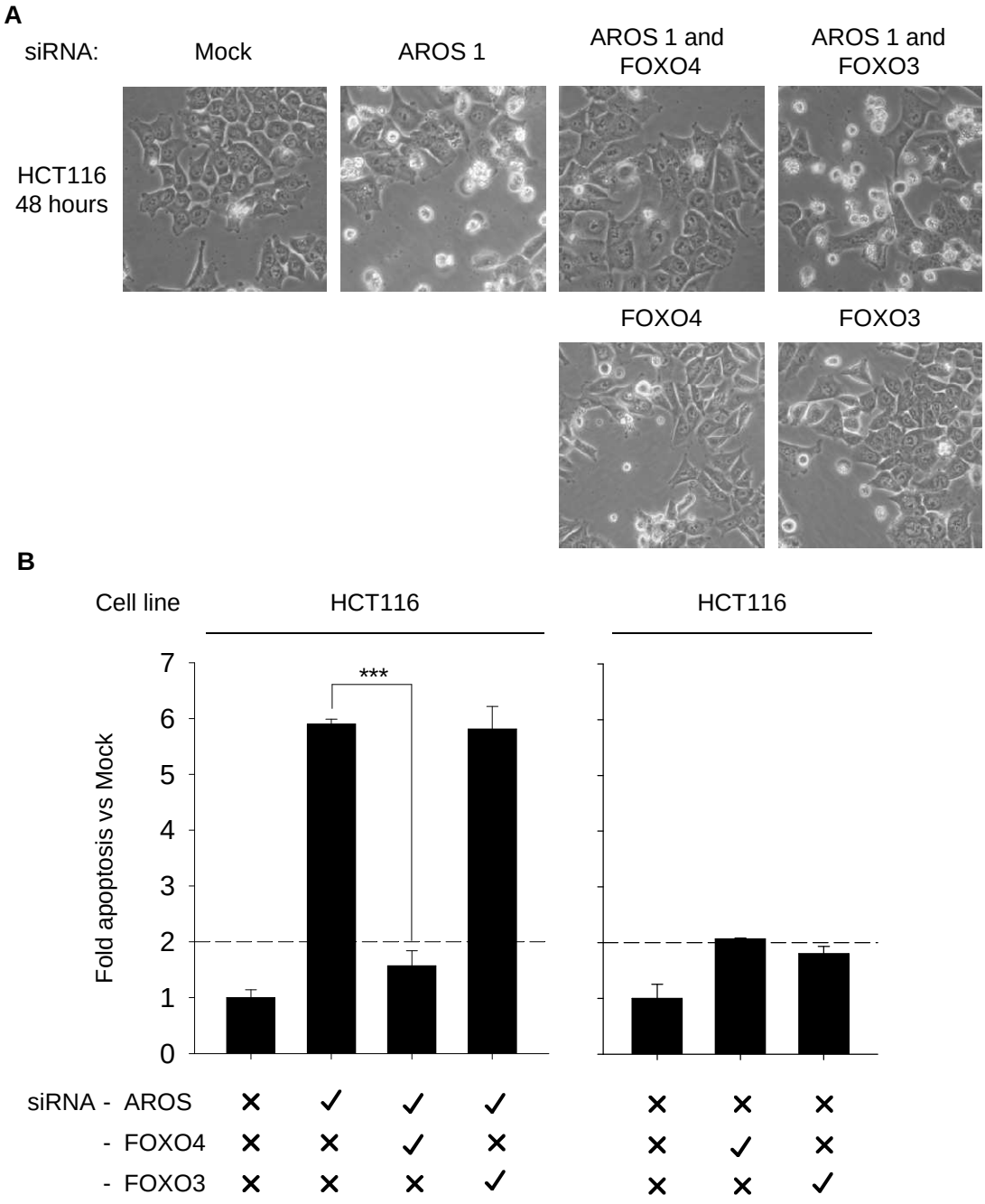

Figure 5.10: FOXO4 expression is required for AROS silencing induced apoptosis

(A) Micrographs from phase contrast microscopy of HCT116 cells treated with basal siRNA transfection as indicated. Cells were exposed to siRNA for 48 hours prior to recording of images. **(B)** Apoptotic induction following siRNA treatments detailed in (A). Data are shown as relative to apoptosis following Mock transfection. Separate graphs indicate separate cell experiments. *** P<0.001.

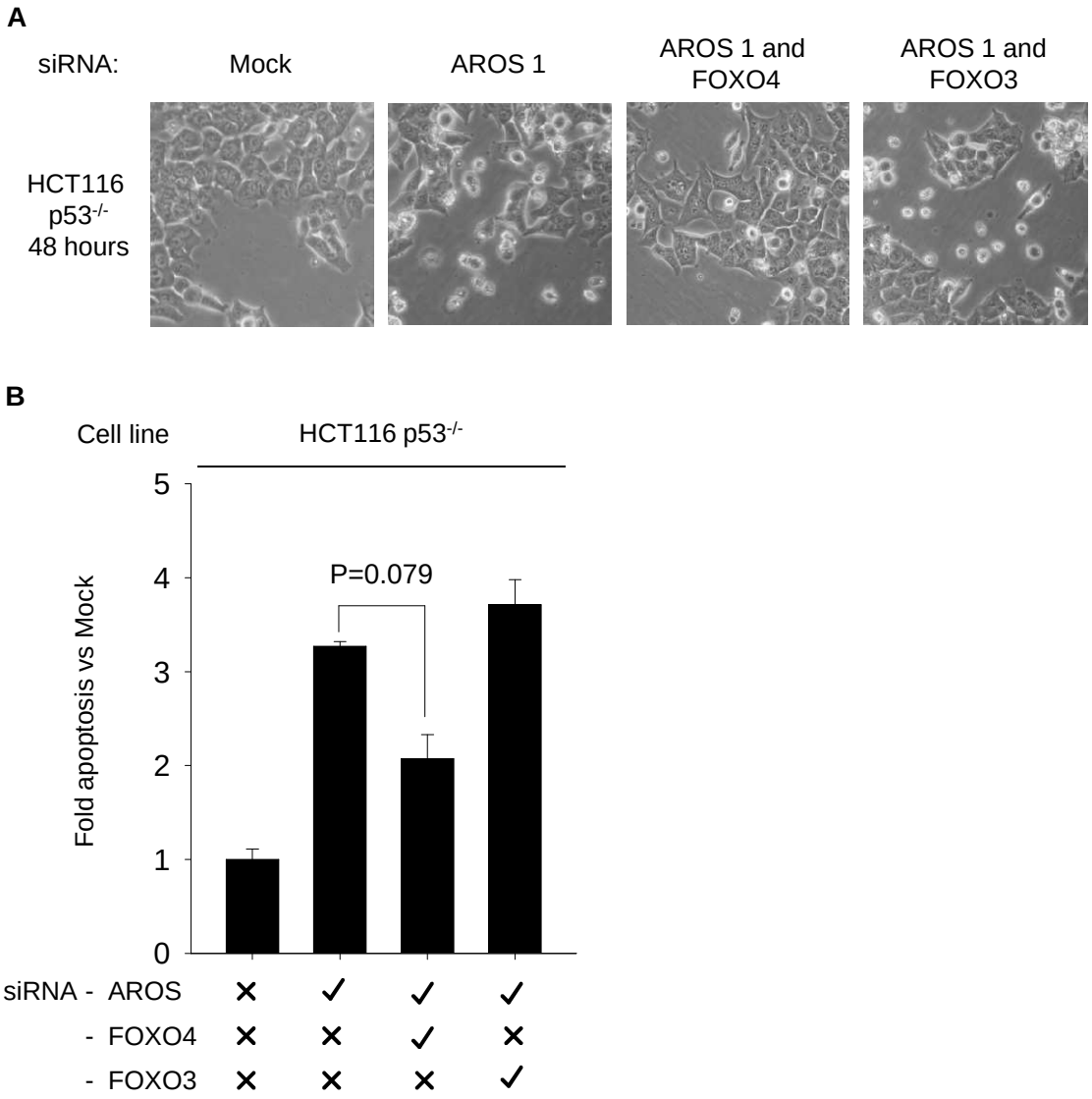

Figure 5.11: FOXO4 expression is required for AROS silencing induced apoptosis, independently of p53

(A) Phase contrast micrographs of HCT116 p53$^{-/-}$ cells 72 hours after basal siRNA treatment targeted against specific mRNA. **(B)** Fold change in apoptosis following basal siRNA transfections as indicated. Cells were harvested for Annexin V staining and flow cytometry analysis 72 hours post-transfection.

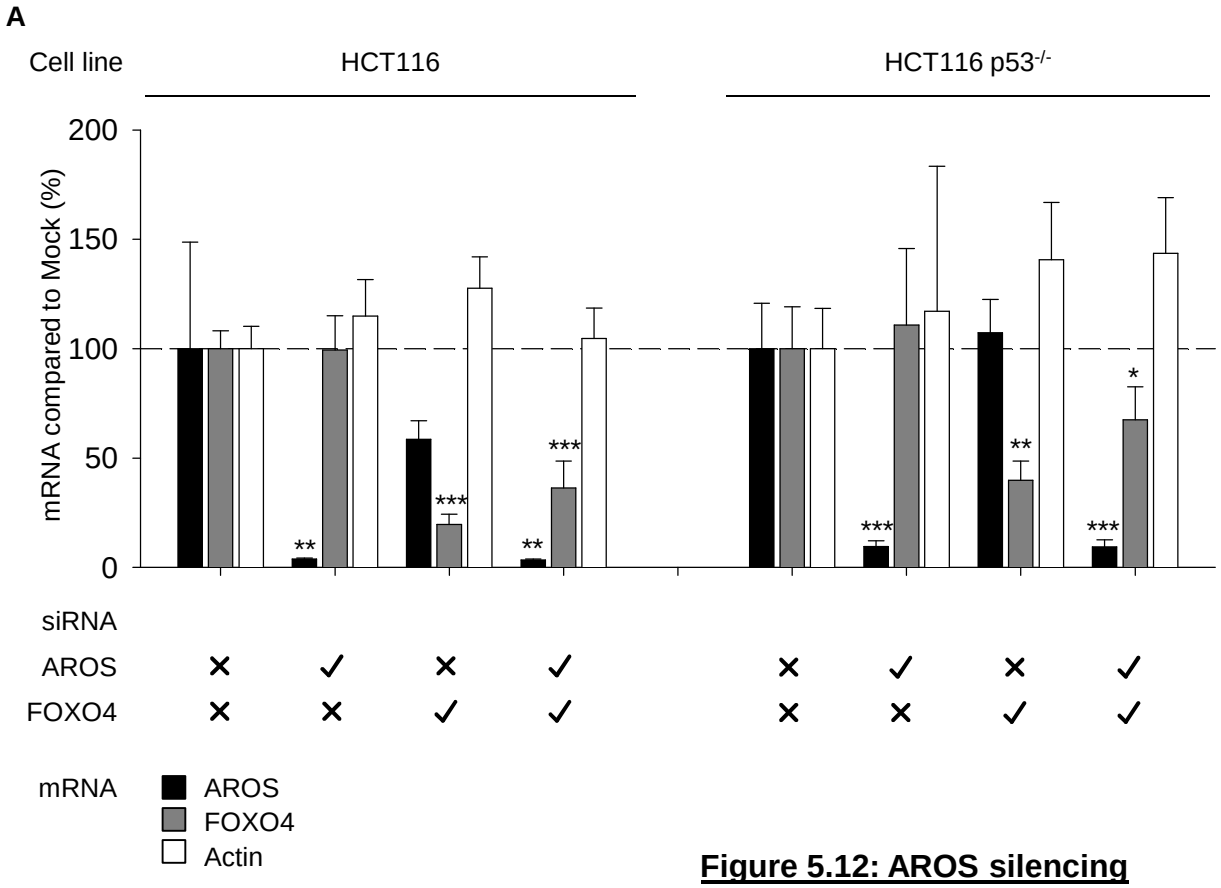

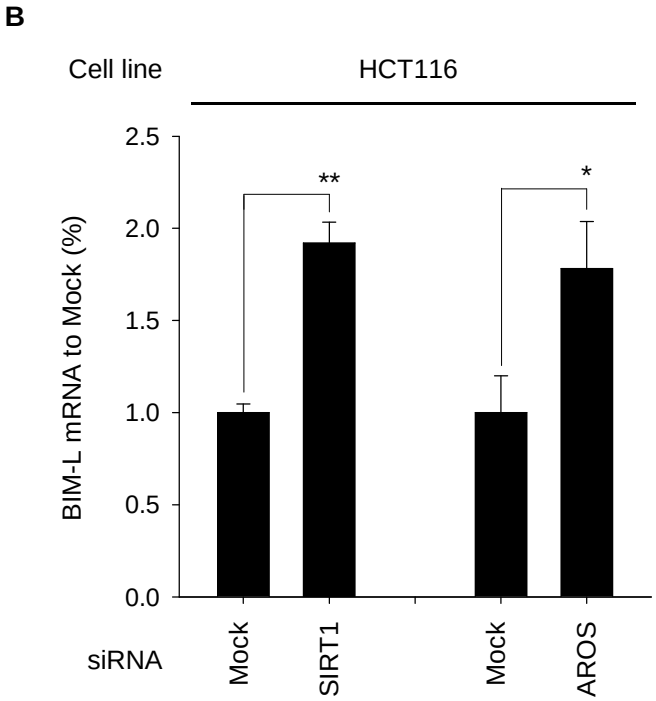

Figure 5.12: AROS silencing induces *BIM-L* expression

(A) Total RNA was harvested 48 hours (HCT116) or 72 hours (HCT116 p53$^{-/-}$) following basal siRNA transfection as indicated. RNA was isolated by the RNeasy method and analysed by qRT-PCR using specific primers for target mRNAs. *Actin* mRNA was used as a loading control. **(B)** HCT116 cells were treated and total RNA isolated as indicated in (A). *BIM-L* mRNA was quantified by qRT-PCR, standardised against *Actin* mRNA expression. Separate graphs indicate separate cell experiments. ** P<0.01, * P<0.05.

5.6 *Discussion*

5.6.1 AROS and apoptosis

AROS anti-apoptotic activity was reported during its original characterisation (Kim et al. 2007); this was under cellular stress caused by etoposide and TSA in two cancer cell lines (HCT116, H1299). This has been expanded here with the observation that AROS is anti-apoptotic in a larger panel of cancer cell lines of both wild-type and null p53 status. AROS appeared to be required for apoptotic evasion in all the cancer cell lines analysed, consistent with the hypothesis that *'AROS is required for cancer cell survival under physiological and stress conditions'*.

Independence from p53 is desirable for putative anti-cancer therapeutic targets due to the high mutation and misregulation rate of p53 in human tumours (Vogelstein et al. 2000; Olivier et al. 2010; Goh et al. 2011). AROS appears to be essential for suppression of basal apoptotic pathways that do not require p53. Thus, targeting of AROS may activate these pathways and induce cancer cell death irrespective of p53 status.

This role of AROS is similar to the reported role of SIRT1 (Ford et al. 2005), which has also been confirmed here. In *Chapter 4* the complete knockdown of AROS was not achieved – a population of AROS persisted in the cytoplasm of HCT116 cells after AROS siRNA treatment. Importantly, this level of knockdown induced apoptosis as recorded here. The molecular data in *Chapter 4* also indicated that AROS did not affect p53 in the HCT116 cell line. This is consistent with the p53 independence in apoptotic induction reported in this *Chapter*.

Strikingly, the fold induction of apoptosis in all cancer cell lines analysed under all conditions is almost identical for both SIRT1 and AROS silencing (*this Chapter*). The values for the fold induction of apoptosis are listed in the *Appendix*. The data are suggestive of a highly similar role in the suppression of apoptosis for both proteins. Furthermore, the similarities between SIRT1 and AROS extend to their downstream effects. Both SIRT1 and AROS suppress FOXO4 pro-apoptotic activity, evinced by requirement for FOXO4 for apoptosis in the absence of SIRT1

or AROS (Ford et al. 2005 and Figures 8 and 9). This is summarised in Figure 5.13A and B.

The correlation between silencing of AROS and SIRT1 appears to extend further downstream of FOXO4. Both AROS and SIRT1 silencing induce expression of *BIM-L* mRNA, a pro-apoptotic target of FOXO4, which is consistent with both AROS and SIRT1 suppressing FOXO4 function, with AROS and SIRT1 likely acting in complex as proposed by Kim and colleagues (2007). This is consistent with the hypothesis that *'AROS is required for SIRT1 suppression of FOXO4'*. These observations represent the first characterisation of regulation of FOXO4 by AROS, and the first characterisation of the effect of AROS on multiple SIRT1 targets – both p53 and FOXO4.

Dependence upon FOXO4 and BIM as pro-apoptotic effectors following targeting prompts the analysis of gene expression in cancer cells. For effective anti-cancer therapeutic targeting of AROS or SIRT1, the *FOXO4* or *BIM* genes may need to be intact. Mutation of either gene would be detrimental for the application of therapeutics against either AROS or SIRT1. Interestingly the mutation rate of the FOXO proteins in primary glioblastomas reported by The Cancer Genome Atlas Research Network (2008) was 1% . Furthermore, no mutations were reported in the *BIM* gene. This indicates that *FOXO4* or *BIM* mutation may be rare in cancer, and is promising for the targeting of AROS or SIRT1 for anti-cancer therapeutic gain.

5.6.2 AROS and the cell cycle

AROS appeared to affect the cell cycle distribution of HCT116 colorectal adenocarcinoma cells only following UV irradiation and in the presence of p53, which is strong evidence that AROS can suppress p53 activity under certain conditions, and that this has a functional significance. This correlates well with the molecular effects seen in *Chapter 4*, with AROS only affecting cell cycle distribution in the single case where it suppressed p53 acetylation in the HCT116 cells.

SIRT1 appeared to regulate the cell cycle under all conditions, in the presence or absence of p53. The observed cases of p53 independence suggest that

SIRT1 *is* able to influence cell cycle distribution via mechanisms not involving p53. This contrasts to the proposed role for AROS, which strictly requires p53 and is consistent with the hypothesis that *'AROS and SIRT1 have different effects on cell phenotype, consistent with different molecular effects'*. These differences are summarised in Figure 5.13A and B. A further implication of the data is that SIRT1 is able to suppress p53, and other targets, without the need for AROS as an activator protein under certain conditions.

5.6.3 AROS as an anti-cancer therapeutic target

AROS is required for survival of multiple cancer cell lines under all conditions analysed. Importantly, AROS does not appear to be required for non-cancer cell survival, based on data presented for 3 non-cancer cell lines (Figure 5.4). These cell lines are from multiple origins: the pigmented retinal epithelium (ARPE10), the mammary gland epithelium (MCF10A) and lung fibroblasts (WI38). Further to this, AROS does not appear to regulate the ARPE19 cell cycle, with only slight alterations in cell cycle distribution seen following silencing (Figure 5.3C). Redundancy for AROS following transient knockdown in relation to survival in these cell lines agrees with the hypothesis that *'AROS is not required for non-cancer cell survival'*, and presents AROS as a cancer-specific survival factor.

The data also suggest that the AROS-SIRT1 interaction is important for regulation of cell survival, mediated via FOXO4 and BIM-L. The opportunity to target this pathway appears feasible. Whether AROS or SIRT1 suppress this pathway in non-cancer cells has not been assessed; however, if suppression does occur it is clear that this is not important in the context of cell viability. Furthermore, the indication that both AROS and SIRT1 govern this pathway suggests that inhibition of this interaction may be sufficient to induce cancer cell death, with little effect on non-cancer cells.

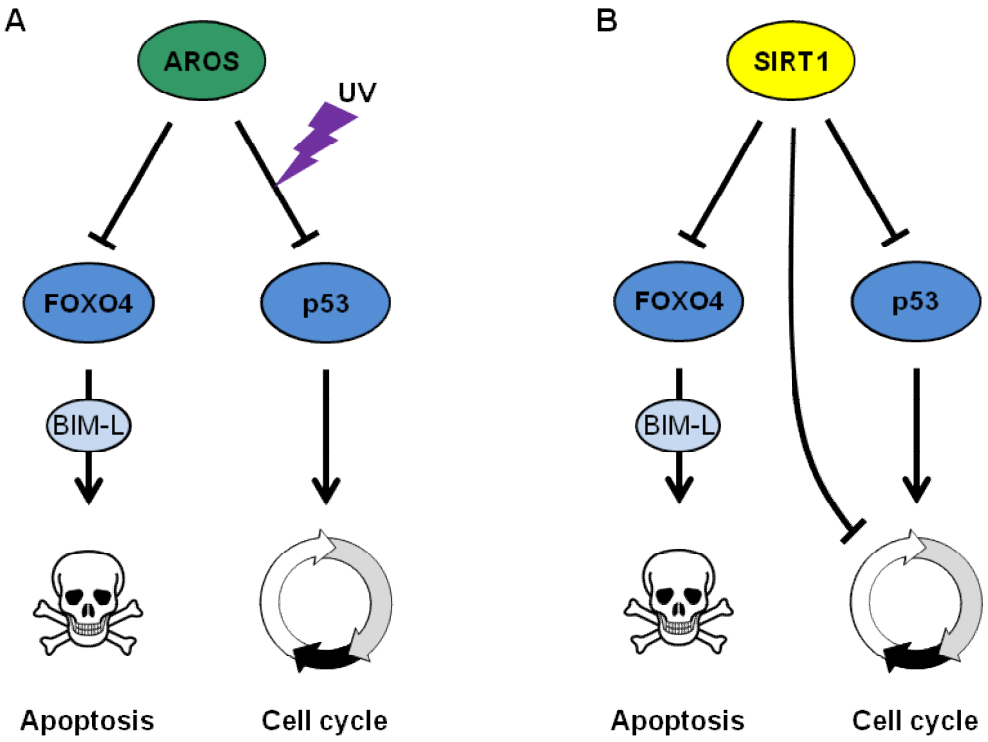

Figure 5.13: AROS and SIRT1 in HCT116 colorectal cancer cells

(A) Schematic of the role of AROS in regulation of FOXO4 and p53 in HCT116 cells. AROS suppresses FOXO4 which is essential for induction of apoptosis following AROS silencing. BIM-L is revealed as a FOXO4 target also suppressed by AROS. AROS also suppresses p53, but only following UV irradiation of HCT116 cells. AROS silencing induced cell cycle alterations appear to be p53-dependent. It is likely that the functions attributed to AROS here are functions of an AROS-SIRT1 complex. **(B)** Schematic as for (A) but for the function of SIRT1. SIRT1 shares the role of AROS in suppression of FOXO4 (Ford et al. 2005). This is similar to the AROS-FOXO4 relationship in (A). SIRT1 suppresses p53 under all conditions analysed. SIRT1 suppression of cell cycle progression acts, at least in part, via p53. However, it is also evident that SIRT1 suppresses cell cycle progression via p53 independent mechanisms.

5.7 *Conclusions*

1. AROS is required for cancer cell survival, but not for non-cancer cell viability. This identifies AROS as a novel anti-cancer therapeutic target.
2. AROS suppresses apoptosis via FOXO4, independent of p53 expression. Similarity to the role of SIRT1 suggests the AROS-SIRT1 interaction as a potential anti-cancer drug target.
3. p53 may be a crucial factor in cell cycle regulation following AROS silencing under specific stress conditions. This differs to regulation of the cell cycle by SIRT1.

Conclusions 2 and 3 are further evidence that the SIRT1-AROS relationship is more complex than obligate activation. AROS appears to be able to influence both the SIRT1 targets, FOXO4 and p53, but this is dependent upon cell context.

6 The relationship between AROS and RPS19

6.1 *Overview*

This *Chapter* extends the analysis of AROS, which was previously analysed in relation to modulation of SIRT1 activity (see *Chapters 4 and 5*). In addition to SIRT1, AROS is also known to interact with a structural component of the small ribosomal subunit, namely RPS19. RPS19 has been linked to cell survival, creating the possibility that AROS promotes cancer cell survival through RPS19. Here the relationship between AROS and RPS19 is explored using the RNAi experimental model also used in the study of the AROS/SIRT1 relationship (*Chapters 4 and 5*).

This *Chapter* outlines an unexpected outcome of this analysis; the presence of a novel autoregulatory loop between AROS and RPS19. Each protein promotes the abundance of the other, but with no effect on reciprocal mRNA level. Following this observation further analysis of the function of the AROS-RPS19 relationship forms the remainder of this *Chapter* as well as *Chapters 7 and 8*.

6.2 *Introduction*

6.2.1 Ribosomal Protein of the Small subunit 19

RPS19 is a 15kDa protein which functions primarily in the synthesis and subsequent translational activity of ribosomes. Consistent with a role in this essential cellular process, *RPS19* mRNA and protein was widely expressed across tissue samples and cell lines (*Chapter 4 – Figure 4.2*). During ribosome biogenesis RPS19 is required for the processing of pre-ribosomal RNA into 18S rRNA (Choesmel et al. 2007; Flygare et al. 2007; Idol et al. 2007). Both RPS19 and 18S rRNA are essential for small ribosomal subunit structure and function (Ben-Shem et al. 2010; Rabl et al. 2011). The role of RPS19 in ribosome biogenesis is discussed and analysed in greater detail in *Chapter 8*.

6.2.2 Ribosomal proteins, p53 and cell fate

As previously discussed in *Chapters 4 and 5*, the p53 tumour suppressor is a key regulator of cell fate. Suppression of p53 is required to facilitate longevity of cancer cells. At least 10 ribosomal proteins have been directly implicated in the regulation of p53. These proteins stabilise p53 by reducing its proteasomal degradation via sequestration of MDM2 (reviewed by Deisenroth and Zhang 2010). Thus, some ribosomal proteins are able to activate p53. This is believed to constitute a mechanism of ribosomal stress monitoring, reducing cell proliferation in response to aberrations in ribosome production or function which could be deleterious for the cell.

Importantly some ribosomal proteins appear to *suppress* p53 in a mechanism independent of the MDM2 degradation pathway. Among this group of ribosomal proteins is RPS19, which suppresses p53 protein accumulation in the mouse and zebrafish (Danilova et al. 2008; McGowan et al. 2008; Dutt et al. 2011; Jaako et al. 2011). Consistent with this, loss of RPS19 resulted in cell death from the erythroid lineage in these animal models. RPS19 was also required for cell survival following RNAi mediated depletion in human cancer cells (Choesmel et al. 2007). Together this suggests that RPS19 is an anti-apoptotic protein able to influence cell fate via p53. Furthermore, RPS19 appears to be a cancer cell survival factor, with its effect in

human non-cancer cells yet to be formally addressed. Although the negative effect on murine and zebrafish erythroid cell viability suggests that RPS19 may have a wider role in promoting cell survival.

6.2.3 RPS19 and AROS

AROS was identified as a direct binding partner of RPS19 in a yeast-two hybrid screen using the mouse proteins (Maeda et al. 2006). This interaction has not been experimentally identified in humans, although it has been predicted by *in silico* analysis (Orru et al. 2007). Importantly, the function of the interaction is entirely unknown. In *Chapter 5*, AROS was found to be anti-apoptotic in cancer cells. This appeared to occur at least in part via SIRT1, but other factors cannot be ruled out. Thus, the anti-apoptotic functions of RPS19 may overlap with the role of AROS in cancer cell survival.

RPS19 suppression of p53 occurs via an unknown mechanism. In *Chapter 4*, AROS was characterised as a context dependent suppressor of p53. This raises the possibility that RPS19 suppresses p53 via AROS, and therefore SIRT1. This could identify a functional network involving AROS and its two binding partners SIRT1 and RPS19. Furthermore, the network could extend beyond suppression of p53 to include specific promotion of cancer cell survival.

6.2.4 Hypotheses

1. AROS and RPS19 affect reciprocal protein function.
2. AROS specifically promotes cancer cell survival via RPS19.
3. RPS19 affects p53 via regulation of AROS.

6.3 *An autoregulatory loop between AROS and RPS19*

6.3.1 AROS promotes RPS19 abundance

RNAi against AROS in the panel of 5 cancer cells reduces AROS protein expression (Figure 6.1A). In the HCT116 $p53^{-/-}$ colorectal adenocarcinoma and MCF7 mammary gland epithelial cancer cell lines AROS protein is efficiently depleted by siRNA. However, in the HCT116, DLD1and LoVo colorectal adenocarcinoma cell lines depletion of total AROS is less evident. This is consistent with the stability of total AROS seen in *Chapter 4*. In that instance, AROS was found to be depleted by siRNA from the nuclear fraction over the abundant cytoplasmic fraction in HCT116 cells. This may contribute to the stability of total AROS seen here. In all 5 cell lines targeting of *AROS* by siRNA resulted in a specific loss of *AROS* mRNA (Figure 6.1B).

Unexpectedly, depletion of *AROS* by siRNA resulted in depletion of RPS19 protein in 3 of the 5 cell lines analysed (Figure 6.1A). In the HCT116, DLD1 and MCF7 cell lines knock down of *AROS* correlated with a loss of RPS19 protein. There was the possibility that this reduction in RPS19 protein was due to off-target RNAi against *RPS19* mRNA from the AROS siRNA. This would manifest as decreased *RPS19* mRNA expression following AROS siRNA treatment. This did not occur in any of the 5 cancer cell lines, with no reduction in *RPS19* mRNA standardised against housekeeping controls (Figure 6.1B). Indeed, in the MCF7 cell line *RPS19* expression was increased by AROS silencing. This may represent a compensatory mechanism attempting to increase RPS19 protein expression.

In the HCT116 $p53^{-/-}$ and LoVo cell lines RPS19 protein did not appear to be affected by AROS siRNA. In the case of the LoVo cell line, silencing of AROS was not efficient, suggesting that greater depletion of AROS may affect RPS19 protein. However, this was not the case for the HCT116 $p53^{-/-}$ cell line, where AROS depletion was efficient (Figure 6.1A). Given that the HCT116 p53 wild-type and p53 null cell lines are otherwise isogenic this data suggests a role for p53 in the promotion of RPS19 protein abundance by AROS.

6.3.2 RPS19 promotes AROS abundance

The data above indicate that AROS may promote RPS19 protein abundance in cancer cell lines (Figure 6.1C). Given this observation, the effect of RPS19 on AROS was analysed in the same panel of cancer cells using siRNA against RPS19. Silencing of RPS19 was efficient at the protein level in all cancer lines in which *RPS19* was targeted (Figure 6.2A). Consistent with this, a significant reduction in *RPS19* mRNA level was seen, standardised against a housekeeping control mRNA (Figure 6.2B).

Similar to the reciprocal analysis above, the abundance of AROS protein was also reduced following targeting of *RPS19*. This appeared to be highly conserved, occurring in all 5 cancer cell lines analysed. This was specific to AROS protein, as standardised *AROS* mRNA expression was not depleted by RPS19 silencing in each of the 5 cancer cell lines (Figure 6.2). Oppositely, the abundance of *AROS* mRNA was significantly *increased* in each cell line following RPS19 silencing.

This suggests that RPS19 maintains AROS protein abundance, completing an autoregulatory loop between AROS and RPS19 (Figure 6.2C). This is the first indication that *'AROS and RPS19 affect reciprocal protein function'*. The increase in *AROS* mRNA may represent a compensatory mechanism to ameliorate the reduced AROS protein levels. However, this response is insufficient to counteract the loss of AROS protein. Thus, loss of RPS19 resulted in loss of AROS protein and a potentially associated increase in *AROS* mRNA.

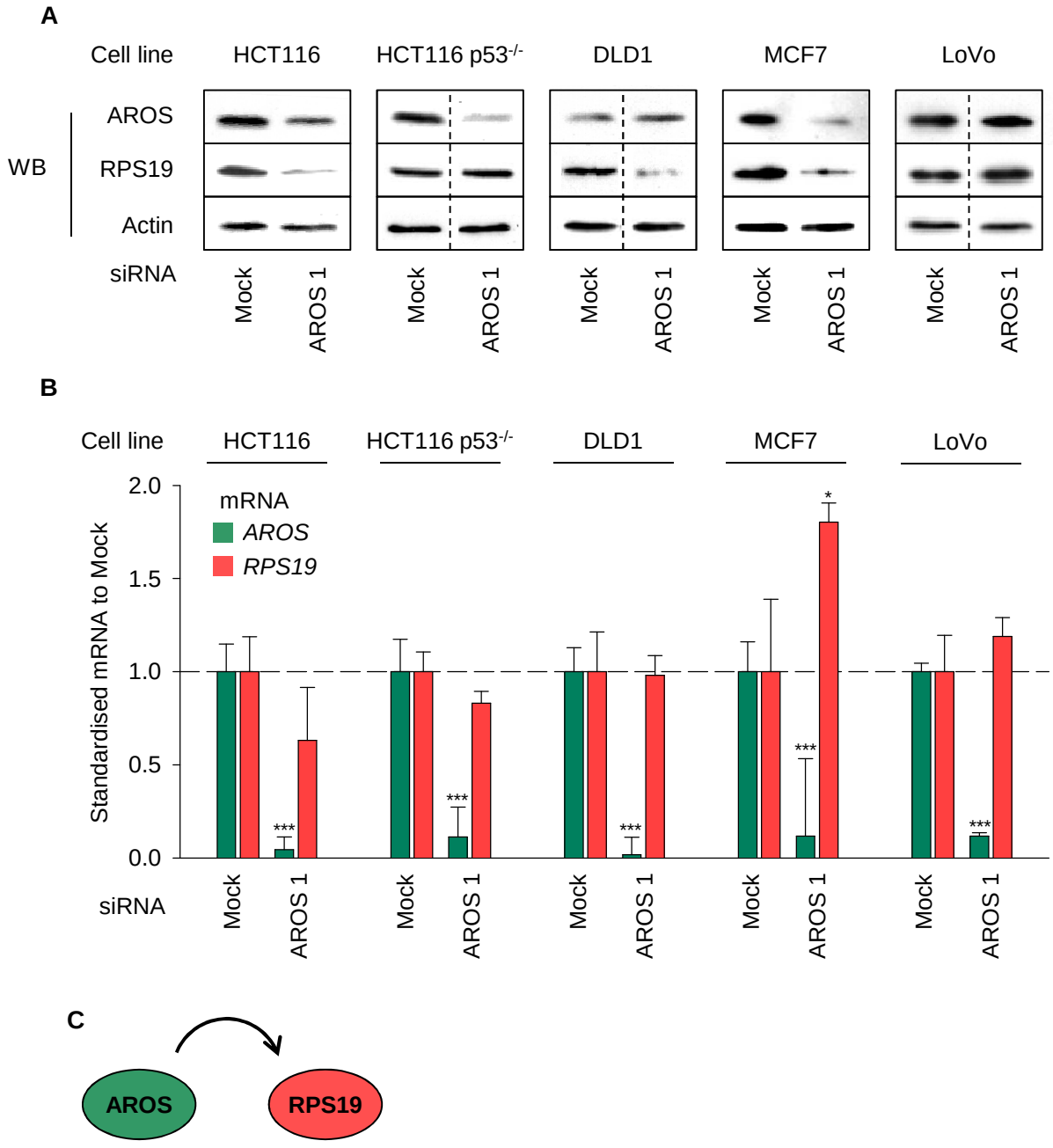

Figure 6.1: AROS silencing results in loss of RPS19 protein

(A) SDS-PAGE and Western blot analysis of protein abundance following AROS siRNA 1 transfection. Cancer cells were transfected and harvested at 48 hours (HCT116 p53$^{-/-}$ at 72 hours) and total protein isolated (see *Methods*). Equivalent protein analysed by mass. Actin expression was used as a loading control. **(B)** Parallel isolation of total RNA by RNeasy method during the transfection detailed in (A). RNA abundance quantified by qRT-PCR and standardised against *Actin* mRNA (*GAPDH* mRNA for MCF7). *** P<0.001, * P<0.05. **(C)** Schematic of the effect of AROS on RPS19 protein.

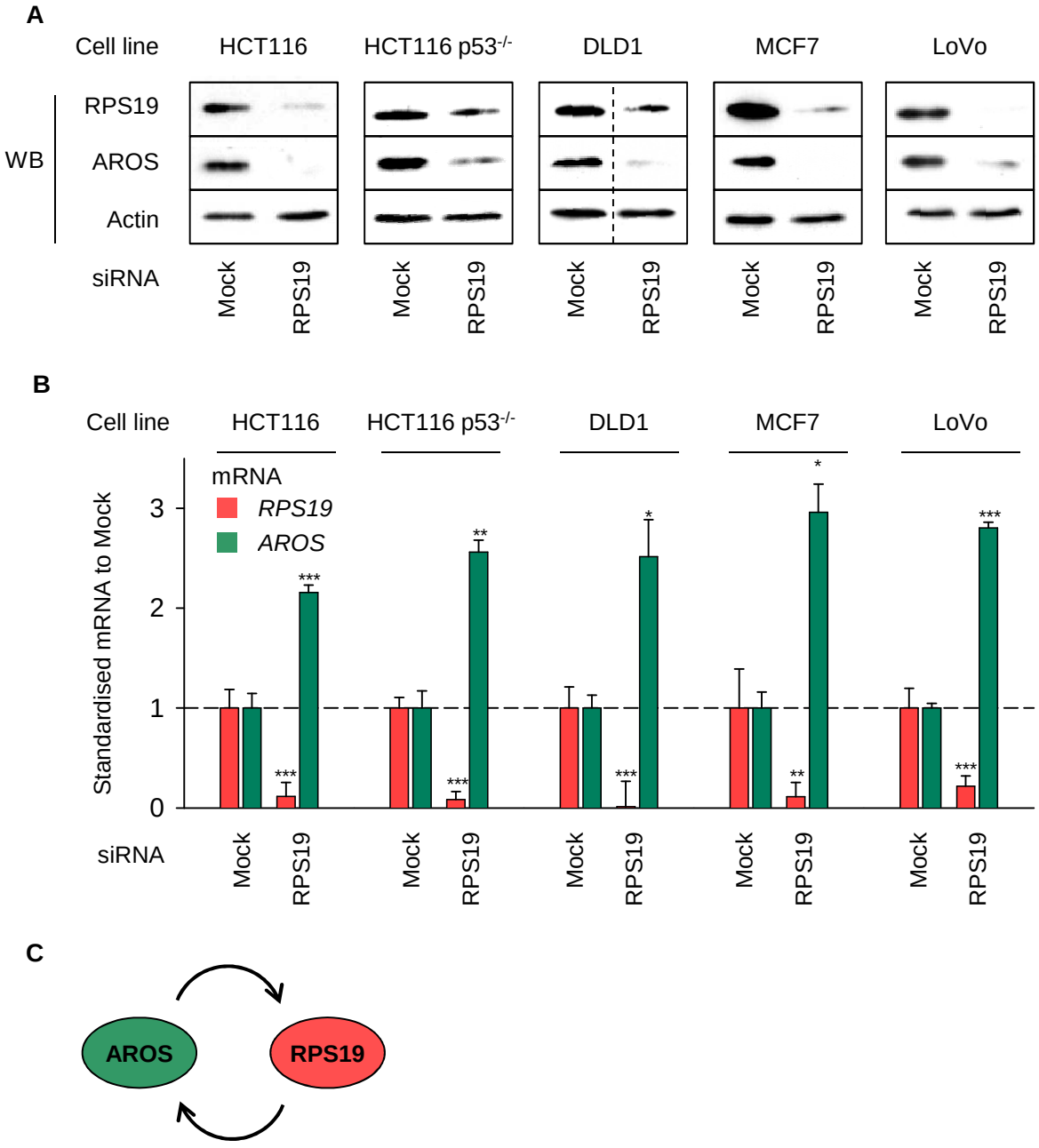

Figure 6.2: RPS19 silencing results in loss of AROS protein

(A) Analysis of protein abundance following RPS19 siRNA transfection in cancer cell lines. Cells were harvested 48 hours (except HCT116 p53$^{-/-}$ – 72 hours) post-transfection and lysed in protein lysis buffer (see *Methods*). Equivalent protein by mass was analysed and Actin expression used as a loading control. **(B)** Total RNA was harvested 48 hours (HCT116, DLD1, MCF7, LoVo) or 72 hours (HCT116 p53$^{-/-}$) after siRNA transfection against *RPS19*. RNA was isolated by the RNeasy method and analysed by qRT-PCR using specific primers for each mRNA, standardised against *Actin* (HCT116, HCT116 p53$^{-/-}$, DLD1, LoVo) or *GAPDH* (MCF7) mRNA expression. **(C)** Schematic of the effect of RPS19 on AROS protein, completing an autoregulatory loop between the two proteins.

6.4 *RPS19 and cancer cell fate*

6.4.1 Cancer cell phenotype

AROS appeared to be a survival factor for cancer cells in *Chapter 5*. RPS19 may also have a role in promoting cancer cell viability, given that knockdown of RPS19 resulted in apoptosis in a human cancer cell line (Choesmel et al. 2007). In order to analyse the role of RPS19 in cancer cell fate, RPS19 siRNA was applied to the panel of cancer cell lines used throughout the *Thesis.* To provide a direct comparison to RPS19 silencing, AROS siRNA1 transfection was carried out in parallel.

RPS19 siRNA resulted in an apparent reduction in cell density in all 5 human cancer cell lines analysed (Figure 6.3). There also appeared to be an increase in cell refringency in each cell line, either due to increased individual cell detachment (DLD1, MCF7), detachment of groups of cells (LoVo) or both (HCT116, HCT116 $p53^{-/-}$). This was potentially indicative of cell death and impaired cell cycle progression. AROS silencing in each cancer cell line correlated with an increase in individual cell refringency, but with little effect on cell density, as previously stated in *Chapter 5*.

6.4.2 Cancer cell apoptosis

Consistent with the alterations in cancer cell phenotype a significant increase in apoptosis was observed in the HCT116 and HCT116 $p53^{-/-}$ cell lines following silencing of RPS19 (Figure 6.4A). Thus, RPS19 appears to be anti-apoptotic in human cancer cells. Further to this, given the apoptosis in the HCT116 $p53^{-/-}$ cell line RPS19 appears to suppress apoptosis independent of p53 status. Silencing of AROS in parallel experiments also induced significant apoptosis in the HCT116 and HCT116 $p53^{-/-}$ cell lines (Figure 6.4A). Silencing of RPS19 therefore has similarities to the roles of AROS in cancer cell apoptotic suppression (see *Chapter 5*), perhaps suggestive of a unified role of the 2 proteins. These observations are consistent with the hypothesis that *'AROS specifically promotes cancer cell survival via RPS19'*.

6.4.3 Cancer cell cycle progression

The reduction in cell density following RPS19 silencing may be attributable to the apparent increase in cell death (Figure 6.4A), but equally may be due to alterations in cell cycle progression. Consistent with this possibility, in the HCT116 cell line RPS19 silencing correlated with a decrease in cells in S phase of the cell cycle and an increased population of G1 and G2/M cells (Figure 6.4Bi). This reduction in S phase cells may contribute to the reduction in HCT116 cell density. In contrast to RPS19 silencing, AROS silencing in the HCT116 cells did not greatly alter the cell cycle distribution from Mock treated cells (Figure 6.4Bi). This is the same data presented in *Chapter 5*. The implication of this difference is that AROS and RPS19 have distinct effects in determining cell cycle distribution in the HCT116 cells.

Interestingly, the cell cycle distribution of the HCT116 $p53^{-/-}$ cell line was not greatly altered by RPS19 silencing, with only a moderate redistribution of cells in G1 and G2/M seen (Figure 6.4Bii). This suggests that alterations in cell cycle status did not contribute to the reduced cell density in this cell line. Further, it suggests that p53 is important for suppressing cell cycle progression following loss of RPS19, and provides further evidence that RPS19 suppresses p53 function.

AROS silencing in the HCT116 $p53^{-/-}$ cell line did not greatly alter the cell cycle distribution from Mock treated cells (Figure 6.4Bii). Thus, AROS does not appear to effect cell cycle distribution in either cell line analysed, whereas RPS19 does affect the cell cycle, but only in the presence of p53. This highlights a difference in the roles of AROS and RPS19 in determining cell fate. This difference is consistent with the phenotypes of the cancer cells analysed following silencing of RPS19 and AROS, which differ in terms of resulting cell density (Figure 6.3); RPS19 silencing reduced cell density but AROS silencing did not appear to have any effect. This suggests that RPS19 and AROS may play distinct roles in determining cancer cell fate. This may disagree with the hypothesis that *'AROS specifically promotes cancer cell survival via RPS19'*.

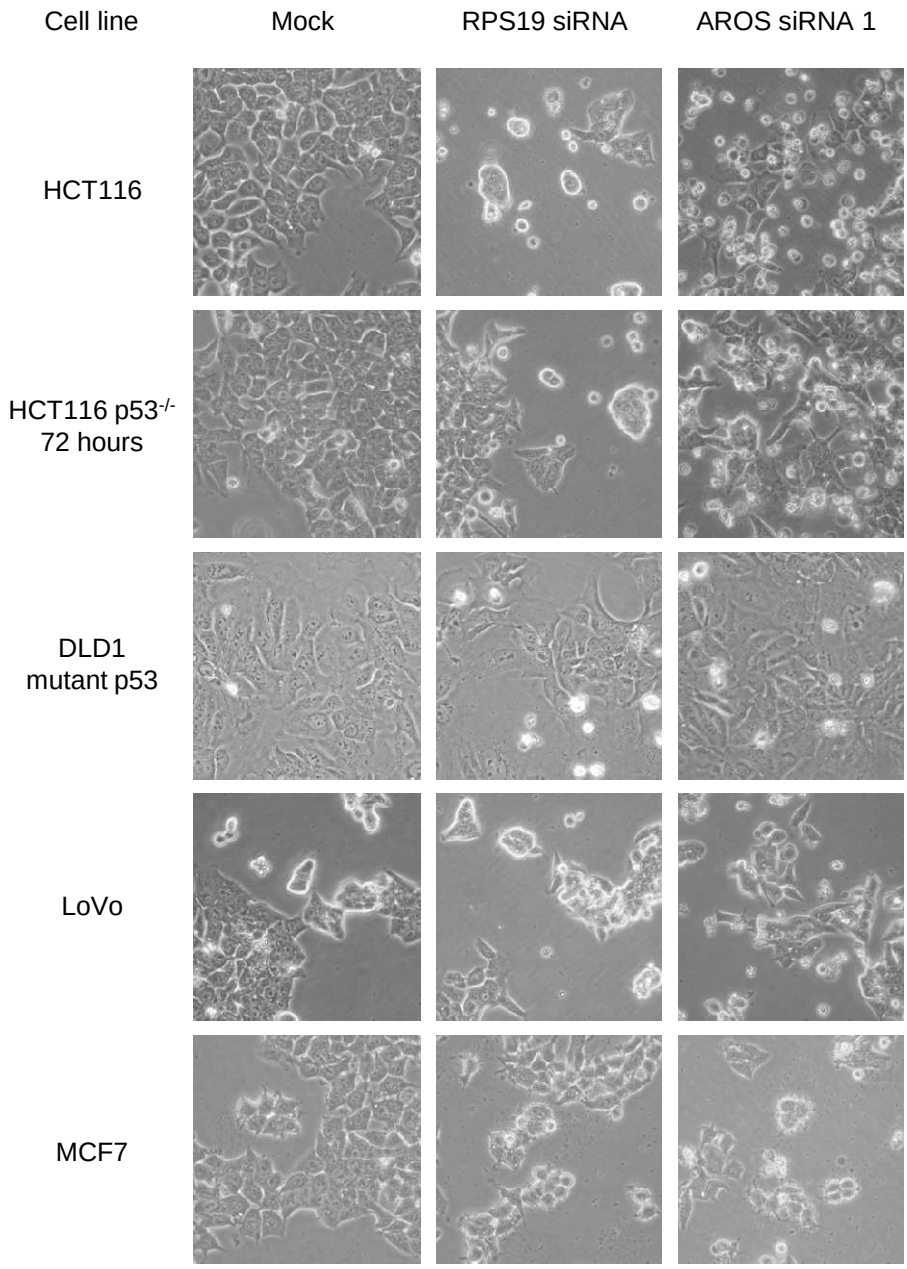

Figure 6.3: RPS19 knockdown causes phenotype alterations in cancer cells

Phase contrast micrographs of HCT116, HCT116 p53$^{-/-}$, DLD1, LoVo and MCF7 cancer cell lines following transfection of siRNAs against *RPS19* or *AROS*. Cells were treated with siRNA and resulting phenotypes recorded 48 hours post-transfection, unless stated.

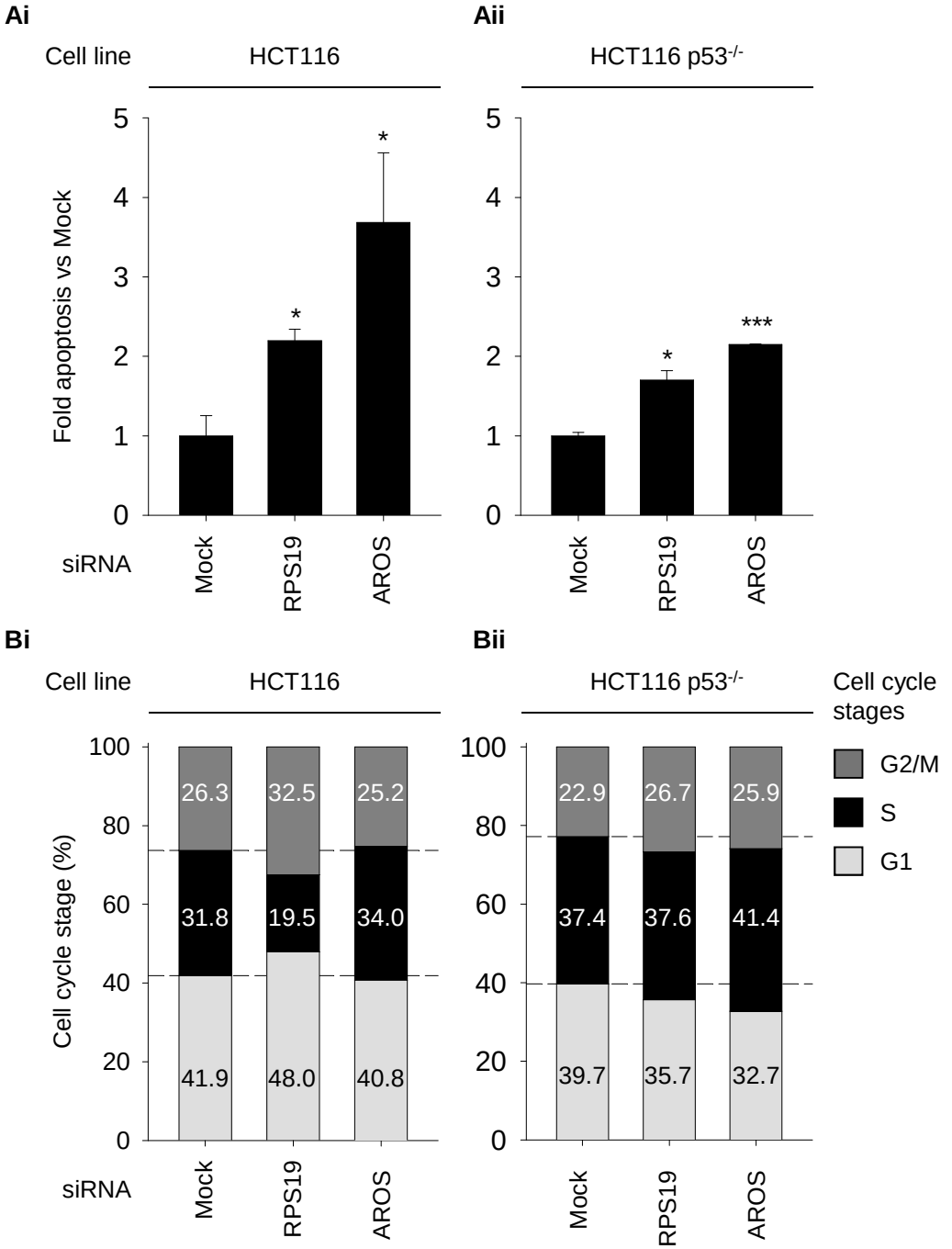

Figure 6.4: The effect of RPS19 on cancer cell apoptosis and cell cycle progression

(Ai) Fold apoptosis compared to Mock treated cells following siRNA transfection in HCT116 cancer cells. Cells treated with siRNA for 48 hours and analysed by Annexin V staining and flow cytometry (See *Methods*). **(Aii)** Data as in (Ai) for the HCT116 p53$^{-/-}$ cell line, treated with siRNA 72 hours prior to harvesting. *** P<0.001, * P<0.05. **(Bi)** Cell cycle distribution according to propidium iodide intercalation and flow cytometry, presented as a percentage of cells for each condition (see *Methods*). HCT116 cells were treated with siRNA as indicated, and harvested 48 hours later. **(Bii)** Data presented as in (Bi) for the HCT116 p53$^{-/-}$ cell line harvested 72 hours post-transfection.

6.5 *The AROS-RPS19 autoregulatory loop in non-cancer cells*

In *Chapter 5* AROS was found to be a cancer specific survival factor, promoting the viability of cancer cells, but not non-cancer cells. With the hypothesis that *'AROS specifically promotes cancer cell survival via RPS19'* the role of RPS19 was analysed in cancer cells, where it was found to be anti-apoptotic in accordance with the role of AROS (see above). Thus, to analyse the potential cancer specificity of RPS19, its role in non-cancer cells was characterised. Firstly, the molecular effects of AROS and RPS19 silencing were assessed in relation to reciprocal protein stability, then the role of RPS19 in determining non-cancer cell fate.

6.5.1 The AROS-RPS19 auto-regulatory loop is present in non-cancer cells

siRNA-mediated targeting of AROS in ARPE19, WI38 and MCF10A non-cancer cell lines was successful at both the protein and mRNA levels (Figure 6.5). As previously seen in cancer cell lines, silencing of AROS reduced the abundance of RPS19 protein in each of the non-cancer cell lines (Figure 6.5A). This was specific to RPS19 protein as the abundance of RPS19 mRNA was not reduced compared to Mock treatment (Figure 6.5B). Thus, the positive effect of AROS depletion on RPS19 protein abundance occurs in both cancer and non-cancer cell lines.

In reciprocal, the silencing of RPS19 was efficient at the mRNA level, which translated to reduced RPS19 protein expression in each of the non-cancer cell lines analysed (Figure 6.6). As seen in the cancer cell lines, the abundance of AROS protein was reduced following targeting of *RPS19*. There was no reduction in *AROS* mRNA standardised against housekeeping controls, consistent with a post-transcriptional effect of RPS19 on AROS (Figure 6.2). In the ARPE19 and WI38 cell lines the abundance of *AROS* mRNA was significantly *increased* following RPS19 silencing. This was previously observed and discussed in cancer cell lines, with the increase in AROS mRNA potentially representing a compensatory mechanism to counteract the reduced AROS protein levels.

Thus, the AROS-RPS19 autoregulatory loop appears to be present in non-cancer cells as well as cancer cells, further supporting the hypothesis that *'AROS and RPS19 affect reciprocal protein function'*. With AROS known to specifically

promote cancer cell survival it is possible that knockdown of RPS19 also has no effect on non-cancer cell survival. Thus, the cellular effect of RPS19 silencing was characterised in the ARPE19, WI38 and MCF10A non-cancer cell lines.

6.5.2 Non-cancer cell fate

Silencing of RPS19 in three non-cancer cell lines appeared to result in a reduction in cell density compared to parallel Mock siRNA treatment (Figure 6.7). RPS19 silencing also appeared to increase the number of refringent cells compared to Mock treatment, indicative of an induction of apoptosis. Consistent with this, RPS19 silencing in the non-cancer ARPE19 retinal epithelial and WI38 lung fibroblast cell lines resulted in a significant induction of apoptosis compared to Mock treatment (Figure 6.8A).

As such, RPS19 appears to be required for survival of not only cancer cells, but also non-cancer cells. This contrasts the role of AROS reported in *Chapter 5*. These data for AROS are shown here for side-by-side comparison to RPS19 silencing. Silencing of AROS has little effect on non-cancer cell phenotype and this correlated with no induction of apoptosis in the ARPE19 and WI38 cell lines (Figure 6.7and Figure 6.8A). This implies that despite the conservation of the AROS-RPS19 molecular relationship between cancer and non-cancer cell lines, the effect each protein has on cell fate is not conserved across cell types. Thus, the hypothesis that *'AROS specifically promotes cancer cell survival via RPS19'* appears to be unlikely.

Further to this, silencing of RPS19 in the ARPE19 cell line appeared to result in a redistribution of cells between stages of the cell cycle (Figure 6.8B). Although the number of cells in S phase was not altered (8%), the G2/M phase population appeared to double with a concomitant reduction in G1 phase cells. This, and the induction of apoptosis seen in Figure 6.8Ai, may contribute to the reduction in cell density observed following RPS19 silencing (Figure 6.7). Silencing of AROS did not have such a significant effect on the cell cycle distribution of ARPE19 cells as silencing of RPS19. This appears consistent with the phenotype of AROS silenced cells shown in Figure 6.7 and indicates another difference between the roles of AROS and RPS19 in cell fate determination.

These phenotypic data strongly indicate that RPS19 is required for cell survival. In contrast to the role of AROS, which was specifically required for cancer cell survival, RPS19 appears to be required for viability of both cancer and non-cancer cells. This requirement for RPS19 may pertain to its role as an essential component of the small ribosomal subunit. Loss of RPS19 is likely to have negative effects on global translation and protein production, which appears here to correlate with a negative effect on cell fate. This suggests that the roles of RPS19 and AROS in cell fate determination do not overlap.

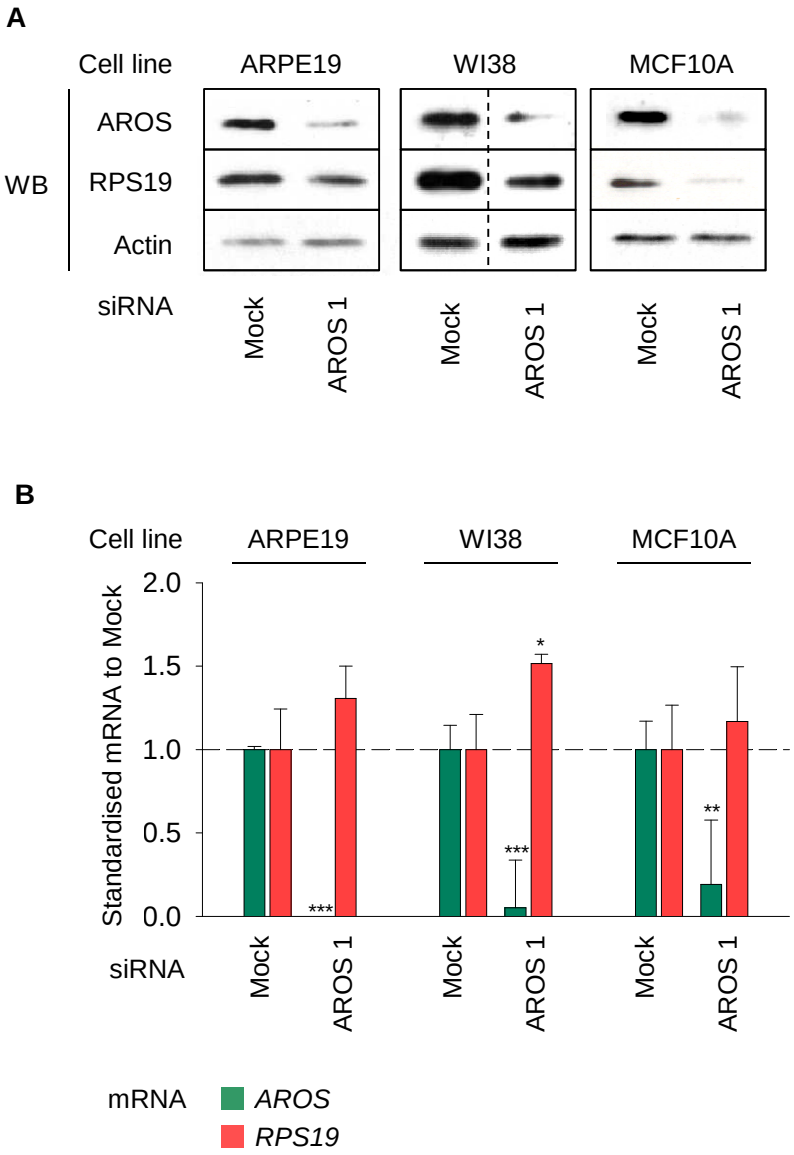

Figure 6.5: AROS silencing results in loss of RPS19 protein in non-cancer cells

(A) SDS-PAGE and Western blot analysis for protein abundance following AROS siRNA 1 transfection. Non-cancer cells were transfected and harvested at 72 hours for total protein (see *Methods*). Equivalent protein loaded by mass. Actin expression was used as a loading control. **(B)** Parallel isolation of total RNA by RNeasy method during the transfection detailed in (A). RNA abundance quantified by qRT-PCR and standardised against *Actin* mRNA (*GAPDH* mRNA for MCF10A). *** P<0.001, ** P<0.01, * P<0.05.

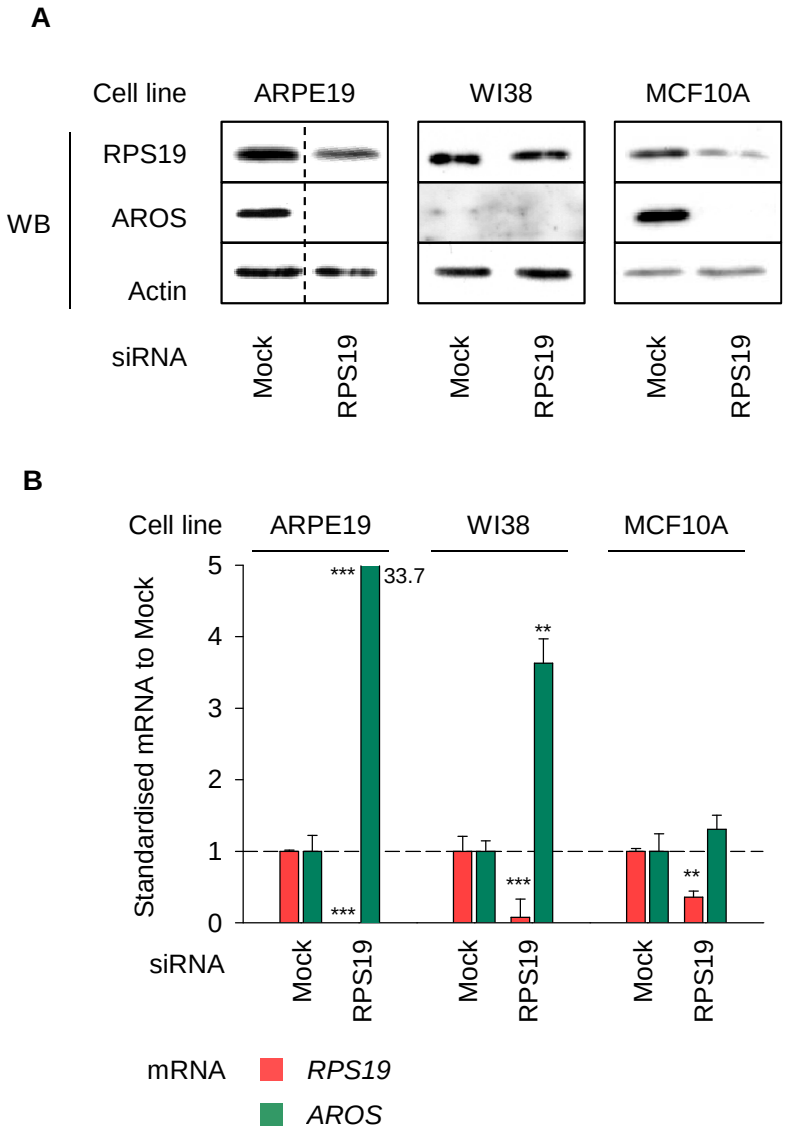

Figure 6.6: RPS19 silencing results in loss of AROS protein in non-cancer cells

(A) Quantification of protein abundance following RPS19 silencing in non-cancer cell lines (ARPE19, WI38 and MCF10A) harvested 72 hours post-transfection. Equivalent protein mass was analysed by SDS-PAGE and Western blotting following lysis of cells. Actin is used as a loading control **(B)** qRT-PCR analysis of mRNA abundance in ARPE19, WI38 and MCF10A non-cancer cell lines 72 hours following *RPS19* siRNA transfection. Data standardised against *Actin* (ARPE19, WI38) or *GAPDH* (MCF10A) mRNA expression. *** P<0.001, ** P<0.01, * P<0.05.

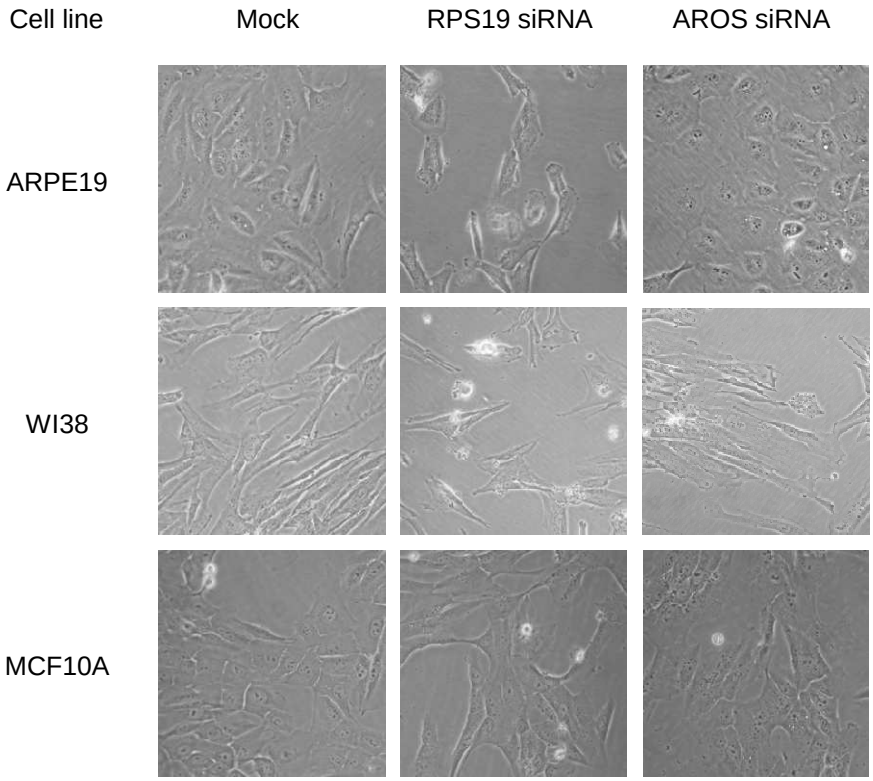

Figure 6.7: RPS19 silencing alters non-cancer cell phenotype

Phase contrast micrographs of ARPE19, WI38 and MCF10A non-cancer cell lines following transfection of siRNAs against *RPS19* or *AROS*. Cells were treated with siRNA and phenotype recorded 72 hours post-transfection in all cases.

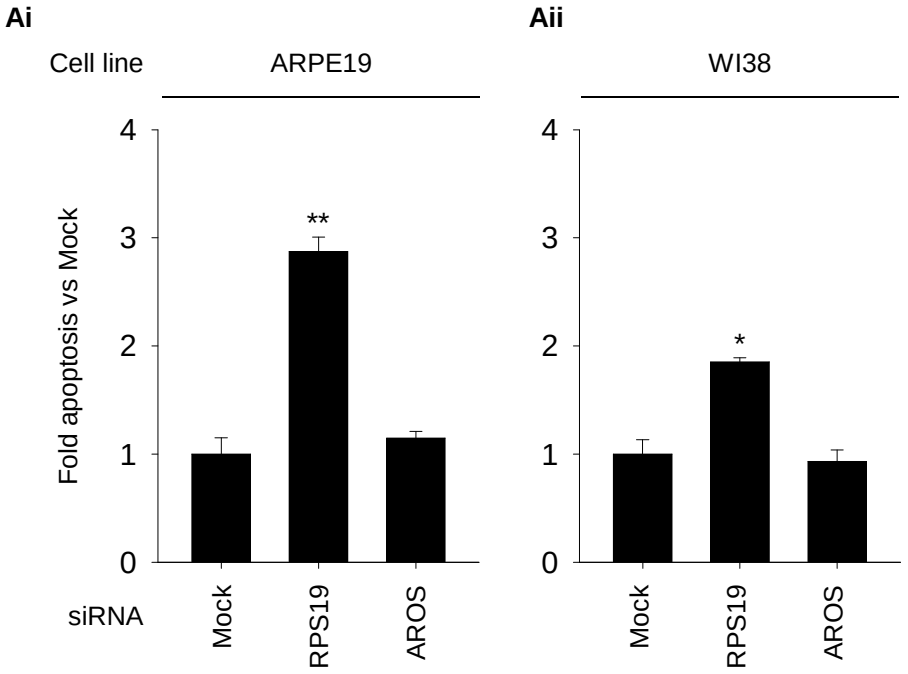

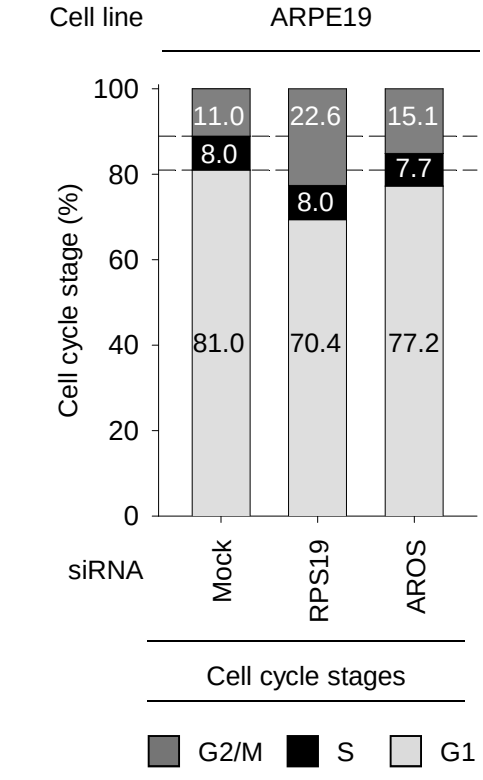

Figure 6.8: The effect of RPS19 on non-cancer cell fate

(Ai) Fold apoptosis compared to Mock treatment in ARPE19 non-cancer cells following RNAi as indicated. Cells treated with siRNA for 72 hours and analysed by Annexin V staining and flow cytometry (See *Methods*). **(Aii)** Data as in (Ai) for the WI38 cell line. ** P<0.01, * P<0.05. **(B)** Propidium iodide intercalation and flow cytometry calculation of cell cycle distribution, presented as a percentage of cells in each stage for each condition (see *Methods*). ARPE19 cells were treated with siRNA as indicated and harvested 72 hours later.

6.6 *AROS-RPS19 autoregulatory loop function*

6.6.1 Suppression of p53

RPS19 suppresses p53 accumulation in animal models, via a mechanism distinct from MDM2-mediated proteasomal degradation (Danilova et al. 2008; McGowan et al. 2008; Dutt et al. 2011; Jaako et al. 2011). This allows the possibility that RPS19 suppresses p53 via AROS, which would be consistent with the observation that RPS19 supports AROS protein abundance. AROS was characterised as a selective activator of SIRT1 activity in *Chapters 4 and 5*. This was observed as a differential effect on acetylated and total p53 levels following knock down of AROS, variable by cell line.

To test the hypothesis that *'RPS19 affects p53 via regulation of AROS'* the abundance of both acetylated and total p53 was determined following basal silencing of RPS19 in seven p53-expressing cell lines (Figure 6.9). These are summarised and compared to the effect AROS silencing reported in *Chapter 4* in Table 6.1.

6.6.1.1 HCT116

Silencing of RPS19 in the HCT116 colorectal adenocarcinoma cell line did not appear to alter the expression of total p53, or increase the acetylation of p53 at lysine 382 (Figure 6.9A). This is consistent with the effect of AROS silencing in this cell line under these conditions (*Chapter 4 – Figure 4.6*). Thus, neither AROS nor RPS19 appears to suppress p53 in the HCT116 cell line under these basal conditions.

6.6.1.2 DLD1

In the DLD1 colorectal adenocarcinoma cell line, silencing of RPS19 did not affect the abundance of p53, but did induce an increase in p53 acetylation at lysine 382 compared to Mock treatment (Figure 6.9A). This is consistent with the effect of silencing AROS in this cell line, where both total and acetylated p53 levels were elevated (*Chapter 4 – Figure 4.7*). The lack of total p53 stabilisation following RPS19 silencing compared to AROS silencing may represent a temporal difference. Increased acetylation of p53 may lead to total p53 stabilisation. As such, the heightened acetylation of p53 following both AROS and RPS19 silencing may only

have stabilised total p53 following AROS silencing at the 48 hour post-transfection time point analysed. Thus, analysis at a later time point may reveal that total p53 stabilisation was yet to occur following RPS19 silencing at 48 hours post-transfection.

6.6.1.3 MCF7

In the MCF7 cancerous mammary gland epithelial cell line RPS19 appeared to stabilise total p53 expression (Figure 6.9A). Unfortunately, acetylated p53 could either not be detected in this cell line under these conditions. However, stabilisation of total p53 correlated with p53 stabilisation seen following AROS silencing in the MCF7 cell line (*Chapter 4 – Figure 4.7*).

6.6.1.4 LoVo

In the LoVo colorectal adenocarcinoma cell line silencing of RPS19 appeared to correlate with an increase in both total and acetylated p53 (Figure 6.9A). This is strikingly similar to the role of AROS reported in *Chapter 4 – Figures 4.7*, where silencing of AROS stabilised both total and acetylated p53 levels.

6.6.1.5 ARPE19

In the ARPE19 non-cancer retinal epithelial cell line, silencing of RPS19 induced a marked stabilisation of p53 protein (Figure 6.9B). Similar to the MCF7 cell line, acetylation status of p53 could not be detected under these conditions in the ARPE19 cell line. However, the data are similar to the stabilisation of p53 observed following AROS silencing in *Chapter 4 – Figure 4.6*. Total p53 was stabilised by AROS knockdown but the effect on acetylated p53 was difficult to interpret.

6.6.1.6 WI38

Total p53 protein levels were stabilised by RPS19 silencing in the WI38 lung fibroblast non-cancer cell line (Figure 6.9B). The effect on acetylated p53 was difficult to indentify due to low levels of acetylation. There appeared to be a band appearing following RPS19 silencing, but this was faint. Nevertheless, the marked

increase in total p53 is consistent with the stabilisation of p53 seen following AROS silencing in *Chapter 4 – Figure 4.8*.

6.6.1.7 MCF10A

Acetylated p53 levels were not analysed in the MCF10A non-cancer mammary gland epithelial cell line due to lack of sample. However, total p53 appeared to be stabilised by RPS19 knockdown in this non-cancer cell line. This is again consistent with the effect of AROS silencing observed in *Chapter 4 – Figure 4.8*.

Overall, the comparison of p53 levels following RPS19 silencing to p53 levels following AROS silencing in *Chapter 4* reveals a striking similarity (see Table 6.1). In all cases the two conditions show some level of identity. When considered with the loss of AROS seen following silencing of RPS19, it appears that RPS19 may promote not only AROS abundance but potentially AROS function in suppression of p53. This is consistent with the hypothesis that '*RPS19 affects p53 via regulation of AROS'*. Thus, the AROS-RPS19 autoregulatory loop appears to be important in the suppression of p53 (Figure 6.9C). Importantly, this could contribute to the unknown mechanism of p53 suppression by RPS19.

6.6.2 SIRT1 abundance

Interestingly, RPS19 appears to effect the expression of the AROS binding partner SIRT1 in 5 of the 8 cell lines analysed. In the HCT116 $p53^{-/-}$ and MCF7 cancer cell lines and ARPE19, WI38 and MCF10A non-cancer cell lines RPS19 silencing resulted in a decrease in the expression of SIRT1 protein (Figure 6.9). Interestingly, the loss of SIRT1 did not correlate with increased p53 acetylation, which would be consistent with the role of SIRT1 in deacetylation of p53 (Luo et al. 2001; Vaziri et al. 2001). However, total p53 protein levels were increased where the p53 gene was intact, suggesting that loss of SIRT1 following silencing of RPS19 may be a factor in the subsequent stabilisation of p53.

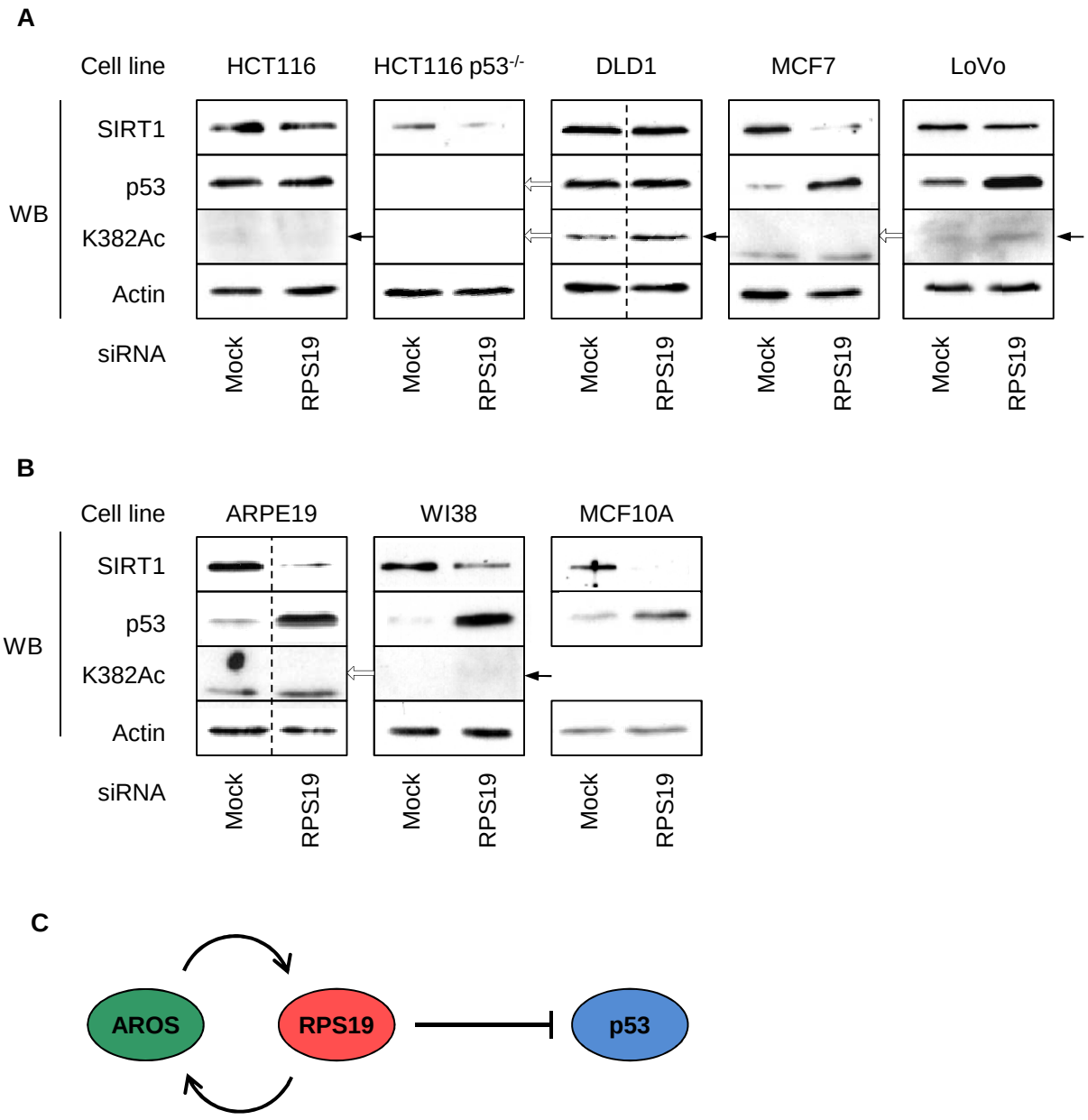

Figure 6.9: The effect of RPS19 silencing on p53

(A) Analysis of SIRT1 and p53 protein abundance following RPS19 siRNA transfection in cancer cell lines. Cells were harvested 48 hours (except HCT116 $p53^{-/-}$ – 72 hours) post-transfection and lysed in protein lysis buffer (see *Methods*). Equivalent protein by mass was analysed and Actin expression used as a loading control. **(B)** Analysis as in (A) for ARPE19, WI38 and MCF10A non-cancer cell lines harvested at 72 hours post-transfection. **(C)** Schematic representation of the AROS-RPS19 autoregulatory loop and the similar effect of each component on p53 protein.

Cell line	***RPS19 suppresses p53***	***Identity to effect of AROS***	***RPS19 effect on SIRT1***
HCT116	✗	✓	~
HCT116 $p53^{-/-}$	-	-	↑
DLD1	✓	✓	~
MCF7	✓	✓	↑
LoVo	✓	✓	~
ARPE19	✓	✓	↑
WI38	✓	✓	↑
MCF10A	✓	✓	↑

Table 6.1: The effect of RPS19 on p53 and SIRT1

Collation of the data from Figure 6.9 regarding the effect of RPS19 silencing on p53. A positive effect on the extent of acetylation and/or total levels of p53 following RPS19 silencing is indicated in Column 2. A tick represents a positive effect, whereas a cross represents no effect. The identity of the data in Column 2 to the effect of AROS silencing seen in *Chapter 4* is indicated by a tick or a cross in Column 3. The effect of RPS19 on SIRT1 protein levels is also shown in Column 4. Arrows indicate the effect of RPS19 on SIRT1 protein expression. '~' indicates no effect seen.

6.7 *Discussion*

6.7.1 Auto-regulation of AROS and RPS19

The data reveal a novel effect of AROS and RPS19 silencing upon reciprocal protein stability. Each protein promotes the abundance of the other in both cancer cell lines (Figure 6.1 and Figure 6.2) and non-cancer cell lines (Figure 6.5 and Figure 6.6). In each case there was no negative effect on reciprocal mRNA levels, implying that the regulation of each protein by the other occurs at the protein level. Given that the two proteins interact in the mouse the association of the proteins seems likely to form part of this regulatory mechanism (Maeda et al. 2006).

The loss of reciprocal protein appears likely to have an effect on the function of that protein. As such, the data indicate that AROS may be required to maintain RPS19 function and vice versa. No significance had previously been attributed to the AROS-RPS19 association, making this the first indication that '*AROS and RPS19 affect reciprocal protein function'*.

The mechanism behind the autoregulatory loop may relate to the functions of AROS and/or RPS19. RPS19 is a structural component of the ribosome (Taylor et al. 2009; Ben-Shem et al. 2010; Rabl et al. 2011), which is also essential for small ribosomal subunit biogenesis (Choesmel et al. 2007; Flygare et al. 2007; Idol et al. 2007). Thus, loss of RPS19 is likely to impact upon ribosome abundance. Therefore, the loss of RPS19 seen following AROS silencing may simply be an indicator of a reduction in ribosome abundance, with a concomitant loss of RPS19. Further, the loss of AROS following RPS19 silencing could be induced by a loss of small ribosomal subunits, should AROS depend on small subunit abundance for stability. The relationship between AROS and the ribosome is explored further in *Chapter 8* in an attempt to address this possibility.

Interestingly, the loop is not present in full in the HCT116 $p53^{-/-}$ cell line, unlike in the wild-type HCT116 cell line. The only difference between these cell lines is the expression of p53 in the HCT116 but not in the HCT116 $p53^{-/-}$. This gives a strong indication that the break in the loop is related to the absence of p53 expression. Silencing of RPS19 reduces AROS expression in the p53 null cell line,

but the reciprocal effect of AROS on RPS19 is lost. The reason for this is unclear, but implies that p53 may be required for regulation of RPS19 by AROS.

6.7.2 RPS19 and suppression of p53

AROS and SIRT1 have similar functions in determining cell fate. For example silencing of each appears to induce a similar level of apoptosis (*Chapter 5*). However, AROS and SIRT1 appeared to act differently in regulation of p53 (*Chapter 4*). Importantly, induction of apoptosis is independent of p53, following AROS, SIRT1 or RPS19 silencing. Thus, the regulation of p53 appears to be disconnected from the regulation of apoptosis in the system. Interestingly, the role of AROS and RPS19 appears to be similar when analysed in terms of the effect each has upon p53.

RPS19 appears to suppress p53 stabilisation in 6 of the 7 p53-expressing cell lines analysed (Table 6.1). Furthermore, RPS19 appears to be required for maintenance of cell cycle profile in a p53-dependent manner (Figure 6.4B). These data are consistent with recent reports from animal models of RPS19 deficiency, where RPS19 suppressed p53 by an unknown mechanism (Danilova et al. 2008; McGowan et al. 2008; Dutt et al. 2011; Jaako et al. 2011). The characterisation here suggests that RPS19 may suppress p53 via AROS and perhaps SIRT1.

The data for suppression of p53 by both AROS and RPS19 are strikingly similar (*Chapter 4, this Chapter* and Table 6.1). AROS appears to be a selective suppressor of p53, dependent upon cell line and context. Interestingly, under conditions where AROS suppressed p53, RPS19 also appeared to suppress p53. Crucially, under conditions where AROS did not appear to suppress p53, RPS19 too had little effect on p53 protein. This correlation is consistent with the autoregulatory loop between AROS and RPS19, with RPS19 knockdown reducing AROS protein abundance and function. The data agree with the hypothesis that '*RPS19 affects p53 via regulation of AROS*'.

Interestingly there may be a more direct effect of RPS19 on SIRT1 than the common binding of AROS. RPS19 appears to affect the expression of SIRT1 protein in 5 of the 8 cell lines analysed. This would directly reduce the SIRT1-mediated

suppression of p53. Consistent with this, the loss of SIRT1 following RPS19 silencing correlated with increased total p53 expression (Figure 6.9). Importantly, AROS silencing under the same conditions does not affect SIRT1 protein abundance (*Chapter 4*). Thus, the effect of RPS19 on SIRT1 abundance is likely to be independent of AROS.

RPS19 is known to suppress p53, but via an unknown mechanism (Danilova et al. 2008; McGowan et al. 2008; Dutt et al. 2011; Jaako et al. 2011). The data here suggest that this may involve RPS19-mediated activation of SIRT1. This could potentially occur via: 1) RPS19 promoting AROS abundance, and subsequent activation of SIRT1 or, 2) RPS19 promoting SIRT1 protein abundance and function. This provides a putative link between RPS19 and SIRT1, which could explain the unknown mechanism of suppression of p53 by RPS19.

6.7.3 RPS19 and cell survival

RPS19 appears to be required for the viability and survival of all cell lines analysed. This is consistent with previous analyses of RPS19 in cell viability (Choesmel et al. 2007; Danilova et al. 2008; McGowan et al. 2008; Dutt et al. 2011; Jaako et al. 2011). The conserved role of RPS19 in promoting cell viability is in contrast to the specific survival functions of AROS, which appears to only promote cancer cell survival (*Chapter 5*). The similarities between AROS and RPS19 in terms of cell viability are limited. The extent of apoptosis, effect on cell cycle and cell phenotype following silencing all appeared to be different. These differences suggest that loss of RPS19 may not be a factor in AROS-silencing-induced cancer cell apoptosis. Therefore, the data do not appear to support the hypothesis that *'AROS specifically promotes cancer cell survival via RPS19'*.

However, it may be possible that RPS19 is involved in this process. Cancer cells undergo rapid proliferation, which will require heightened function of ribosomes. In contrast, non-cancer cells grow more slowly. Targeting of the ribosome in cancer cells may be selective for these rapidly dividing cells (Silvera et al. 2010). It is possible that AROS only influences RPS19 function to a critical extent in cancer cells. This could account for the cancer specificity for AROS in cell

viability. This, and the potential modes of AROS anti-apoptotic function, is discussed in *Chapter 9*.

6.8 *Conclusions*

1. AROS and RPS19 form a functional autoregulatory loop.
2. RPS19 appears to be essential for survival of all cells, both cancerous and non-cancerous .
3. RPS19 suppresses p53, via a mechanism potentially involving regulation of AROS and SIRT1.

7 AROS and RPS19 complexes

7.1 *Overview*

Chapter 6 indicated that AROS and RPS19 form an autoregulatory loop, promoting reciprocal protein abundance and function. This presumably involves the association of the two proteins, given the known interaction in the mouse (Maeda et al. 2006). This *Chapter* aims to identify the AROS-RPS19 association between the proteins in human cells. Exogenous expression of tagged proteins and immunoprecipitation are used for this purpose.

Chapter 6 also revealed a potential link between RPS19 and SIRT1 function. Given that both proteins interact with AROS, the potential for an interaction between RPS19 and SIRT1 was also analysed. This considered a newly identified splice variant form of SIRT1, termed SIRT1-Δ8. Again using exogenous expression and immunoprecipitation a specific interaction between RPS19 and SIRT1-Δ8 is identified, and analysed further for potential functional consequences.

7.2 *Introduction*

7.2.1 RPS19 interactions

RPS19 is a structural component of the small ribosomal subunit, intercalating 18S ribosomal RNA (Taylor et al. 2009; Ben-Shem et al. 2010; Rabl et al. 2011). RPS19 is also required for the synthesis of ribosomes, which occurs within the subnuclear structure, the nucleolus (Choesmel et al. 2007; Flygare et al. 2007; Idol et al. 2007). As such, RPS19 associates with ribosomal proteins and ribosome biogenesis factors, likely in both the cytoplasm where ribosomes function and in the nucleus/nucleolus during ribosome synthesis.

This role in ribosome biogenesis was evident in the published protein interactome of RPS19, but also revealed that RPS19 forms associations with many non-ribosomal factors (Orru et al. 2007). RPS19 associated with proteins involved in cellular activities such as mRNA processing, transcription and signal transduction. Thus, RPS19 is believed to have distinct extra-ribosomal functions. One such function appears to be the suppression of p53, via an unknown mechanism (Danilova et al. 2008; McGowan et al. 2008; Dutt et al. 2011; Jaako et al. 2011).

Human RPS19 was predicted to interact with AROS, based on the association reported in the mouse (Maeda et al. 2006; Orru et al. 2007). Data presented in *Chapter 6* were consistent with the mechanism of p53 suppression by RPS19 potentially occurring via AROS and SIRT1. The aim of this *Chapter* is to analyse the complexes formed by AROS and RPS19 to gain insight into this potential mechanism. The potential for interaction with *SIRT1* gene products was analysed, which encompassed association with a novel SIRT1 splice variant.

7.2.2 SIRT1 splice variation

In parallel with this study, other members of the YCR p53 Research Unit discovered and characterised the first splice variant of the *SIRT1* gene, namely SIRT1-Δ8 (Lynch et al. 2010). SIRT1-Δ8 differs from SIRT1-FL (the ‘full length’ form of the *SIRT1* gene) in its omission of exon 8. The novel SIRT1-Δ8 isoform has reduced deacetylase activity, but is nonetheless able to suppress p53 lysine 382

acetylation (Lynch et al. 2010). Thus it is possible that SIRT1-Δ8 plays a role in RPS19-mediated regulation of p53.

One difference between SIRT1-Δ8 and SIRT1-FL is during the response to applied stress. Following stress SIRT1-Δ8 is significantly upregulated, in contrast to SIRT1-FL which is down-regulated (Lynch et al. 2010). Interestingly, this upregulation is p53-dependent, identifying an autoregulatory loop between p53 and SIRT1-Δ8. Furthermore, this suggests a role for SIRT1-Δ8 but not SIRT1-FL during the cellular response to applied stress.

Importantly for the analysis carried out thus far in the *Thesis*, the siRNA used to target *SIRT1* is specific for SIRT1-FL. The 'SIRT1 siRNA' targets a region in exon 8 of SIRT1-FL, which is absent in the SIRT1-Δ8 isoform. Thus the previous analyses of SIRT1 function can be attributed to SIRT1-FL. Targeting of SIRT1-Δ8 by RNAi is possible using an siRNA specific to the splice junction sequence created in this isoform from exon 7 to 9 (Lynch et al. 2010). This is used herein for analysis of SIRT1-Δ8 function.

Initially the analysis here focuses on the complexes formed by AROS and RPS19. Importantly, association of the two proteins has yet to be reported in human cells. Confirmation of this association will supplement the autoregulatory loop identified between the proteins in *Chapter 6*. A further focus of this *Chapter* is on the potential for RPS19 to interact with SIRT1-FL and/or SIRT1-Δ8. This potential association has not been previously reported, but may have implications for RPS19 suppression of p53. Additionally the possibility for regulation of RPS19 by the *SIRT1* isoforms is analysed.

7.2.3 Hypotheses

1. AROS and RPS19 associate in human cells.
2. RPS19 associates with SIRT1-FL and/or SIRT1-Δ8.
3. The *SIRT1* gene regulates RPS19.

7.3 *Molecular interactions of AROS*

Immunoprecipitation of endogenous AROS or RPS19 was attempted but proved unsuccessful with a range of antibodies. Given the small size of AROS and RPS19 (both less than 16kDa) the inability to co-immunoprecipitate endogenous protein may represent occlusion of their binding domains as a result of interaction with antibody, which have a molecular weight of ~150kDa. To address this, exogenously expressed Flag-tagged AROS and RPS19 proteins were employed to allow immunoprecipitation of each protein without perturbation of protein interactions. The limitations of exogenous protein expression and immunoprecipitation were combated by attempting reciprocal immunoprecipitations where possible. Overexpression of exogenous constructs did not greatly alter cell phenotypes in all cases (*Appendix*).

7.3.1 Flag-AROS and endogenous RPS19

Exogenous Flag-tagged AROS was successfully expressed in HCT116 cells following the scheme in Figure 7.1A. The exogenous Flag-AROS (indicated by a *) migrated behind endogenous AROS (indicated by a †) upon SDS-PAGE (Figure 7.1B). This is demonstrated in the 'Input' samples (lanes 1 and 2), which also evidence the higher expression of the exogenous AROS, consistent with over-expression. Flag-AROS was pulled down by Flag-immunoprecipitation when over-expressed (lane 5) with no immunoprecipitation from the no lysate and control transfection immunoprecipitations (lanes 3 and 4 - Figure 7.1B). In all 3 cases an anti-Flag antibody was used for immunoprecipitation.

Endogenous RPS19 was enriched by immunoprecipitation of Flag-AROS compared to the controls (Figure 7.1B – lane 5 compared to lanes 3 and 4). This indicates that endogenous RPS19 associates with Flag-AROS, consistent with the hypothesis that *'AROS and RPS19 associate in human cells'*. Negative control Actin protein was not co-immunoprecipitated by Flag-AROS, indicating that co-immunoprecipitation of RPS19 was not due to non-specific binding. Examples of full Western blots from a repeat of this experiment are shown in the *Appendices*.

Input and Flag-IP protein was loaded in known quantities. This allows the quantification of the fraction of endogenous RPS19 that associated with Flag-AROS in Figure 7.1B. The quantity of total protein that was used in immunoprecipitation (Flag-IP protein) was loaded in excess compared to original Input protein, as indicated in Figure 7.1B. Thus, 2-fold more Flag-IP protein was loaded compared to Input in the lower RPS19 and Actin Western blot analyses. Quantification revealed that over one third of total RPS19 protein appeared to associate with Flag-AROS in the HCT116 cell line (Figure 7.1C – left graph).

7.3.2 Flag-AROS and endogenous SIRT1

Flag-AROS also appeared to associate with endogenous SIRT1 protein (Figure 7.1B). This represents SIRT1-FL and is consistent with the published interaction between the proteins (Kim et al. 2007). A 100-fold excess of Flag-IP protein compared to Input protein was required to visualise the SIRT1 protein that co-immunoprecipitated with Flag-AROS. Thus, the fraction of endogenous SIRT1 (1.72%) that co-immunoprecipitates with Flag-AROS is lower than the fraction of endogenous RPS19 (Figure 7.1C).

7.3.3 Nuclear interactions of AROS

Flag-AROS interacts with both RPS19 and SIRT1 (see above). In *Chapter 4* a novel population of AROS was observed in the cytoplasm, with lower expression in the nucleus (Figure 4.5). Both RPS19 and SIRT1 are known to reside in both the nucleus and the cytoplasm (Da Costa et al. 2003; Tanno et al. 2007). This raises the question of whether Flag-AROS associates specifically with RPS19 and SIRT1 in different compartments or across the whole cell.

To analyse this immunoprecipitation of Flag-AROS was undertaken, following the protocol outlined in Figure 7.1A, with subcellular fractionation at the point of harvesting according to Figure 7.2A. Flag-AROS expressed in the Input of the cytoplasmic fraction, migrating behind endogenous AROS upon SDS-PAGE (lane 6 –Figure 7.2B). AROS was not detected in the Input of the nuclear fraction, presumably due to the lower expression of AROS in this fraction (*Chapter 4 – Figure 4.5*). Despite this Flag-AROS was immunoprecipitated with anti-Flag

antibody in the nuclear fraction (lane 4 –Figure 7.2B). Flag-AROS was not immunoprecipitated in the cytoplasmic fraction which was not amenable with immunoprecipitation. Nevertheless the cytoplasmic Input indicates even loading of immunoprecipitations within the experiment, and lack of Lamin AC expression compared to the nuclear fraction demonstrates efficient subcellular fractionation.

The interaction between Flag-AROS and RPS19 occurs in the nuclear fraction of HCT116 colorectal adenocarcinoma cells (Figure 7.2B). This interaction was quantified as representing 2.24% of nuclear RPS19 protein interacting with nuclear Flag-AROS (Figure 7.1C – left graph). Flag-AROS appeared to associate with one third of RPS19 protein in total cell lysate (Figure 7.1C), compared to less than 3% of nuclear RPS19. This lower interaction in the nucleus may imply that the total interaction seen is achieved in the cytoplasmic fraction. Perhaps consistent with this is the relative expression of AROS between fractions reported in *Chapter 4 – Figure 4.5*, where the dominant fraction of AROS was cytoplasmic. As such, these data do not formally identify a cytoplasmic Flag-AROS-RPS19 interaction but may allow its inference from comparison of whole cell and nuclear extract data.

SIRT1 was present in the nuclear fraction but did not appear to co-immunoprecipitate with Flag-AROS (Figure 7.2B and C). This suggests that Flag-AROS does not associate with SIRT1 in the nucleus, and thus that the Flag-AROS-SIRT1 interaction may be exclusively cytoplasmic. This has implications for the regulation of SIRT1 by AROS, which was shown to require a direct interaction between the proteins (Kim et al. 2007). Whether AROS regulates SIRT1 in the nucleus is questioned by this observation.

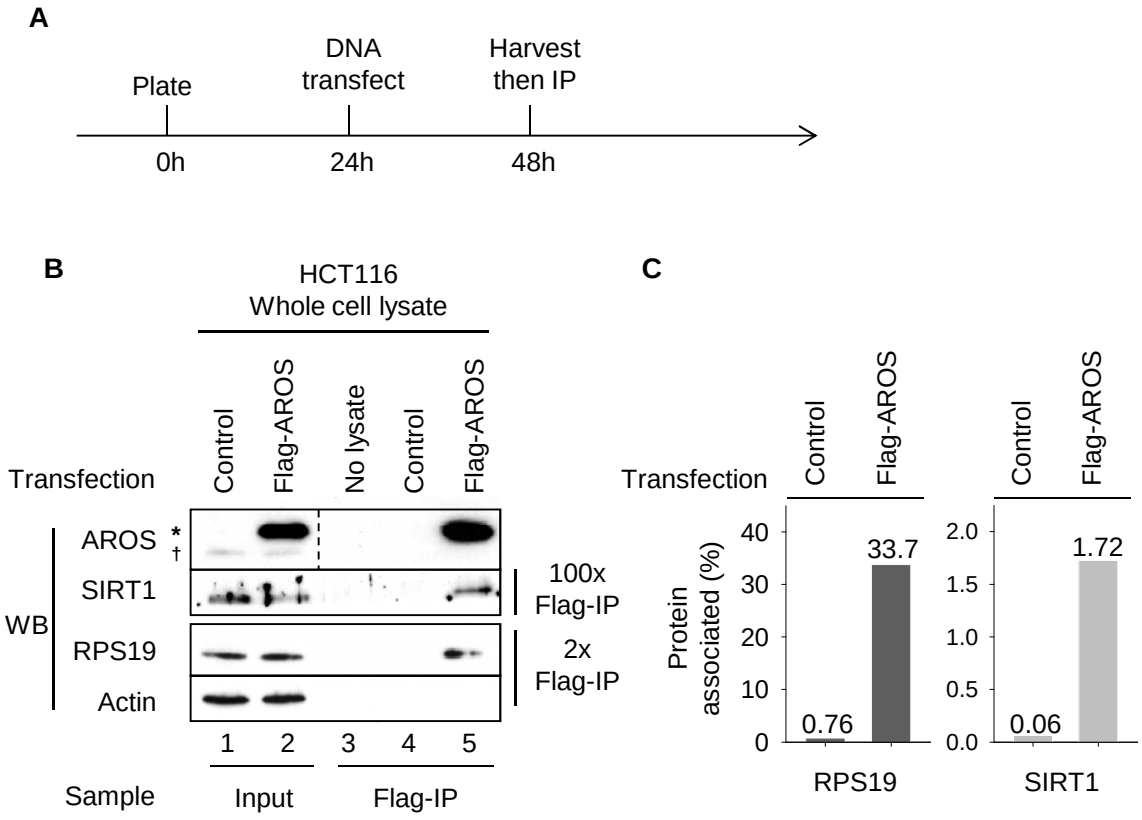

Figure 7.1: AROS interacts with RPS19 and SIRT1

(A) Time course of Flag-immunoprecipitation protocol. Cells were plated, then transfected with Flag-AROS pcDNA3 in liposomes 24 hours later. Control transfection was with liposomes only. After expression for 24 hours a known quantity of protein from cell lysate was used in Flag-immunoprecipitation for each condition. Flag-AROS expressing lysate was immunoprecipitated with anti-Flag conjugated beads, in parallel to lysate with no Flag-AROS overexpression (Control transfection). 'No lysate' control immunoprecipitation was run using lysis buffer only. Flag peptide was used to elute co-immunoprecipitated proteins for subsequent analysis. **(B)** Co-immunoprecipitated proteins were loaded for SDS-PAGE according to original quantity of protein loaded for immunoprecipitation. This was analysed in excess as indicated (2 or 100 fold) against a known quantity of original Input protein. Actin was used as a negative control that did not co-immunoprecipitate. Dashed line represents different exposures. (*) represents exogenous Flag-AROS, (†) represents endogenous AROS. **(C)** Quantification of co-immunoprecipitated endogenous RPS19 and SIRT1 using Quantity One software. Values represent the percentage of total RPS19 and SIRT1 protein found to co-immunoprecipitate with Flag-AROS.

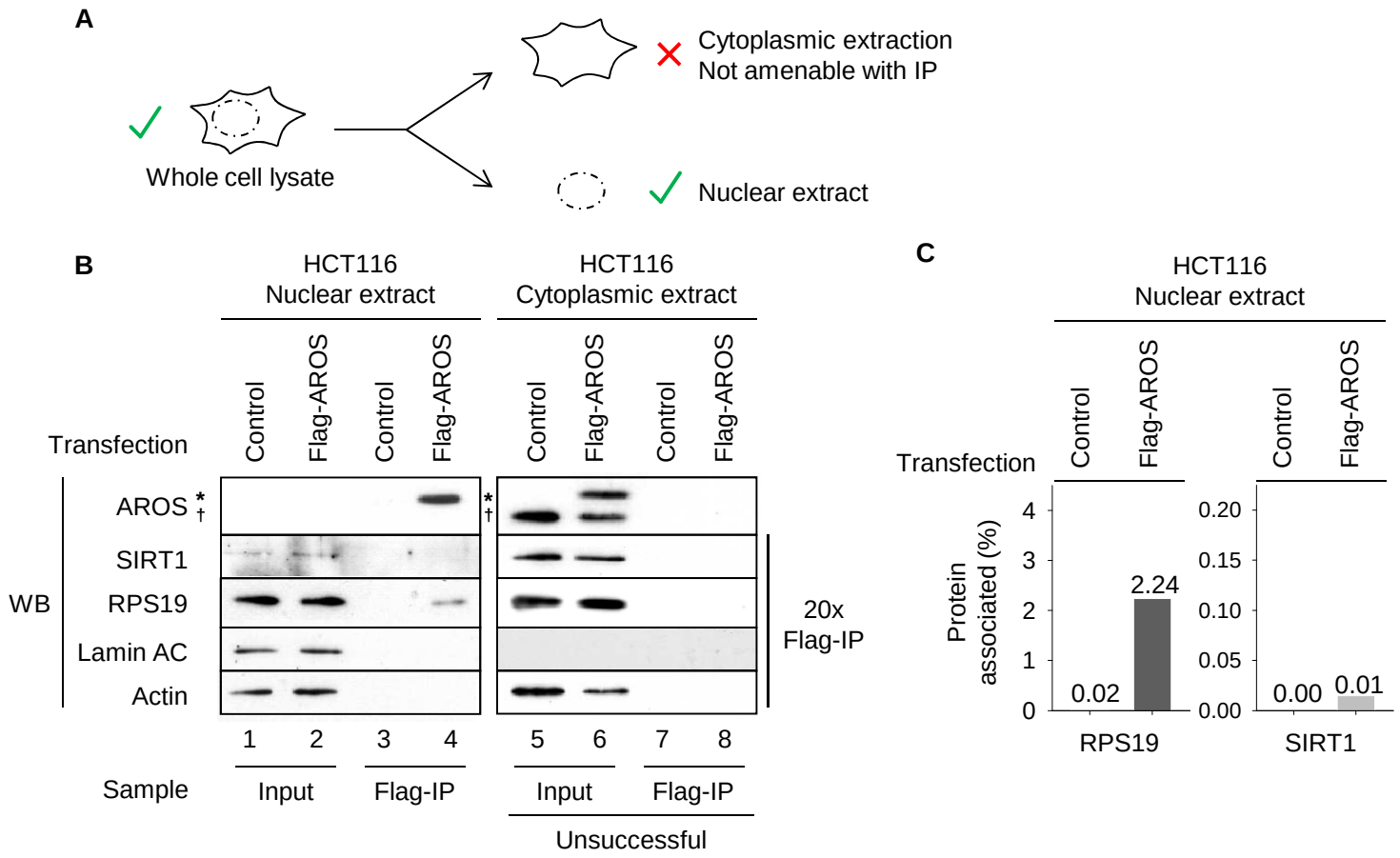

Figure 7.2: Nuclear AROS interacts with RPS19

(A) Subcellular fractionation protocol to analyse Flag-AROS interactions in nuclear and cytoplasmic compartments. HCT116 cells were separated into nuclear and cytoplasmic extracts and analysed by Flag-IP (see *Methods*). Immunoprecipitation protocol was not possible from cytoplasmic extract due to buffer constraints. **(B)** Analysis of nuclear and cytoplasmic immunoprecipitation. Lamin AC was used as a nuclear marker protein, present in the nuclear Input only. (*) represents exogenous Flag-AROS, (†) represents endogenous AROS. Data represents 20-fold more protein loaded in Flag-IP than Input. **(B)** Quantification of the percentage of total RPS19 and SIRT1 that co-immunoprecipitated with Flag-AROS. Data calculated using Quantity One software.

7.4 *Molecular interactions of RPS19*

Given the AROS-RPS19 and AROS-SIRT1 interactions confirmed above, there was potential for an RPS19-SIRT1 interaction in the experimental system. To analyse this tagged RPS19 protein was overexpressed in HCT116 cancer cells according to the protocol shown in Figure 7.3A. This allowed Flag immunoprecipitation as carried out for Flag-AROS. The recently discovered SIRT1 splice variant form (SIRT1-Δ8) was also analysed as a potential binding partner for RPS19, given that SIRT1-Δ8 interacts with AROS (Lynch et al. 2010). The analysis was carried out using exogenous SIRT1-FL and SIRT1-Δ8, because the endogenous SIRT1-Δ8 could not be detected by antibody. Given that AROS is known to interact with both isoforms of the *SIRT1* gene, Flag-AROS was used as a positive control to immunoprecipitate SIRT1-FL and SIRT1-Δ8.

7.4.1 RPS19 auto-association

Flag-Myc-RPS19 was detected in both experimental conditions when overexpressed (lanes 1 and 3 –Figure 7.3B). The exogenous Flag-Myc-RPS19 (*) migrated behind endogenous RPS19 (†) by SDS-PAGE and expressed at a similar level. Myc-SIRT1-FL was detected when overexpressed (lane 1) as was Myc-SIRT1-Δ8 (lane 3). Thus, co-expression of exogenous RPS19 and the SIRT1 isoform proteins was possible.

Flag-Myc-RPS19 was immunoprecipitated by Flag antibody, being detected in the immunoprecipitation lanes 5 and 7 (Figure 7.3B). Interestingly, where exogenous Flag-Myc-RPS19 was immunoprecipitated a fraction of endogenous RPS19 was also immunoprecipitated (Figure 7.3B). This implies that Flag-Myc-RPS19 interacts with endogenous RPS19, potentially in a dimer. A role for covalent RPS19 dimers has been characterised in relation to the immune response to apoptosis (Yamamoto 2007). This auto-association may represent a non-covalent precursor to this dimeric form.

7.4.2 Flag-Myc-RPS19 and endogenous AROS

The successful over-expression and immunoprecipitation of Flag-Myc-RPS19 allows the association of exogenous RPS19 and endogenous AROS to be analysed. This forms the reciprocal analysis to those above using exogenous Flag-AROS (Figure 7.1B). Endogenous AROS was co-immunoprecipitated by Flag-Myc-RPS19, indicating that the two proteins associated (Figure 7.3C). This provides further evidence in support of the hypothesis that '*AROS and RPS19 associate in human cells'*.

7.4.3 RPS19 specifically associates with SIRT1-Δ8

Similar to endogenous AROS, overexpressed Myc-SIRT1-Δ8 co-immunoprecipitated with Flag-Myc-RPS19 (Figure 7.3B). Importantly, exogenous RPS19 did not appear to co-immunoprecipitate Myc-SIRT1-FL. Together this implies that RPS19 is able to specifically complex with SIRT1-Δ8 over SIRT1-FL (Figure 7.3C). Importantly, this is the first instance of a protein specifically interacting with SIRT1-Δ8 over SIRT1-FL, and indicates that *'RPS19 associates with SIRT1-Δ8*'. Furthermore, RPS19 and SIRT1-Δ8 may influence reciprocal protein functions via this interaction. This is analysed later in the *Chapter*. First, the specificity of the novel RPS19-SIRT1-Δ8 interaction was confirmed by analysis of the interaction of the SIRT1 isoform with Flag-AROS.

7.4.4 Flag-AROS interactions as a positive control

AROS is known to interact with both SIRT1-FL and SIRT1-Δ8 (Lynch et al. 2010) and was used here as a positive control for interaction with both proteins. Flag-AROS was over-expressed in parallel immunoprecipitations to those above for Flag-Myc-RPS19 (Figure 7.4A and B). In these experiments Flag-AROS appeared to co-immunoprecipitate both exogenous Myc-SIRT1-FL (o) and Myc-SIRT1-Δ8 (‡), as well as endogenous SIRT1-FL (<). Endogenous SIRT1-Δ8 could not be detected by antibody. Nevertheless, these data indicate that AROS interacts with both variants of the *SIRT1* gene (Figure 7.4C). This is consistent with the previously reported binding capacities of AROS (Kim et al. 2007; Lynch et al. 2010). This also provides

a repeat analysis of the Flag-AROS-RPS19 interaction, which occurs as expected (Figure 7.4B and C).

7.4.5 RPS19 binds SIRT1-Δ8 following applied stress

SIRT1-Δ8 is upregulated following the application of stress, and may suppress the stress response by deacetylating p53 (Lynch et al. 2010). This implies that SIRT1-Δ8 is important during the cellular response to stress. Thus, with exogenous RPS19 and SIRT1-Δ8 able to associate in the absence of applied stress (Figure 7.3B) the potential for an association following applied stress was analysed. For this a modified overexpression protocol was used, with an extra 24 hours between cDNA transfection and harvesting to allow for UV stress treatment (Figure 7.5A). The quantity of cDNA used for over-expression was reduced by half accordingly.

Flag-Myc-RPS19 and Myc-SIRT1-Δ8 co-immunoprecipitated following the application of UV irradiation stress to HCT116 cells (Figure 7.4B). This indicates that the RPS19-SIRT1-Δ8 interaction may persist under conditions where SIRT1-Δ8 may have great physiological relevance.

Interestingly the interaction between Flag-Myc-RPS19 and endogenous AROS was not observed following the application of UV stress (Figure 7.5B). This may be attributable to the lower relative expression of exogenous Flag-Myc-RPS19 following applied stress compared to in the absence of applied stress (Figure 7.3B compared to Figure 7.5B) As such, the abundant endogenous RPS19 may compete for AROS protein following UV irradiation to a greater extent than in the absence of applied stress. This could also explain the apparent loss of RPS19 dimer associations following applied stress.

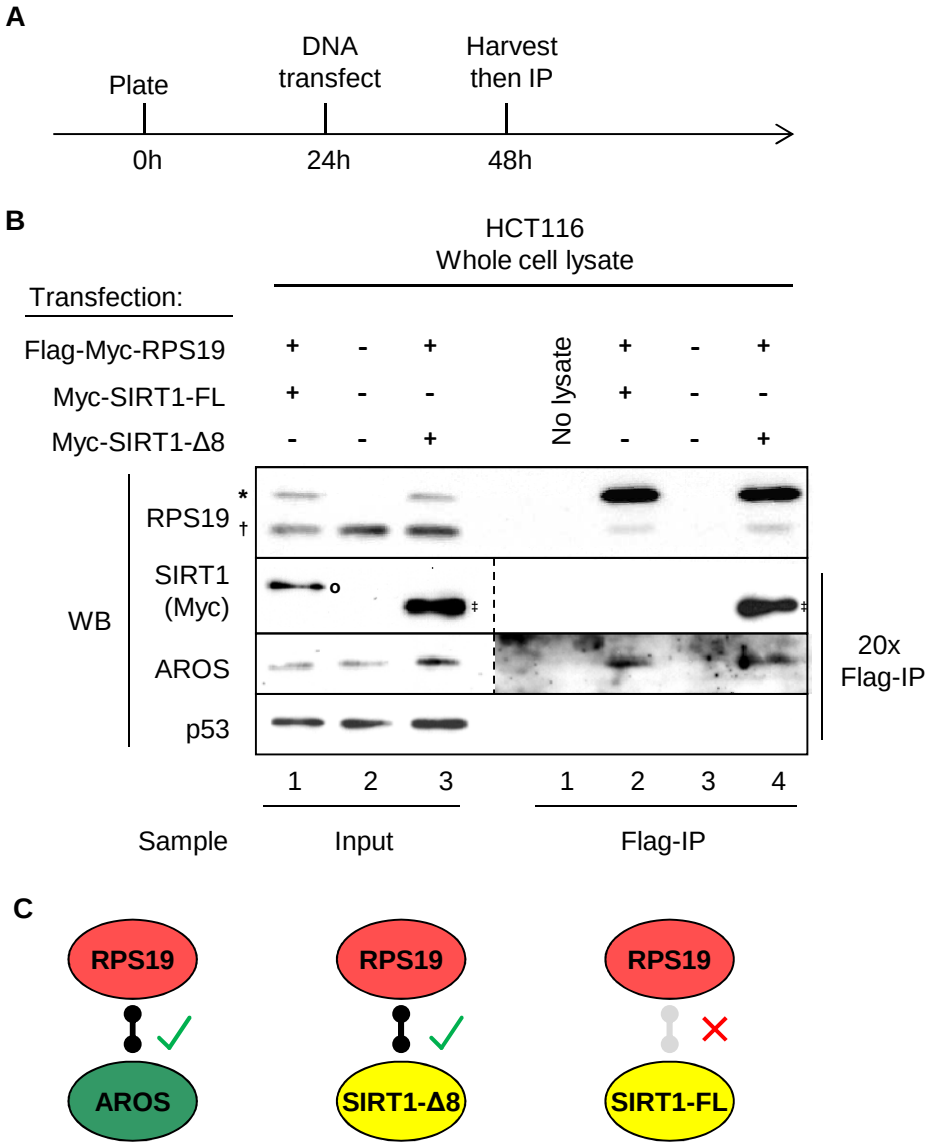

Figure 7.3: RPS19 interacts with SIRT1-Δ8

(A) Time course of Flag-immunoprecipitation experiments. HCT116 cells were plated then transfected 24 hours later with cDNA encoding Flag-Myc-RPS19 and the SIRT1 splice variant constructs. Flag-Myc-RPS19 was immunoprecipitated from whole cell lysates 24 hours after transfection by Flag-antibody conjugated to agarose beads. Control transfected cells were treated with liposomes only, and then used in identical parallel immunoprecipitation. Elution was with excess Flag peptide. **(B)** Samples were analysed by SDS-PAGE and Western blotting with 20-fold excess immunoprecipitated protein loaded compared to Input protein. Overexpressed Flag-Myc-RPS19 (*) migrated behind endogenous RPS19 (†). Overexpressed Myc-SIRT1-FL (o) migrated behind Myc-SIRT1-Δ8 (‡). 'No lysate' represents immunoprecipitation using lysis buffer only. p53 was used as a protein that did not interact with Flag-Myc-RPS19. **(C)** Schematic of RPS19 interactions. Flag-Myc-RPS19 associated with endogenous AROS and exogenous SIRT1-Δ8. No association was seen with exogenous SIRT1-FL.

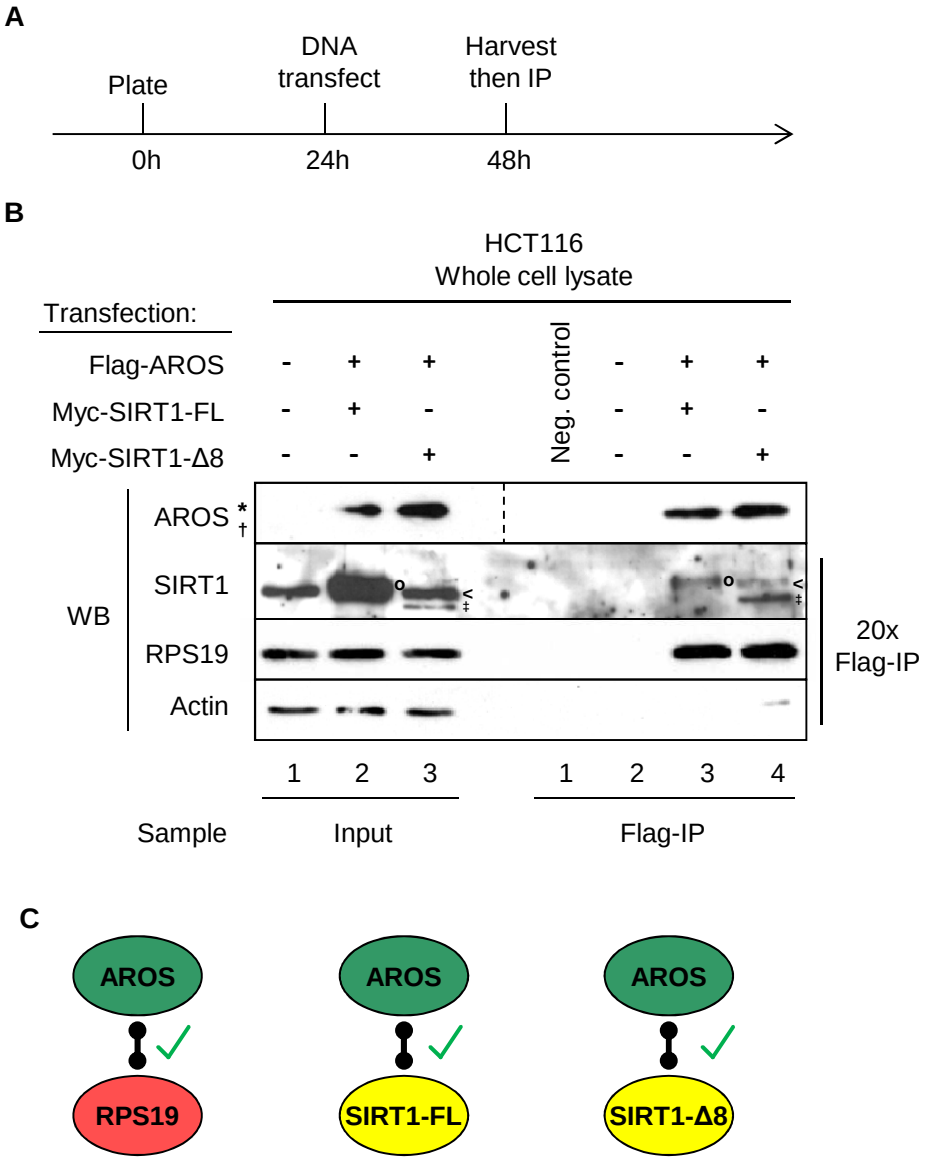

Figure 7.4: AROS interacts with SIRT1-FL and SIRT1-Δ8

(A) Time course of Flag-immunoprecipitation experiments. HCT116 cells were plated then transfected with cDNA encoding Flag-AROS and the SIRT1 splice variant constructs 24 hours later. Flag-AROS was immunoprecipitated from whole cell lysates 24 hours after transfection using Flag-antibody conjugated to agarose beads. Control transfected cells were treated with liposomes only then used in parallel identical immunoprecipitation. Elution was with excess Flag peptide. **(B)** Samples analysed by SDS-PAGE and Western blotting. Overexpressed Flag-AROS (*) migrated behind endogenous AROS (†). Overexpressed SIRT1-FL (o) migrated behind endogenous SIRT1 (<). SIRT1-Δ8 (‡) migrated ahead of endogenous SIRT1. 'No lysate' lane represents immunoprecipitation using lysis buffer only. Actin was used as a negative control for interaction with Flag-AROS. **(C)** Schematic of AROS interactions. Flag-AROS interacts with endogenous RPS19 and SIRT1-FL, as well as exogenous SIRT1-Δ8.

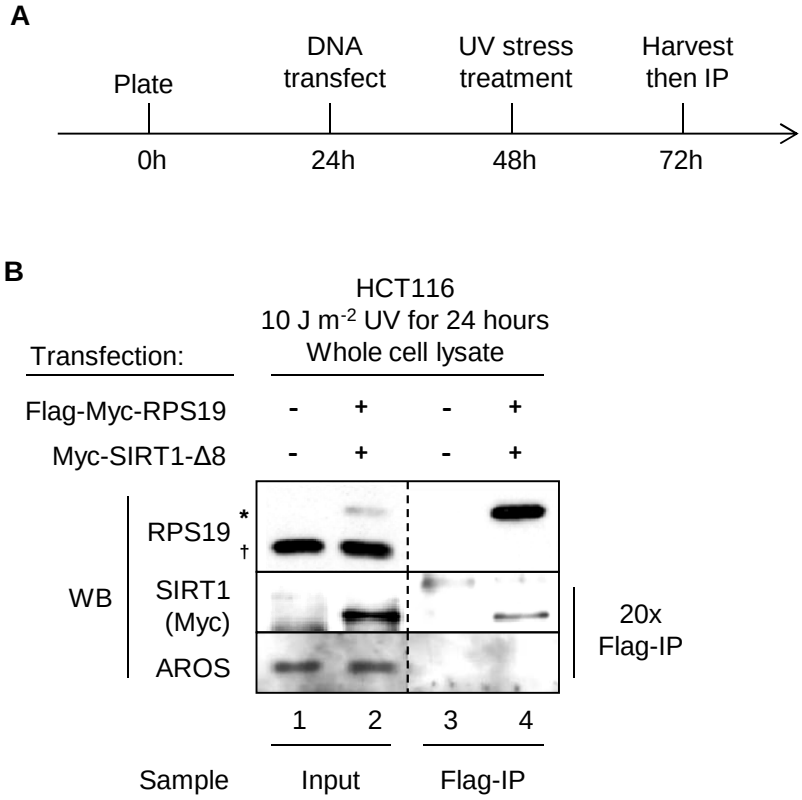

Figure 7.5: RPS19 interacts with SIRT1-Δ8 following UV stress

(A) Time course of Flag-immunoprecipitation and UV stress experiments. HCT116 cells were plated then transfected 24 hours later with cDNA encoding Flag-Myc-RPS19 and Myc-SIRT1-Δ8. 24 hours after transfection cells were stressed by the application of UV irradiation at 10J m^{-2}. Flag-Myc-RPS19 was immunoprecipitated from whole cell lysates 48 hours after transfection (24 hours after UV stress) by Flag-antibody conjugated to agarose beads. Control transfected cells were treated with liposomes only and used in parallel identical immunoprecipitation. Elution was with excess Flag peptide. **(B)** Samples analysed by SDS-PAGE and Western blotting. Overexpressed Flag-Myc-RPS19 (*) migrated behind endogenous RPS19 (†).

7.5 *SIRT1-Δ8 regulation of RPS19*

The immunoprecipitation data above indicate that RPS19 forms a specific interaction with the SIRT1-Δ8 splice variant of the *SIRT1* gene. The remainder of this *Chapter* analyses the potential regulation of RPS19 by SIRT1-Δ8 via this molecular interaction. This utilises a specific siRNA against the SIRT1-Δ8 isoform, which targets the novel splice junction between exons 7 and 9 in SIRT1-Δ8.

7.5.1 mRNA knockdown

Use of SIRT1-Δ8 siRNA in the HCT116 cell line depleted *SIRT1-Δ8* mRNA expression compared to control, as analysed by RT-PCR (Figure 7.6A). Due to the requirement to use a primer across the SIRT1-Δ8 exon 7 to 9 splice junction, qRT-PCR could not be performed to amplify *SIRT1-Δ8* mRNA (Lynch et al. 2010). Commercially available antibodies are unable to detect endogenous human SIRT1-Δ8 protein. Thus, analysis of the resulting knockdown of SIRT1-Δ8 was not possible.

7.5.2 Cell phenotype

Targeting of SIRT1-Δ8 across 4 cell lines of cancerous (HCT116, DLD1 and MCF7) and non-cancerous (WI38) origin did not greatly alter the phenotype compared to Mock treatment (Figure 7.6B). In the MCF7 cell line there was an apparent effect. SIRT1-Δ8 siRNA appeared to reduce cell density compared to Mock treatment, with the cells appearing refringent under phase contrast microscopy. This may be indicative of suppression of cell cycle progression in MCF7 cells, perhaps consistent with SIRT1-Δ8 suppressing p53 (Lynch et al. 2010). In the other 3 cell lines silencing of SIRT1-Δ8 did not greatly affect cell density or morphology compared to Mock treatment.

7.5.3 SIRT1-Δ8 promotes RPS19 protein

SIRT1-Δ8 appeared to affect RPS19 protein abundance upon analysis by Western blot. In each of the 4 cell lines analysed targeting of SIRT1-Δ8 reduced the protein abundance of RPS19 compared to Mock treatment of cells (Figure 7.7A). *RPS19* mRNA was not negatively affected by loss of SIRT1-Δ8 (Figure 7.7B),

suggesting that the effect SIRT1-Δ8 has upon RPS19 occurs at the protein level. In the MCF7 cell line silencing of SIRT1-Δ8 actually increased *RPS19* mRNA expression compared to Mock treatment. This has parallels to the protein level regulation of RPS19 by AROS in *Chapter 6*, suggesting that SIRT1-Δ8 may play a role in the regulation of RPS19 by AROS (Figure 7.7C). This possibility is perhaps supported by the association of AROS and SIRT1-Δ8 (Lynch et al. 2010), which both also interact with RPS19 (*this Chapter*).

Knockdown of SIRT1-Δ8 had a variable effect of AROS abundance across the 4 cell lines analysed. In the HCT116 and DLD1 cancer cell lines the protein abundance of AROS was not affected by knockdown of SIRT1-Δ8 (Figure 7.7A). This is despite the loss of RPS19, which was previously seen to result in loss of AROS in *Chapter 6*. In the HCT116 cell line targeting of SIRT1-Δ8 reduced the abundance of *AROS* mRNA compared to Mock treatment (Figure 7.7B) but this did not translate to a reduction in total AROS protein. Stability of AROS may be attributable to apparent higher stability of AROS in these colorectal adenocarcinoma cell lines (see *Chapter 4*).

In the MCF7 mammary epithelial cancer cell line AROS protein abundance was reduced by SIRT1-Δ8 knockdown, despite no reduction in *AROS* mRNA (Figure 7.7A and B). Similarly, in the WI38 cell line AROS protein, but not mRNA, abundance may have been reduced by knockdown of SIRT1-Δ8, although the Western blot is open to interpretation. Together these data suggest that SIRT1-Δ8 may promote AROS protein abundance in a similar manner to its apparent promotion of RPS19 protein above. This could give SIRT1-Δ8 an important role in the AROS-RPS19 autoregulatory loop.

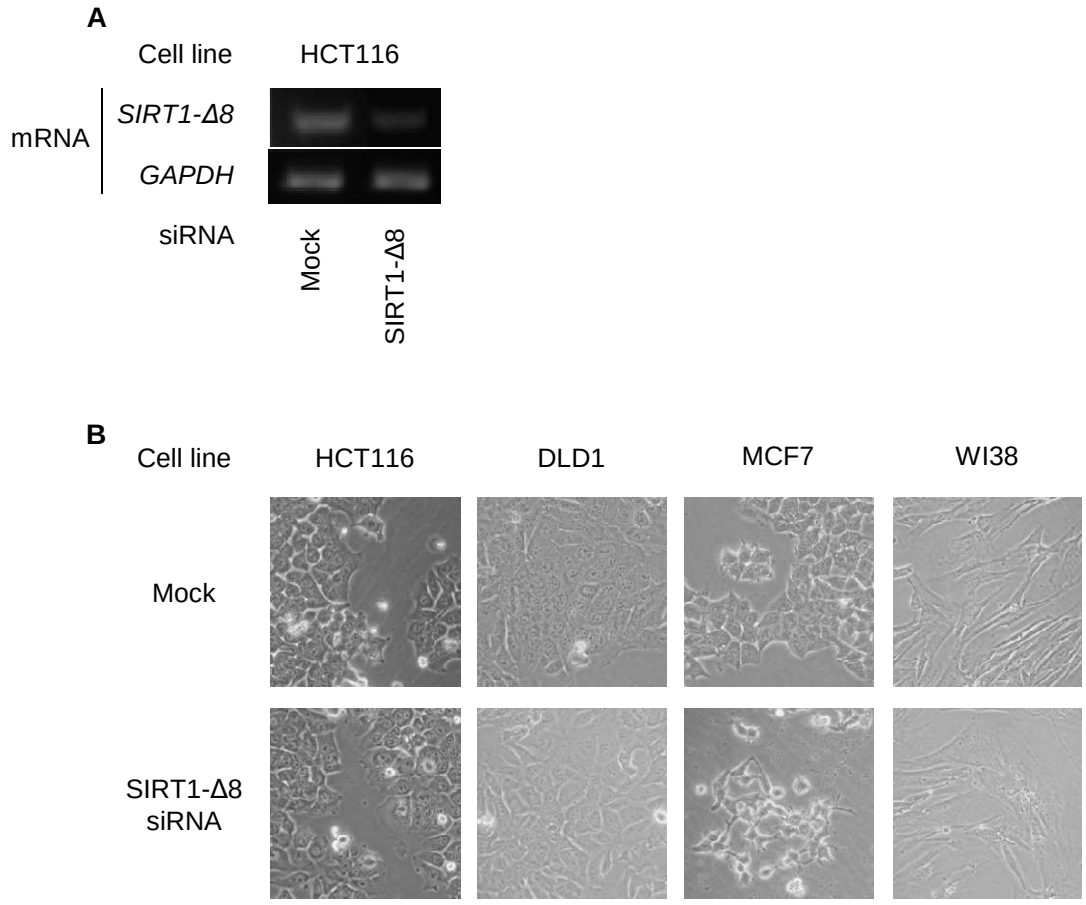

Figure 7.6: Targeting SIRT1-Δ8 by siRNA

(A) mRNA abundance of *SIRT1-Δ8* and *GAPDH* in HCT116 cells treated with SIRT1-Δ8 siRNA. Total RNA was isolated by RNeasy method and analysed by RT-PCR. cDNA product was visualised by agarose gel electrophoresis using ethidium bromide and UV transillumination. **(B)** Phase contrast micrographs of cell lines treated with RNAi specifically against SIRT1-Δ8 prior to harvesting at 48 hours (HCT116, DLD1 and MCF7) or 72 hours (WI38) post-transfection.

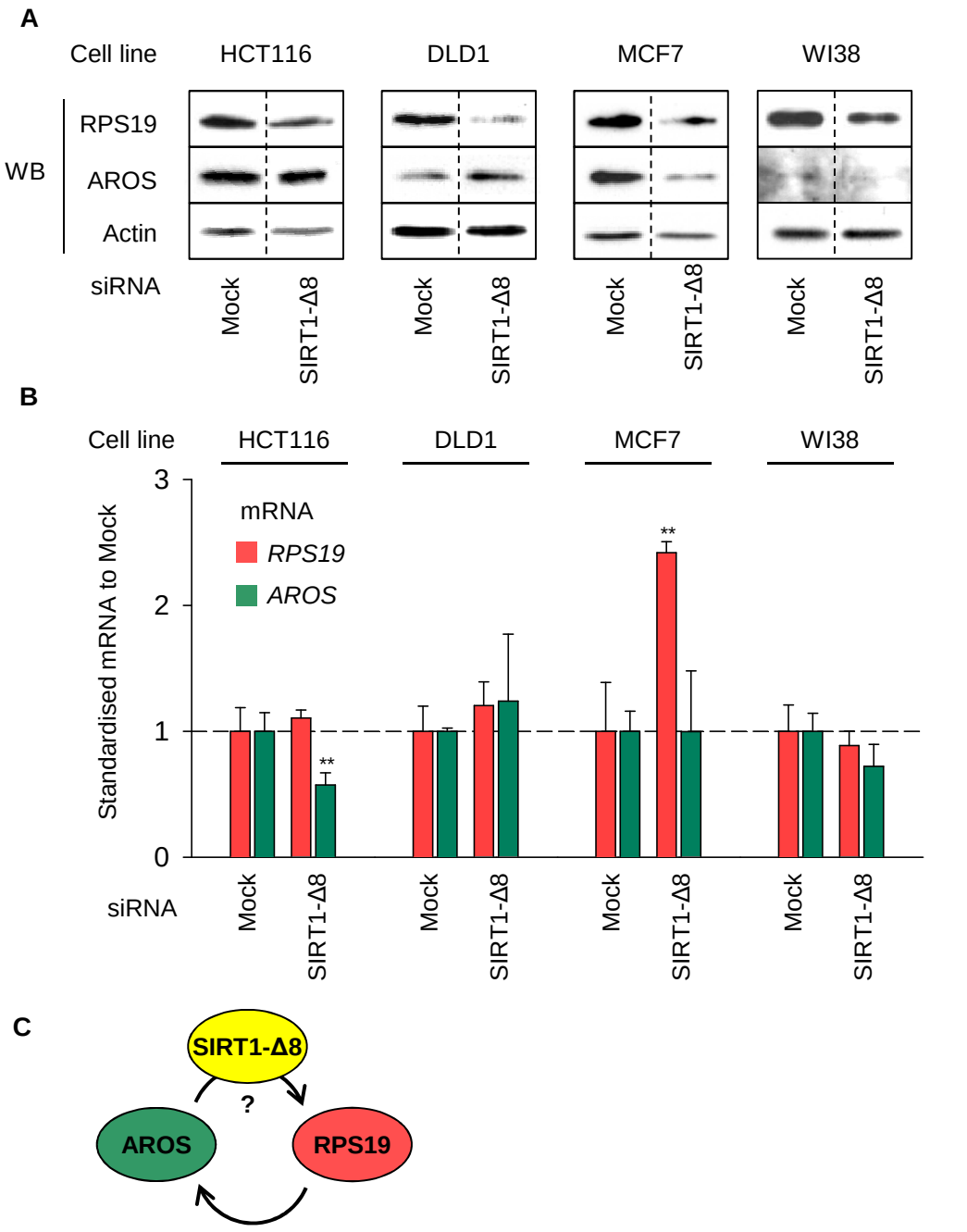

Figure 7.7: SIRT1-Δ8 knock down results in loss of RPS19 protein

(A) Expression of AROS and RPS19 proteins following targeting of SIRT1-Δ8 by siRNA. Cell lines were transfected with siRNA then harvested 48 hours (HCT116, DLD1 and MCF7) or 72 hours (WI38) post-transfection. Whole cell protein was isolated and loaded onto SDS-PAGE according to calculated protein mass. Actin was used as a loading control. **(B)** Expression of *AROS* and *RPS19* mRNA following targeting of SIRT1-Δ8 by siRNA. RNA was isolated by RNeasy method and analysed by qRT-PCR (*Methods*). mRNA abundance was standardised against *Actin* (HCT116, DLD1 and WI38) or *GAPDH* (MCF7) mRNA abundances. ** P<0.01. **(C)** Schematic of potential regulation of the AROS-RPS19 autoregulatory loop by SIRT1-Δ8.

7.6 *Discussion*

7.6.1 Implications of the AROS-RPS19 association

The observation of an association between exogenous Flag-AROS and endogenous RPS19 (Figure 7.1B), and the reciprocal association between Flag-Myc-RPS19 and AROS (Figure 7.3B) is compelling evidence for conservation of the AROS-RPS19 interaction originally identified in the mouse (Maeda et al. 2006). This appears to confirm the hypothesis that *'AROS and RPS19 associate in human cells'*. The original AROS-RPS19 association was characterised as a direct interaction between the two proteins, suggesting that the association seen here is also a direct interaction.

The interaction of AROS and RPS19 has implications for the autoregulatory loop identified between the proteins (*Chapter 6*). It appears likely that the AROS-RPS19 autoregulatory loop involves the direct interaction of the proteins. One possibility is that the AROS-RPS19 complex is less liable to degradation than the individual proteins. RPS19 was recently reported to be actively degraded by the proteasome (Cretien et al. 2008), potentially supporting this hypothesis. The data suggest that interaction with AROS may reduce the proteasomal degradation of RPS19. Given the reciprocal nature of the AROS-RPS19 relationship, this also appears to protect AROS from degradation. Future analysis into the proteasomal degradation of RPS19 and/or AROS would be required to analyse this. Importantly this data does not rule out a mechanism governing AROS and RPS19 protein stability linked to ribosome stability, which remains a possibility.

Interestingly the AROS-RPS19 interaction appears to occur in the nucleus of HCT116 cells, whereas the AROS-SIRT1 interaction was less prevalent in this compartment (Figure 7.2B). RPS19 is required for ribosome synthesis, which occurs within the nucleolus, a subnuclear structure (Choesmel et al. 2007; Flygare et al. 2007; Idol et al. 2007). The interaction between AROS and RPS19 within the nucleus may be indicative of a functional role of AROS in ribosome synthesis. This possibility is analysed in *Chapter 8*.

7.6.2 Auto-association of RPS19

In Figure 7.3 exogenous Flag-Myc-RPS19 co-immunoprecipitated endogenous RPS19 protein. This implies that RPS19 is able to form dimers. RPS19 acts as a monomeric protein during ribosome biogenesis and subsequent activity. However, a covalently ligated dimeric form of RPS19 has been identified and characterised (Nishiura et al. 1998). The non-covalent RPS19 dimer potentially identified here could represent a precursor to this covalent dimeric form.

The RPS19 dimer is formed during apoptosis by the ligation of lysine 122 from one RPS19 molecule to glutamine 137 of a second RPS19 molecule (reviewed by Yamamoto 2007). Extracellular RPS19 dimer acts as a selective chemo-attractant for monocytes over neutrophils, which assists in the clearance of post-apoptotic cell debris (Oda et al. 2008). The outcome of this is an acute immune response to routine cell death promoted by monocytes, as opposed to a chronic inflammatory response which would arise from neutrophil recruitment and activation.

During the analyses of RPS19 no covalently bound dimeric forms were observed, which would migrate slower by SDS-PAGE. This is consistent with the documented excretion of the covalent dimeric form from the cell, and does not rule out the possibility that the dimer observed here contributes to the covalent dimer described.

The presence of RPS19-RPS19 interactions may influence binding to AROS. As such, the high abundance of the RPS19 interaction with AROS may be attributable to dimerisation of RPS19. The dimerisation may increase the apparent total RPS19 co-immunoprecipitated by Flag-AROS as multiple protein molecules may have associated with a single Flag-AROS. However, the RPS19 dimerisation appears to be a low abundance interaction and may or may not occur when AROS associates with RPS19. Thus, although not confirmed, it seems likely that the majority of the Flag-AROS-RPS19 association is not the result of RPS19 dimerisation, and that the AROS-RPS19 association is highly abundant.

7.6.3 RPS19 association with SIRT1-Δ8

RPS19 appeared to specifically interact with a splice variant of SIRT1 and not the full length protein (Figure 7.3B). The RPS19-SIRT1-Δ8 interaction appeared to be abundant, but is of unknown significance. Interestingly, AROS interacts with both the SIRT1-FL and SIRT1-Δ8 variants of the *SIRT1* gene (This work and Lynch et al. 2010). The effect of AROS on SIRT1-Δ8 is not known, and this data does not indicate whether AROS and RPS19 are able to bind SIRT1-Δ8 simultaneously.

The specificity of the interaction raises the question of how does RPS19 interact with SIRT1-Δ8 but not SIRT1-FL? Other than lacking exon 8 the two proteins are identical. However the SIRT1-Δ8 protein has a novel peptide sequence across the splice junction, which may permit specific interactions (Figure 7.8A). Furthermore, SIRT1-Δ8 lacks residues that bind substrates in SIRT1-FL, suggesting that substrate specificity may be altered between the two isoforms (Lynch et al. 2010). There is no evidence of acetylation of RPS19 in the literature, suggesting that it is not party to reversible modification in this way. However, given the role of SIRT1-Δ8 as a deacetylase enzyme, the possibility that RPS19 is a specific substrate for SIRT1-Δ8 cannot be ruled out (Figure 7.8A).

Conversely, specificity may be mediated by the SIRT1-FL interactome. RPS19 binding to SIRT1-FL may be occluded by association of proteins that bind in exon 8, meaning that loss of exon 8 in the SIRT1-Δ8 isoform promotes association of RPS19 (Figure 7.8A). These hypothetical mechanisms of the specific interaction between SIRT1-Δ8 and RPS19 require further analysis to validate. However, this was not undertaken here, with the focus instead on functions of the SIRT1-Δ8-RPS19 association.

7.6.4 RPS19 in SIRT1-Δ8 function

Both SIRT1-Δ8 and RPS19 suppress p53 acetylation (Danilova et al. 2008; McGowan et al. 2008; Lynch et al. 2010; Dutt et al. 2011; Jaako et al. 2011). SIRT1-Δ8 suppresses p53 via direct deacetylation, which is required for transactivation of p53 target genes (Tang et al. 2008). The mechanism of RPS19 suppression of p53 is

unknown. It is possible that RPS19 suppresses p53 via its association with SIRT1-Δ8.

In *Chapter 6* RPS19 promoted AROS protein stability, suggesting that RPS19 promotes p53 suppression by AROS. RPS19 also appeared to promote SIRT1-FL protein stability in some cell lines, suggesting that RPS19 may suppress p53 via SIRT1-FL. The data here suggest that the RPS19 does not promote SIRT1-FL protein abundance via association. However, the data do indicate that RPS19 may be able to suppress p53 via a number of distinct mechanisms involving AROS and multiple isoforms of the *SIRT1* gene (Figure 7.8B).

7.6.5 SIRT1-Δ8 in RPS19 function

Knockdown of SIRT1-Δ8 resulted in a reduction in RPS19 protein abundance in four cell lines (Figure 7.7A). This may have also resulted in loss of AROS protein, which has been associated with RPS19 knockdown. Thus it appears that SIRT1-Δ8 may promote RPS19 abundance and possibly function. This may occur via the interaction between SIRT1-Δ8 and RPS19 which is also reported in this *Chapter*. The potential for a role of AROS in the function of RPS19 was identified in *Chapter 6*, and supplemented by the observation of AROS-RPS19 association in this *Chapter*. RPS19 is essential for specific steps during ribosome biogenesis in human cells (Choesmel et al. 2007; Flygare et al. 2007; Idol et al. 2007). Thus, the next *Chapter* focuses on a potential role for both AROS and SIRT1-Δ8 in ribosome biogenesis.

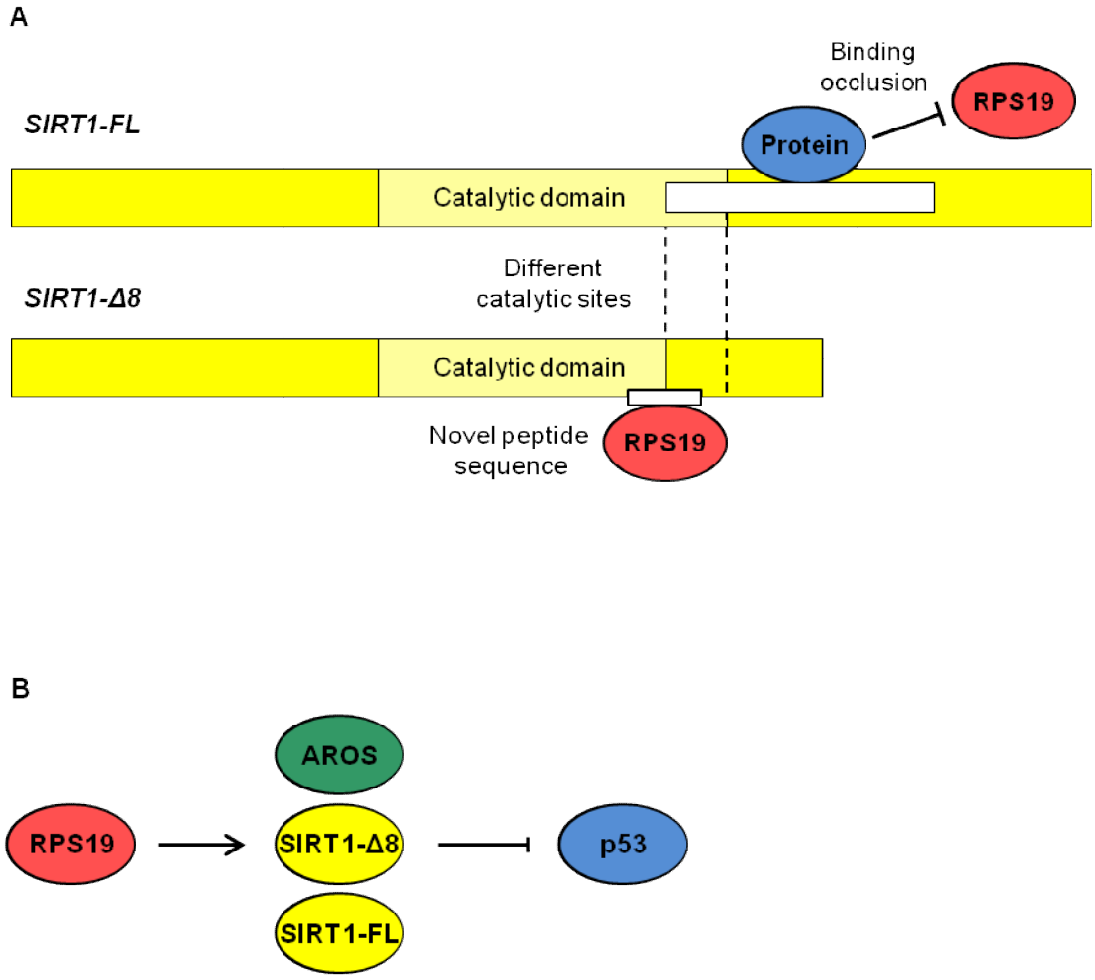

Figure 7.8: RPS19 and isoforms of *SIRT1*

(A) Schematic representation of SIRT1-FL and SIRT1-Δ8, showing potential mechanisms for the specific interaction of RPS19 with SIRT1-Δ8. These are, occlusion of RPS19 from binding SIRT1-FL, differences in the catalytic site of the two isoforms and RPS19 binding to the novel peptide sequence of SIRT1-Δ8. **(B)** Suppression of p53 by RPS19 may occur via modulation of AROS and *SIRT1* isoform function.

7.7 *Conclusions*

1. AROS and RPS19 associate in human cells.
2. RPS19 specifically associates with SIRT1-Δ8 over SIRT1-FL.
3. SIRT1-Δ8 promotes RPS19 protein level abundance.

8 Regulation of ribosome biogenesis

8.1 *Overview*

This final results *Chapter* analyses the role of AROS and SIRT1-Δ8 in the regulation of RPS19 during ribosome biogenesis. This builds on *Chapter 6 and Chapter 7*, where molecular interactions and relationships between AROS, RPS19 and SIRT1-Δ8 were characterised. Analysis utilised siRNAs against AROS and SIRT1-Δ8 to compare the outcome against the use of RPS19 siRNA.

AROS is found to have a role in ribosome biogenesis, with parallels to the role of RPS19. AROS specifically affects 40S ribosomal RNA and proteins. Furthermore, sucrose density ultracentrifugation identifies an association of AROS with 40S subunits and mature 80S ribosomes. Finally, SIRT1-Δ8 is found to have a role in ribosome biogenesis, building on the specific interaction between SIRT1-Δ8 and RPS19 seen in *Chapter 7*.

8.2 *Introduction*

8.2.1 The eukaryotic ribosome

Ribosomes catalyse the synthesis of protein, doing so with high fidelity at high speed according to the sequence of mRNA. Ribosomes are essential to translate the nucleotide encoded genetic code into the functional form that is the proteome. All cells, from single celled bacteria to mammalian cells, including plant cells, archaea and fungi, rely on ribosomes for production of protein. It is thought that ribosomes represent one of the earliest developments that allowed cellular life to exist. Over millennia of evolution the function of ribosomes in each branch of life has remained the same, but the specific structures have diverged (Hage and Tollervey 2004; Dinman 2009).

Translating ribosomes are in fact the association of two ribosomal subunits upon mRNA. These are termed the small and the large subunit. In higher eukaryotes these are referred to as 40S and 60S respectively, due to their relative density upon sedimentation (Figure 8.1A). Together the 40S and 60S subunits form the 80S ribosome. 40S and 60S subunits are free in the cytoplasm prior to mRNA binding to a 40S subunit. Binding triggers association of the 60S subunit and the initiation of translation.

Ribosomes are ribonucleoproteins as they consist of both RNA and protein elements. There are four ribosomal RNAs (rRNAs) and 80 ribosomal proteins in the eukaryotic ribosome. The 40S subunit contains a single rRNA (the 18S rRNA) and 33 ribosomal proteins (Figure 8.1A). The 60S subunit is larger and comprises 3 rRNAs (the 5S, 5.8S and 28S rRNAs) and 47 proteins (Figure 8.1A). Recent structures of the eukaryotic ribosome reveal the location of the ribosomal proteins and RNAs across each subunit (Taylor et al. 2009; Ben-Shem et al. 2010; Rabl et al. 2011). This will be used as a powerful tool for interpretation of the results presented in this *Chapter*.

8.2.2 Ribosome biogenesis

Unsurprisingly for such large and complex macromolecules the synthesis of ribosomes is highly complex, energy consuming and regulated in the cell. Ribosome biogenesis involves the coordinated function of transcription machinery to produce rRNA and ribosomal protein mRNA, synthesis of the ribosomal proteins and assembly of each subunit from its component parts. Add to this the actions of a multitude of ribosome biogenesis factors, which are both proteins and small RNAs, and the number of molecules that are involved in synthesis of each ribosome is in the 100s (Freed et al. 2010; Kressler et al. 2010).

Ribosome biogenesis occurs primarily in nucleoli, which are subnuclear organelles centred on the ribosomal DNA genes (rDNA). However, the complex process stretches beyond the nucleus, with elements such as ribosomal protein synthesis and the final nucelolytic cleavage of pre-18S rRNA occurring in the cytoplasm (Figure 8.1A and Rouquette et al. 2005). This adds an extra level to ribosome biogenesis, with subcellular trafficking both into and out of the nucleus demanding further regulation and consumption of energy.

Importantly, biogenesis of each ribosomal subunit occurs independently via parallel pathways (Figure 8.1A and Hadjiolova et al. 1993). This is maintained at a stoichiometric ratio of 1:1 by the co-transcription of rRNA components for both the small and large subunits. rDNA is transcribed into a single long pre-rRNA termed the 45S pre-rRNA. The sequences that ultimately form the 18S, 5.8S and 28S rRNAs are present within this pre-rRNA, separated by transcribed spacers (Figure 8.1B). Endonucleolytic cleavage within the 5’ internal transcribed spacer separates the 40S subunit constituent (18S rRNA) from the 60S subunit components (5.8S and 28S rRNA). 5S rRNA is transcribed independently of 45S pre-rRNA transcription to contribute to the 60S subunit.

Further nucelolytic cleavages of pre-rRNA yield the final rRNA forms present in each subunit (Figure 8.1B). This occurs in parallel to ribosomal protein loading onto rRNAs in macromolecular complexes called the small and large subunit processomes. Indeed ribosomal proteins are not passive during pre-rRNA

processing, being required for the nucelolytic steps in synthesis of each ribosomal subunit (Robledo et al. 2008). This indicates that ribosomal protein association is essential for rRNA processing. As such, the biogenesis of each subunit from rRNA and protein occurs while the rRNA is being processed (Figure 8.1A).

8.2.3 The role of RPS19 in ribosome biogenesis

As previously discussed, RPS19 is a structural component of the small ribosomal subunit, present in the head region of the eukaryotic ribosome (Taylor et al. 2009; Ben-Shem et al. 2010; Rabl et al. 2011). However, as well as being a structural component, RPS19 is essential for the synthesis of 40S ribosomal subunits. RPS19 is required for the final nuclear cleavage of the 3' end of precursor rRNA which ultimately yields the 18S rRNA of the 40S subunit in human cells (cleavage step indicated by [*] in Figure 8.1B). Thus, reduction in RPS19 expression results in reduced abundance of mature 40S subunits and a concomitant reduction in 80S ribosomes (Choesmel et al. 2007; Flygare et al. 2007; Idol et al. 2007).

The mechanism by which RPS19 promotes this cleavage event is unknown. It has been proposed that RPS19 is required for recruitment of factors involved in the cleavage of the 3' end of 18S rRNA (Taylor et al. 2009). RPS19 is surface accessible in structures of the 40S subunit and located in proximity to the hypothesised position of the 3' end of pre-18S rRNA prior to cleavage (Rabl et al. 2011). The nuclease required for this cleavage has yet to be formally recognised. RCL1 has been proposed as this nuclease, but current data is conflicting (Horn et al. 2011; Tanaka et al. 2011). Nevertheless the role for RPS19 has been well demonstrated and given the positive effect of both AROS and SIRT1-Δ8 upon RPS19 protein abundance (*Chapter 6* and *Chapter 7*), the roles of these two proteins in RPS19 function are analysed and discussed below.

8.2.4 AROS and SIRT1-Δ8 in ribosome function

Any role for AROS in relation to the ribosome would be a novel observation. The possibility of a ribosomal association of AROS was first identified in *Chapter 4*, where a large proportion of AROS protein was seen to reside in the cytoplasm of both HCT116 and ARPE19 cells. The possibility of association also draws upon the

observation that AROS directly interacts with RPS19 in the mouse (Maeda et al. 2006), with the association of the two proteins also observed in *Chapter 7*.

In *Chapter 6* AROS was seen to promote RPS19 protein abundance. Thus it appears possible that AROS may influence the function of RPS19 via promoting its abundance. This could reveal a novel role for AROS in regulating the ribosome. Similarly, SIRT1-Δ8 promotes RPS19 abundance (see *Chapter 7*) revealing the possibility that SIRT1-Δ8 too has a role in regulating ribosome function. These possibilities form the analysis in this *Chapter*.

8.2.5 Hypotheses

1. AROS associates with the ribosome.
2. AROS promotes ribosome biogenesis via RPS19.
3. AROS promotes cancer cell survival by promoting ribosome biogenesis.
4. SIRT1-Δ8 has a role in ribosome biogenesis.

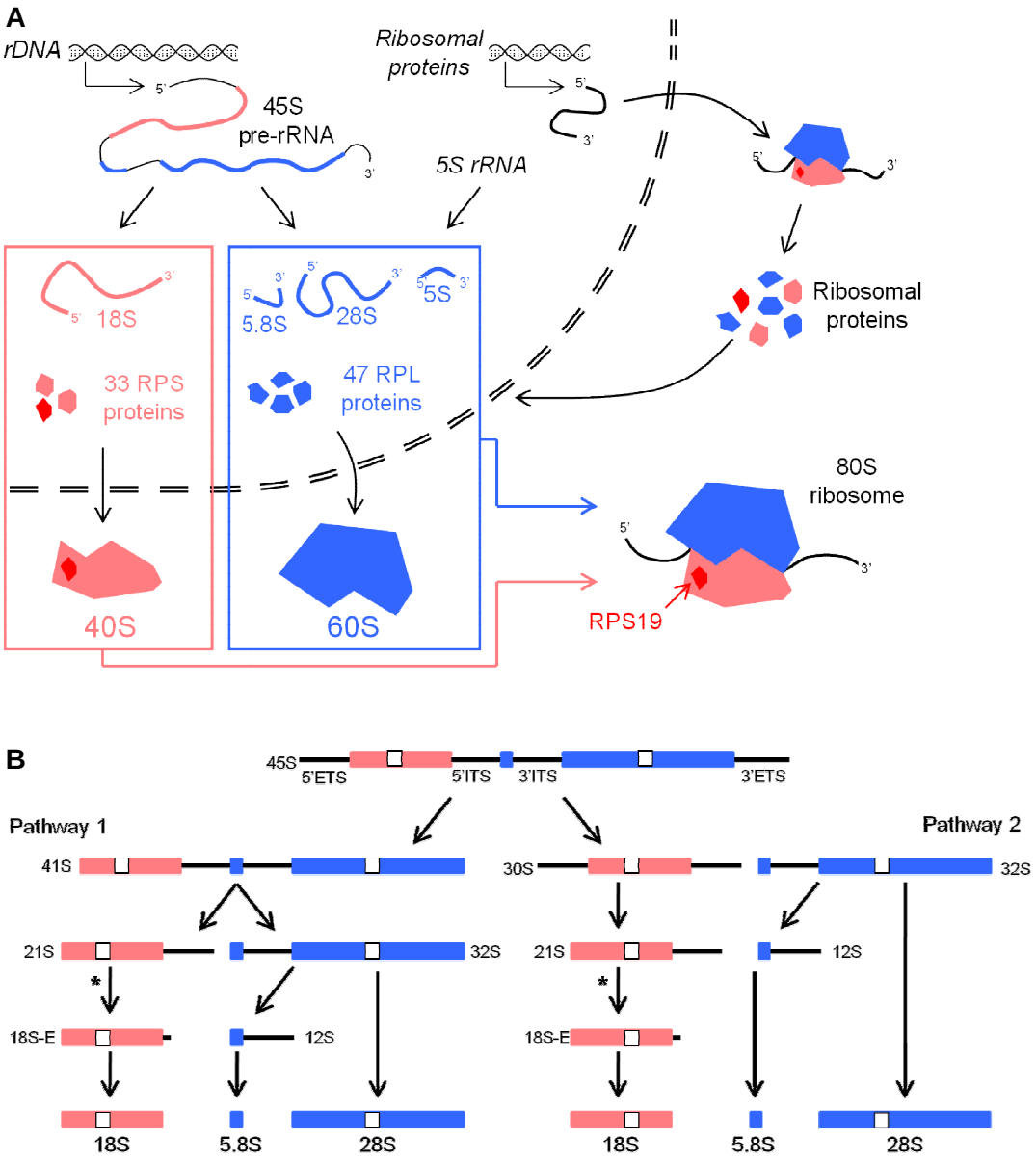

Figure 8.1: Schematics of ribosome biogenesis

(A) Ribosomal RNA is transcribed from rDNA into a precursor termed the 45S pre-rRNA. This is cleaved into 18S (small subunit) and 5.8S and 28S (both large subunit) rRNAs. 5S rRNA is produced independently and is required in the large subunit. Ribosomal protein genes are transcribed then translated into the 80 ribosomal proteins. Assembly of 40S small subunits and 60S large subunits is parallel and stoichiometric, due to early cleavage of 45S pre-rRNA. Subunits combine upon mRNA to form translating 80S ribosomes. **(B)** Human 45S pre-rRNA processing pathways by endonucleolytic cleavage. 45S pre-rRNA is shown annotated with internal (ITS) and external (ETS) transcribed spacers. Processing can occur via either of two pathways dependent on the order of cleavage events. The final products are identical. qRT-PCR amplicons for 18S and 28S rRNA precursors are indicated as white boxes. * = cleavage of pre-rRNA that requires RPS19.

8.3 *Association of AROS with ribosomes*

8.3.1 Ribosomal subunits and mature ribosomes

Quantification of RNA abundance through a sucrose density ultracentrifuge gradient of cytoplasmic lysate from cycling untreated HCT116 cells revealed distinct peaks for ribosomal subunits and the 80S ribosome (Figure 8.2A). This is a characteristic profile of ribosomal subunits and ribosomes seen in such experiments (for example see Choesmel et al. 2007). The 80S ribosome migrates furthest into the gradient due to its high relative density. Here 80S ribosomes penetrated into the 11th and 12th fractions taken from the gradient. Polysomes were not detected at high abundance in any sucrose density gradients and thus did not form part of the analysis. The 60S large ribosomal subunit is less dense, settling above the 80S ribosome, predominantly in fraction 9. Less dense again was the 40S small subunit, giving a peak in fractions 6 and 7. The RNA content in the higher fractions (lanes 5 and below) represents non-ribosome associated mRNAs, tRNAs and other miscellaneous small RNAs with lower density.

The distribution of these peaks was confirmed by analysis of ribosomal proteins from both the small and large ribosomal subunits by Western blotting (Figure 8.2B). Two 40S subunit proteins – RPS6 and RPS19 – were found in two distinct populations within the fractions of the gradient: lanes 6 to 8, representing free small ribosomal subunits; and lanes 11 to 13, representing 80S ribosomes. A large subunit protein, RPL3, was also found in lanes 11 to 13, consistent with these fractions representing the 80S ribosome. RPL3 protein in fractions 9 and 10 appears to represent free large ribosomal subunits, also given the absence of small ribosomal proteins from these fractions. RPL3 is known to form inter-subunit links in the eukaryotic ribosome (Ben-Shem et al. 2010), suggesting that RPL3 in lanes 5 to 7 represents an association with the small ribosomal subunit.

Application of antibodies against AROS and SIRT1 across these fractions revealed the potential for association of AROS with the ribosome, but no association of SIRT1 (Figure 8.2B). AROS was detected in a population in lanes 6 and 7, which represents the small ribosomal subunit (see above). This is consistent with the association between AROS and the small ribosomal subunit protein RPS19

identified in *Chapter 7* and the hypothesis that *'AROS associates with the ribosome'*. However, the detection of AROS in these lanes was weak, leaving this interpretation open to debate. AROS also appeared to associate with 80S ribosomes, with protein seen in fractions 11 to 13. AROS in fractions 14 and 15 may represent association with polysomes. SIRT1 protein was not found in any of the fractions analysed, suggestive of no interaction with either ribosomal subunit. This acts as a negative control protein within this analysis. This represents SIRT1-FL protein, SIRT1-Δ8 association with ribosomes was not analysed.

8.3.2 Ribosomal proteins

Immunoprecipitation of Flag-AROS allowed the interaction between AROS and ribosomal proteins to be assessed. This was carried out on the same samples shown in *Chapter 7 – Figure 7.5A*, where SIRT1-FL and SIRT1-Δ8 were overexpressed with Flag-AROS (Figure 8.3). The data are similar for overexpression of each splice variant, suggesting that their expression did not alter the association of AROS with other proteins.

Flag-AROS co-immunoprecipitated both endogenous RPS19 and RPS6 from the small ribosomal subunit (Figure 8.3). RPS19 and RPS6 reside on opposite sides of the 40S subunit, indicating that the interaction of AROS with both proteins may represent an interaction with the small subunit as a whole (Taylor et al. 2009; Ben-Shem et al. 2010; Rabl et al. 2011). This adds greatly to the hypothesis that *'AROS associates with the ribosome'*.

Interestingly, the Flag-AROS association with RPS19 represents a larger proportion of this ribosomal protein than the Flag-AROS interaction with RPS6. RPS19 and RPS6 are present in the 40S subunit in equal stoichiometric quantity. This could indicate that the AROS-RPS19 interaction is at least in part extra-ribosomal, due to the higher proportion of RPS19 that interacts compared to RPS6.

Flag-AROS also appeared to co-immunoprecipitate RPL3 from the large ribosomal subunit (Figure 8.3). This interaction represented a small but significant fraction of the total RPL3. This suggests that AROS associates with large ribosomal subunits, presumably in association with 40S subunits. This is supported by the

sucrose density ultracentrifuge analysis where AROS was found in fractions attributed to the 80S ribosome, but not 60S large ribosomal subunit (Figure 8.2). However, it is possible that RPL3 associates with small ribosomal subunits via its known location at the subunit interface, which may explain the AROS association with RPL3.

Taken together, the sucrose density ultracentrifuge and immunoprecipitation data suggest that *'AROS associates with the ribosome'*, specifically the small ribosomal subunit (Figure 8.4A). This appears to be specific to small subunits, with association not seen with the large ribosomal subunit (Figure 8.4B). Small ribosomal subunit association is presumably mediated by the direct interaction between AROS and RPS19 reported in the mouse (Maeda et al. 2006), and likely conserved in human (*Chapter 7* and Orru et al. 2007). The co-immunoprecipitation of 3 ribosomal proteins with Flag-AROS, from both the small and large subunits is suggestive of an association with the translating 80S ribosome (Figure 8.4C). An association with the small ribosomal subunit may also indicate a role in ribosome biogenesis. This was investigated using siRNA against AROS and analysing the effect on ribosomal proteins, rRNAs and ribosomal subunits.

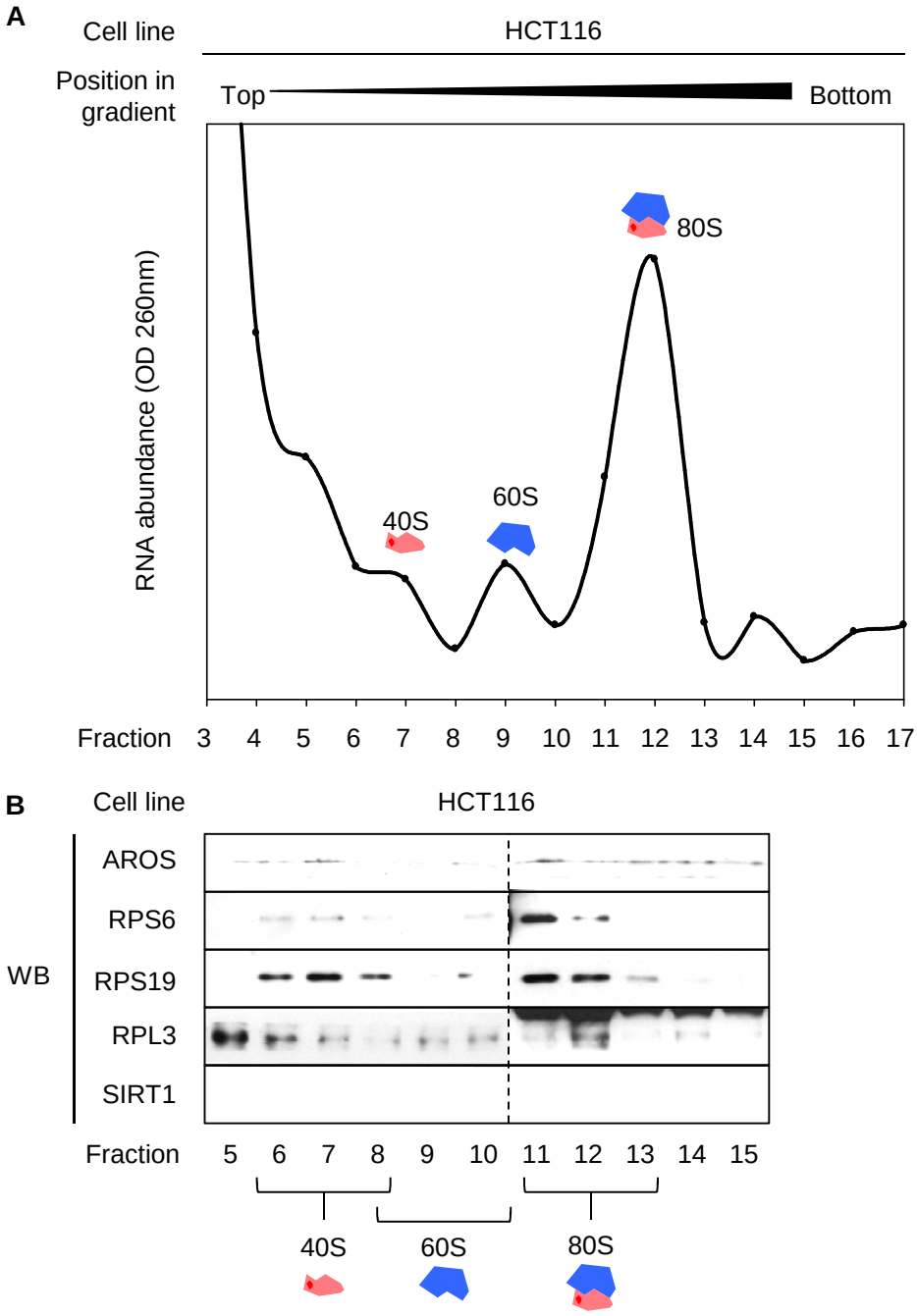

Figure 8.2: AROS associates with small ribosomal subunits and 80S ribosomes

(A) OD260nm analysis of ribosomal subunit rRNA from HCT116 cytoplasmic lysate. HCT116 cytoplasm was isolated and separated by sucrose density ultracentrifugation (see *Methods*). RNA content of subsequent fractions were analysed for RNA content by optical density (OD) at 260nm. Peaks corresponding to 40S and 60S subunits as well as the 80S ribosome are annotated. **(B)** SDS-PAGE separation and Western blotting analysis of fractions generated in (A). Fractions were loaded by equivalent volume. Samples were probed for ribosomal proteins, AROS and SIRT1 as indicated. SIRT1 protein was detected in a positive control sample included in the Western blot.

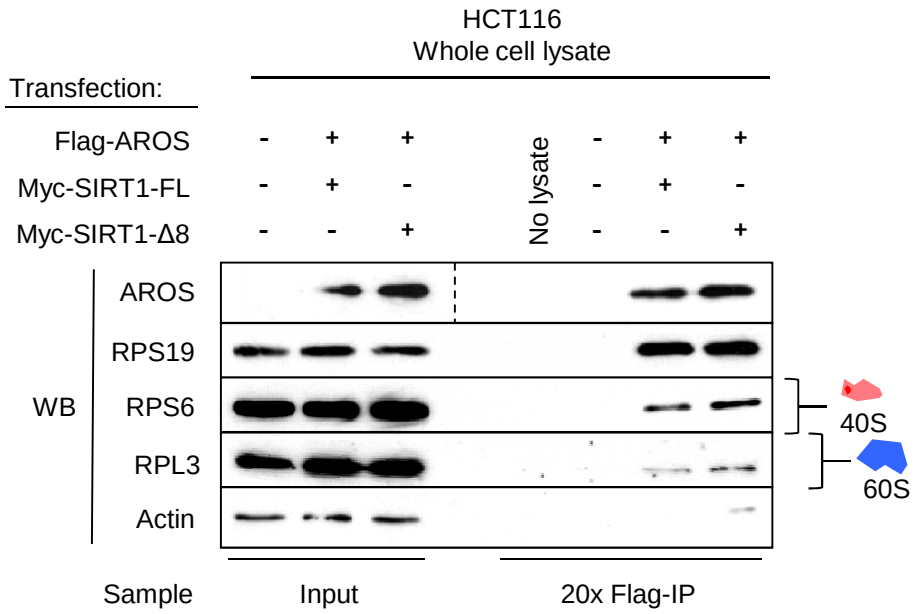

Figure 8.3: Flag-AROS co-immunoprecipitates ribosomal proteins

Analysis of ribosomal proteins that co-immunoprecipitate with Flag-AROS. HCT116 cells were transfected with pcDNA3 Flag-AROS, Myc-SIRT1-FL or Myc-SIRT1-Δ8 constructs as indicated. Flag-AROS was immunoprecipitated from whole cell lysates 24 hours after transfection by Flag-antibody conjugated to agarose beads. Elution was with excess Flag peptide. Samples were analysed by SDS-PAGE and Western blotting for indicated protein abundance. Data represents samples as analysed in Figure 7.5.

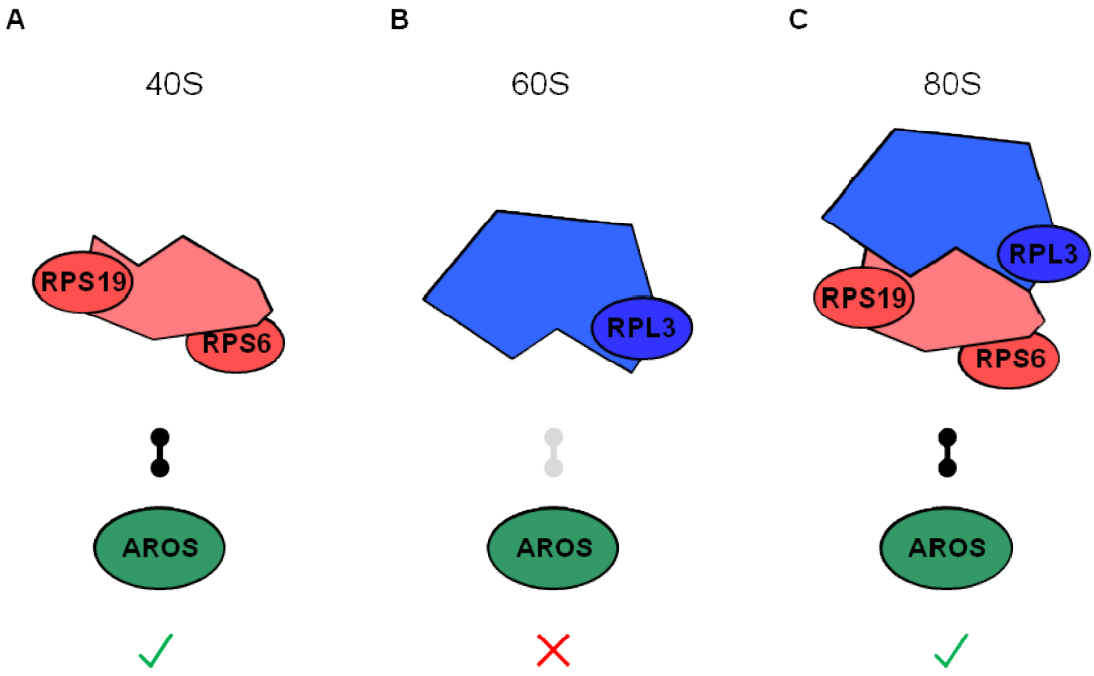

Figure 8.4: Schematic of AROS association with the ribosome

Schematics of the interactions of AROS with ribosomal subunits and ribosomal proteins. **(A)** AROS associates with free small ribosomal subunits. This potentially explains the association with RPS19 and RPS6, which reside on opposite sides of the small subunit. **(B)** AROS does not appear to associate with free large subunits, indicated by grey bar. **(C)** AROS does associate with 80S ribosomes, comprising of small and large subunits. This may explain the association with RPL3 protein, which is a component of the large subunit.

8.4 *AROS and ribosome biogenesis in cancer cells*

8.4.1 AROS and ribosomal proteins

AROS promotes the abundance of RPS19 protein in an autoregulatory loop (see *Chapter 6*). This effect is again observed here in the HCT116 and MCF7 cells lines (Figure 8.5A). Loss of p53 negates the effect AROS has upon RPS19, reported in *Chapter 6* and shown again here (Figure 8.5A). To expand this analysis the effect of AROS silencing on two further ribosomal proteins was analysed – RPS6 from the small subunit and RPL3 from the large subunit – in parallel to RPS19 silencing.

Silencing of RPS19 resulted in depletion of RPS6 protein in all 3 human cancer cell lines analysed – the HCT116, HCT116 $p53^{-/-}$ and MCF7 lines (Figure 8.5A). RPS19 had no effect on RPL3 protein expression in the HCT116 and HCT116 $p53^{-/-}$ cell lines, with a slight reduction seen in the MCF7 cell line. This is largely consistent with a small ribosomal subunit specific effect following RPS19 silencing.

Parallel silencing of AROS decreased the abundance of RPS6 protein compared to Mock treatment in the HCT116 and MCF7 cell lines (Figure 8.5A). This occurred to a similar extent as the reduction in RPS6 seen following RPS19 silencing in the HCT116 cell line (both giving RPS6:Actin ratio of 0.8), but to a lesser extent in the MCF7 cell line. In the HCT116 $p53^{-/-}$ cell line RPS6 protein was not greatly depleted compared to Mock treatment. This correlates with the lack of RPS19 depletion following AROS silencing in this p53 null cell line. As such, it appears that loss of RPS6 protein correlates with depletion of RPS19, either following RPS19 siRNA treatment or loss of RPS19 associated with knock down of AROS. RPL3 protein abundance did not appear to be affected following RNAi against AROS in all cancer 3 cell lines. This is consistent with a small ribosomal subunit specific effect role for AROS, and is the first indication that *'AROS promotes ribosome biogenesis via RPS19'*.

8.4.2 AROS and ribosomal RNAs

Ribosomes comprise of both protein and RNA, and it is the RNA element that performs the key catalytic and regulatory functions to ensure rapid translation with high fidelity. Transcription of the 18S and 28S ribosomal RNAs occurs in tandem from ribosomal DNA genes, producing stoichiometric biogenesis pathways yielding the 40S and 60S subunits (see *Introduction* and Hadjiolova et al. 1993). Thus, factors effecting the transcription of rRNA affect the abundance of both 18S and 28S forms, whereas factors specifically effecting one rRNA may have a role in the synthesis of the relevant ribosomal subunit. A specific effect of RPS19 on 18S, 40S subunit, rRNA has previously been reported (Choesmel et al. 2007; Flygare et al. 2007; Idol et al. 2007).

To analyse the role of AROS and RPS19 in regulating rRNA abundance, amplicons specific to regions within the 18S and 28S mature rRNAs were designed, as indicated schematically in Figure 8.1. These were used on isolated nuclear RNA, such that the amplicons amplified regions from the nuclear precursors of each mature rRNA, as shown in Figure 8.1. The analysis was restricted to the nuclear fraction because this is the site of ribosome synthesis, with rRNA in this fraction likely to alter the greatest should modulation of ribosome biogenesis occur. Analysis of nuclear rRNAs also removes the effect of pre-existing ribosomes in the cytoplasm, which may dilute the effects in the nucleus.

Consistent with a role in small subunit synthesis, silencing of RPS19 resulted in a specific reduction in the 18S rRNA amplicon within nuclei of HCT116 and HCT116 $p53^{-/-}$ cells (Figure 8.5B). Nuclear 40S subunit RNA content is reduced to below 60% of control cells in both cases. In contrast no alteration in the abundance of 28S rRNA from the large ribosomal subunit was observed. This is consistent with a specific role for RPS19 in small ribosomal subunit synthesis (Choesmel et al. 2007; Flygare et al. 2007; Idol et al. 2007), and the data for ribosomal protein abundance following RPS19 silencing (Figure 8.5A).

Silencing of AROS resulted in a reduction in the 18S rRNA amplicon in the HCT116 cell line (Figure 8.5B). The reduction was comparable to that seen

following silencing of RPS19, and is consistent with the reduction in RPS19 protein following AROS knock down (Figure 8.5A). 28S rRNA from the large subunit did not appear to be affected by silencing of AROS, with abundance similar to that of Mock treated cells. As such, it appears that AROS promotion of RPS19 protein abundance correlates with potential AROS promotion of RPS19 function in maintaining nuclear small ribosomal subunit rRNA levels. As such, this supports the hypothesis that *'AROS promotes ribosome biogenesis via RPS19'*. However, it is equally possible that AROS regulates ribosome biogenesis and RPS19 simultaneously, given the crucial role of RPS19 in ribosome biogenesis.

Maintenance of RPS19 protein abundance following silencing of AROS in the HCT116 $p53^{-/-}$ cell line correlated with no effect on small ribosomal subunit rRNA (Figure 8.5A and B). Silencing of AROS in the HCT116 $p53^{-/-}$ cell line did not affect nuclear 18S or 28S rRNA abundance compared to Mock treatment. This suggests that the effect AROS has upon ribosomal proteins and rRNA are linked – reduction in ribosomal protein correlates with reduction in rRNA. This is further evidence that the presence of p53 is important for AROS in the regulation of RPS19, and also suggests a role for p53 in the regulation of ribosome biogenesis.

It appears that AROS affects RPS19 abundance as well as the stability of other small ribosomal subunit proteins (RPS6) and 18S rRNA precursors. This may occur by a number of mechanisms; AROS may regulate extra-ribosomal RPS19, which in turn regulates small ribosomal subunit component abundance, or AROS may directly regulate the small ribosomal subunit, presumably via its direct interaction with RPS19 (Maeda et al. 2006). The association of AROS with small ribosomal subunits and 80S ribosomes is perhaps suggestive of the latter possibility (Figure 8.2B).

8.4.3 AROS and ribosomal subunits

Given the effect of AROS and RPS19 silencing on ribosomal proteins and RNA in the HCT116 colorectal adenocarcinoma cell line, the effect this has upon cytoplasmic subunits and mature ribosomes was analysed by sucrose density

ultracentrifugation. RPS19 is known to specifically affect small ribosomal subunits in this context and was thus used as a positive control.

Analysis of isolated cytoplasm from Mock treated cells in parallel to RPS19 silencing revealed OD260nm peaks for 40S subunits, 60S subunit and 80S ribosomes as annotated (Figure 8.6A). Following silencing of RPS19 the 40S peak appeared to be reduced compared to Mock treatment, indicative of a reduction in the abundance of synthesised 40S subunits. There was little effect on the abundance of 60S subunits, consistent with RPS19 specifically effecting the small ribosomal subunit. 80S ribosomes consist of 40S and 60S subunits, with a reduction in 40S subunits likely to result in reduced 80S ribosome abundance. Thus the reduction in 40S subunits following RPS19 silencing correlated with a reduction in 80S ribosomes compared to Mock treatment (Figure 8.6A).

Silencing of AROS was carried out in a separate analysis in HCT116 cells. Variation was evident in the OD260nm profile of the Mock treatment between experiments (Figure 8.6A compared to B). 80S ribosomes gave a distinct peak, as did the 60S ribosomal subunit. However, instead of a peak for the 40S subunits, a shoulder from the descending smaller RNA species curve was present. This variation could be attributable to any number of experimental factors (effectiveness of cycloheximide treatment, total cell number for example, formation of sucrose gradient), and stresses the point to compare within individual experiments only.

To this end, AROS silencing compared to the Mock treatment in Figure 8.6B resulted in loss of the 40S subunit shoulder and a slight reduction in the 60S subunit peak (Figure 8.6B). This suggests that AROS, like RPS19, is required for small subunit abundance, consistent with the specific effects on ribosomal proteins and rRNAs outlined in Figure 8.5. The data are consistent with the hypothesis that *'AROS promotes ribosome biogenesis via RPS19'*. There was also a reduction in the 80S ribosome peak following AROS silencing, which was almost completely lost. This indicates that AROS promotes the production of translation competent ribosomes, and indicates a role for AROS in translational control by provision of ribosomes. This is summarised in Figure 8.6C, with the novel AROS-RPS19

regulatory loop effecting 40S subunit and 80S ribosomes, but not influencing 60S subunits.

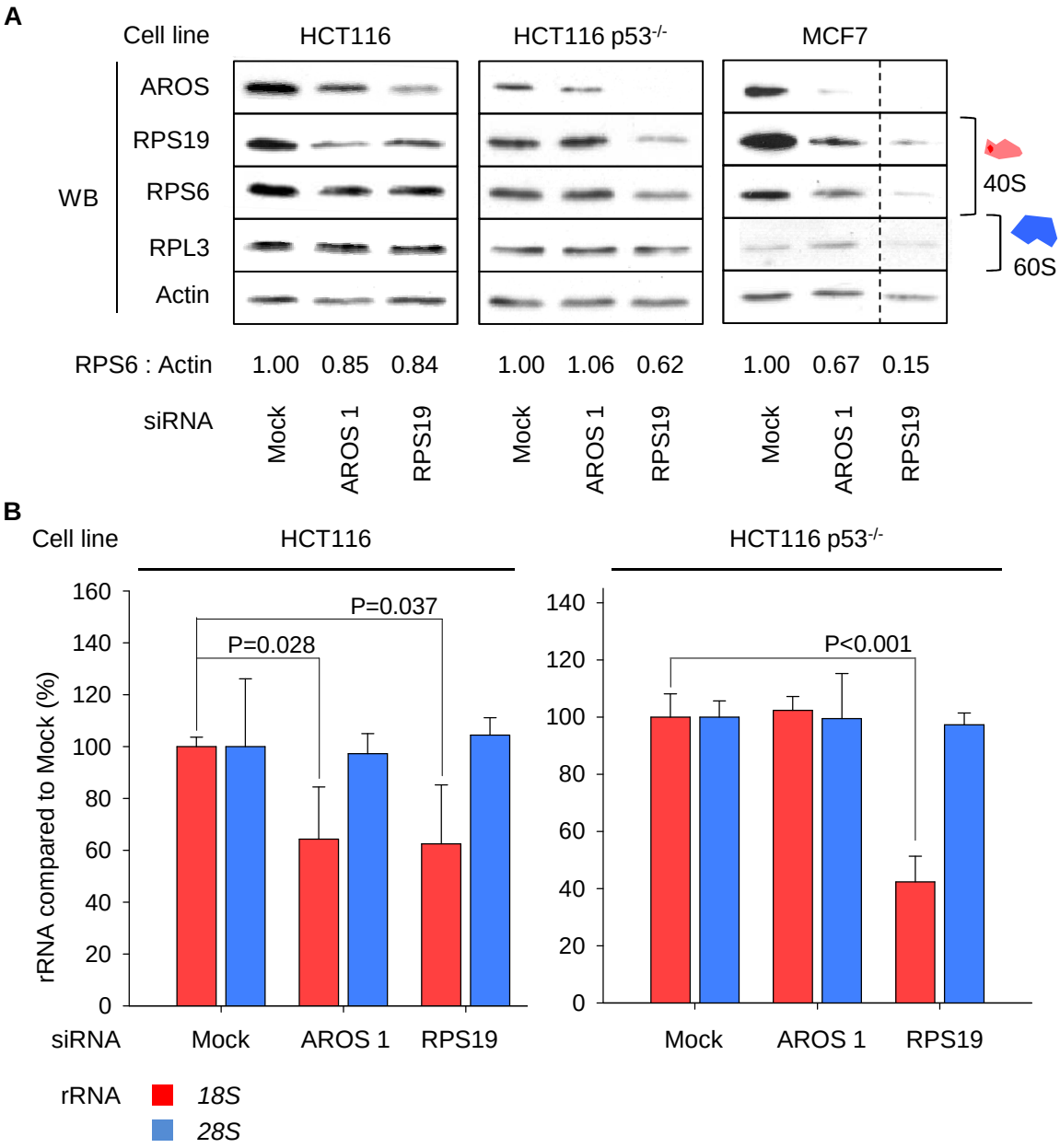

Figure 8.5: The effect of RPS19 and AROS on component ribosome abundance

(A) Analysis of ribosomal protein abundance following RNAi against *AROS* or *RPS19*. HCT116 and MCF7 cancer cells were harvested 48 hours after siRNA transfection – HCT116 p53$^{-/-}$ at 72 hours. Total cell protein was separated by SDS-PAGE, loaded by equivalent mass, and protein abundance determined by Western blotting. The 'RPS6:Actin' ratio was calculated using Quantity One densitometry as the change in RPS6 abundance compared to Mock treatment standardised against Actin expression. **(B)** Expression of nuclear pre-ribosomal RNA, quantified by qRT-PCR. HCT116 and HCT116 p53$^{-/-}$ cells were transfected as in (A) then nuclear RNA was isolated and analysed for 18S and 28S rRNA qRT-PCR amplicon abundance.

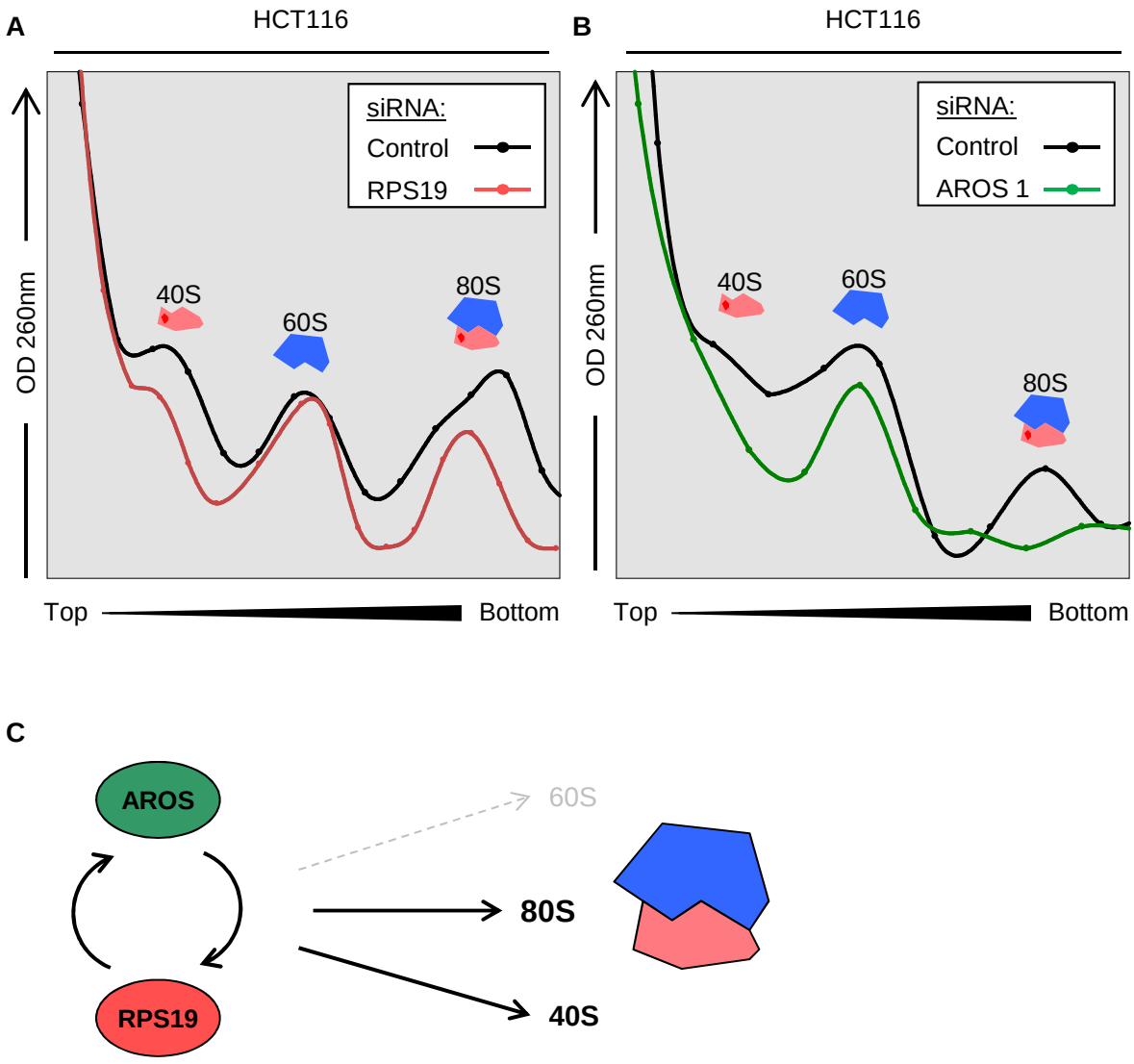

Figure 8.6: The effect of RPS19 and AROS silencing on 40S subunit and 80S ribosome abundance

(A) Aligned OD260nm analysis of HCT116 cytoplasmic lysates from Mock and RPS19 siRNA treatment. HCT116 cytoplasm was isolated and separated by sucrose density ultracentrifugation. Subsequent fractions were analysed for RNA content by reading OD at 260nm. **(B)** Data as for (A), following AROS siRNA 1 transfection. **(C)** Schematic representation of the AROS-RPS19 relationship and its regulation of small ribosomal subunits and mature ribosomes. The black arrows indicate promotion of 40S and 80S abundance. The dashed grey arrow indicates no apparent effect on 60S subunits.

8.5 *AROS and ribosome biogenesis in non-cancer cells*

AROS and RPS19 form an autoregulatory loop in both cancer and non-cancer cell lines (*Chapter 6*). Despite this, AROS is specifically required for cancer but not non-cancer cell survival (*Chapter 5*). In this *Chapter* AROS appears to affect RPS19 function in promoting ribosome abundance in cancer cells. Thus, the question arises over whether AROS regulation of ribosome biogenesis is specific to cancer cells. It is possible that AROS is not required for ribosome abundance in non-cancer cells, which may explain its cancer specificity for cell survival. Alternatively, AROS may regulate ribosomes in both cancer and non-cancer cells, but this may only promote cell viability in cancer cells. It is also possible that AROS does not promote cancer cell survival via the ribosome. This was investigated using the ARPE19 cell line as a model non-cancer cell line.

8.5.1 AROS and ribosomal proteins

Firstly, ribosomal protein abundance was analysed in the ARPE19 retinal epithelial cell line. Silencing of AROS did not appear to effect RPS6 protein expression, perhaps suggestive of a cancer specific function of AROS (Figure 8.7A). Surprisingly, RPL3 abundance may have been depleted by AROS silencing in the ARPE19 cell line, which is in contrast to the small ribosomal subunit specific effects seen in cancer cell lines (Figure 8.5A). However, AROS does effect RPS19 protein abundance (Figure 8.7A), indicative of a consistent effect towards the small subunit.

8.5.2 AROS and ribosomal RNAs

ARPE19 nuclear rRNA abundance was analysed using the 18S and 28S rRNA amplicons following AROS silencing. A significant reduction in the 18S amplicon was observed following AROS silencing (Figure 8.7B), indicating that AROS promotes the abundance 18S rRNA precursors. This is similar to the role of AROS in HCT116 cancer cells (Figure 8.5B). Unlike in the HCT116 cell line, the abundance of the 28S amplicon was significantly increased following AROS silencing in the ARPE19 line (Figure 8.7B). This may suggest that AROS suppresses the abundance of nuclear 28S rRNA forms, presumably at the post-transcriptional level. The mechanism behind this is unclear. However, the data *do* suggest that

AROS specifically promotes 18S rRNA precursor abundance in the ARPE19 and HCT116 cell lines (Figure 8.7B and Figure 8.5B). These data may contradict the hypothesis that *'AROS promotes cancer cell survival by promoting ribosome biogenesis'*.

8.5.3 AROS and ribosomal subunits

The analysis of HCT116 cancer cells correlated a reduction in small ribosomal subunit protein and RNA with a reduction in synthesised small subunits following AROS silencing (Figure 8.5 and Figure 8.6). Consistent with a conserved role of AROS across cell lines, in the ARPE19 non-cancer cell line the abundance of small ribosomal subunits was reduced following AROS silencing (Figure 8.7C). The 40S peak in OD260nm analysis was smaller following AROS silencing compared to parallel Mock treatment. This indicates that the role for AROS in ribosome biogenesis is not cancer specific.

In contrast the 60S peak appeared markedly increased following AROS silencing (Figure 8.7C). This is consistent with a role for AROS in specifically promoting small subunit over large subunit abundance, and parallels the modulation of nuclear rRNA levels following AROS silencing (Figure 8.7B). Furthermore, this suggests that AROS suppresses 60S subunit biogenesis. However, the increase in 60S subunits could be attributable to release of these from 80S ribosomes following the loss of small ribosomal subunits.

In agreement with this possibility AROS silencing resulted in a decrease in 80S ribosomes compared to Mock treatment. The 80S peak in the Mock treated sample was almost completely lost following AROS silencing (Figure 8.7C). This is again similar to the result seen in the HCT116 cancer cell line, which together suggests that AROS has a conserved role in maintaining 40S subunit and 80S ribosome abundance. The hypothesis that *'AROS promotes cancer cell survival by promoting ribosome biogenesis'* requires consideration as a result (see *Discussion*).

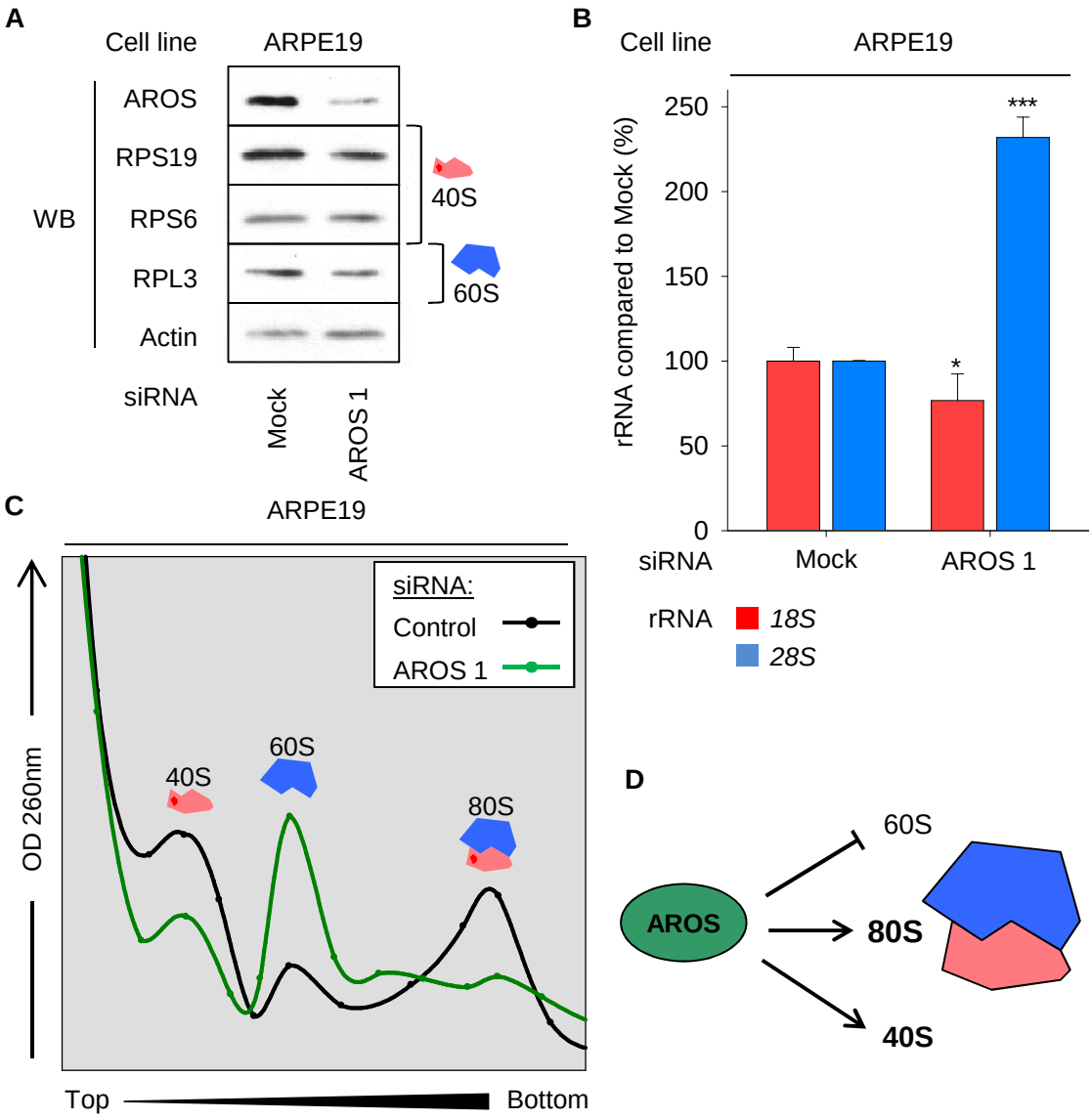

Figure 8.7: The role of AROS for small subunit and 80S ribosome abundance in non-cancer cells

(A) Expression of ribosomal proteins following silencing of AROS. ARPE19 cells were treated with AROS siRNA 1 then harvested 72 hours later. Total protein was loaded on SDS-PAGE according to equivalent mass and analysed by western blotting. Actin is used as a loading control. **(B)** Relative expression of nuclear pre-ribosomal RNAs, quantified by qRT-PCR. ARPE19 cells were transfected 72 hours prior to isolation of nuclear RNA (see *Methods*) analysed for abundance of PCR amplicons within the 18S and 28S rRNAs. *** P<0.001, * P<0.05. **(C)** Aligned OD260nm analysis of ARPE19 cytoplasmic lysates from Mock and AROS siRNA 1 treatment. ARPE19 cytoplasm was isolated and separated by sucrose density ultracentrifugation and subsequent fractions analysed for RNA content by reading optical density at 260nm. **(D)** Schematic of the effect of AROS on small (positive) and large (potentially negative) ribosomal subunits and 80S ribosomes.

8.6 *SIRT1-Δ8 and ribosome biogenesis*

The recently identified splice variant of the *SIRT1* gene, SIRT1-Δ8 appears to promote RPS19 abundance (*Chapter 7*). This potentially occurs via interaction between RPS19 and SIRT1-Δ8, as the two proteins were also seen to specifically associate in *Chapter 7*. Thus, with the role of RPS19 in ribosome biogenesis well characterised the possibility that SIRT1-Δ8 promotes ribosome biogenesis via RPS19 was explored in HCT116 cancer cells.

8.6.1 Ribosomal proteins and RNAs

The abundances of RPS6 and RPL3 were analysed following silencing of SIRT1-Δ8 in the HCT116 cell line. Levels of both proteins, which represent the 40S and 60S subunits respectively, were not reduced following SIRT1-Δ8 knockdown (Figure 8.8A). This is in contrast to silencing of RPS19 in the same cell line, after which levels of RPS6 were specifically reduced compared to RPL3 (Figure 8.5A). This may suggest that the reduction in RPS19 following silencing of SIRT1-Δ8 is distinct from reduction of RPS19 targeting by siRNA. Surprisingly the levels of RPL3 may have increased as a result of SIRT1-Δ8 silencing, while the abundance of RPS6 is entirely unchanged (Figure 8.8A).

This is in contrast to the effect of silencing SIRT1-Δ8 on the nuclear abundance of the rRNA amplicons. SIRT1-Δ8 knockdown resulted in a reduction in both 18S and 28S rRNA, to less than 50% of Mock treated samples (Figure 8.8B). This suggests that SIRT1-Δ8 is involved in either the transcription of rRNA from rDNA or the processing and biogenesis of *both* ribosomal subunits, and is an indication that *'SIRT1-Δ8 has a role in ribosome biogenesis'*. The maintenance of RPS6 and RPL3 proteins following SIRT1-Δ8 knockdown could suggests that regulation of rRNA transcription is more likely. However, the effect of SIRT1-Δ8 upon RPS19 protein remains, suggesting that SIRT1-Δ8 does affect post-transcriptional components of ribosome biogenesis.

8.6.2 Ribosomal subunits and mature ribosomes

The effect of SIRT1-Δ8 silencing on both small and large subunit rRNA suggests a role in ribosome biogenesis. Thus, the effect of SIRT1-Δ8 on ribosome subunit and mature ribosome abundance was analysed by sucrose density ultracentrifugation. As previously, Mock treatment produced distinct peaks for 40S and 60S ribosome subunits and a peak for the 80S translating ribosome (Figure 8.8C). Silencing of SIRT1-Δ8 reduced the abundance of both 40S and 60S subunits below the levels in Mock treatment. There was an almost complete loss of free 40S and 60S ribosomal subunits following silencing of SIRT1-Δ8. This is in agreement with the hypothesis that *'SIRT1-Δ8 has a role in ribosome biogenesis'*.

Interestingly silencing of SIRT1-Δ8 did not result in a large reduction in the abundance of 80S ribosomes compared to Mock (Figure 8.8C). There appeared to be a similar quantity of 80S ribosomes, despite the apparent reduction in abundance of both subunits. The specific effect of SIRT1-Δ8 knockdown on ribosomal subunits but not the translating ribosome is depicted in Figure 8.8D.

The loss of both ribosomal subunits appears to correlate with the loss of both rRNAs following SIRT1-Δ8 silencing (Figure 8.8B). Reduced ribosomal RNA availability may contribute to the loss of ribosomal subunits. Interestingly, this may be independent from ribosomal protein availability, which was not negatively affected by SIRT1-Δ8 siRNA. Together this appears to support the hypothesis that *'SIRT1-Δ8 has a role in ribosome biogenesis'* and suggest that SIRT1-Δ8 contributes to the transcription of rRNA at the beginning of the process.

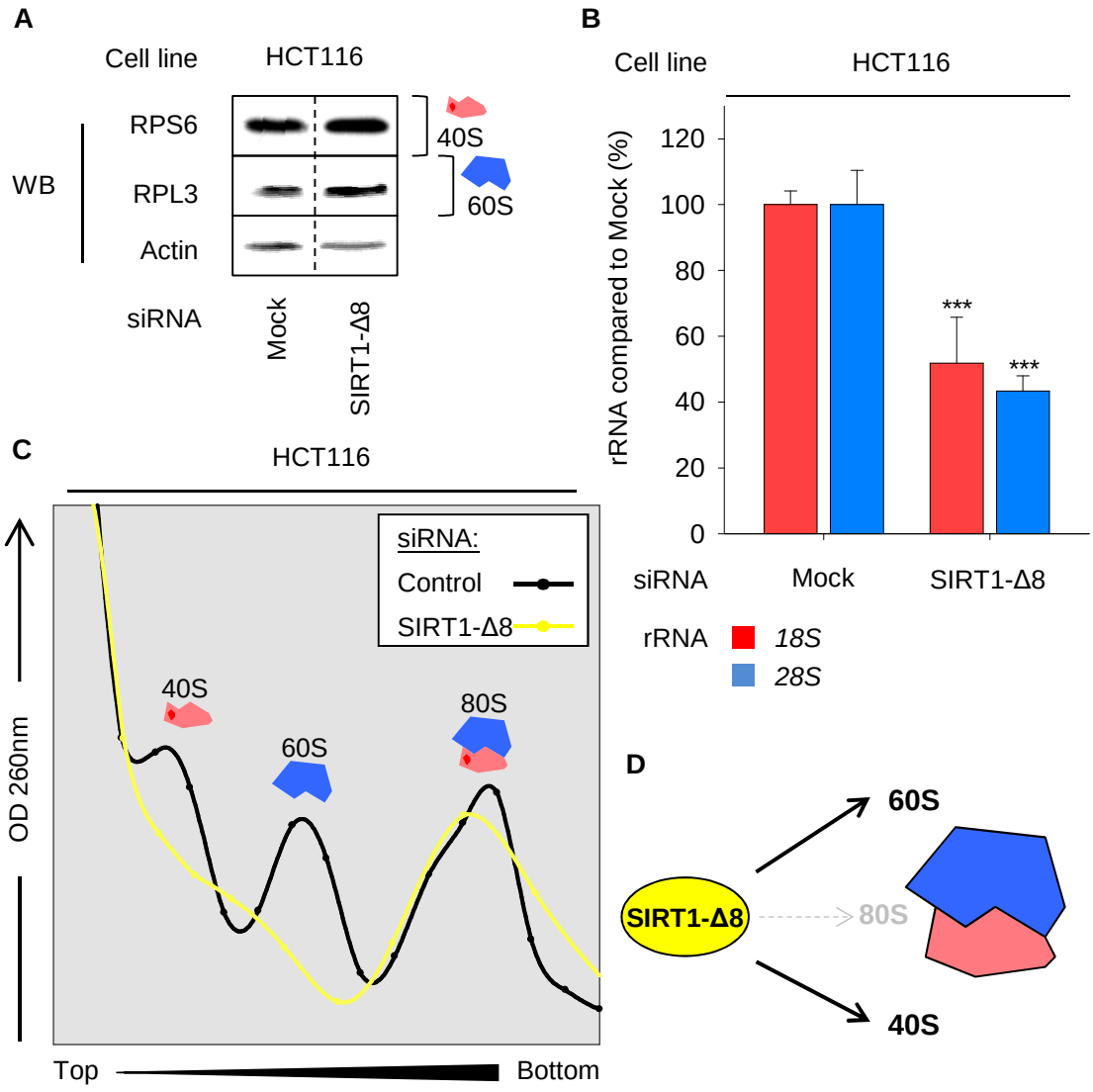

Figure 8.8: SIRT1-Δ8 may have a role in maintaining ribosome subunit abundance

(A) Ribosomal protein abundance following SIRT1-Δ8 siRNA treatment in the HCT116 cancer cell line. Cells were treated with siRNA then harvester 48 hours later. Total protein was analysed by SDS-PAGE and specific antibody Western blotting. Actin was used as a loading control. **(B)** Relative expression of pre-18S and pre-28S ribosomal RNAs in isolated nuclear fractions, quantified by qRT-PCR. HCT116 cells were transfected 48 hours prior to isolation of nuclear RNA (see *Methods*) and analysed for abundance of PCR amplicons within the 18S and 28S rRNAs. *** P<0.001. **(C)** Aligned OD260nm analysis of HCT116 cytoplasmic lysates from Mock and SIRT1-Δ8 treatment. HCT116 cytoplasm was isolated and separated by sucrose density ultracentrifugation with isolated fractions analysed for RNA content by reading optical density at 260nm. **(D)** Schematic of the regulation of small and large ribosomal subunits by SIRT1-Δ8 in HCT116 cancer cells. Black arrows indicate promotion of 40S and 60S abundance. Dashed grey arrow represents no apparent effect on 80S ribosomes.

8.7 *Discussion*

8.7.1 AROS in ribosome biogenesis

The data here reveal that AROS promotes ribosome biogenesis in both HCT116 cancer and ARPE19 non-cancer cells. This suggests a conserved role for AROS during the ubiquitous process of ribosome synthesis. The role of AROS appears similar to the role of RPS19. Taken together with the autoregulatory loop between AROS and RPS19 reported in *Chapter 6*, this is highly suggestive that AROS promotes ribosome biogenesis via RPS19. This could occur via direct promotion of ribosome biogenesis via the association of AROS with RPS19 and ribosomes (see discussion below) or via extra-ribosomal association of AROS and RPS19, which in turn promotes ribosome biogenesis. The association of AROS with the ribosome reported in this *Chapter* and the localisation of AROS to nucleoli, the site of ribosome biogenesis (Maeda et al. 2006; Kim et al. 2007), support the former option. However, as stated previously, the regulation of RPS19 and ribosome biogenesis by AROS could be synchronous. It is difficult to interpret whether AROS regulation of RPS19 impacts on ribosome biogenesis, or vice versa, as negative effects on either RPS19 or ribosome biogenesis will likely result in the effects seen on the opposite. Perhaps most likely is a co-regulation of RPS19 and ribosome biogenesis by AROS, given the intrinsic link between the two.

Interestingly, p53 is important for the regulation of RPS19 and ribosome biogenesis by AROS (*This Chapter and Chapter 6*). In the absence of p53 AROS does not promote RPS19 protein abundance or ribosome biogenesis. Thus the role of p53 appears to be suppression of RPS19 protein abundance following knockdown of AROS. As such, p53 appears to support the role of AROS in promoting RPS19 abundance and ribosome biogenesis. p53 may have a defined role in the process, but this cannot be essential as p53 null cells are able to synthesise ribosomes.

AROS is able to suppress activation of p53 via promoting its deacetylation by SIRT1 (*Chapter 4* and Kim et al. 2007). Thus with AROS able to suppress p53 and p53 appearing to suppress RPS19 following AROS knockdown, this creates a putative mechanism whereby AROS promotes RPS19 protein abundance (Figure 8.9). In turn, maintenance of RPS19 protein abundance would allow AROS to

promote 40S ribosomal subunit biogenesis. p53 is known to localise to the nucleoli, which does not rule out the possibility that this regulation occurs during ribosome biogenesis (Rubbi and Milner 2000). This putative mechanism would also require the deacetylase activity of SIRT1 to suppress p53. SIRT1-Δ8 also appeared to have a role in ribosome biogenesis (discussed below) and is known to deacetylate p53. Thus the suppression of p53 supported by AROS may involve SIRT1-Δ8.

8.7.2 SIRT1-Δ8 in ribosome biogenesis

SIRT1-Δ8 silencing had a similar effect on 40S subunits as silencing of either AROS or RPS19. This is consistent with SIRT1-Δ8 playing a part in the regulation of RPS19 and subsequently ribosome biogenesis. Preliminary analysis of SIRT1-FL in relation to ribosome biogenesis did not indicate a role for the protein, indicating that the effect of SIRT1-Δ8 is specific for this isoform of the gene. SIRT1-Δ8 subcellular localisation is similar to that of SIRT1-FL, which is known to localise to the cytoplasm, nucleus and nucleolus (Tanno et al. 2007; Murayama et al. 2008; Lynch et al. 2010). Thus, SIRT1-Δ8 may be able to directly participate in ribosome biogenesis in the nucleolus and across the cell.

SIRT1-FL protein regulates ribosomal RNA transcription in response to cellular energy status (Murayama et al. 2008). SIRT1 senses energy status via its requirement for NAD^+ and is able to silence rDNA transcription via methylation in complex with an epigenetic silencing complex. NAD^+ levels are inversely proportional to glucose availability, promoting SIRT1 to suppress rDNA transcription during low nutrient availability. Whether SIRT1-Δ8 can also perform this function is unknown. SIRT1-Δ8 appears to regulate synthesis of both small and large ribosomal subunit rRNA, suggesting an early role in ribosome biogenesis, such as during transcription (Figure 8.8). However, SIRT1-FL has a suppressive effect on rRNA synthesis, in contrast to the positive effect seen for SIRT1-Δ8. One possibility is that silencing of SIRT1-Δ8 removes its use of NAD^+ as a co-substrate, thus increasing NAD^+ availability to promote SIRT1-FL function. This could result in the silencing of rDNA and reduction in rRNA observed following SIRT1-Δ8 knockdown.

The apparent maintenance of 80S ribosomes despite the loss of 40S and 60S subunits suggests that SIRT1-Δ8 has a more direct role in translation than the provision of ribosomal subunits. Thus, it appears that SIRT1-Δ8 suppresses the formation of 80S ribosomes from 40S and 60S subunits. This is based on the observation that following SIRT1-Δ8 silencing a higher proportion of the 40S and 60S subunits formed 80S ribosomes than were present as individual free subunits (Figure 8.8C). How this may occur is entirely unknown, but would suggest an association between SIRT1-Δ8 and ribosomal subunits.

8.7.3 Association of AROS with ribosomes

AROS appears to associate specifically with 40S ribosomal subunits over 60S subunits (Figure 8.2B), supporting the hypothesis that *'AROS associates with the ribosome'*. This interaction is supported by immunoprecipitation data indicating that AROS associates with both RPS19 and RPS6 from the small subunit (Figure 8.3). These two ribosomal proteins reside on opposite faces of the eukaryotic 40S subunit, suggesting that AROS interacts with the subunit as a whole (Taylor et al. 2009; Ben-Shem et al. 2010; Rabl et al. 2011). Of course, there is the possibility that AROS interacts with both RPS19 and RPS6 independently of the ribosome. However, given the sucrose density gradient analysis, association with 40S subunits seems the better explanation of these ribosomal protein associations.

This association is likely to occur via the direct interaction between AROS and RPS19 (Maeda et al. 2006). RPS19 protein resides in the head region of the eukaryotic ribosome, and is believed to act as a binding site for specific factors during ribosome biogenesis (Taylor et al. 2009; Rabl et al. 2011). The location of RPS19 is thus amenable to binding of extra-ribosomal factors, especially factors as small as AROS, which is only 15.4kDa in size. This *Chapter* has identified a putative role for AROS during the biogenesis of 40S subunits. However, AROS associates with mature 40S subunits, potentially contradicting a role as a ribosome biogenesis factor. These are usually recycled after use to permit further biogenesis, and thus do not remain associated with the 40S subunit (Kressler et al. 2010).

AROS also associated with RPL3 from the large subunit (Figure 8.3). This may suggest an association with the 60S subunit as a whole. However, the sucrose density gradient data do not correlate with this (Figure 8.2A). AROS does appear to associate with 80S ribosomes, which contain both small and large subunits. Thus, this association is likely to explain the association with RPL3 (Figure 8.4C). This provides compelling evidence that AROS not only associates with the mature 40S subunits, but also the translation competent 80S ribosome. This lends further support to a role of AROS beyond ribosome biogenesis.

The association with 80S ribosomes may suggest a role in translation beyond the provision of 40S ribosomal subunits. How and why this occurs falls beyond the remit of this work. It is easy to speculate an association between SIRT1-Δ8 and the ribosome, given the association observed between RPS19 and SIRT1-Δ8 in *Chapter 7*. SIRT1-FL was not detected in the sucrose density gradient, suggesting that any association would be specific for SIRT1-Δ8. Should SIRT1-Δ8 associate with the ribosome, AROS may be an important mediator in the interaction. These themes allow scope for future work into a putative role for the *SIRT1* gene during ribosome biogenesis and possibly translation.

8.7.4 Ribosome biogenesis and cell fate

Loss of ribosomal subunits and 80S ribosomes is likely to have an impact at the cellular level. Reduced 80S ribosome abundance seen in HCT116 cancer cells following silencing of RPS19 or AROS likely correlates with a reduction in active translation, and concomitant reduction in overall protein production. Consistent with this effecting cell fate, silencing of either RPS19 or AROS resulted in apoptosis in the HCT116 cancer cell line (*Chapter 6 – Figure 6.4*). However, silencing of each factor also resulted in activation of tumour suppressors, which may contribute to this apoptosis.

In the non-cancer ARPE19 cell line AROS is not required for cell survival (*Chapter 5*), but does appear to be required for 40S subunit biogenesis (Figure 8.7). Thus, AROS affects ribosome biogenesis in a variety of cell types. This also appears

to contradict the theory that AROS promotes cancer cell survival via promoting ribosome biogenesis.

However, it is possible that AROS promotion of ribosome biogenesis is only required to promote cancer cell survival. Cancer cells proliferate rapidly, leaving them susceptible to pharmacological targeting of processes required for such rapid division. For example, many anti-cancer therapeutics target DNA replication, due to its increased rate in cancer cells when compared to most non-cancer cells. However, these treatments are not specific, resulting in death of rapidly dividing non-cancer cells and genotoxic stress across all cells. A requirement for rapid protein translation may also mean that the ribosome is an Achilles' Heel for cancer cells (Silvera et al. 2010). Targeting ribosomes would also have no genotoxic side effects, unlike DNA damaging agents. Thus, targeting of AROS could provide a means to expose a dependence upon rapid growth.

The data following SIRT1-Δ8 silencing supports the theory that loss of 80S ribosomes reduces translation and contributes to apoptosis. HCT116 cells depleted of SIRT1-Δ8 exhibit neither a decrease in 80S ribosome abundance nor an apoptotic phenotype compared to Mock treated cells (Figure 8.8C and Figure 7.7B). Thus, it appears that maintenance of 80S correlates with cancer cell survival for the HCT116 cell line.

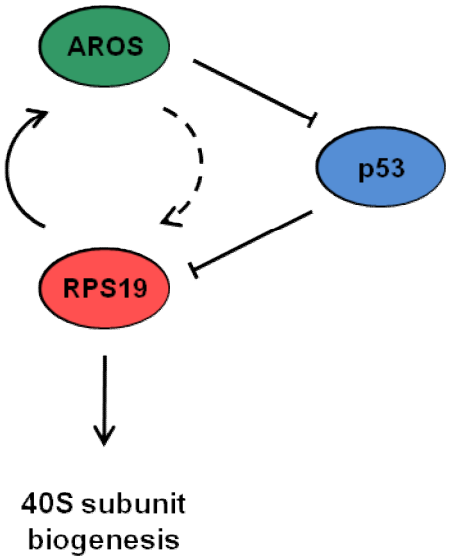

Figure 8.9: Regulation of RPS19 and ribosome biogenesis by AROS

Schematic of the role of p53 in the regulation of RPS19 by AROS. AROS suppresses p53 via promoting deacetylation and p53 appears capable of suppression of RPS19 abundance. This may contribute to the positive regulation of RPS19 by AROS.

8.8 *Conclusions*

1. AROS may specifically associate with 40S subunits and 80S ribosomes.
2. AROS promotes the biogenesis of 40S subunits in cancer and non-cancer cell lines.
3. Cancer cell survival may require AROS function to support ribosome biogenesis.
4. SIRT1-Δ8 has a role in biogenesis of 40S and 60S subunits.

9 Conclusions

9.1 *LDH-A suppresses p53 acetylation*

The role of LDH-A as a decision maker during carbon metabolism has long been known (Baumberger et al. 1933), as has the altered metabolism employed by cancer cells, which appears to rely on LDH-A activity (Warburg 1956). However, only recently has the possibility that LDH-A acts as a cancer specific survival factor been analysed. LDH-A was identified as a survival factor in cancer in two recent independent studies (Fantin et al. 2006; Le et al. 2010). In the work outlined in *Chapter 3* this has been augmented with the observation that LDH-A suppresses p53 acetylation, via a mechanism likely to involve activation of SIRT1.

9.1.1 LDH-A potentiates SIRT1 activity

In *Chapter 3*, suppression of LDH-A resulted in an increase in p53 acetylation, which correlated with apoptosis in cancer cell lines. This was specific for LDH-A, with no effect seen following LDH-B suppression. Further, LDH-A was potentially specifically required for cancer cell survival, as a non-cancer cell line was not affected by loss of LDH-A. The mechanism of LDH-A suppression induced cancer cell death has previously been attributed to impaired metabolism, resulting in failure to meet energetic demands (Fantin et al. 2006; Le et al. 2010). Although this is likely to contribute to cancer cell viability, the analysis here identifies an intersection between cancer metabolism and apoptotic signalling pathways.

LDH-A promotes glycolysis by coupling the recycling of the reducing agent NAD^+ to the synthesis of lactate from pyruvate. It is this activity that is believed to be upregulated in cancer to promote growth, and potentially allow targeting of LDH-A as an anti-cancer target (Knight and Milner 2011). The analysis in *Chapter 3* was undertaken based on the assumption that provision of NAD^+ by LDH-A can support SIRT1 activity, given that SIRT1 is an NAD^+-dependent deacetylase (Imai et al. 2000; Landry et al. 2000; Smith et al. 2000). The data are consistent with LDH-A sustaining SIRT1 activity towards the tumour suppressors p53 and FOXO4, and

represent the first indication that cancer metabolism can influence SIRT1-mediated anti-apoptotic signalling (Figure 9.3).

The data are a strong indication that LDH-A acts via SIRT1 to, at least in part, promote cancer cell survival. The elucidation of the exact mechanism of LDH-A was undertaken in parallel in the YCR p53 Research Unit and supports a mechanism for LDH-A acting via provision of NAD^+ for SIRT1 activity.

9.1.2 LDH-A is a p53-independent cancer cell survival factor

Further to providing the first indication that LDH-A can directly influence apoptotic signalling, the effect of LDH-A on cancer cell survival was found to be independent of p53 expression (*Chapter 3*). The analyses undertaken here are the first observation that LDH-A is required for cancer cell survival where p53 is wild-type, mutant or null. This is consistent with LDH-A-mediated promotion of SIRT1 activity as SIRT1 cancer cell survival function is p53-independnet. Independence from p53 expression is important from a therapeutic point of view, as p53 is mutated or misregulated in the majority of cancers (Vogelstein et al. 2000; Olivier et al. 2010; Goh et al. 2011). Thus, the ability to induce cancer cell death in the absence of p53 is an indicator of potential therapeutic success.

9.1.3 SIRT1 regulation by cancer metabolism

Upregulation of SIRT1 protein has been reported in various cancers (see *Chapter 1*). However, the ability of SIRT1 protein to promote cancer cell survival is presumably dependent on the provision of NAD^+ as a co-enzyme (Imai et al. 2000; Landry et al. 2000; Smith et al. 2000). This study identifies a putative mechanism by which SIRT1 activity is potentially increased in cancer. Importantly, it appears likely that LDH-A-mediated upregulation of SIRT1 does not depend upon increased SIRT1 abundance. Furthermore, the increased activity of LDH-A may be a consequence of altered cancer metabolism (Warburg 1956). This suggests that aberrant upregulation of SIRT1 may be a consequence of specific alterations in cancer cell energy production. Crucially this may allow cancer specific targeting of SIRT1 via suppression of LDH-A.

9.2 *AROS is a selective activator of SIRT1*

AROS was originally characterised as an activator of SIRT1 activity (Kim et al. 2007). In *Chapter 4* and *Chapter 5*, analysis of well characterised targets of SIRT1-mediated deacetylation indicated that AROS function has differences and similarities to SIRT1. From this it was inferred that AROS acts as a selective activator of SIRT1. For example, under basal conditions in HCT116 colorectal adenocarcinoma cells AROS appears to suppress FOXO4 but not p53, both of which are targets of SIRT1 suppression. Interestingly, AROS *did* suppress p53 following the application of stress in the same cell line, indicating that selective activation of SIRT1 by AROS is dynamic. The work here is the first indication of a complex AROS-SIRT1 relationship and that SIRT1 can function in the absence of AROS.

9.2.1 How is selective activation modulated?

From the data outlined in *Chapter 4* and *Chapter 5*, it seems unlikely that regulation of SIRT1 by AROS occurs in an 'on' and 'off' fashion. For example, SIRT1 appeared to be able to suppress FOXO4 but not p53 following AROS silencing under the same conditions in HCT116 cells. Thus, AROS appears to promote FOXO4 suppression over p53 suppression. This also implies that SIRT1 does not require AROS association for all catalytic activity, as p53 is still deacetylated and suppressed. Therefore, as well as being dynamic in response to stimuli it appears that AROS can modulate SIRT1 activity according to substrate. One possible explanation for this type of relationship may be modulation of AROS and/or SIRT1 by external factors.

Regulation of SIRT1 is an emerging field, with at least 12 protein level activators or suppressors of SIRT1 activity identified (see *Chapter 1*). Regulation of AROS is an entirely unexplored field, but future analyses are likely to reveal multiple regulatory mechanisms. Regulation of both SIRT1 and AROS is likely to integrate external stimuli, such as stress, into the relationship between the proteins. Indeed, SIRT1 is subject to phosphorylation by multiple kinases known to be modulated under stress conditions – JNK1(Nasrin et al. 2009), JNK2 (Ford et al. 2008) and mTOR (Back et al. 2011). Phosphorylation by these kinases may alter the

ability of AROS to bind SIRT1 and affect SIRT1 function, potentially contributing to the dynamic relationship between AROS and SIRT1 (Figure 9.1).

9.2.2 AROS as a director of SIRT1 activity

The observation that AROS selectively modulates SIRT1 activity leads to the question of why. What is the function of AROS in the wider role of SIRT1? As described above AROS may modulate SIRT1 function differently in response to stress. SIRT1 is an important component of the cell stress response via its modulation of important participants such as p53 and the FOXO proteins. It is possible that AROS acts as an extra, but potentially subvertable, level of regulation within this system. For example, modification of AROS (or SIRT1) following stress may be required for AROS-mediated promotion of certain SIRT1 targets, or conversely modification may suppress the existing regulation of SIRT1 by AROS (Figure 9.1).

Interestingly, the modulation of SIRT1 by AROS appears to contribute to the role of SIRT1 as a cancer cell survival factor, as AROS is also specifically required for cancer cell survival (*Chapter 5*). It is possible that AROS specifically modulates SIRT1 activity towards substrates involved in cancer cell longevity over other substrates with alternative functions. As such, the relationship between AROS and SIRT1 may be constitutively modified in cancer compared to non-cancer cells. Should this be the case, there is an opportunity to exploit this for anti-cancer therapeutic gain. The role of AROS in cancer cell survival is discussed at greater length in Section 9.6 below.

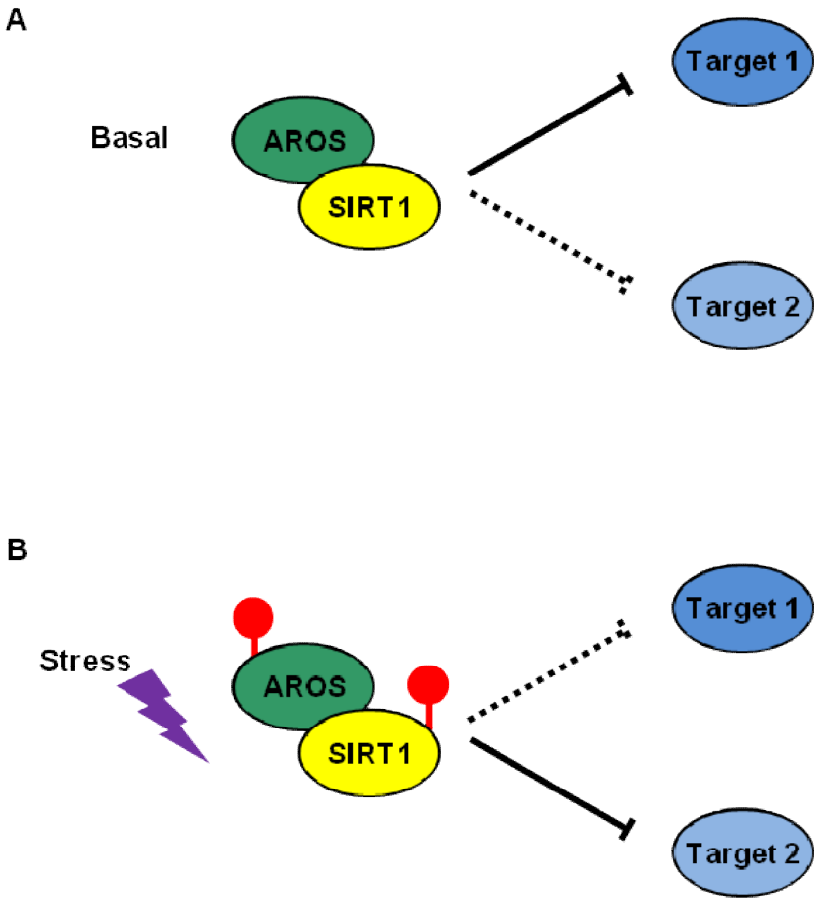

Figure 9.1: Selective modulation of SIRT1 by AROS

(A) AROS is able to selectively promote SIRT1 activity towards certain substrates but not others, giving AROS a role as a specific modulator of SIRT1. The mechanism behind this modulation is unknown. **(B)** AROS-mediated regulation of SIRT1 activity alters following the application of stress. This may be able to direct SIRT1 activity towards different substrates, and may be attributable to reversible alterations to AROS and/or SIRT1 proteins.

9.3 *AROS and RPS19 form an autoregulatory feedback loop*

The relationship between AROS and the structural component of the 40S ribosomal subunit, RPS19, was outlined in *Chapter 6*. This supplements the observation in the mouse that the two proteins form a direct interaction (Maeda et al. 2006). Association between the human homologues of AROS and RPS19 was observed for the first time in *Chapter 7*. The data in *Chapter 6* provide the most significant contribution to the knowledge of these two proteins, attributing a function to the interaction for the first time. Each protein appears to promote the protein level abundance of the other in a reciprocal autoregulatory loop. This raises questions regarding the mechanism of autoregulation, and has implications in a rare disease linked to *RPS19* mutation.

9.3.1 Mechanism of autoregulation

It appears likely that the mechanism behind AROS and RPS19 autoregulation is linked to degradation. This is based on the observation that abundance of reciprocal mRNA is *not* affected by knockdown of each protein (*Chapter 6*), indicating that synthesis is not likely to be a factor. Interestingly overexpression of AROS or RPS19 did not increase reciprocal protein abundance (*Chapter 7*), suggesting that each protein is required but not sufficient to promote reciprocal protein abundance, again appearing to correlate with a mechanism linked to degradation.

A mechanism involving degradation may relate to the association of AROS and RPS19 in human cells (*Chapter 7*) likely via the direct interaction seen in mouse cells (Maeda et al. 2006). The formation of the AROS-RPS19 complex may be crucial to support the stability of each protein. Hypothetically, association may negate degradation by blocking ubiquitination, which is known to regulate RPS19 stability (Cretien et al. 2008). Alternatively, association may promote modification of either protein, which may subsequently increase stability.

In opposition to a mechanism involving degradation, there is the possibility that translational control plays a part in the autoregulation. A recent report has highlighted a role for RPS19 in selective translation (Horos et al. 2011). Silencing of

RPS19 in this study resulted in reduced expression of specific proteins despite maintenance of the respective mRNA. This was attributed to selective translation mediated by RPS19, and is strikingly similar to the regulation of AROS by RPS19 observed in *Chapter 6*. Thus, *AROS* mRNA may be selectively translated in the presence of RPS19, such that knockdown of RPS19 reduces translation and subsequent protein expression. Crucially this would have no effect on *AROS* mRNA levels.

The apparent association of AROS with 40S ribosomal subunits (*Chapter 8*) raises the possibility that AROS and RPS19 stability is linked to the stability of ribosomes. RPS19 stability will almost certainly be linked to that of ribosomes given its role as a structural component of the 40S subunit. The ribosomal association observed for AROS may link loss of ribosomes to loss of AROS protein. Similarly, loss of RPS19 protein following AROS silencing may be a consequence of the role of AROS in 40S subunit biogenesis observed in *Chapter 8* and discussed below. Thus, the regulation of ribosome biogenesis may be at the heart of the AROS-RPS19 relationship. Inhibition of ribosome biogenesis (for example by RNAi against other ribosomal proteins) and the subsequent effect on AROS stability would reveal whether AROS and RPS19 stability is dependent or independent of ribosome stability. This analysis would also allow analysis of the putative regulation of p53 in response to ribosome biogenesis, which may signal through AROS and SIRT1.

9.3.2 Implications in disease – Diamond-Blackfan Anaemia

RPS19 was the first ribosomal protein gene to be linked to a disease. 25% of cases of the erythroblastopenia, Diamond-Blackfan Anaemia (DBA), present deleterious heterozygous mutations in the *RPS19* gene (Draptchinskaia et al. 1999; Willig et al. 1999). DBA has since been linked to mutation in a further 12 ribosomal protein genes, which in total constitute up to 54% of disease incidence (Boria et al. 2010; Ito et al. 2010). This led to the definition of DBA as the first ribosomopathy, a disease linked to mutations in ribosomal protein genes (Luft 2010). Interestingly, the mutated ribosomal protein genes contribute to both the small and large ribosomal subunits and are not confined to one region of the ribosome (Ben-Shem et al. 2010; Boria et al. 2010; Ito et al. 2010; Rabl et al. 2011). This implies that the aetiology of

the disease may be linked to the ribosome as a whole, and not extra-ribosomal functions of the ribosomal proteins.

AROS appears to promote RPS19 protein abundance in 6 cell lines from multiple origins in *Chapter 6*, raising the possibility that AROS can influence RPS19 abundance in DBA. DBA is a disease specific to the erythroid lineage of haematopoiesis, with cells in this lineage reduced in number resulting in an anaemic phenotype (Diamond and Blackfan 1938). RPS19 expression is required in erythroid progenitor cells to ensure survival (Choesmel et al. 2007; Flygare et al. 2007; Idol et al. 2007). Thus, should AROS-mediated promotion of RPS19 abundance occur in erythroid cells, AROS too may be required for survival of cells into mature erythrocytes. The role of RPS19 in ribosome biogenesis has also been linked to DBA (Choesmel et al. 2007; Flygare et al. 2007; Idol et al. 2007), perhaps consistent with the disease being a ribosomopathy (Luft 2010). AROS promoted ribosome biogenesis in a fashion similar to RPS19 in *Chapter 8*. This may be linked to the role of RPS19 in DBA, adding further to a putative role for AROS in DBA.

The effect of AROS on other ribosomal proteins implicated in DBA has not been assessed in this study. It is possible that AROS also promotes their expression, potentially creating a link between these apparently disparate proteins. However, even if this is not the case the conserved effect of AROS on RPS19 abundance, which likely occurs via direct interaction (Maeda et al. 2006), warrants further investigation of AROS in the context of DBA. The work here represents the first implication of AROS as a potential factor in DBA.

9.4 *RPS19 may suppress p53 via AROS/SIRT1*

Silencing of RPS19 correlated with an increase in p53 levels, either acetylated p53, total p53 or both (*Chapter 6*). This agrees with previous indications that RPS19 suppresses p53 (Danilova et al. 2008; McGowan et al. 2008; Dutt et al. 2011; Jaako et al. 2011), and further, the data outlined in *Chapter 6* and *Chapter 7* are the first indication that RPS19 suppression of p53 may occur via AROS and/or *SIRT1*. Three possible mechanisms of p53 suppression by RPS19 were identified, which are likely to overlap.

9.4.1 Multiple mechanisms

RPS19 may act via AROS to suppress p53. This is based on the correlation between the effect of RPS19 on p53 and selective role outlined for AROS in the suppression of p53 activation in *Chapter 4*. Variation in AROS-mediated suppression of p53 was almost exactly replicated by RPS19.

RPS19 may also suppress p53 via two *SIRT1* gene products, SIRT1-FL and SIRT1-Δ8 (*Chapter 6* and *Chapter 7*). SIRT1-FL is capable of direct deacetylation and suppression of p53 (Luo et al. 2001; Vaziri et al. 2001; Ford et al. 2005), as is SIRT1-Δ8, although at a reduced rate compared to SIRT1-FL (Lynch et al. 2010). Suppression of p53 by AROS is likely to occur via activation of SIRT1-FL by AROS (Kim et al. 2007), and potentially activation of SIRT1-Δ8 by AROS. However, more direct modulation of SIRT1-FL and SIRT1-Δ8 by RPS19 may also contribute to p53 suppression.

SIRT1-FL expression was reduced by loss of RPS19 in 5 cell lines analysed in *Chapter 6*. This raises the possibility that RPS19 modulates SIRT1-FL-mediated suppression of p53 by promoting SIRT1 protein abundance. Similarly, the molecular interactions identified in *Chapter 7* indicated that RPS19 associates with SIRT1-Δ8. The function of this interaction is unknown, but may allow RPS19 to upregulate SIRT1-Δ8 activity, which may in turn suppress p53. Thus, RPS19 appears to be capable of multiple mechanisms which could suppress p53, potentially acting via the AROS-SIRT1 axis detailed in *Chapter 4* and *Chapter 5*.

9.4.2 Implications in disease – Diamond-Blackfan Anaemia

Stabilisation of p53 as a result of reduced RPS19 expression has been reported in animal models of Diamond-Blackfan Anaemia (Danilova et al. 2008; McGowan et al. 2008; Dutt et al. 2011; Jaako et al. 2011). The data reported here prompted the proposal of various mechanisms which could lead to activation of p53 following loss of RPS19 (see above). These involve proteins that have yet to be characterised in DBA: AROS, SIRT1-FL and SIRT1-Δ8. Almost half of the cases of DBA have no known genetic cause. The work here suggests that reduced or altered expression from the *AROS* or *SIRT1* genes could contribute to DBA and that these genes may be mutated in the disease.

9.5 *AROS has a role in ribosome biogenesis*

Chapter 8 followed the observation that AROS promotes RPS19 stability with characterisation of a known RPS19 function following silencing of AROS. The role of RPS19 in 40S ribosomal subunit biogenesis was well established, allowing analysis of the role of AROS and direct comparison to RPS19. Specifically RPS19 is known to promote 40S subunit abundance by facilitating the processing of rRNA in the nucleolus (Choesmel et al. 2007; Flygare et al. 2007; Idol et al. 2007). The role identified for AROS is the first indication that AROS has a function in ribosome biogenesis.

9.5.1 AROS in 40S biogenesis

AROS appeared to specifically promote 40S subunit abundance in the cytoplasm, and the abundance of 40S subunit rRNA in the nucleus of two cell lines of different origins – the HCT116 and ARPE19 (*Chapter 8*). Furthermore, the whole cell abundance of the 40S subunit proteins RPS19 and RPS6 was decreased following silencing of AROS in the HCT116 cells. This appeared to be specific to the 40S subunit as the abundance of 60S subunits, rRNA and protein was not decreased in either cell line. The data correlate well with the role of RPS19 in ribosome biogenesis, either analysed in parallel (*Chapter 8*) or upon comparison to previous publications (Choesmel et al. 2007; Flygare et al. 2007; Idol et al. 2007).

It is possible that AROS promotes 40S subunit biogenesis independently of RPS19, potentially acting via association with alternative ribosomal proteins or ribosomal RNA. However, analysis of a range of 40S subunit proteins identified distinct roles for each in ribosome biogenesis (Robledo et al. 2008), suggesting that the correlation between AROS and RPS19 function observed here is due to similar functions. Together with the observation that AROS and RPS19 form a direct interaction (Maeda et al. 2006), this adds further to the theory that AROS acts via, or together with, RPS19 to promote ribosome biogenesis

9.5.2 AROS association with ribosomes

AROS appeared to associate with 40S subunits and 80S ribosomes in the cytoplasm of HCT116 cancer cells (*Chapter 8*). The association is likely to occur for a reason, potentially allowing AROS to influence ribosome function. This is the first observation that AROS may have a role in the function of ribosomes. The association also suggests that AROS interacts with pre-ribosomes in the nucleus, although this analysis was not undertaken. However, given the specific role of AROS in 40S subunit synthesis an association would appear likely.

The association of AROS with the 40S subunits and 80S ribosomes is likely related to the interaction between AROS and RPS19 (Maeda et al. 2006). The structure of the 40S subunit appears amenable to association of non-ribosomal proteins with RPS19 (Taylor et al. 2009; Ben-Shem et al. 2010; Rabl et al. 2011), especially proteins as small as AROS. Thus, AROS seems likely to interact with ribosomes via RPS19.

9.5.3 AROS and translational control

As well as identifying a role for AROS in the biogenesis of 40S subunits the data in *Chapter 8* also reveal a putative role for AROS in the control of translation. Translation requires the formation of 80S ribosomes, which was impaired following depletion of AROS. Thus, AROS appears to be able to promote translation by providing sufficient 40S subunits for formation of translation competent ribosomes.

As well as this global function in translational control, AROS may also be able to impart translational control via its association with 40S subunits and 80S ribosomes. Classic ribosome biogenesis factors dissociate after carrying out their function, to be recycled to promote further ribosome biogenesis (Freed et al. 2010; Kressler et al. 2010). AROS does not appear to act like a classical ribosome biogenesis factor, as it remains associated with ribosomes beyond their synthesis. This raises the possibility that AROS fulfils a function via this prolonged association, potentially in the control of translation.

40S subunits bind mRNA prior to association with 60S subunits and the initiation of translation. This gives 40S subunits the ability to select mRNAs for translation. AROS association with 40S subunits in the cytoplasm suggests that it may play a part in this function. This possibility is aided by the recent observation that RPS19, with which AROS interacts and forms an autoregulatory loop (*Chapter 6* and *Chapter 7*), imparts specific control of translation in erythroid precursors (Horos et al. 2011). Whether AROS is involved in this process merits further investigation.

9.6 *AROS selectively promotes cancer cell survival*

Chapter 5 revealed that AROS protein is required in 3 cancer cell lines to avoid apoptosis, with phenotypes consistent with apoptosis following knockdown of AROS in 2 further cancer cell lines. In contrast 3 non-cancer cell lines did not require AROS expression to maintain viability, leading to the conclusion that AROS is a putative '*novel anti-cancer therapeutic target*'. The exact mechanism by which AROS promotes cancer cell survival may involve two routes, acting via modulation of SIRT1 activity and/or promotion of ribosome biogenesis. This represents the first identification of AROS as a specific survival factor for cancer cells, and a significant addition to potential mechanisms by which AROS suppresses cancer cell apoptosis.

9.6.1 Selective SIRT1 activation

SIRT1 is a cancer specific survival factor, promoting cancer cell viability but being redundant for non-cancer cell survival (see *Introduction* and Ford et al. 2005). Thus, the characterisation of AROS in *Chapter 4* and *Chapter 5* has parallels to the functions of SIRT1. As such, it appears likely that AROS promotes cancer cell survival, at least in part, via activation of SIRT1 (Figure 9.2).

9.6.2 Promoting ribosome biogenesis

AROS also appears to promote ribosome biogenesis (see above). Although this appears to occur in cell lines of cancerous and non-cancerous origins, whereas only cancer cells appear to require AROS for survival. However, the dramatic effect on 40S subunit and 80S ribosome abundance this may have a negative effect on cell viability. The requirement for translation is perhaps greater in rapidly dividing cancer cells such as the HCT116 cells analysed here, than in non-cancer cells, such as the ARPE19 cells used. Targeting translation as a means to target cancer is not a new concept (Silvera et al. 2010), but AROS may represent a novel target (Figure 9.2).

9.6.3 AROS as an anti-cancer target

The data presented within the *Thesis* identify AROS as a putative anti-cancer therapeutic target. The data indicate further that AROS is able to promote cancer cell

survival independently of p53 expression. Thus, targeting of AROS in p53 deficient cancers, which occurs in 50% of cancers (Vogelstein et al. 2000; Olivier et al. 2010; Goh et al. 2011), should result in cancer cell death. The potential to promote cancer cell growth via two distinct mechanisms (See above and Figure 9.2) adds further to the prospects of targeting AROS in cancer. Multiple mechanisms could enhance the effect of targeting AROS compared to targeting of each mechanism individually. Furthermore, this may allow AROS targeting to remain effective should the influence of one pathway in promoting cancer survival be diminished.

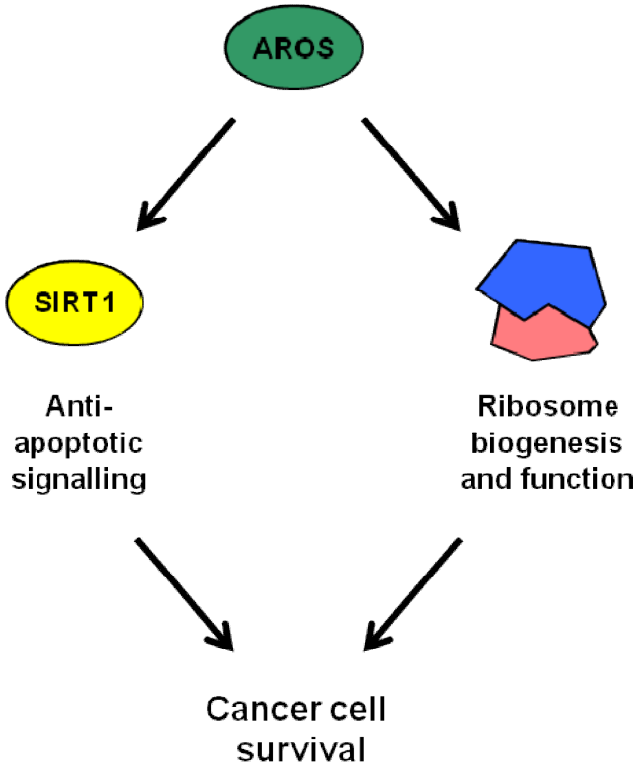

Figure 9.2: Potential mechanism for AROS as a cancer cell survival factor

AROS appears capable of promoting cancer cell survival via activation of SIRT1 anti-apoptotic signalling and via promotion of ribosome biogenesis. It is possible that both mechanisms are important, which could increase the efficacy of anti-cancer targeting of AROS.

9.7 *SIRT1-Δ8 has a role in ribosome biogenesis*

SIRT1-Δ8 was identified as an alternatively spliced form of the *SIRT1* gene, which is translated into a protein with reduced but detectable deacetylase activity (Lynch et al. 2010). No distinct function has previously been attributed to the SIRT1-Δ8 form to differentiate it from the SIRT1-FL protein. SIRT1-Δ8 protein is likely to retain the relationship SIRT1-FL has with NAD^+ availability for function. Thus, SIRT1-Δ8 may be responsive to cell metabolism. SIRT1-Δ8 but not SIRT1-FL *is* responsive to stress, being upregulated after cellular insult, but this relates to SIRT1-Δ8 regulation not function (Lynch et al. 2010).

Here, SIRT1-Δ8 appears to specifically interact with RPS19, with no interaction detectable between RPS19 and SIRT1-FL (*Chapter 7*). Thus, RPS19 is the first protein identified that preferentially associates with SIRT1-Δ8 over SIRT1-FL. This association may also affect RPS19 abundance, as silencing of SIRT1-Δ8 appears to reduce RPS19 abundance (*Chapter 7*).

SIRT1-Δ8 was shown to promote the nuclear abundance of 40S and 60S subunit rRNA and the cytoplasmic abundance of mature 40S and 60S subunits (*Chapter 8*). This is the first indication that SIRT1-Δ8 regulates ribosome biogenesis, which could have great important in linking cellular metabolism with ribosome biogenesis (see below).

9.7.1 Subunit specific or wider effects?

How SIRT1-Δ8 affects ribosome biogenesis is not clear from the data presented here. The data appear to suggest a role in global provision of rRNA, with levels of nuclear 18S and 28S pre-rRNA reduced by SIRT1-Δ8 silencing (*Chapter 8*). In *Chapter 8* this was hypothesised to relate to a known function for SIRT1-FL in regulating rDNA loci (see below also). However, the specific association with and promotion of RPS19 suggests that SIRT1-Δ8 may influence the function of RPS19 in ribosome biogenesis. This should be specific to the synthesis of 40S subunits, apparently contradicting the loss of both 40S and 60S subunits following SIRT1-Δ8 knockdown.

However, it is possible that SIRT1-Δ8 influences both subunits at the post-transcriptional level, potentially via a similar association with a 60S subunit protein(s) to that seen with RPS19. This could represent a post-transcriptional method for regulation of ribosome synthesis, governed by a stress and metabolism responsive signalling enzyme in SIRT1-Δ8.

9.7.2 Linking ribosomes and *SIRT1*

Ribosome biogenesis has been linked to control by SIRT1 via SIRT1-mediated epigenetic regulation of the rDNA loci in mammalian cells (Murayama et al. 2008). rDNA is silenced in response to reduced carbon metabolism, which is proportional to NAD^+ availability and thus SIRT1 deacetylase activity. This is believed to suppress the energy consuming process of ribosome biogenesis in response to low nutrient availability (Grummt and Ladurner 2008). The data presented here suggest that SIRT1-Δ8 may be able to influence ribosome biogenesis post transcription. This is based on the AROS-SIRT1-Δ8 and RPS19-SIRT1-Δ8 interactions, and the possibility that AROS requires SIRT1-Δ8 for its role in ribosome biogenesis.

Furthermore, the association between AROS and ribosomes raises the possibility that SIRT1-Δ8 also associates with 40S subunits and/or 80S ribosomes. No association was detected between SIRT1-FL and the ribosome (*Chapter 8*), but SIRT1-Δ8 was not analysed. Furthermore, the putative association may have a functional role during ribosome function, modulating translation. A recent report has identified a role for SIRT1 in regulating translation via modulation of eIF2 (Ghosh et al. 2011). However, the analysis was carried out using SIRT1 null cells or RNAi which will have depleted both SIRT1-FL and SIRT1-Δ8. Thus, it is possible that SIRT1-Δ8 participates in translational control if the function attributed to SIRT1 is in fact carried out by SIRT1-Δ8.

Together, the work detailed here is the first indication of a specific role for SIRT1-Δ8 to differentiate it from SIRT1-FL. Furthermore, a putative role for SIRT1-Δ8 is proposed during ribosome biogenesis, which could link global ribosome abundance, translation and cellular energy and stress status.

9.8 *Cancer metabolism, ribosome biogenesis and cancer cell survival*

The *Thesis* aimed to identify links between the metabolism of cancer cells, ribosome biogenesis and cancer cell survival. This was based on the well characterised role of LDH-A in metabolic regulation and a predicted role for AROS in ribosome biogenesis. The schematic Venn diagram drawn in *Chapter 1* has been populated throughout the course of the studies to produce Figure 9.3.

9.8.1 Cancer metabolism and cancer cell survival

Cancer metabolism appears to promote cancer cell survival, in part via regulation of p53 and FOXO4 by SIRT1, which appears to be linked to LDH-A activity. The increase in Aerobic Glycolysis in cancer cells may drive NAD^+ synthesis by LDH-A and subsequently SIRT1 activity in response to increased NAD^+ availability. In this relationship SIRT1 acts as the central node, linking cancer metabolism to cancer cell survival. Interestingly, SIRT1 also appears to have the capacity to alter metabolism, potentially doing so in cancer to promote metabolic alterations that may in turn promote cancer cell survival (Knight and Milner 2011). LDH-A represents a crucial link between cancer metabolism and cancer cell survival, as illustrated in Figure 9.3.

9.8.2 Ribosome biogenesis and cancer cell survival

AROS appears to play an important role in promoting ribosome biogenesis and cancer cell survival. Thus, AROS is placed at the intersection of these two areas in Figure 9.3. As discussed above, AROS-mediated promotion of cancer cell survival may be linked to SIRT1, or attributable to regulation of ribosome biogenesis. Interaction between ribosome biogenesis and the *SIRT1* gene is also evident, highlighted by the characterisation of SIRT1-Δ8 as a potential regulator of RPS19 and ribosome biogenesis. Thus, the data highlights interplay between AROS and its roles in ribosome biogenesis and cancer cell survival, potentially involving both SIRT1-FL and SIRT1-Δ8.

9.8.3 Cancer metabolism and ribosome biogenesis

The potential for cancer metabolism to affect ribosome biogenesis is highlighted by the data presented here. This did not form a large part of the analysis, leaving room for speculation. NAD^+ availability has previously been linked to ribosome biogenesis via SIRT1 activity (Murayama et al. 2008). However, the possibility that altered cancer metabolism promotes ribosome biogenesis has not been formally assessed. It may be advantageous for cancer cells to upregulate ribosome biogenesis in order to facilitate proliferation. As such, increased SIRT1 activity driven by cancer metabolism may affect ribosome biogenesis as well as cancer cell survival via the putative model outlined here. It is also possible that SIRT1-Δ8 participates in linking cancer metabolism to ribosome biogenesis, as it also requires NAD^+ and appears to promote both 40S and 60S subunit synthesis.

9.8.4 Concluding remarks

The broad aim of this work, identified in *Chapter 1*, was to analyse the protein level regulation of SIRT1 in an attempt to discover and characterise novel anti-cancer therapeutic targets. During the course of the analysis two factors were found with such properties, LDH-A and AROS. LDH-A had previously been identified as a survival factor in cancer cells (Fantin et al. 2006; Le et al. 2010), but this work supplements this with the addition of a putative mechanism acting via SIRT1-mediated anti-apoptotic signalling. The characterisation of AROS as a specific survival factor is entirely novel, with AROS only previously being shown to promote cancer cell survival (Kim et al. 2007). Furthermore, the characterisation of a previously unknown role for AROS in ribosome biogenesis identified a possible link between anti-apoptotic signalling and protein synthesis. Together this work has allowed novel regulation of SIRT1 to be integrated with cancer metabolism, ribosome biogenesis and cancer cell survival.

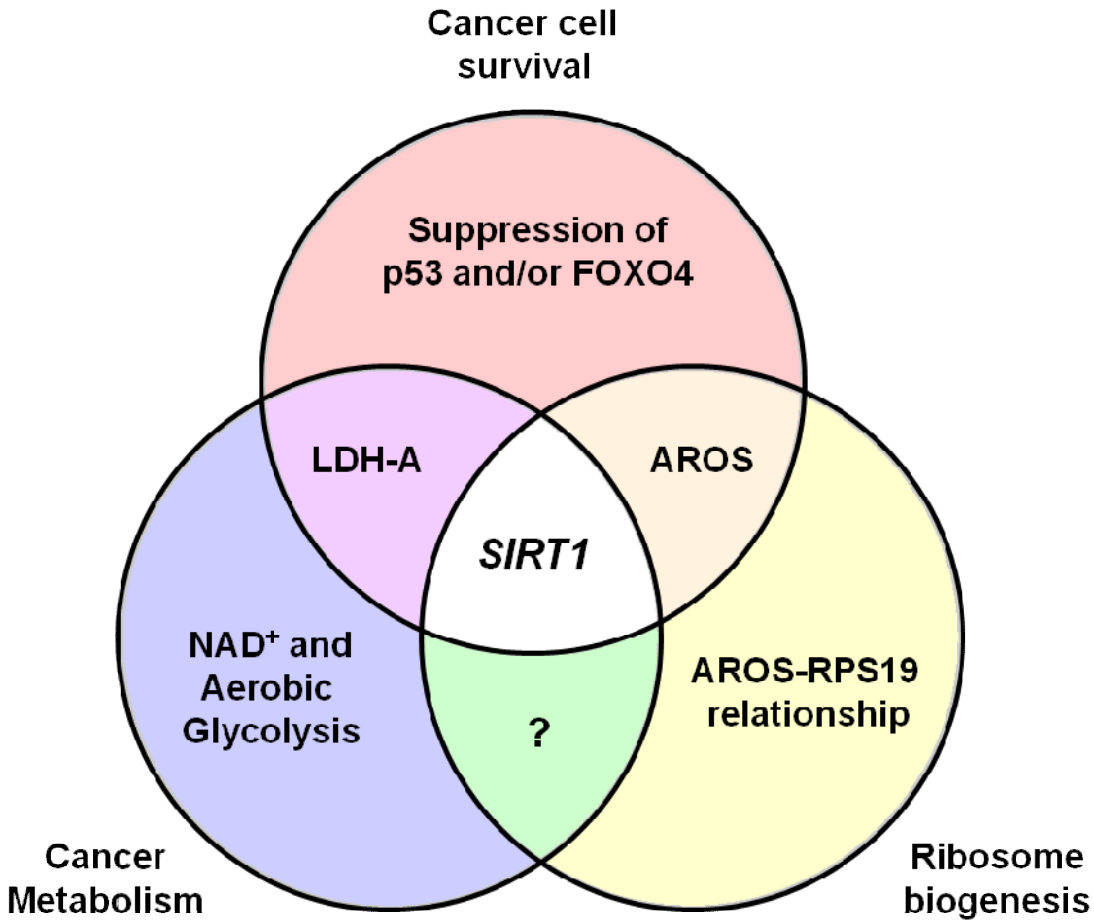

Figure 9.3: Cancer metabolism, ribosome biogenesis and cancer cell survival

The interplay between cancer metabolism and ribosome biogenesis in contributing to cancer cell survival. The *SIRT1* gene occupies the centre of the relationship, as it influences and/or is influenced by each of the three factors. LDH-A was characterised as a link between cancer metabolism and cancer cell survival, linking Aerobic Glycolysis with SIRT1 activity via NAD^+ availability. AROS links ribosome biogenesis with cancer cell survival in the system, via *SIRT1* for the latter function. There is the possibility that cancer metabolism affects ribosome biogenesis within the system, but this was not formally assessed.

10 Appendices

Processing of apoptosis data

Other supplementary data

Table 10.1: Annexin V / FACS data for Chapter 3 – Figures 3.7, 3.8 and 3.10

Cell line and siRNA	*Average (% cells)*	*Standard deviation*	*Fold change to mock*	*Standard deviation to fold*
Cancer cell lines				
HCT116				
Mock	4.33	0.15	1.00	0.03
LDH-A	19.59	0.48	4.53	0.02
LDH-B	2.77	0.10	0.64	0.04
LDH-A & B	12.78	0.77	2.95	0.06
HCT116 $p53^{-/-}$				
Mock	3.23	0.13	1.00	0.04
LDH-A	8.92	0.59	2.76	0.07
LDH-B	2.92	0.16	0.90	0.06
LDH-A & B	8.74	0.06	2.71	0.01
DLD1				
Mock	2.03	0.26	1.00	0.13
Lamin AC	3.10	0.32	1.53	0.16
LDH-A	10.30	0.00	5.09	0.00
MCF7				
Mock	1.78	0.81	1.00	0.45
LDH-B	3.16	0.19	1.77	0.11
LDH-A	9.50	1.73	5.33	0.97
Non-cancer cell line				
ARPE19				
Mock	0.64	0.20	1.00	0.31
LDH-A	0.93	0.03	1.45	0.03
LDH-B	0.91	0.21	1.41	0.23
LDH-A & B	1.04	0.01	1.62	0.01
FOXO4 rescue data				
HCT116				
Mock	2.56	0.12	1.00	0.05
LDH-A	11.52	0.06	4.51	0.02
+ FOXO4	6.28	0.41	2.46	0.16

Table 10.2: Annexin V / FACS data for Chapter 5 - Figure 5.2

Cell line and siRNA	***Average (% cells)***	***Standard deviation***	***Fold change to mock***	***Standard deviation to fold***
Cancer cell lines				
HCT116				
Mock	4.33	0.15	1.00	0.03
Lamin AC	7.25	0.46	1.68	0.06
SIRT1	21.38	1.88	4.94	0.09
AROS 1	19.11	0.22	4.42	0.01
HCT116 – 72h				
Mock	4.58	0.49	1.00	0.11
Lamin AC	6.61	0.35	1.44	0.08
SIRT1	18.30	0.28	4.00	0.06
AROS 1	16.15	0.31	3.53	0.07
AROS 2	10.46	0.74	2.29	0.16
HCT116 $p53^{-/-}$				
Mock	3.23	0.13	1.00	0.04
Lamin AC	5.54	0.23	1.72	0.04
SIRT1	8.33	0.62	2.58	0.07
AROS 1	8.66	0.07	2.68	0.01
MCF7				
Mock	2.00	0.20	1.00	0.10
SIRT1	6.22	0.47	3.22	0.08
AROS 1	6.52	0.47	3.11	0.07

Table 10.3: Annexin V / FACS data for Chapter 5 - Figure 5.5

Cell line and siRNA	*Average (% cells)*	*Standard deviation*	*Fold change to mock*	*Standard deviation to fold*
Non-cancer cell lines				
ARPE19				
Mock	0.64	0.20	1.00	0.31
Lamin AC	0.89	0.11	1.38	0.12
SIRT1	1.21	0.18	1.89	0.15
AROS 1	0.89	0.15	1.38	0.17
WI38				
Mock	1.68	0.25	1.00	0.15
Lamin AC	2.22	0.03	1.32	0.01
SIRT1	1.67	0.01	0.99	0.01
AROS 1	2.12	2.12	1.26	0.17
MCF10A				
Mock	1.29	0.26	1.00	0.20
SIRT1	1.58	0.22	1.23	0.14
AROS 1	2.15	0.45	1.67	0.21

Table 10.4: Annexin V / FACS data for Chapter 5 - Figure 5.7

Cell line and siRNA	*Average (% cells)*	*Standard deviation*	*Fold change to mock*	*Standard deviation to fold*
HCT116				
Mock	7.07	0.30	1.00	0.04
+ Etoposide / TSA				
Mock	12.78	1.41	1.81	0.20
SIRT1	32.98	1.68	4.66	0.24
AROS 1	32.96	1.82	4.66	0.26
ARPE19				
Mock	4.14	0.90	1.00	0.22
+ Etoposide / TSA				
Mock	4.53	2.67	1.09	0.64
SIRT1	11.78	1.04	2.85	0.25
AROS 1	5.41	0.28	1.31	0.07

Table 10.5: Annexin V / FACS data for Chapter 5 - Figures 5.8 and 5.9

Cell line and siRNA	*Average (% cells)*	*Standard deviation*	*Fold change to mock*	*Standard deviation to fold*
HCT116				
Mock	3.75	0.33	1.00	0.09
+ UV treatment				
Mock	11.76	0.11	3.13	0.03
Lamin AC	17.34	0.09	4.62	0.02
SIRT1	26.00	1.30	6.93	0.35
AROS 1	25.22	3.12	6.72	0.83
HCT116 p53$^{-/-}$				
Mock	3.23	0.13	1.00	0.04
+ UV treatment				
Mock	5.45	0.83	1.69	0.26
Lamin AC	11.19	1.38	3.46	0.43
SIRT1	15.58	1.14	4.82	0.35
AROS 1	18.80	0.78	5.82	0.24

Table 10.6: Annexin V / FACS data for Chapter 5 - Figures 5.10 and 5.11

Cell line and siRNA	*Average (% cells)*	*Standard deviation*	*Fold change to mock*	*Standard deviation to fold*
HCT116				
Mock	3.77	0.53	1.00	0.14
AROS 1	22.22	0.33	5.90	0.09
+ FOXO4	5.93	0.35	1.57	0.27
+ FOXO3	21.87	1.00	5.81	0.41
Mock	4.79	1.21	1.00	0.25
FOXO4	9.90	0.06	2.07	0.01
FOXO3	8.63	0.61	1.80	0.13
HCT116 p53$^{-/-}$				
Mock	3.61	0.39	1.00	0.11
AROS 1	11.78	0.17	3.27	0.05
+ FOXO4	7.46	0.93	2.07	0.26
+ FOXO3	13.38	0.98	3.71	0.27

Table 10.7: Annexin V / FACS data for Chapter 6 – Figures 6.4 and 6.8

Cell line and siRNA	*Average (% cells)*	*Standard deviation*	*Fold change to mock*	*Standard deviation to fold*
Cancer cell lines				
HCT116				
Mock	4.79	1.21	1.00	0.25
RPS19	10.51	0.70	2.20	0.15
AROS	17.64	4.18	3.69	0.87
HCT116 $p53^{-/-}$				
Mock	4.76	0.21	1.00	0.04
RPS19	8.08	0.57	1.70	0.12
AROS	10.22	0.04	2.15	0.01
Non-cancer cell lines				
ARPE19				
Mock	1.08	0.16	1.00	0.15
RPS19	3.09	0.14	2.87	0.13
AROS	1.24	0.06	1.15	0.06
WI38				
Mock	2.65	0.35	1.00	0.13
RPS19	4.91	0.10	1.85	0.04
AROS	2.47	0.28	0.93	0.11

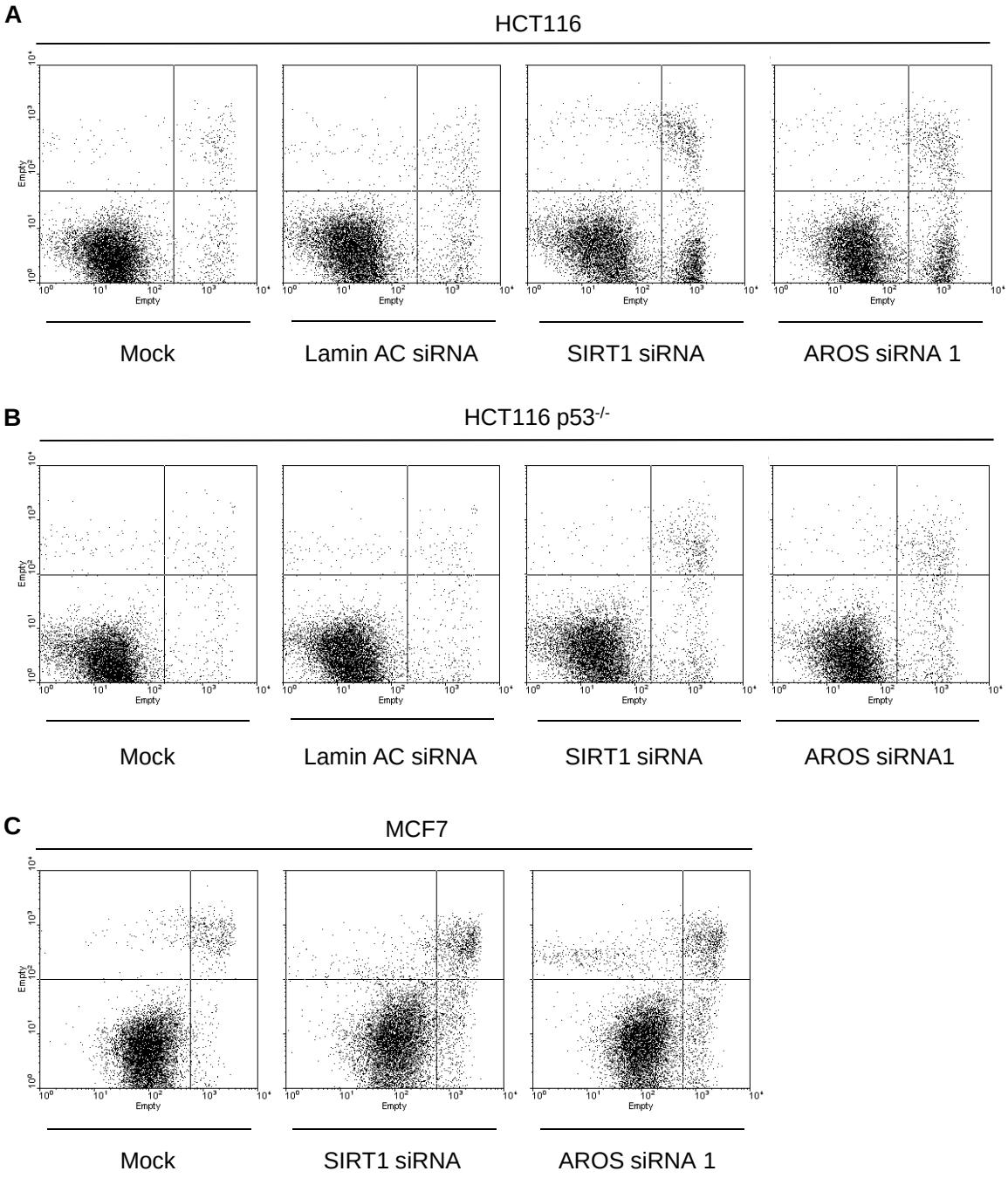

Figure 10.1: FACS scatter plot for Chapter 5 - Figure 5.2

(A) Scatter plots from Annexin V (x-axis) and propidium iodide (y-axis) staining of HCT116 colorectal adenocarcinoma cells following siRNA treatment as indicated. Analysis was carried out as described in the *Methods* at 48 hours post-transfection giving values for apoptotic induction as shown in Table 10.2. **(B)** Data as in (A) for the colorectal adenocarcinoma HCT116 $p53^{-/-}$ cell line at 72 hours post-transfection. **(C)** Data as in (A) for the MCF7 mammary gland epithelial cancer cell line at 48 hours post-transfection.

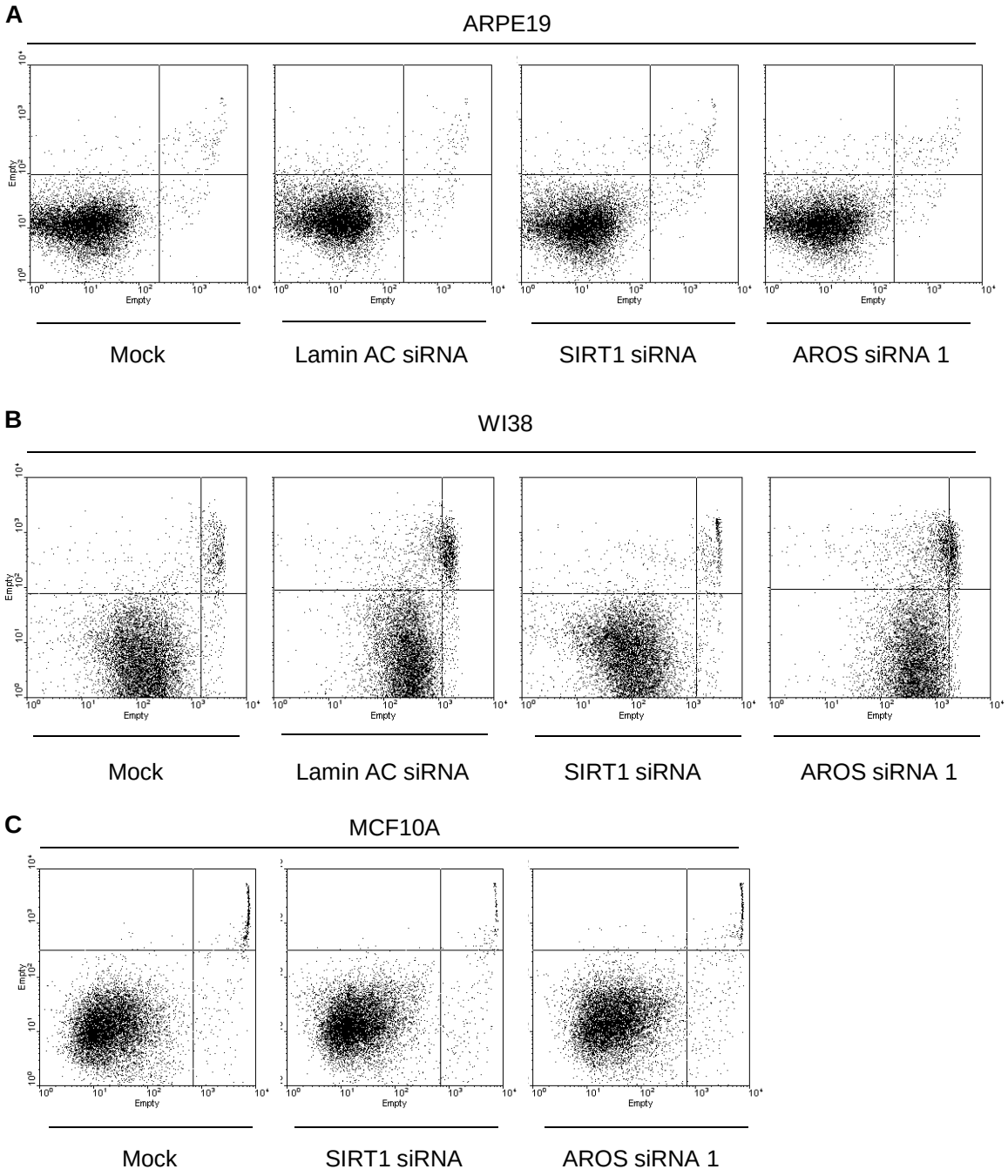

Figure 10.2: FACS scatter plot for Chapter 5 - Figure 5.5

(A) Scatter plots from Annexin V (x-axis) and propidium iodide (y-axis) staining of ARPE19 retinal epithelial cells following siRNA treatment as indicated. Analysis was carried out as described in the *Methods* at 72 hours post-transfection giving values for apoptotic induction as shown in Table 10.2. **(B)** Data as in (A) for the WI38 lung fibroblast cell line at 72 hours post-transfection. **(C)** Data as in (A) for the MCF10A mammary gland epithelial cell line at 72 hours post-transfection.

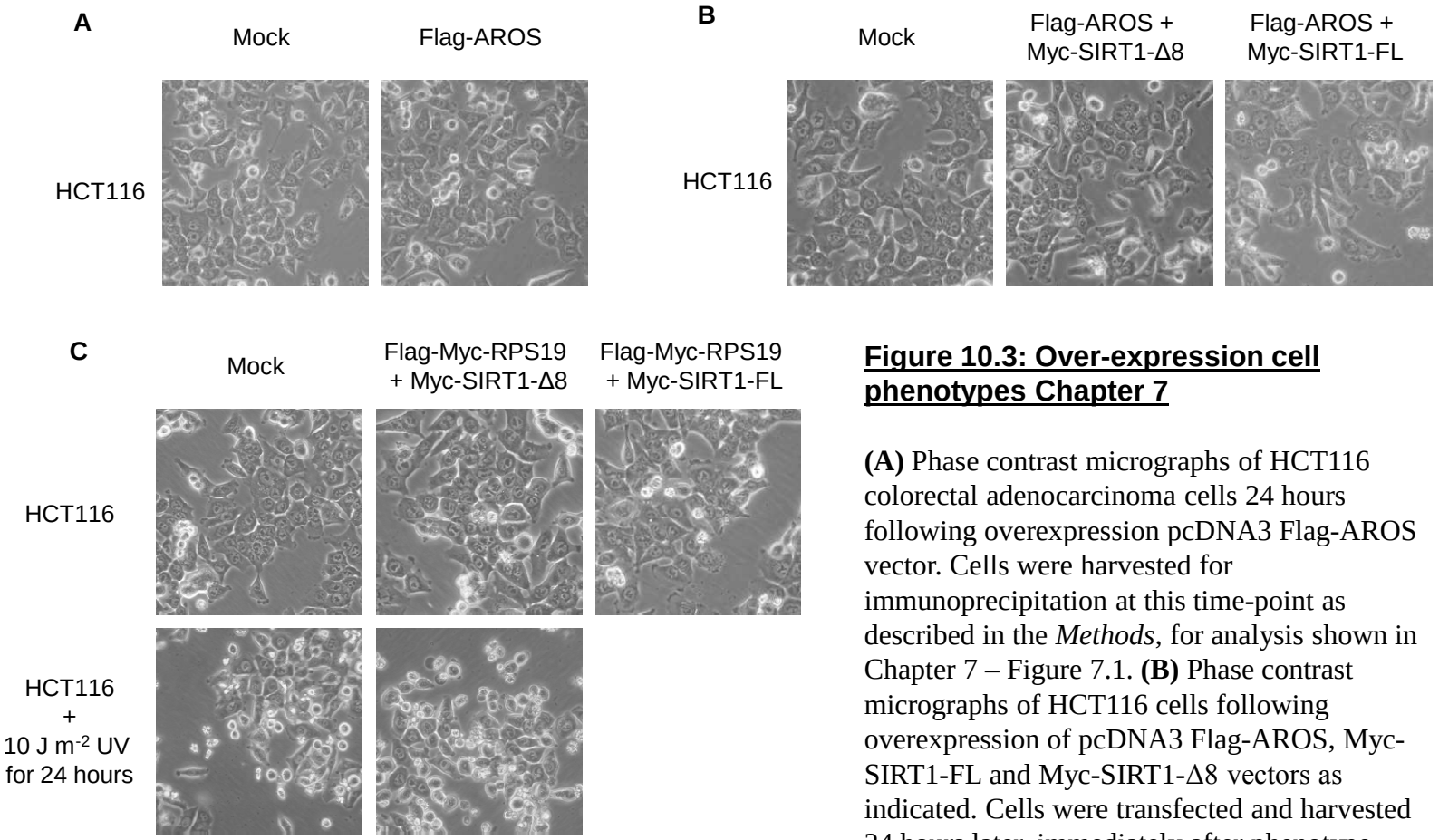

Figure 10.3: Over-expression cell phenotypes Chapter 7

(A) Phase contrast micrographs of HCT116 colorectal adenocarcinoma cells 24 hours following overexpression pcDNA3 Flag-AROS vector. Cells were harvested for immunoprecipitation at this time-point as described in the *Methods*, for analysis shown in Chapter 7 – Figure 7.1. **(B)** Phase contrast micrographs of HCT116 cells following overexpression of pcDNA3 Flag-AROS, Myc-SIRT1-FL and Myc-SIRT1-Δ8 vectors as indicated. Cells were transfected and harvested 24 hours later, immediately after phenotype was recorded, for immunoprecipitation analysis shown in Chapter 7 – Figure 7.4. **(C)** Phase contrast micrographs of HCT116 cells following overexpression of pCMV6 Flag-Myc-RPS19, pcDNA3 Myc-SIRT1-FL and pcDNA3 Myc-SIRT1-Δ8 vectors as indicated. Cells were transfected and harvested 24 hours later for immunoprecipitation analysis shown in Chapter 7 – Figure 7.3. For Chapter 7 – Figure 7.5, cells were transfected then UV irradiated 24 hours later, incubated for a further 24 hours then harvested for immunoprecipitation.

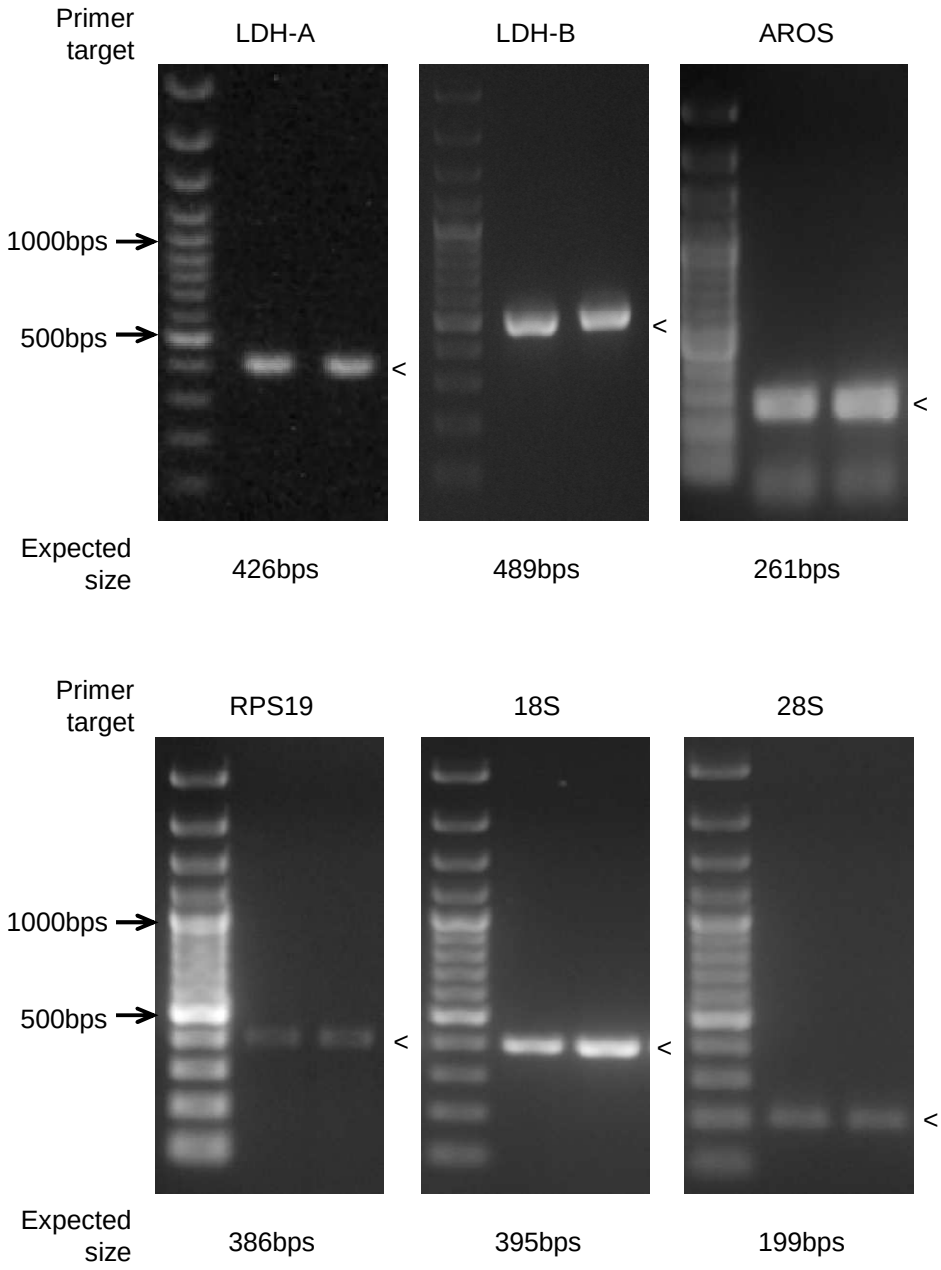

Figure 10.4: cDNA primer products from PCR analyses

Verification of single cDNA product of the correct size following PCR analysis of target mRNAs as indicated. The products from PCR analyses were separated by agarose gel electrophoresis and stained with ethidium bromide (see *Methods*). Two independent reactions were analysed next to a 100bp ladder to verify cDNA size, as shown beneath each image. Arrows indicate the product band. The smaller band in the AROS cDNA products represents a product of primer dimerisation. This was omitted from qRT-PCR analyses by use of a melt step prior to reading.

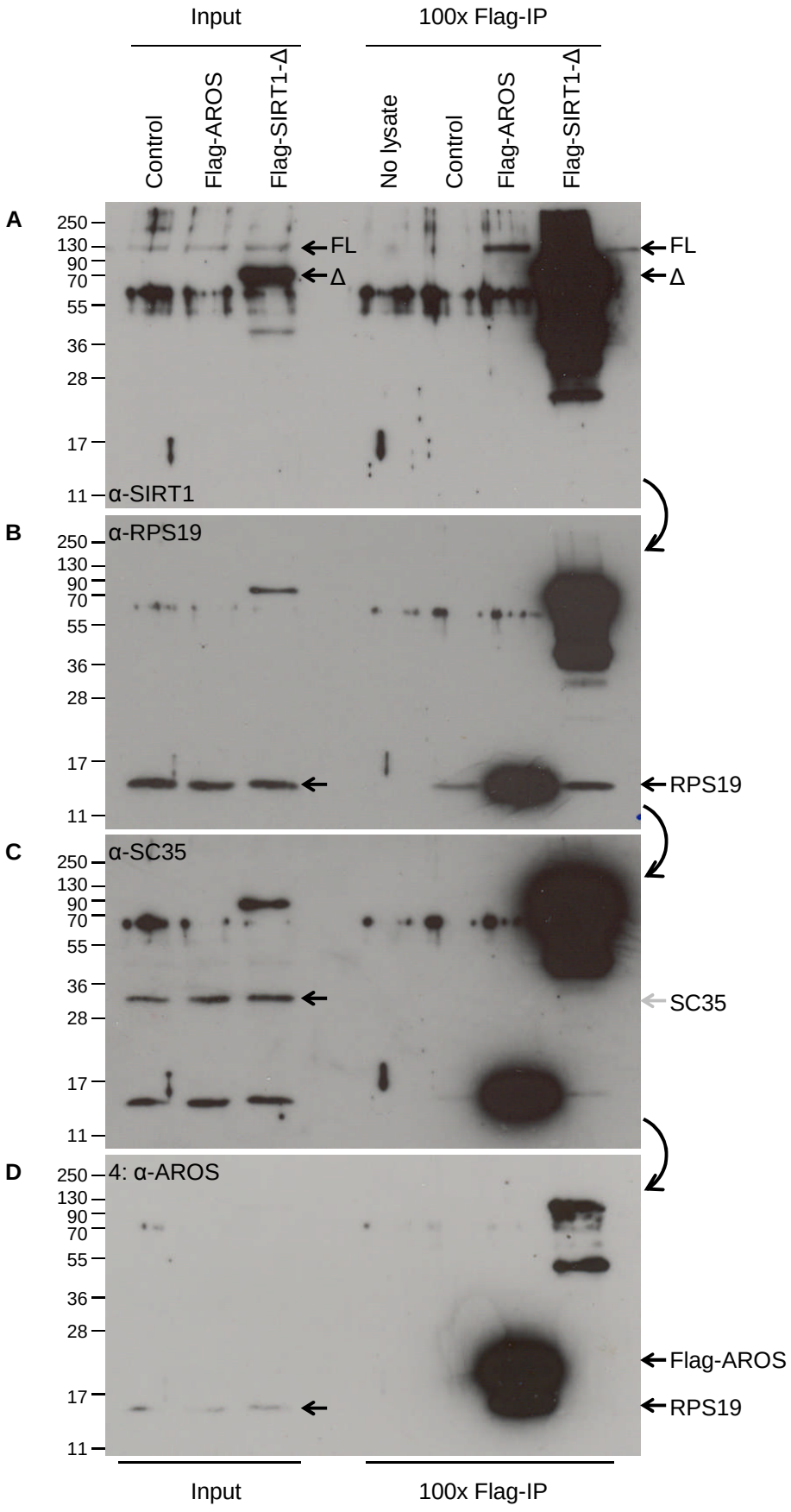
Input
100x Flag-IP
Control
Flag-AROS
Flag-SIRT1-Δ
No lysate
Control
Flag-AROS
Flag-SIRT1-Δ
A
250
130
90
70
55
36
28
17
11
FL
Δ
α-SIRT1
B
α-RPS19
RPS19
C
α-SC35
SC35
D
4: α-AROS
Flag-AROS
RPS19
Input
100x Flag-IP

Figure 10.5: Western blotting from Flag-AROS immunoprecipitation

Sequential Western blotting analyses of a single nitrocellulose membrane containing sample from immunoprecipitation of Flag-AROS. Flag-immunoprecipitation was carried out as detailed in the *Methods* and *Chapter 7*. This data represents a repeat of the Flag-AROS immunoprecipitation data presented in *Chapter 7 – Figure 7.1*. Also analysed in parallel on this membrane was a Flag-SIRT1-Δ construct which lacks residues 1-217, the region that interacts with AROS (Kim et al. 2007). Panel **(A)** probed with anti-SIRT1 antibody indicates the Flag-AROS-SIRT1-FL association, and expression and immunoprecipitation of the SIRT1-Δ construct. Panel **(B)** probed with anti-RPS19 antibody reveals the association of Flag-AROS with RPS19. Panel **(C)** probed with anti-SC35 antibody is used in place of Actin as a negative control for no interaction with Flag-AROS (grey arrow). The region for Actin expression (~43kDa) is masked in the SIRT1-Δ immunoprecipitation lane, leading to the use of SC35 antibody. Panel **(D)** probed with anti-AROS antibody indicates the immunoprecipitation and thus expression of Flag-AROS. Endogenous or Flag-AROS was not detected in the Input samples at this exposure. To detect AROS in the Input, a new analysis was undertaken with an altered loading ratio between 'Input' and 'Flag-IP' samples.

List of Abbreviations

40S	Small ribosomal subunit
60S	Large ribosomal subunit
80S	40S and 60S subunits associated on mRNA
ADAM10	Disintegrin and metalloproteinase domain-containing protein 10
ADP	Adenosine diphosphate
AMPK	AMP-activated protein kinase
ARF	Alternate reading frame protein
AROS	Active regulator of SIRT1
ATM	Ataxia telangiectasia mutated protein
ATP	Adenosine triphosphate
BIM-L	Bcl-2 interacting mediator of cell death – long isoform
BLAST	Basic Local Alignment Search Tool
bps	Base pairs
BRCA1	Breast cancer type 1 susceptibility protein
CaM kinase Iα	Ca^{2+}/calmodulin-dependent protein kinase Iα
cDNA	Complementary DNA
ChREBP	Carbohydrate response-element-binding protein
CK2	Casein Kinase II
CMV	Cytomegalovirus
CO_2	Carbon dioxide
CREB	Cyclic-AMP responsive element binding
DBA	Diamond-Blackfan Anaemia
DBC1	Deleted in breast cancer 1
DMEM	Dulbecco's Modified Eagle Medium
DMSO	Dimethyl sulfoxide
DNA	Deoxyribonucleic acid
DTT	Dithiothreitol
DYRK	Dual-specificity tyrosine phosphorylation regulated kinase
E2F1	E2F transcription factor 1
EDTA	Ethylenediaminetetraacetic acid
ESA	Essential for SIRT1 activity
ETO	Etoposide
ETS	External transcribed spacer
FACS	Fluorescence activated cell sorter
FCS	Foetal calf serum
FL	Full length
FOXO	Forkhead box O
g	Gravity
G1	Growth phase 1
G2	Growth phase 2
GAPDH	Glyceraldehyde 3-phosphate dehydrogenase
HDAC	Histone deacetylase
HDM2	Human MDM2
hEGF	Human epidermal growth factor
HEPES	4-(2-hydroxyethyl)-1-piperazineethanesulfonic acid
HIC1	Hypermethylated in breast cancer 1

HIF	Hypoxia inducible factor
HRP	Horse radish peroxidase
HuR	Hu-antigen R
IgG	Immunoglobulin G
IP	Immunoprecipitation
ITS	Internal transcribed spacer
J m^{-2}	Joules per square metre
J/m^2/s	Joules per square metre per second
JNK	c-Jun N-terminal kinase
K382Ac	Acetylated lysine 382
kDa	Kilo-Daltons
L	Long exposure (on Western blots)
LDH-A	Lactate dehydrogenase A
LDH-B	Lactate dehydrogenase B
LDH-C	Lactate dehydrogenase C
M	Mitosis
MDM2	Mouse Double Minute 2
MEBM	Mammary epithelial cell basal media
MEM	Modified Eagle Medium
mRNA	Messenger RNA
MST1	Mammalian Sterile 20-like kinase 1
mTOR	Mammalian Target Of Rapamycin
NAD^+	Nicotinamide adenine dinucelotide (oxidised)
NADH	Nicotinamide adenine dinucelotide (reduced)
NAM	Nicotinamide
NAMPT	Nicotinamide phosphoribosyltransferase
NEAA	Non-essential amino acids
NES	Nuclear export signal
NLS	Nuclear localisation sequence
NMN	Nicotinamide mononucleotide
NMNAT	Nicotinamide mononucleotide adenylyl transferase
OD	Optical density
OXPHOS	Oxidative phosphorylation
p300/CBP	300kDa protein / CREB binding protein
p53	53kDa protein
PAGE	Poly-acrylamide gel electrophoresis
PARP	Poly-ADP ribose polymerase
PBS	Phosphate buffered saline
PCAF	p300/CBP-associated factor
PCR	Polymerase chain reaction
PGC-1α	Peroxisome proliferator-activated receptor gamma coactivator-1α
PI	Propidium iodide
POD	Peroxidase
qRT	Quantitative reverse transcription
RAS	Rat sarcoma protein
rDNA	Ribosomal DNA
RNA	Ribonucleic acid
RNAi	RNA interference
RPL11	Ribosomal protein of the large subunit 11

RPL3	Ribosomal protein of the large subunit 3
rpm	Revolutions per minute
RPMI	Roswell Park Memorial Institute (media)
RPS19	Ribosomal protein of the small subunit 19
RPS6	Ribosomal protein of the small subunit 6
rRNA	Ribosomal RNA
RT	Reverse transcription
S	Short exposure (on Western blots)
S	Synthesis phase
SDS	Sodium dodecyl sulphate
SENP1	Sentrin-specific protease 1
SET7/9	SET domain containing 7/9
shRNA	Short hairpin RNA
Sir2	Silent information regulator 2
siRNA	Short interfering RNA
SIRT1	Silent information regulator type 1
SIRT3	Silent information regulator type 3
SIRT6	Silent information regulator type 6
SUMO	Small ubiquitin-like modifier
TAE	TRIS base, Acetic acid and EDTA
TBS(T)	TRIS buffered saline (plus tween)
TP53	Tumor protein 53 (gene)
TRIS	*Tris*(hydroxymethyl)aminomethane
tRNA	Transfer RNA
TSA	Trichostatin A
TSC2	Tuberous sclerosis protein 2
U	Enzyme units
UV	Ultra-violet
V	Volts
WB	Western blot
YCR	Yorkshire Cancer Research
Δ8	Missing exon 8

Bibliography

Abdelmohsen K, Lal A, Kim HH and Gorospe M. 2007a. Posttranscriptional Orchestration of an Anti-Apoptotic Program by HuR. *Cell Cycle* **6**: 1288-1292.

Abdelmohsen K, Pullmann Jr R, Lal A, Kim HH, Galban S, Yang X, Blethrow JD, Walker M, Shubert J, Gillespie DA, Furneaux H and Gorospe M. 2007b. Phosphorylation of HuR by Chk2 Regulates SIRT1 Expression. *Molecular Cell* **25**: 543-557.

Ahmed SU and Milner J. 2009. Basal cancer cell survival involves JNK2 suppression of a novel JNK1/c-Jun/Bcl-3 apoptotic network. *PLoS One* **4**: e7305.

Alhazzazi TY, Kamarajan P, Verdin E and Kapila YL. 2011. SIRT3 and cancer: Tumor promoter or suppressor? *Biochimica Et Biophysica Acta-Reviews on Cancer* **1816**: 80-88.

Allison SJ and Milner J. 2007. SIRT3 is Pro-Apoptotic and Participates in Distinct Basal Apoptotic Pathways. *Cell Cycle* **6**: 2669-2677.

Autiero I, Costantini S and Colonna G. 2009. Human Sirt-1: Molecular Modeling and Structure-Function Relationships of an Unordered Protein. *PLoS One* **4**.

Back JH, Rezvani HR, Zhu Y, Guyonnet-Duperat V, Athar M, Ratner D and Kim AL. 2011. Cancer Cell Survival Following DNA Damage-mediated Premature Senescence Is Regulated by Mammalian Target of Rapamycin (mTOR)-dependent Inhibition of Sirtuin 1. *Journal of Biological Chemistry* **286**: 19100-19108.

Bai P, Canto C, Brunyanszki A, Huber A, Szanto M, Cen Y, Yamamoto H, Houten SM, Kiss B, Oudart H, Gergely P, Menissier-de Murcia J, Schreiber V, Sauve AA and Auwerx J. 2011a. PARP-2 regulates SIRT1 expression and whole-body energy expenditure. *Cell Metabolism* **13**: 450-460.

Bai P, Canto C, Oudart H, Brunyanszki A, Cen Y, Thomas C, Yamamoto H, Huber A, Kiss B, Houtkooper RH, Schoonjans K, Schreiber V, Sauve AA, Menissier-de Murcia J and Auwerx J. 2011b. PARP-1 inhibition increases mitochondrial metabolism through SIRT1 activation. *Cell Metabolism* **13**: 461-468.

Banks AS, Kon N, Knight C, Matsumoto M, Gutiérrez-Juárez R, Rossetti L, Gu W and Accili D. 2008. SirT1 Gain of Function Increases Energy Efficiency and Prevents Diabetes in Mice. *Cell Metabolism* **8**: 333-341.

Barak Y, Juven T, Haffner R and Oren M. 1993. mdm2 expression is induced by wild type p53 activity. *EMBO Journal* **12**: 461-468.

Barlow AL, van Drunen CM, Johnson CA, Tweedie S, Bird A and Turner BM. 2001. dSIR2 and dHDAC6: Two Novel, Inhibitor-Resistant Deacetylases in Drosophila melanogaster. *Experimental Cell Research* **265**: 90-103.

Baumberger JP, Jurgensen JJ and Bardwell K. 1933. The Coupled Redox Potential of the Lactate-Enzyme-Pyruvate System. *The Journal of General Physiology* **16**: 961-976.

Bell SD, Botting CH, Wardleworth BN, Jackson SP and White MF. 2002. The Interaction of Alba, a Conserved Archaeal Chromatin Protein, with Sir2 and Its Regulation by Acetylation. *Science* **296**: 148-151.

Ben-Shem A, Jenner L, Yusupova G and Yusupov M. 2010. Crystal Structure of the Eukaryotic Ribosome. *Science* **330**: 1203-1209.

Blackwell M. 2011. The Fungi: 1, 2, 3 … 5.1 million species? *American Journal of Botany* **98**: 426-438.

Boehler C, Gauthier LR, Mortusewicz O, Biard DS, Saliou JM, Bresson A, Sanglier-Cianferani S, Smith S, Schreiber V, Boussin F and Dantzer F. 2011. Poly(ADP-ribose) polymerase 3 (PARP3), a newcomer in cellular response to DNA damage and mitotic progression. *Proceedings of the National Academy of Sciences of the United States of America* **108**: 2783-2788.

Boria I, Garelli E, Gazda HT, Aspesi A, Quarello P, Pavesi E, Ferrante D, Meerpohl JJ, Kartal M, Da Costa L, Proust A, Leblanc T, Simansour M, Dahl N, Frojmark AS, Pospisilova D, Cmejla R, Beggs AH, Sheen MR, Landowski M, Buros CM, Clinton CM, Dobson LJ, Vlachos A, Atsidaftos E, Lipton JM, Ellis SR, Ramenghi U and Dianzani I. 2010. The ribosomal basis of Diamond-Blackfan Anemia: mutation and database update. *Human Mutation* **31**: 1269-1279.

Bou Kheir T, Futoma-Kazmierczak E, Jacobsen A, Krogh A, Bardram L, Hother C, Gronbaek K, Federspiel B, Lund AH and Friis-Hansen L. 2011. miR-449 inhibits cell proliferation and is down-regulated in gastric cancer. *Molecular Cancer* **10**: 29.

Brameier M, Krings A and MacCallum RM. 2007. NucPred—Predicting nuclear localization of proteins. *Bioinformatics* **23**: 1159-1160.

Braunstein M, Rose AB, Holmes SG, Allis CD and Broach JR. 1993. Transcriptional silencing in yeast is associated with reduced nucleosome acetylation. *Genes & Development* **7**: 592-604.

Braunstein M, Sobel RE, Allis CD, Turner BM and Broach JR. 1996. Efficient transcriptional silencing in Saccharomyces cerevisiae requires a heterochromatin histone acetylation pattern. *Molecular and Cellular Biology* **16**: 4349-4356.

Brooks C and Gu W. 2011. The impact of acetylation and deacetylation on the p53 pathway. *Protein & Cell* **2**: 456-462.

Brunet A, Kanai F, Stehn J, Xu J, Sarbassova D, Frangioni JV, Dalal SN, DeCaprio JA, Greenberg ME and Yaffe MB. 2002. 14-3-3 transits to the nucleus and participates in dynamic nucleocytoplasmic transport. *The Journal of Cell Biology* **156**: 817-828.

Brunet A, Sweeney LB, Sturgill JF, Chua KF, Greer PL, Lin YX, Tran H, Ross SE, Mostoslavsky R, Cohen HY, Hu LS, Cheng HL, Jedrychowski MP, Gygi SP, Sinclair DA, Alt FW and Greenberg ME. 2004. Stress-dependent regulation of FOXO transcription factors by the SIRT1 deacetylase. *Science* **303**: 2011-2015.

Bryk M, Banerjee M, Murphy M, Knudsen KE, Garfinkel DJ and Curcio MJ. 1997. Transcriptional silencing of Ty1 elements in the RDN1 locus of yeast. *Genes & Development* **11**: 255-269.

Bunz F, Dutriaux A, Lengauer C, Waldman T, Zhou S, Brown JP, Sedivy JM, Kinzler KW and Vogelstein B. 1998. Requirement for p53 and p21 to sustain G2 arrest after DNA damage. *Science* **282**: 1497-1501.

Calnan DR and Brunet A. 2008. The FoxO code. *Oncogene* **27**: 2276-2288.

Cantó C and Auwerx J. 2011. Targeting Sirtuin 1 to Improve Metabolism: All You Need Is NAD+? *Pharmacological Reviews*.

Canto C, Gerhart-Hines Z, Feige JN, Lagouge M, Noriega L, Milne JC, Elliott PJ, Puigserver P and Auwerx J. 2009. AMPK regulates energy expenditure by modulating NAD+ metabolism and SIRT1 activity. *Nature* **458**: 1056-1060.

Chen GL, Yang L, Rowe TC, Halligan BD, Tewey KM and Liu LF. 1984. Nonintercalative antitumor drugs interfere with the breakage-reunion reaction

of mammalian DNA topoisomerase II. *Journal of Biological Chemistry* **259**: 13560-13566.

Chen J, Zhang B, Wong N, Lo AW, To KF, Chan AW, Ng MH, Ho CY, Cheng SH, Lai PB, Yu J, Ng HK, Ling MT, Huang AL, Cai XF and Ko BC. 2011a. Sirtuin 1 Is Upregulated in a Subset of Hepatocellular Carcinomas where It Is Essential for Telomere Maintenance and Tumor Cell Growth. *Cancer Research* **71**: 4138-4149.

Chen R, Dioum EM, Hogg RT, Gerard RD and Garcia JA. 2011b. Hypoxia increases sirtuin 1 expression in a hypoxia-inducible factor-dependent manner. *Journal of Biological Chemistry* **286**: 13869-13878.

Chen WY, Wang DH, Yen RC, Luo J, Gu W and Baylin SB. 2005. Tumor Suppressor HIC1 Directly Regulates SIRT1 to Modulate p53-Dependent DNA-Damage Responses. *Cell* **123**: 437-448.

Choesmel V, Bacqueville D, Rouquette J, Noaillac-Depeyre J, Fribourg S, Cretien A, Leblanc T, Tchernia G, Da Costa L and Gleizes PE. 2007. Impaired ribosome biogenesis in Diamond-Blackfan anemia. *Blood* **109**: 1275-1283.

Chuikov S, Kurash JK, Wilson JR, Xiao B, Justin N, Ivanov GS, McKinney K, Tempst P, Prives C, Gamblin SJ, Barlev NA and Reinberg D. 2004. Regulation of p53 activity through lysine methylation. *Nature* **432**: 353-360.

Cretien A, Hurtaud C, Moniz H, Proust A, Marie I, Wagner-Ballon O, Choesmel V, Gleizes PE, Leblanc T, Delaunay J, Tchernia G, Mohandas N and Da Costa L. 2008. Study of the effects of proteasome inhibitors on ribosomal protein S19 (RPS19) mutants, identified in patients with Diamond-Blackfan anemia. *Haematologica* **93**: 1627-1634.

Da Costa L, Tchernia G, Gascard P, Lo A, Meerpohl J, Niemeyer C, Chasis JA, Fixler J and Mohandas N. 2003. Nucleolar localization of RPS19 protein in normal cells and mislocalization due to mutations in the nucleolar localization signals in 2 Diamond-Blackfan anemia patients: potential insights into pathophysiology. *Blood* **101**: 5039-5045.

Danilova N, Sakamoto KM and Lin S. 2008. Ribosomal protein S19 deficiency in zebrafish leads to developmental abnormalities and defective erythropoiesis through activation of p53 protein family. *Blood* **112**: 5228-5237.

Deisenroth C and Zhang Y. 2010. Ribosome biogenesis surveillance: probing the ribosomal protein-Mdm2-p53 pathway. *Oncogene* **29**: 4253-4260.

Dhanasekaran DN and Reddy EP. 2008. JNK signaling in apoptosis. *Oncogene* **27**: 6245-6251.

Diamond LK and Blackfan KD. 1938. Hypoplastic anemia. *American Journal of Diseases of Children* **56**: 464–467.

Dinman JD. 2009. The Eukaryotic Ribosome: Current Status and Challenges. *Journal of Biological Chemistry* **284**: 11761-11765.

Dioum EM, Chen R, Alexander MS, Zhang Q, Hogg RT, Gerard RD and Garcia JA. 2009. Regulation of hypoxia-inducible factor 2alpha signaling by the stress-responsive deacetylase sirtuin 1. *Science* **324**: 1289-1293.

Donmez G and Guarente L. 2010. Aging and disease: connections to sirtuins. *Aging Cell* **9**: 285-290.

Donmez G, Wang D, Cohen DE and Guarente L. 2010. SIRT1 suppresses beta-amyloid production by activating the alpha-secretase gene ADAM10. *Cell* **142**: 320-332.

Draptchinskaia N, Gustavsson P, Andersson B, Pettersson M, Willig TN, Dianzani I, Ball S, Tchernia G, Klar J, Matsson H, Tentler D, Mohandas N, Carlsson B and Dahl N. 1999. The gene encoding ribosomal protein S19 is mutated in Diamond-Blackfan anaemia. *Nature Genetics* **21**: 169-175.

Drewinko B, Romsdahl MM, Yang LY, Ahearn MJ and Trujillo JM. 1976. Establishment of a Human Carcinoembryonic Antigen-producing Colon Adenocarcinoma Cell Line. *Cancer Research* **36**: 467-475.

Du J, Zhou Y, Su X, Yu JJ, Khan S, Jiang H, Kim J, Woo J, Kim JH, Choi BH, He B, Chen W, Zhang S, Cerione RA, Auwerx J, Hao Q and Lin H. 2011. Sirt5 Is a NAD-Dependent Protein Lysine Demalonylase and Desuccinylase. *Science* **334**: 806-809.

Dutt S, Narla A, Lin K, Mullally A, Abayasekara N, Megerdichian C, Wilson FH, Currie T, Khanna-Gupta A, Berliner N, Kutok JL and Ebert BL. 2011. Haploinsufficiency for ribosomal protein genes causes selective activation of p53 in human erythroid progenitor cells. *Blood* **117**: 2567-2576.

Eades G, Yao Y, Yang M, Zhang Y, Chumsri S and Zhou Q. 2011. miR-200a Regulates SIRT1 Expression and Epithelial to Mesenchymal Transition (EMT)-like Transformation in Mammary Epithelial Cells. *Journal of Biological Chemistry* **286**: 25992-26002.

Essers MAG, Weijzen S, de Vries-Smits AMM, Saarloos I, de Ruiter ND, Bos JL and Burgering BMT. 2004. FOXO transcription factor activation by oxidative stress mediated by the small GTPase Ral and JNK. *EMBO Journal* **23**: 4802-4812.

Fang S, Jensen JP, Ludwig RL, Vousden KH and Weissman AM. 2000. Mdm2 Is a RING Finger-dependent Ubiquitin Protein Ligase for Itself and p53. *Journal of Biological Chemistry* **275**: 8945-8951.

Fantin VR, St-Pierre J and Leder P. 2006. Attenuation of LDH-A expression uncovers a link between glycolysis, mitochondrial physiology, and tumor maintenance. *Cancer Cell* **9**: 425-434.

Finley LW, Carracedo A, Lee J, Souza A, Egia A, Zhang J, Teruya-Feldstein J, Moreira PI, Cardoso SM, Clish CB, Pandolfi PP and Haigis MC. 2011. SIRT3 opposes reprogramming of cancer cell metabolism through HIF1alpha destabilization. *Cancer Cell* **19**: 416-428.

Firestein R, Blander G, Michan S, Oberdoerffer P, Ogino S, Campbell J, Bhimavarapu A, Luikenhuis S, de Cabo R, Fuchs C, Hahn WC, Guarente LP and Sinclair DA. 2008. The SIRT1 deacetylase suppresses intestinal tumorigenesis and colon cancer growth. *PLoS One* **3**: e2020.

Firth JD, Ebert BL and Ratcliffe PJ. 1995. Hypoxic Regulation of Lactate Dehydrogenase A. *Journal of Biological Chemistry* **270**: 21021-21027.

Flygare J, Aspesi A, Bailey JC, Miyake K, Caffrey JM, Karlsson S and Ellis SR. 2007. Human RPS19, the gene mutated in Diamond-Blackfan anemia, encodes a ribosomal protein required for the maturation of 40S ribosomal subunits. *Blood* **109**: 980-986.

Ford J, Ahmed S, Allison S, Jiang M and Milner J. 2008. JNK2-dependent regulation of SIRT1 protein stability. *Cell Cycle* **7**: 3091-3097.

Ford J, Jiang M and Milner J. 2005. Cancer-specific functions of SIRT1 enable human epithelial cancer cell growth and survival. *Cancer Research* **65**: 10457-10463.

Freed EF, Bleichert F, Dutca LM and Baserga SJ. 2010. When ribosomes go bad: diseases of ribosome biogenesis. *Molecular BioSystems* **6**: 481-493.

Frye RA. 2000. Phylogenetic Classification of Prokaryotic and Eukaryotic Sir2-like Proteins. *Biochemical and Biophysical Research Communications* **273**: 793-798.

Ghosh HS, McBurney M and Robbins PD. 2010. SIRT1 Negatively Regulates the Mammalian Target of Rapamycin. *PLoS One* **5**: e9199.

Ghosh HS, Reizis B and Robbins PD. 2011. SIRT1 associates with eIF2-alpha and regulates the cellular stress response. *Nature Scientific Reports* **1**.

Gilley J, Coffer PJ and Ham J. 2003. FOXO transcription factors directly activate bim gene expression and promote apoptosis in sympathetic neurons. *The Journal of Cell Biology* **162**: 613-622.

Gillings AS, Balmanno K, Wiggins CM, Johnson M and Cook SJ. 2009. Apoptosis and autophagy: BIM as a mediator of tumour cell death in response to oncogene-targeted therapeutics. *Federation of European Biochemical Societies Journal* **276**: 6050-6062.

Goh AM, Coffill CR and Lane DP. 2011. The role of mutant p53 in human cancer. *The Journal of Pathology* **223**: 116-126.

Goldberg E, Eddy EM, Duan C and Odet F. 2010. LDHC: the ultimate testis-specific gene. *Journal of Andrology* **31**: 86-94.

Goldman RD, Kaplan NO and Hall TC. 1964. Lactic Dehydrogenase in Human Neoplastic Tissues. *Cancer Research* **24**: 389-399.

Gottschling DE, Aparicio OM, Billington BL and Zakian VA. 1990. Position effect at S. cerevisiae telomeres: Reversible repression of Pol II transcription. *Cell* **63**: 751-762.

Greiss S and Gartner A. 2009. Sirtuin/Sir2 phylogeny, evolutionary considerations and structural conservation. *Molecules and Cells* **28**: 407-415.

Grummt I and Ladurner AG. 2008. A Metabolic Throttle Regulates the Epigenetic State of rDNA. *Cell* **133**: 577-580.

Gu W and Roeder RG. 1997. Activation of p53 Sequence-Specific DNA Binding by Acetylation of the p53 C-Terminal Domain. *Cell* **90**: 595-606.

Guo H, Ingolia NT, Weissman JS and Bartel DP. 2010a. Mammalian microRNAs predominantly act to decrease target mRNA levels. *Nature* **466**: 835-840.

Guo X, Williams JG, Schug TT and Li X. 2010b. DYRK1A and DYRK3 promote cell survival through phosphorylation and activation of SIRT1. *Journal of Biological Chemistry*.

Hadjiolova KV, Nicoloso M, Mazan S, Hadjiolov AA and Bachellerie J-P. 1993. Alternative pre-rRNA processing pathways in human cells and their

alteration by cycloheximide inhibition of protein synthesis. *European Journal of Biochemistry* **212**: 211-215.

Hage AE and Tollervey D. 2004. A Surfeit of Factors: Why is Ribosome Assembly So Much More Complicated in Eukaryotes than Bacteria? *RNA Biology* **1**: 9-14.

Hamaguchi M, Meth JL, von Klitzing C, Wei W, Esposito D, Rodgers L, Walsh T, Welcsh P, King M-C and Wigler MH. 2002. DBC2, a candidate for a tumor suppressor gene involved in breast cancer. *Proceedings of the National Academy of Sciences* **99**: 13647-13652.

Hanahan D and Weinberg RA. 2011. Hallmarks of cancer: the next generation. *Cell* **144**: 646-674.

Hao C-M and Haase VH. 2010. Sirtuins and Their Relevance to the Kidney. *Journal of the American Society of Nephrology* **21**: 1620-1627.

Haupt Y, Maya R, Kazaz A and Oren M. 1997. Mdm2 promotes the rapid degradation of p53. *Nature* **387**: 296-299.

Herranz D, Iglesias G, Munoz-Martin M and Serrano M. 2011. Limited role of Sirt1 in cancer protection by dietary restriction. *Cell Cycle* **10**.

Hintz M and Goldberg E. 1977. Immunohistochemical localization of LDH-x during spermatogenesis in mouse testes. *Developmental Biology* **57**: 375-384.

Honda R, Tanaka H and Yasuda H. 1997. Oncoprotein MDM2 is a ubiquitin ligase E3 for tumor suppressor p53. *Federation of the Societies of Biochemistry Letters* **420**: 25-27.

Honda R and Yasuda H. 2000. Activity of MDM2, a ubiquitin ligase, toward p53 or itself is dependent on the RING finger domain of the ligase. *Oncogene* **19**: 1473-1476.

Horn DM, Mason SL and Karbstein K. 2011. Rcl1 Protein, a Novel Nuclease for 18 S Ribosomal RNA Production. *Journal of Biological Chemistry* **286**: 34082-34087.

Horos R, IJspeert H, Pospisilova D, Sendtner R, Andrieu-Soler C, Taskesen E, Nieradka A, Cmejla R, Sendtner M, Touw IP and von Lindern M. 2011. Ribosomal deficiencies in Diamond-Blackfan anemia impair translation of transcripts essential for differentiation of murine and human erythroblasts. *Blood*.

Hsu C-P, Zhai P, Yamamoto T, Maejima Y, Matsushima S, Hariharan N, Shao D, Takagi H, Oka S and Sadoshima J. 2010. Silent Information Regulator 1 Protects the Heart From Ischemia/Reperfusion / Clinical Perspective. *Circulation* **122**: 2170-2182.

http://www.lsbm.org. "Reference database for gene Expression Analysis (RefExA)." Retrieved 27.09.2011, 2011.

Huffman DM, Grizzle WE, Bamman MM, Kim J-s, Eltoum IA, Elgavish A and Nagy TR. 2007. SIRT1 Is Significantly Elevated in Mouse and Human Prostate Cancer. *Cancer Research* **67**: 6612-6618.

Idol RA, Robledo S, Du HY, Crimmins DL, Wilson DB, Ladenson JH, Bessler M and Mason PJ. 2007. Cells depleted for RPS19, a protein associated with Diamond Blackfan Anemia, show defects in 18S ribosomal RNA synthesis and small ribosomal subunit production. *Blood Cells, Molecules & Diseases* **39**: 35-43.

Imai S. 2011. Dissecting systemic control of metabolism and aging in the NAD World: The importance of SIRT1 and NAMPT-mediated NAD biosynthesis. *FEBS Letters* **585**: 1657-1662.

Imai S, Armstrong CM, Kaeberlein M and Guarente L. 2000. Transcriptional silencing and longevity protein Sir2 is an NAD-dependent histone deacetylase. *Nature* **403**: 795-800.

Ito E, Konno Y, Toki T and Terui K. 2010. Molecular pathogenesis in Diamond-Blackfan anemia. *International Journal of Hematology* **92**: 413-418.

Jaako P, Flygare J, Olsson K, Quere R, Ehinger M, Henson A, Ellis S, Schambach A, Baum C, Richter J, Larsson J, Bryder D and Karlsson S. 2011. Mice with ribosomal protein S19 deficiency develop bone marrow failure and symptoms like patients with Diamond-Blackfan anemia. *Blood*.

Kaeberlein M, McVey M and Guarente L. 1999. The SIR2/3/4 complex and SIR2 alone promote longevity in Saccharomyces cerevisiae by two different mechanisms. *Genes & Development* **13**: 2570-2580.

Kang H, Suh J-Y, Jung Y-S, Jung J-W, Kim Myung K and Chung Jay H. 2011. Peptide Switch Is Essential for Sirt1 Deacetylase Activity. *Molecular Cell* **44**: 203-213.

Kanno T, Sudo K, Maekawa M, Nishimura Y, Ukita M and Fukutake K. 1988. Lactate dehydrogenase M-subunit deficiency: a new type of hereditary exertional myopathy. *Clinica Chimica Acta* **173**: 89-98.

Kawahara TLA, Michishita E, Adler AS, Damian M, Berber E, Lin M, McCord RA, Ongaigui KCL, Boxer LD, Chang HY and Chua KF. 2009. SIRT6 Links Histone H3 Lysine 9 Deacetylation to NF-ºB-Dependent Gene Expression and Organismal Life Span. *Cell* **136**: 62-74.

Kim EJ, Kho JH, Kang MR and Um SJ. 2007. Active regulator of SIRT1 cooperates with SIRT1 and facilitates suppression of p53 activity. *Molecular Cell* **28**: 277-290.

Kim JE, Chen J and Lou Z. 2008. DBC1 is a negative regulator of SIRT1. *Nature* **451**: 583-586.

Knight JRP and Milner J. 2011. SIRT1, metabolism and cancer. *Current Opinion in Oncology*: In press: 10.1097/CCO.1090b1013e32834d32813b.

Koslowski M, Tureci O, Bell C, Krause P, Lehr HA, Brunner J, Seitz G, Nestle FO, Huber C and Sahin U. 2002. Multiple splice variants of lactate dehydrogenase C selectively expressed in human cancer. *Cancer Research* **62**: 6750-6755.

Kresge N, Simoni RD and Hill RL. 2005. Otto Fritz Meyerhof and the Elucidation of the Glycolytic Pathway. *Journal of Biological Chemistry* **280**: e3.

Kressler D, Hurt E and Bassler J. 2010. Driving ribosome assembly. *Biochimica et Biophysica Acta* **1803**: 673-683.

Krishnakumar R and Kraus WL. 2010. The PARP Side of the Nucleus: Molecular Actions, Physiological Outcomes, and Clinical Targets. *Molecular Cell* **39**: 8-24.

Kubbutat MHG, Jones SN and Vousden KH. 1997. Regulation of p53 stability by Mdm2. *Nature* **387**: 299-303.

la Cour T, Kiemer L, Mølgaard A, Gupta R, Skriver K and Brunak S. 2004. Analysis and prediction of leucine-rich nuclear export signals. *Protein Engineering Design and Selection* **17**: 527-536.

Landry J, Sutton A, Tafrov ST, Heller RC, Stebbins J, Pillus L and Sternglanz R. 2000. The silencing protein SIR2 and its homologs are NAD-dependent protein deacetylases. *Proceedings of the National Academy of Sciences* **97**: 5807-5811.

Lane DP. 1992. p53, guardian of the genome. *Nature* **358**: 15-16.

Larionov A, Krause A and Miller W. 2005. A standard curve based method for relative real time PCR data processing. *BMC Bioinformatics* **6**: 62.

Le A, Cooper CR, Gouw AM, Dinavahi R, Maitra A, Deck LM, Royer RE, Vander Jagt DL, Semenza GL and Dang CV. 2010. Inhibition of lactate dehydrogenase A induces oxidative stress and inhibits tumor progression. *Proceedings of the National Academy of Sciences* **107**: 2037-2042.

Lee JT and Gu W. 2010. The multiple levels of regulation by p53 ubiquitination. *Cell Death & Differentiation* **17**: 86-92.

Leiblich A, Cross SS, Catto JW, Phillips JT, Leung HY, Hamdy FC and Rehman I. 2006. Lactate dehydrogenase-B is silenced by promoter hypermethylation in human prostate cancer. *Oncogene* **25**: 2953-2960.

Lewis B, Shim H, Li Q, Wu C, Lee L, Maity A and Dang C. 1997. Identification of putative c-Myc-responsive genes: characterization of rcl, a novel growth-related gene. *Molecular and Cellular Biology* **17**: 4967-4978.

Li M, Luo J, Brooks CL and Gu W. 2002. Acetylation of p53 inhibits its ubiquitination by Mdm2. *Journal of Biological Chemistry* **277**: 50607-50611.

Li S, Banck M, Mujtaba S, Zhou M-M, Sugrue MM and Walsh MJ. 2010. p53-Induced Growth Arrest Is Regulated by the Mitochondrial *SirT3* Deacetylase. *PLoS One* **5**: e10486.

Lim JH, Lee YM, Chun YS, Chen J, Kim JE and Park JW. 2010. Sirtuin 1 modulates cellular responses to hypoxia by deacetylating hypoxia-inducible factor 1alpha. *Molecular Cell* **38**: 864-878.

Liu X, Wang D, Zhao Y, Tu B, Zheng Z, Wang L, Wang H, Gu W, Roeder RG and Zhu W-G. 2011. Methyltransferase Set7/9 regulates p53 activity by interacting with Sirtuin 1 (SIRT1). *Proceedings of the National Academy of Sciences* **108**: 1925-1930.

Lohrum MA, Ashcroft M, Kubbutat MH and Vousden KH. 2000. Contribution of two independent MDM2-binding domains in p14(ARF) to p53 stabilization. *Current Biology* **10**: 539-542.

Lombard DB, Alt FW, Cheng H-L, Bunkenborg J, Streeper RS, Mostoslavsky R, Kim J, Yancopoulos G, Valenzuela D, Murphy A, Yang Y, Chen Y, Hirschey MD, Bronson RT, Haigis M, Guarente LP, Farese RV, Jr., Weissman S, Verdin E and Schwer B. 2007. Mammalian Sir2 Homolog

SIRT3 Regulates Global Mitochondrial Lysine Acetylation. *Molecular and Cellular Biology* **27**: 8807-8814.

Luft F. 2010. The rise of a ribosomopathy and increased cancer risk. *Journal of Molecular Medicine* **88**: 1-3.

Luo J, Nikolaev AY, Imai S, Chen D, Su F, Shiloh A, Guarente L and Gu W. 2001. Negative control of p53 by Sir2alpha promotes cell survival under stress. *Cell* **107**: 137-148.

Luo J, Su F, Chen D, Shiloh A and Gu W. 2000. Deacetylation of p53 modulates its effect on cell growth and apoptosis. *Nature* **408**: 377-381.

Lynch CJ, Shah ZH, Allison SJ, Ahmed SU, Ford J, Warnock LJ, Li H, Serrano M and Milner J. 2010. SIRT1 undergoes alternative splicing in a novel auto-regulatory loop with p53. *PLoS One* **5**: e13502.

Maeda N, Toku S, Kenmochi N and Tanaka T. 2006. A novel nucleolar protein interacts with ribosomal protein S19. *Biochemical and Biophysical Research Communications* **339**: 41-46.

Maeda N, Toku S, Naito Y, Nishiura H, Tanaka T and Yamamoto H. 2009. Phosphorylation of ribosomal protein S19 at Ser59 by CaM kinase I alpha. *Journal of Neurochemistry* **109**: 393-402.

Majmundar AJ, Wong WJ and Simon MC. 2010. Hypoxia-inducible factors and the response to hypoxic stress. *Molecular Cell* **40**: 294-309.

Markert CL, Shaklee JB and Whitt GS. 1975. Evolution of a gene. Multiple genes for LDH isozymes provide a model of the evolution of gene structure, function and regulation. *Science* **189**: 102-114.

Maya R, Balass M, Kim ST, Shkedy D, Leal JF, Shifman O, Moas M, Buschmann T, Ronai Z, Shiloh Y, Kastan MB, Katzir E and Oren M. 2001. ATM-dependent phosphorylation of Mdm2 on serine 395: role in p53 activation by DNA damage. *Genes & Development* **15**: 1067-1077.

McGowan KA, Li JZ, Park CY, Beaudry V, Tabor HK, Sabnis AJ, Zhang W, Fuchs H, de Angelis MH, Myers RM, Attardi LD and Barsh GS. 2008. Ribosomal mutations cause p53-mediated dark skin and pleiotropic effects. *Nature Genetics* **40**: 963-970.

Michishita E, McCord RA, Berber E, Kioi M, Padilla-Nash H, Damian M, Cheung P, Kusumoto R, Kawahara TLA, Barrett JC, Chang HY, Bohr VA, Ried T,

Gozani O and Chua KF. 2008. SIRT6 is a histone H3 lysine 9 deacetylase that modulates telomeric chromatin. *Nature* **452**: 492-496.

Min S-W, Cho S-H, Zhou Y, Schroeder S, Haroutunian V, Seeley WW, Huang EJ, Shen Y, Masliah E, Mukherjee C, Meyers D, Cole PA, Ott M and Gan L. 2010. Acetylation of Tau Inhibits Its Degradation and Contributes to Tauopathy. *Neuron* **67**: 953-966.

Mitchell P. 1961. Coupling of Phosphorylation to Electron and Hydrogen Transfer by a Chemi-Osmotic type of Mechanism. *Nature* **191**: 144-148.

Momand J, Zambetti GP, Olson DC, George D and Levine AJ. 1992. The mdm-2 oncogene product forms a complex with the p53 protein and inhibits p53-mediated transactivation. *Cell* **69**: 1237-1245.

Mostoslavsky R, Chua KF, Lombard DB, Pang WW, Fischer MR, Gellon L, Liu P, Mostoslavsky G, Franco S, Murphy MM, Mills KD, Patel P, Hsu JT, Hong AL, Ford E, Cheng H-L, Kennedy C, Nunez N, Bronson R, Frendewey D, Auerbach W, Valenzuela D, Karow M, Hottiger MO, Hursting S, Barrett JC, Guarente L, Mulligan R, Demple B, Yancopoulos GD and Alt FW. 2006. Genomic Instability and Aging-like Phenotype in the Absence of Mammalian SIRT6. *Cell* **124**: 315-329.

Motta MC, Divecha N, Lemieux M, Kamel C, Chen D, Gu W, Bultsma Y, McBurney M and Guarente L. 2004. Mammalian SIRT1 represses forkhead transcription factors. *Cell* **116**: 551-563.

Murayama A, Ohmori K, Fujimura A, Minami H, Yasuzawa-Tanaka K, Kuroda T, Oie S, Daitoku H, Okuwaki M, Nagata K, Fukamizu A, Kimura K, Shimizu T and Yanagisawa J. 2008. Epigenetic Control of rDNA Loci in Response to Intracellular Energy Status. *Cell* **133**: 627-639.

Nadtochiy SM, Redman E, Rahman I and Brookes PS. 2011. Lysine deacetylation in ischaemic preconditioning: the role of SIRT1. *Cardiovascular Research* **89**: 643-649.

Nasrin N, Kaushik VK, Fortier E, Wall D, Pearson KJ, de Cabo R and Bordone L. 2009. JNK1 Phosphorylates SIRT1 and Promotes Its Enzymatic Activity. *PLoS One* **4**: e8414.

Nemoto S, Fergusson MM and Finkel T. 2004. Nutrient Availability Regulates SIRT1 Through a Forkhead-Dependent Pathway. *Science* **306**: 2105-2108.

Nemoto S, Fergusson MM and Finkel T. 2005. SIRT1 functionally interacts with the metabolic regulator and transcriptional coactivator PGC-1alpha. *Journal of Biological Chemistry*.

Network TCGAR. 2008. Comprehensive genomic characterization defines human glioblastoma genes and core pathways. *Nature* **455**: 1061-1068.

Nishioka K, Chuikov S, Sarma K, Erdjument-Bromage H, Allis CD, Tempst P and Reinberg D. 2002. Set9, a novel histone H3 methyltransferase that facilitates transcription by precluding histone tail modifications required for heterochromatin formation. *Genes & Development* **16**: 479-489.

Nishiura H, Shibuya Y and Yamamoto T. 1998. S19 ribosomal protein cross-linked dimer causes monocyte-predominant infiltration by means of molecular mimicry to complement C5a. *Laboratory Investigation* **78**: 1615-1623.

Noriega LG, Feige JN, Canto C, Yamamoto H, Yu J, Herman MA, Mataki C, Kahn BB and Auwerx J. 2011. CREB and ChREBP oppositely regulate SIRT1 expression in response to energy availability. *EMBO Reports* **12**: 1069-1076.

O'Connor L, Strasser A, O'Reilly LA, Hausmann G, Adams JM, Cory S and Huang DC. 1998. Bim: a novel member of the Bcl-2 family that promotes apoptosis. *EMBO Journal* **17**: 384-395.

Oberdoerffer P, Michan S, McVay M, Mostoslavsky R, Vann J, Park SK, Hartlerode A, Stegmuller J, Hafner A, Loerch P, Wright SM, Mills KD, Bonni A, Yankner BA, Scully R, Prolla TA, Alt FW and Sinclair DA. 2008. SIRT1 redistribution on chromatin promotes genomic stability but alters gene expression during aging. *Cell* **135**: 907-918.

Oda Y, Tokita K, Ota Y, Li Y, Taniguchi K, Nishino N, Takagi K, Yamamoto T and Nishiura H. 2008. Agonistic and Antagonistic Effects of C5a-Chimera Bearing S19 Ribosomal Protein Tail Portion on the C5a Receptor of Monocytes and Neutrophils, Respectively. *Journal of Biochemistry* **144**: 371-381.

Ohkubo S, Tanaka T, Taya Y, Kitazato K and Prives C. 2006. Excess HDM2 Impacts Cell Cycle and Apoptosis and Has a Selective Effect on p53-dependent Transcription. *Journal of Biological Chemistry* **281**: 16943-16950.

Olivier M, Hollstein M and Hainaut P. 2010. TP53 Mutations in Human Cancers: Origins, Consequences, and Clinical Use. *Cold Spring Harbor Perspectives in Biology* **2**.

Orru S, Aspesi A, Armiraglio M, Caterino M, Loreni F, Ruoppolo M, Santoro C and Dianzani I. 2007. Analysis of the ribosomal protein S19 interactome. *Molecular & Cellular Proteomics* **6**: 382-393.

Ozdag H, Teschendorff A, Ahmed A, Hyland S, Blenkiron C, Bobrow L, Veerakumarasivam A, Burtt G, Subkhankulova T, Arends M, Collins VP, Bowtell D, Kouzarides T, Brenton J and Caldas C. 2006. Differential expression of selected histone modifier genes in human solid cancers. *BMC Genomics* **7**: 90.

Pan D. 2010. The Hippo Signaling Pathway in Development and Cancer. *Developmental Cell* **19**: 491-505.

Potente M, Ghaeni L, Baldessari D, Mostoslavsky R, Rossig L, Dequiedt F, Haendeler J, Mione M, Dejana E, Alt FW, Zeiher AM and Dimmeler S. 2007. SIRT1 controls endothelial angiogenic functions during vascular growth. *Genes & Development* **21**: 2644-2658.

Pruitt K, Zinn RL, Ohm JE, McGarvey KM, Kang SHL, Watkins DN, Herman JG and Baylin SB. 2006. Inhibition of SIRT1 reactivates silenced cancer genes without loss of promoter DNA hypermethylation. *Plos Genetics* **2**: 344-352.

Rabl J, Leibundgut M, Ataide SF, Haag A and Ban N. 2011. Crystal Structure of the Eukaryotic 40S Ribosomal Subunit in Complex with Initiation Factor 1. *Science* **331**: 730-736.

Read JA, Winter VJ, Eszes CM, Sessions RB and Brady RL. 2001. Structural basis for altered activity of M- and H-isozyme forms of human lactate dehydrogenase. *Proteins* **43**: 175-185.

Revollo JR, Grimm AA and Imai S-i. 2004. The NAD Biosynthesis Pathway Mediated by Nicotinamide Phosphoribosyltransferase Regulates Sir2 Activity in Mammalian Cells. *Journal of Biological Chemistry* **279**: 50754-50763.

Rine J and Herskowitz I. 1987. Four Genes Responsible for a Position Effect on Expression From HML and HMR in Saccharomyces cerevisiae. *Genetics* **116**: 9-22.

Rippin TM, Freund SM, Veprintsev DB and Fersht AR. 2002. Recognition of DNA by p53 core domain and location of intermolecular contacts of cooperative binding. *Journal of Molecular Biology* **319**: 351-358.

Robledo S, Idol RA, Crimmins DL, Ladenson JH, Mason PJ and Bessler M. 2008. The role of human ribosomal proteins in the maturation of rRNA and ribosome production. *RNA* **14**: 1918-1929.

Rodgers JT, Lerin C, Haas W, Gygi SP, Spiegelman BM and Puigserver P. 2005. Nutrient control of glucose homeostasis through a complex of PGC-1alpha and SIRT1. *Nature* **434**: 113-118.

Rogina B and Helfand SL. 2004. Sir2 mediates longevity in the fly through a pathway related to calorie restriction. *Proceedings of the National Academy of Sciences* **101**: 15998-16003.

Roth J, Dobbelstein M, Freedman DA, Shenk T and Levine AJ. 1998. Nucleo-cytoplasmic shuttling of the hdm2 oncoprotein regulates the levels of the p53 protein via a pathway used by the human immunodeficiency virus rev protein. *EMBO Journal* **17**: 554-564.

Rouquette J, Choesmel V and Gleizes PE. 2005. Nuclear export and cytoplasmic processing of precursors to the 40S ribosomal subunits in mammalian cells. *EMBO Journal* **24**: 2862-2872.

Rubbi CP and Milner J. 2000. Non-activated p53 co-localizes with sites of transcription within both the nucleoplasm and the nucleolus. *Oncogene* **19**: 85-96.

Saunders LR and Verdin E. 2007. Sirtuins: critical regulators at the crossroads between cancer and aging. *Oncogene* **26**: 5489-5504.

Schreiber V, Dantzer F, Ame JC and de Murcia G. 2006. Poly(ADP-ribose): novel functions for an old molecule. *Nature Reviews Molecular Cell Biology* **7**: 517-528.

Semenza GL. 2003. Targeting HIF-1 for cancer therapy. *Nature reviews. Cancer* **3**: 721-732.

Shim H, Dolde C, Lewis BC, Wu C-S, Dang G, Jungmann RA, Dalla-Favera R and Dang CV. 1997. c-Myc transactivation of LDH-A: Implications for tumor metabolism and growth. *Proceedings of the National Academy of Sciences* **94**: 6658-6663.

Silvera D, Formenti SC and Schneider RJ. 2010. Translational control in cancer. *Nature Reviews Cancer* **10**: 254-266.

Smith JS and Boeke JD. 1997. An unusual form of transcriptional silencing in yeast ribosomal DNA. *Genes & Development* **11**: 241-254.

Smith JS, Brachmann CB, Celic I, Kenna MA, Muhammad S, Starai VJ, Avalos JL, Escalante-Semerena JC, Grubmeyer C, Wolberger C and Boeke JD. 2000. A phylogenetically conserved NAD+-dependent protein deacetylase activity in the Sir2 protein family. *Proceedings of the National Academy of Sciences* **97**: 6658-6663.

Soucek L and Evan GI. 2010. The ups and downs of Myc biology. *Current Opinion in Genetics & Development* **20**: 91-95.

Sunayama J, Tsuruta F, Masuyama N and Gotoh Y. 2005. JNK antagonizes Akt-mediated survival signals by phosphorylating 14-3-3. *The Journal of Cell Biology* **170**: 295-304.

Tanaka N, Smith P and Shuman S. 2011. Crystal structure of Rcl1, an essential component of the eukaryal pre-rRNA processosome implicated in 18s rRNA biogenesis. *RNA* **17**: 595-602.

Tang Y, Zhao W, Chen Y, Zhao Y and Gu W. 2008. Acetylation is indispensable for p53 activation. *Cell* **133**: 612-626.

Tanner KG, Landry J, Sternglanz R and Denu JM. 2000. Silent information regulator 2 family of NAD- dependent histone/protein deacetylases generates a unique product, 1-O-acetyl-ADP-ribose. *Proceedings of the National Academy of Sciences* **97**: 14178-14182.

Tanno M, Sakamoto J, Miura T, Shimamoto K and Horio Y. 2007. Nucleocytoplasmic Shuttling of the NAD+-dependent Histone Deacetylase SIRT1. *Journal of Biological Chemistry* **282**: 6823-6832.

Tao W and Levine AJ. 1999. Nucleocytoplasmic shuttling of oncoprotein Hdm2 is required for Hdm2-mediated degradation of p53. *Proceedings of the National Academy of Sciences* **96**: 3077-3080.

Taylor DJ, Devkota B, Huang AD, Topf M, Narayanan E, Sali A, Harvey SC and Frank J. 2009. Comprehensive molecular structure of the eukaryotic ribosome. *Structure* **17**: 1591-1604.

Thompson JS, Ling X and Grunstein M. 1994. Histone H3 amino terminus is required for telomeric and silent mating locus repression in yeast. *Nature* **369**: 245-247.

Tissenbaum HA and Guarente L. 2001. Increased dosage of a sir-2 gene extends lifespan in Caenorhabditis elegans. *Nature* **410**: 227-230.

van der Vos KE and Coffer PJ. 2011. The extending network of FOXO transcriptional target genes. *Antioxidants & Redox Signaling* **14**: 579-592.

Vaziri H, Dessain SK, Ng Eaton E, Imai SI, Frye RA, Pandita TK, Guarente L and Weinberg RA. 2001. hSIR2(SIRT1) functions as an NAD-dependent p53 deacetylase. *Cell* **107**: 149-159.

Vita M and Henriksson M. 2006. The Myc oncoprotein as a therapeutic target for human cancer. *Seminars in Cancer Biology* **16**: 318-330.

Vogelstein B, Lane D and Levine AJ. 2000. Surfing the p53 network. *Nature* **408**: 307-310.

von Heideman A, Berglund Å, Larsson R and Nygren P. 2010. Safety and efficacy of NAD depleting cancer drugs: results of a phase I clinical trial of CHS 828 and overview of published data. *Cancer Chemotherapy and Pharmacology* **65**: 1165-1172.

Wales MM, Biel MA, Deiry WE, Nelkin BD, Issa J-P, Cavenee WK, Kuerbitz SJ and Baylin SB. 1995. p53 activates expression of HIC-1, a new candidate tumour suppressor gene on 17p13.3. *Nature Medicine* **1**: 570-577.

Wang B, Hasan MK, Alvarado E, Yuan H, Wu H and Chen WY. 2011a. NAMPT overexpression in prostate cancer and its contribution to tumor cell survival and stress response. *Oncogene* **30**: 907-921.

Wang C, Chen L, Hou X, Li Z, Kabra N, Ma Y, Nemoto S, Finkel T, Gu W, Cress WD and Chen J. 2006. Interactions between E2F1 and SirT1 regulate apoptotic response to DNA damage. *Nature Cell Biology* **8**: 1025-1031.

Wang R-H, Kim H-S, Xiao C, Xu X, Gavrilova O and Deng C-X. 2011b. Hepatic Sirt1 deficiency in mice impairs mTorc2/Akt signaling and results in hyperglycemia, oxidative damage, and insulin resistance. *The Journal of Clinical Investigation* **121**: 4477-4490.

Wang R-H, Zheng Y, Kim H-S, Xu X, Cao L, Lahusen T, Lee M-H, Xiao C, Vassilopoulos A, Chen W, Gardner K, Man Y-G, Hung M-C, Finkel T and Deng C-X. 2008a. Interplay among BRCA1, SIRT1, and Survivin during BRCA1-Associated Tumorigenesis. *Molecular Cell* **32**: 11-20.

Wang RH, Sengupta K, Li C, Kim HS, Cao L, Xiao C, Kim S, Xu X, Zheng Y, Chilton B, Jia R, Zheng ZM, Appella E, Wang XW, Ried T and Deng CX. 2008b. Impaired DNA damage response, genome instability, and tumorigenesis in SIRT1 mutant mice. *Cancer Cell* **14**: 312-323.

Warburg O. 1956. On respiratory impairment in cancer cells. *Science* **124**: 269-270.

Warburg O and Christian W. 1936. Pyridin, der wasserstoffubertragende bestandteil von garungsfermenten. *Biochemische Zeitschrift* **287**: 291–328.

Weber JD, Taylor LJ, Roussel MF, Sherr CJ and Bar-Sagi D. 1999. Nucleolar Arf sequesters Mdm2 and activates p53. *Nature Cell Biology* **1**: 20-26.

Willig TN, Draptchinskaia N, Dianzani I, Ball S, Niemeyer C, Ramenghi U, Orfali K, Gustavsson P, Garelli E, Brusco A, Tiemann C, Perignon JL, Bouchier C, Cicchiello L, Dahl N, Mohandas N and Tchernia G. 1999. Mutations in ribosomal protein S19 gene and diamond blackfan anemia: wide variations in phenotypic expression. *Blood* **94**: 4294-4306.

Wu X, Bayle JH, Olson D and Levine AJ. 1993. The p53-mdm-2 autoregulatory feedback loop. *Genes & Development* **7**: 1126-1132.

Wu Z, Zheng S and Yu Q. 2009. The E2F family and the role of E2F1 in apoptosis. *The International Journal of Biochemistry* **41**: 2389-2397.

Xu D, Takeshita F, Hino Y, Fukunaga S, Kudo Y, Tamaki A, Matsunaga J, Takahashi R-u, Takata T, Shimamoto A, Ochiya T and Tahara H. 2011. miR-22 represses cancer progression by inducing cellular senescence. *The Journal of Cell Biology* **193**: 409-424.

Yamakuchi M, Ferlito M and Lowenstein CJ. 2008. miR-34a repression of SIRT1 regulates apoptosis. *Proceedings of the National Academy of Sciences* **105**: 13421-13426.

Yamamoto T. 2007. Roles of the ribosomal protein S19 dimer and the C5a receptor in pathophysiological functions of phagocytic leukocytes. *Pathol Int* **57**: 1-11.

Yang T and Sauve AA. 2006. NAD metabolism and sirtuins: metabolic regulation of protein deacetylation in stress and toxicity. *The American Association of Pharmaceutical Scientists Journal* **8**: E632-643.

Yang Y, Fu W, Chen J, Olashaw N, Zhang X, Nicosia SV, Bhalla K and Bai W. 2007. SIRT1 sumoylation regulates its deacetylase activity and cellular response to genotoxic stress. *Nature Cell Biology* **9**: 1253-1262.

Yecies J and Manning B. 2011. mTOR links oncogenic signaling to tumor cell metabolism. *Journal of Molecular Medicine* **89**: 221-228.

Ying W. 2008. NAD(+)/ NADH and NADP(+)/NADPH in cellular functions and cell death: Regulation and biological consequences. *Antioxidants & Redox Signaling* **10**.

Yoshida M, Kijima M, Akita M and Beppu T. 1990. Potent and specific inhibition of mammalian histone deacetylase both in vivo and in vitro by trichostatin A. *Journal of Biological Chemistry* **265**: 17174-17179.

Yoshino J, Mills Kathryn F, Yoon Myeong J and Imai S-i. 2011. Nicotinamide Mononucleotide, a Key NAD+ Intermediate, Treats the Pathophysiology of Diet- and Age-Induced Diabetes in Mice. *Cell Metabolism* **14**: 528-536.

Yu J-K, Satou Y, Holland ND, Shin-I T, Kohara Y, Satoh N, Bronner-Fraser M and Holland LZ. 2007. Axial patterning in cephalochordates and the evolution of the organizer. *Nature* **445**: 613-617.

Yuan F, Xie Q, Wu J, Bai Y, Mao B, Dong Y, Bi W, Ji G, Tao W, Wang Y and Yuan Z. 2011. MST1 Promotes Apoptosis through Regulating Sirt1-dependent p53 Deacetylation. *Journal of Biological Chemistry* **286**: 6940-6945.

Yuan J, Minter-Dykhouse K and Lou Z. 2009. A c-Myc–SIRT1 feedback loop regulates cell growth and transformation. *The Journal of Cell Biology* **185**: 203-211.

Zhang T, Berrocal JG, Frizzell KM, Gamble MJ, DuMond ME, Krishnakumar R, Yang T, Sauve AA and Kraus WL. 2009. Enzymes in the NAD+ salvage pathway regulate SIRT1 activity at target gene promoters. *Journal of Biological Chemistry*.

Zhao G, Cui J, Zhang JG, Qin Q, Chen Q, Yin T, Deng SC, Liu Y, Liu L, Wang B, Tian K, Wang GB and Wang CY. 2011. SIRT1 RNAi knockdown induces apoptosis and senescence, inhibits invasion and enhances chemosensitivity in pancreatic cancer cells. *Gene Therapy*.

Zhao W, Kruse JP, Tang Y, Jung SY, Qin J and Gu W. 2008. Negative regulation of the deacetylase SIRT1 by DBC1. *Nature* **451**: 587-590.

Zhong L, D'Urso A, Toiber D, Sebastian C, Henry RE, Vadysirisack DD, Guimaraes A, Marinelli B, Wikstrom JD, Nir T, Clish CB, Vaitheesvaran B, Iliopoulos O, Kurland I, Dor Y, Weissleder R, Shirihai OS, Ellisen LW, Espinosa JM and Mostoslavsky R. 2010. The histone deacetylase Sirt6 regulates glucose homeostasis via Hif1alpha. *Cell* **140**: 280-293.

Zhong L and Mostoslavsky R. 2010. SIRT6: A master epigenetic gatekeeper of glucose metabolism. *Transcription* **1**: 17-21.

Zschoernig B and Mahlknecht U. 2009. Carboxy-terminal phosphorylation of SIRT1 by protein kinase CK2. *Biochemical and Biophysical Research Communications* **381**: 372-377.

Publications and Presentations

Publication

Knight JRP, and Milner J. (2011) SIRT1, metabolism and cancer. Current Opinion in Oncology. (PMID: 22080944).

Oral presentations

Annual Graduate Symposium, March 2011, University of York; 'AROS, the nucleolus and cancer cell survival' – resulted in the award of the KM Stott prize.

YCR Annual Scientific Meeting, June 2010, Harrogate; 'AROS, the nucleolus and cancer cell survival'

Poster presentations

EMBL Protein Synthesis and Translational Control Conference, September 2011, Heidelberg, Germany; 'AROS: A novel factor in ribosome biogenesis'

Wellcome Trust Sub-Nuclear Structures and Disease Conference, July 2010, Cambridge; 'RPS19 and AROS: The regulation of pre-rRNA processing'

Genes and Cancer Conference, December 2009, Warwick; 'AROS protein is essential for cancer cell survival but not for SIRT1 activity'

YCR Annual Scientific Meeting, June 2009, Harrogate; 'Is AROS required for SIRT1 function and cancer cell survival?'